UNIVERSITY OF CALIFORNIA, SAN DIEGO

Metal Complexes of Tripodal N-Heterocyclic Carbene Ligands: Synthesis, Structure, Bonding, and Reactivity

A dissertation submitted in partial satisfaction of the

requirements for the degree Doctor of Philosophy

in

Chemistry

by

Xile Hu

Committee in charge:

Professor Karsten Meyer, Chair

Professor David N. Hendrickson

Professor Melvin Okamura

Professor Charles L. Perrin

Professor William C. Trogler

2004

The dissertation of Xile Hu is approved, and it is acceptable in quality and form for publication on microfilm.

_____

_____

_____

_____

_____

Chair

University of California, San Diego

2004

Dedicated with love and appreciation to my mother

Xiulan Lin and my father Fusheng Hu

Habe nun, ach! Philosophie,	*I've studied now Philosophy*
Juristerei und Medizin,	*And Jurisprudence, Medicine,*
Und leider auch Theologie,	*And even, alas! Theology*
Durchaus studiert, mit heissem Bemuehn.	*All through and through with ardour keen!*
Da steh' ich nun, ich armer Tor,	*Here now I stand, poor fool, and see*
Und bin so klug als wie zuvor!	*I'm just as wise as formerly.*
Heisse Magister, heisse Doktor gar,	*Am called a Master, even Doctor too,*
Und ziehe schon an die zehen Jahr'	*And now I've nearly ten years through*
Herauf, herab und quer und krumm	*Pulled my students by their noses to and fro*
Meine Schueler an der Nase herum --	*And up and down, across, about,*
Und sehe, dass wir nichts wissen koennen!	*And see there's nothing we can know!*

----Goethe "Faust"

TABLE OF CONTENTS

LIST OF SYMBOLS AND ABBREVIATIONS

Å	angstrom
δ	chemical shift
Δ	difference
^{o}	degree
ε	molar extinction coefficient
μ	magnetic moment
μ_B	Bohr magneton
χ	magnetic susceptibility
λ	wavelength
ADF	Amsterdam density functional
atm.	atmosphere
ave.	average
BP86	Becke's 88 exchange functional and Perdew's 88 correlation functional
BPh_4	tetraphenylborate
br	broad
Bu	butyl
Bz	benzyl
calcd	calculated
CCDC	Cambridge crystallographic data center
CCSD(T)	couple cluster single double triple excitation
COD	1,5-cyclooctadiene

Cp	cyclopentadienyl
CV	cyclic voltammogram
De	bond dissociation energy
deg.	degree
DFT	density functional theory
DMSO	dimethyl sulfoxide
dtbpe	1,2-bis(di-*tert*-butylphosphino)ethane
EDA	energy decomposition analysis
EPR	electron paramagnetic resonance
equiv.	equivalent
Et	ethyl
FAB	fast atom bombardment
Fc	ferrocene
Fc^+	ferrocenium
FT-IR	Fourier transform infrared
g	gram
GC-MS	gas chromatography mass spectrometry
GOF	goodness of fitting
HOMO	highest occupied molecular orbital
hr	hour
HR-MS	high resolution mass spectrometry
Hz	hertz

IM	imidazol-2-ylidene
IMes	1,3-dimesitylimidazol-2-ylidene
^{i}Pr	iso-propyl
K	kelvin
kcal	kilo-calorie
KOe	kilo-oersteds
L	liter
LUMO	lowest unoccupied molecular orbital
M	metal
M	mol L^{-1}
Me	methyl
Me_2NN	2,4-bis(2,6-dimethylphenyllimido)pentane
mes	mesitylene
mg	mili-gram
MHZ	mega-hertz
mL	mili-liter
mmol	mili-mole
MO	molecular orbital
mol	mole
mT	mili-tesla
mV	mili-volt
n-Bu	normal-butyl

NHC	N-heterocyclic carbene
nm	nano-meter
NMR	nuclear magnetic resonance
ORTEP	oak ridge thermal ellipsoid presentation
OTf	triflate
ox.	oxidation
Ph	phenyl
PhINTs	[N-(p-toluenesulfonyl)imino]phenyliodinane
ppm	part per million
red.	reduction
s	second
SOMO	singly occupied molecular orbital
SQUID	superconducting quantum interface device
STO	Slater-type orbital
T	tesla
TBA	tetra-butyl ammonium
t-Bu	tertial-butyl
t-BuOK	potassium tert-butoxide
TCNE	tetracyanoethylene
tert	tertial
THF	tetrahydrofuran
TIME	1,1,1-tris[(imidazole-2-ylidene)methyl]ethane

TIMEN	[tris(2-imidazol-2-ylidene)ethyl]amine
TM	transition metal
TMS	trimethyl silyl
Tp	hydridotris(pyrazolyl)borate
TZP	triple zeta polarization
UV/vis	ultra-violet/visible
V	volt
VWN	Vosko, Wilk, and Nusair local density approximation
xyl	xylene
ZORA	zeroth-order regular approximation

LIST OF FIGURES

Chapter 1

Chapter 2

Chapter 3

Chapter 4

LIST OF SCHEMES

LIST OF TABLES

Chapter 2

Chapter 3

Chapter 4

Chapter 5

Chapter 6

ACKNOWLEDGEMENTS

First and foremost I would like to thank my advisor, Professor Karsten Meyer, for his unconditional and infinite support throughout my Ph.D. study. None of the work with this dissertation would have been possible without his encouragement and guidance. In many ways, he has helped to shape me into the scientist I am today. Thank you Karsten!

During these years, I have the great pleasure to work, side by side, with the "Puerto Rican turkey", Ingrid Castro Rodriguez. Thank you Ingrid, for all the crystal structures you solved for me, for all the rides you gave me for free, and for always being there when I needed you. I apologize for my sometimes unintentional negligence of you. I will miss you, turkey!

I am very grateful to Dr. Kristian Olsen, for leading me into the door of computational chemistry. My discussions with him on the electronic structure of inorganic compounds have inspired the work presented in chapter 6.

I would also like to thank other past and present members of the Meyer group. Dr. Hidetaka Nakai had been a wonderful person to work with. Dr. Yongjun Tang synthesized some imidazolium salts in the early period of this study.

I am indebted to Dr. Christina Hauser, who has proof-read almost all of my papers. Her enthusiasm on our work is greatly appreciated.

I acknowledge Dr. Peter Gantzel, Dr. Lev N. Zakharov, and Professor Arnold L. Rheingold for their help on X-ray crystallography. I thank Dr. Roger Issacson

(Department of Physics) for teaching me how to use the EPR instrument. The support from these people has been tremendous.

My thanks also go to Nelda Hann, Chia Her, Lynne Keith-McMullin, and Jill Weller for their administrative support.

I have had many friends in San Diego. Thanks to them, I am not alone here in the U.S., some 10,000 miles away from my hometown back in China. The fun we had together has become memories, but the friendship we build will last forever.

The text, schemes, and figures of chapter two, three, four, five, and six, in part or full, are reprints of the materials previous published, or submitted for publication, as listed in the publication list at page xxxi. The dissertation author was the primary researcher and author. The co-authors listed in these publications also participated in the research. The permissions to reproduce these papers are granted by the American Chemical Society and the Royal Chemical Society.

VITA

June 2000	B.S. in Chemistry, Peking University, Beijing, P. R. China
2000-2004	Teaching Assistant and Research Assistant, Department of Chemistry and Biochemistry, University of California, San Diego
June 2002	M.S. in Chemistry, University of California, San Diego
December 2004	Ph.D. in Chemistry, University of California, San Diego

PRESENTATIONS

1. *"Cobalt Complexes of Nitrogen-Anchored Tripodal N-Heterocyclic Carbene Ligands: Coordination Chemistry and Reactivity Study"*
   228th American Chemical Society National Meeting, **Philadelphia**, PA, August **2004**.
   Poster presentation

2. "*Dioxygen Activation and Imido Transfer Chemistry Supported by Cobalt Tris-Carbene Complexes*"
   Gordon Research Conference in Organometallic Chemistry, **Newport**, RI, July **2004**.
   Poster presentation

3. "*Metal Complexes of Novel Tripodal N-Heterocyclic Carbene Ligands: Synthesis, Structure, Bonding, and Reactivity*"
   Los Alamos National Laboratory, Chemistry Division, **Los Alamos**, NM, July **2004**.
   Invited Talk

4. "*Tripodal N-Heterocyclic Carbene Ligands and Their Metal Complexes: Synthesis, Structure, and Bonding*"
   Gordon Research Conference in Organometallic Chemistry, **Newport**, RI, July **2003**.
   Poster presentation

5. "*Synthesis and Characterization of Tripodal Percarbene Ligands and Their Corresponding Metal Complexes*"
2nd Annual San Diego Organometallic Meeting, **La Jolla**, CA, December **2002**.
Oral presentation

6. "*Identification of Iron Cyclam Complexes Encapsulated inside Zeolite-Y*"
1st "PacChem" Super-Group Meeting, **UC San Diego**, CA, February **2002**.
Oral presentation

7. *"Quest for High Valent Iron Species"*
13th International Zeolite Conference, **Montpellier**, France, July **2001**.
Poster presentation

PUBLICATIONS

1. Terminal Cobalt(III) Imido Complexes Supported by Tris(Carbene) Ligands: Imido Insertion into the Cobalt—Carbene Bond
Hu, **X**.; Meyer, K*.
J. Am. Chem. Soc. ASAP article, DOI: 10.1021/ja044271b.

2. Dioxygen Activation by a Low-Valent Cobalt Complex with a Flexible Tripodal N-Heterocyclic Carbene Ligand
Hu, **X**.; Castro-Rodriguez, I.; Meyer, K*.
J. Am. Chem. Soc. **2004**, *126*, 13464-13473.

3. Synthesis and Characterization of Electron-Rich Nickel Tris-Carbene Complexes.
Hu, **X**.; Castro-Rodriguez, I.; Meyer, K*.
Chem. Comm. **2004**, 2164-2165.

4. Group 11 Metal Complexes of N-Heterocyclic Carbene Ligands: Nature of the Metal—Carbene Bond
Hu, **X**.; Castro-Rodriguez, I.; Olsen, K.; Meyer, K*.
Organometallics **2004**, *23*, 755-764.

5. Synthesis and Characterization of N-Heterocyclic Carbene Complexes of Uranium(III)
Nakai, H.; **Hu**, **X**.; Zakharov, L. N.; Rheingold, A.; Meyer, K*.
Inorg. Chem. **2004**, *43*, 855-857.

6. Cationic and Neutral Four-Coordinate Alkylidene Complexes of Vanadium(IV) Containing Short V=C Bonds
Basuli, F.; Kilgore, U.; **Hu**, **X**.; Meyer, K.; Pink, M.; Huffman, J. C.; Mindiola, D. J*
Angew. Chem. Int. Ed., **2004**, *43*, 3156-3159.

7. Copper Complexes of Nitrogen-Anchored Tripodal N-Heterocyclic Carbene Ligands
Hu, **X**.; Castro-Rodriguez, I.; Meyer, K*.
J. Am. Chem. Soc. **2003**, *125*, 12237-12245.

8. A Bis-Carbenealkenyl Copper(I) Complex From a Tripodal Carbene Ligand
Hu, **X**.; Castro-Rodriguez, I.; Meyer, K*.
Organometallics **2003**, *22*, 3016-3018.

9. Silver Complexes of a Novel Tripodal N-Heterocyclic Carbene Ligand: Evidence for Significant Metal—Carbene π-Interaction
Hu, **X**.; Tang, Y.-J.; Gantzel, P.; Meyer, K*.
Organometallics **2003**, *22*, 612-614.

10. Identification of Iron Cyclam Complexes Encapsulated Inside Zeolite Y
Hu, **X**; Meyer, K*.
Inorg. Chim. Acta. **2002**, *337*, 53-58. Special Edition in Honor of Karl Wieghardt's 60th Birthday

ABSTRACT OF THE DISSERTATION

Metal Complexes of Tripodal N-Heterocyclic Carbene Ligands: Synthesis, Structure, Bonding, and Reactivity

by

Xile Hu

Doctor of Philosophy in Chemistry

University of California, San Diego, 2004

Professor Karsten Meyer, Chair

N-Heterocyclic carbenes are important ligands for homogeneous catalysis, but their potential for small molecule activation has not been exploited. Synthesis of mono-dentate carbenes and chelating bis-carbenes as well as their coordination to transition metals is well documented, but little work has been reported on poly-carbene ligands and complexes. The main goal of this dissertation work was to develop tripodal carbene ligand systems for transition metal coordination and subsequent application in small molecule activation chemistry.

The carbon-anchored tripodal N-heterocyclic carbene ligands $TIME^R$ (R = Me, *t*-Bu) were synthesized. The methyl derivative forms a tri-nuclear silver complex

$[(TIME^{Me})_2Ag_3]^{3+}$, which is able to transfer the carbene ligand to other group 11 metal ions, yielding iso-structural complexes $[(TIME^{Me})_2M_3]^{3+}$ (M = Cu, Au). The *tert*-butyl derivative forms a di-nuclear bis(carbene)alkenyl Cu(I) complex $[(TIME^{t\text{-}Bu})_2Cu_2]^{2+}$. NMR spectroscopy and X-ray crystallography revealed "normal" as well as "abnormal" binding modes in the complex.

The nitrogen-anchored tripodal N-heterocyclic carbene ligand system TIMEN was developed to favor the 1:1 metal ligand binding mode (κ^3). While the methyl derivative produces a tri-nuclear Cu(I) complex $[(TIMEN^{Me})_2Cu_3]^{3+}$, other alkyl-substituted TIMEN ligands give rise to mono-nuclear Cu(I)/(II) complexes $[(TIMEN^{R})Cu]^{+}$ (R = *t*-Bu, Bz).

The tris(carbene) ligand $TIMEN^{t\text{-}Bu}$ yields electron-rich nickel complexes $[(TIMEN^{t\text{-}Bu})Ni]^{0/+1}$. Spectroscopic, electrochemical, and structural characterizations of these complexes are described.

The aryl-substituted TIMEN ligands ($TIMEN^{Ar}$, Ar = xylene, mesitylene) were synthesized and coordinated to cobalt(I). The cobalt(I) complex $[(TIMEN^{xyl})Co]^{+}$ reacts with organic chlorides, carbon monoxide, and dioxygen to yield cobalt (I)/(II)/(III) complexes $[(TIMEN^{xyl})Co(CO)]^{+}$, $[(TIMEN^{xyl})Co(Cl)]^{+}$, and $[(TIMEN^{xyl})Co(O_2)]^{+}$, respectively. Spectroscopic, structural, reactivity, and DFT studies on these complexes are described. The cobalt(I) complexes $[(TIMEN^{Ar})Co]^{+}$ (Ar = xyl, mes) reacted with arylazides to form terminal cobalt(III) imido complexes $[(TIMEN^{Ar})Co(NAr')]^{+}$ (Ar' = 4-methoxyphenyl, 4-methylphenyl). The cobalt—

imido fragment in these complexes is electrophilic and accordingly, the imido group readily inserts into one of the cobalt—carbene bonds in solution.

The nature of the metal—carbene bond in group 11 metal N-heterocyclic carbene complexes and related species was analyzed by DFT methods. Qualitative molecular orbital analysis and quantitative energy decomposition analysis revealed the existence of non-negligible and even significant π-bonding between electron-rich late metals and N-heterocyclic carbenes.

Chapter 1. Introduction to Carbenes and N-Heterocyclic Carbenes

1.1. Carbenes

Carbenes are compounds containing a divalent carbon atom with only six valence-shell electrons. Introduced by Doering to organic chemistry in the 1950s[1] and by Fischer to organometallic chemistry in 1964,[2] these fascinating species have sparked the interest of organic,[3,4] inorganic,[5] and theoretical chemists[6] like no other single class of molecules. This is probably due to their intriguing molecular and electronic structures, challenging syntheses, and versatile properties, varying from nucleophilic to electrophilic and even ambiphilic character.[7]

In a prototypical carbene molecule –C–, the carbon atom can be either linear or bent. A linear geometry gives rise to a sp-hybridized carbene center with two degenerate nonbonding orbitals (p_x and p_y). Bending the molecule removes the degeneracy and renders the carbene atom sp^2-hybridized. As a result, the former p_x orbital is stabilized by acquiring s character (it is therefore called σ) while the p_y orbital remains almost intact and is often called p_π (Figure 1-1).[4] Most carbenes are bent and their frontier orbitals can be systematically labeled as σ and p_π.

The ground-state spin multiplicity is a fundamental property of carbenes. Four electronic configurations can be envisioned (Figure 1-2).[4] A triplet carbene contains two non-bonding electrons in two different orbitals with parallel spins ($\sigma^1 p_\pi^1$, $^3B_1$ state). A singlet carbene, on the other hand, may have two non-bonding electrons paired in the same σ or p_π orbitals (σ^2 or p_π^2, $^1A_1$ state), or paired in two different orbitals ($\sigma^1 p_\pi^1$, $^1B_1$ state); the σ^2 state is generally more stable. The ground state spin multiplicity dictates the reactivity of carbenes. Singlet carbenes have a filled and an

empty orbital, and thus are generally ambiphilic; triplet carbenes have two half-occupied orbitals and behave like diradicals.

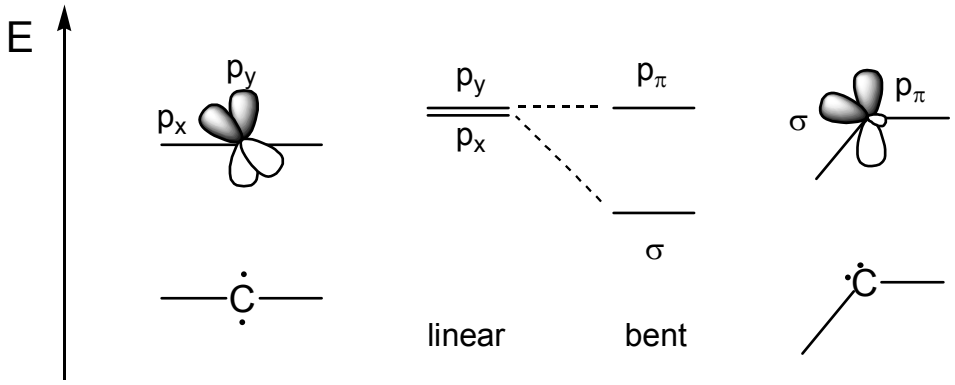

Figure 1-1. Frontier orbitals of prototypical linear and bent carbenes.

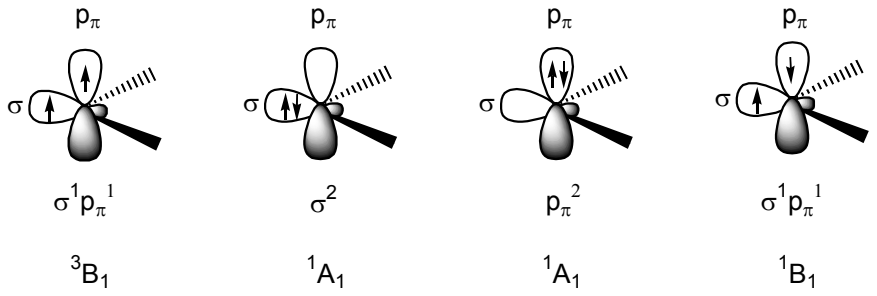

Figure 1-2. Four possible electronic configurations of a carbene.

A carbene's ground-state electronic configuration is related to the relative energies of its σ and p_π orbitals. A large σ-p_π separation favors the singlet state and Hoffmann suggested that a value of about 2 eV is required to enforce a singlet ground state.[8] The σ-p_π separation is largely influenced by the substituents on the carbenes. The σ orbitals of diamino carbenes are stabilized by the inductive effect of the electronegative neighboring nitrogen atoms and the p_π orbitals are greatly destabilized

by the strong π-donation of the lone pair electrons from the same nitrogens. Such carbenes have a very large σ-p$_\pi$ separation and are normally singlet. Dialkyl carbenes, on the contrary, are often triplet.

1.2. N-Heterocyclic Carbenes

During the last 15 years, carbene chemistry has advanced in a dramatic fashion with the preparation of persistent triplet diarylcarbenes[9] and the isolation of heteroatom-substituted singlet carbenes.[4,10,11] In 1991, Arduengo et al. reported ground-breaking work on the synthesis of "*A Stable Crystalline Carbene*".[12] The diadamantyl-substituted imidazol-2-ylidene (**1**) was prepared by deprotonation of the corresponding imidazolium salt with sodium or potassium hydride in the presence of catalytic amounts of *t*-BuOK or DMSO (Scheme 1-1). The free carbene was isolated and found to be remarkably stable. Soon after, it was realized that the bulky adamantyl groups in **1** are not required for the stabilization of the free carbene, and a whole family of imadazol-2-ylidenes bearing different substituents (**2**) were prepared following similar methods.[13] Together with their saturated counterparts (**3**), these carbenes are now commonly called N-heterocyclic carbenes (NHCs) (Figure 1-3).[14]

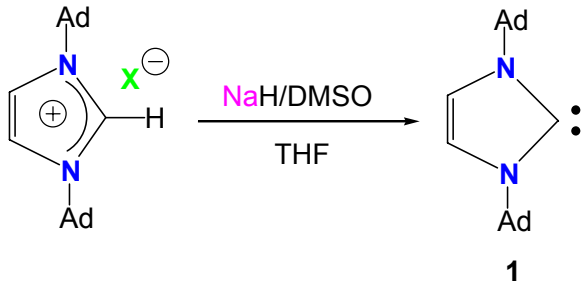

1

Scheme 1-1. Preparation of the First N-Heterocyclic Carbene.

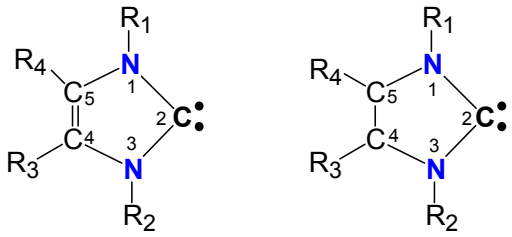

2 **3**

Figure 1-3. Unsaturated and saturated N-heterocyclcic carbenes.

1.3. Molecular and Electronic Structure of N-Heterocyclic Carbenes

The molecular structure of **1** exhibits features characteristic for an unsaturated NHC (Figure 1-4).[12] Particularly notable is the small N—$C_{carbene}$—N angle of 102.2°. This angle is significantly reduced from the 109.7° found in the corresponding imidazolium salt. Other significant structural differences between an NHC and its imidazolium precursor include the C_2—$N_{1/3}$, N_1—C_5, and N_3—C_4 distances. They are increased from those of the imidazolium salt, while the C_4—C_5 bond lengths are reduced slightly. These structural changes indicate an increase of *p* character in the

C_2—N bonds and a decrease of π-delocalization in the imidazole ring upon deprotonation of the imidazolium ion.[15,16]

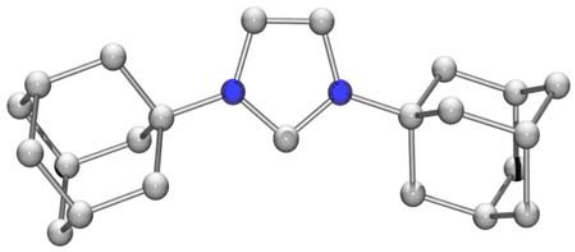

Figure 1-4. Solid-state molecular structure of carbene **1**[12].

The electronic structures of NHCs have been subjected to a few theoretical studies.[15-19] While the calculated structural data for the singlet ground state agree well with the experimental determined values, the triplet geometries are quite different. For model compound 1,2-dihydroimidazol-2-ylidene, the singlet-triplet gap is reportedly 79.4 kcal/mol.[15] This suggests that the reactivity of NHCs should be dominated by their singlet ground-state, which has been confirmed by experimental findings. The carbene center is almost charge neutral. The proton affinity of the carbene center is remarkably high, with a calculated value of 257.3 kcal/mol at MP2 level.[15] The stability of an NHC is mainly due to electronic effects, although steric hindrance may also play an important role. The interaction between the carbene centers with the π-donating, σ-accepting amino substitutes provides most of the stabilizing energy,[15,18,19]and the aromaticity of the imidazole ring brings an additional stabilization of about 25 kcal/mol.[19]

1.4. Reactivity and Ligand Properties of N-Heterocyclic Carbenes

Both saturated and unsaturated NHCs display nucleophilic reactivity.[4,11] Unlike transient carbenes, a stable NHC does not undergo cyclopropanation with normal olefins and C—H insertion into hydrocarbons. A saturated NHC is prone to dimerization, but an unsaturated NHC hardly dimerizes due to a large singlet-triplet gap.

Because of its high Lewis basicity, the NHC behaves like a very good donor ligand. Reports on the use of NHCs as ligands appeared as early as the 1960s when Őfele et al. and Wanzlick et al. prepared the first metal NHC complexes by reacting imidazolium salts with basic metal precursors.[20] Unfortunately, the limitation of this method hampered the potential of NHC ligands. Arduengo's isolation of stable carbenes immediately led to a renaissance of carbene chemistry, including its coordination chemistry. It has been shown that NHCs can coordinate to virtually every metal in the periodic table, in both low and high oxidation states.[11] Surprisingly, it is not trivial to classify NHCs as either "soft" or "hard" ligands.[21] At first glance, given the neutral carbon donor, an NHC should be a soft ligand, and it does exhibit many features similar to those of basic tertiary phosphine ligands. On the other hand, NHCs are also known to coordinate to "hard" metal fragments such as high-valent early transition metal, lanthanide, and actinide ions. This mixed character indeed makes NHCs potentially useful for supporting various redox events at a coordinated metal center.

1.5. N-Heterocyclic Carbenes in Homogeneous Catalysis

Current interests in metal complexes of NHC ligands arise from reports of their remarkable activity in homogeneous catalysis. In 1995, Hermann et al. found that palladium(II) bis-carbene complexes **4** and **5** are very efficient catalysts for Heck-coupling reactions (Figure 1-5).[22] The carbene ligands in these complexes appear to stabilize both Pd(II) and Pd(0) species resulting in very high catalytic turnover numbers. This study provided, as stated in the title of Hermann's paper, "a new structural principle" for catalyst design. Subsequently, numerous metal complexes bearing NHC ligands have been synthesized and show improved activities in various catalytic reactions including C—N coupling,[23] hydrosilation,[24] ethylene/carbon monoxide copolymerization,[25] C—H activation,[26] hydrogenation,[27] hydroformylation,[28] furan synthesis,[29] dehalogenation,[30] atom-transfer radical polymerization,[31] and particularly C—C bond formation (Suzuki[32], Heck,[22,33] Sonogashira,[34] Stille,[35] and Grignard[36] cross coupling reactions) and olefin metathesis[37] reactions.

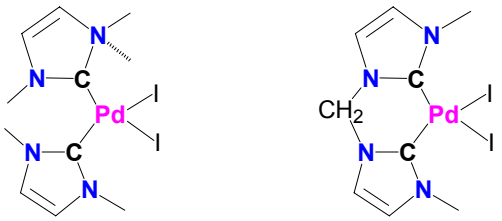

4 **5**

Figure 1-5. Palladium bis-carbene complexes that catalyze Heck-reactions

The superior performance of the NHC catalysts in these reactions results from the pronounced donor properties of NHC ligands. Experiments have confirmed that typical NHCs are more electron-releasing than even the most basic phosphines.[38] NHC complexes have high thermal and hydrolytic durability and reactions can often be carried out in the air. Unlike phosphines, NHCs hardly dissociate from the metal ions thus there is no need for excess ligands. NHCs stabilize both low and high valent species formed in catalysis resulting in higher turnover numbers and longer catalyst lifetimes. In light of the vast numbers of applications and their distinctive advantages, NHCs have now become a guiding "concept" in organometallic catalysis.[39]

1.6. Bi- and Polydentate N-Heterocyclic Carbene Ligands

Bi- and polydentate NHC ligands received increased attention in recent years. Crabtree et al. has worked on pincer-type CNC hybrid carbene ligands, and found palladium complex **6** robust enough to catalyze Heck reactions at 180°C in the air (Figure 1-6).[40] A number of other chelating NHCs, mostly containing other hetero-atom donors, have also been synthesized and show improved stability.[25,41]

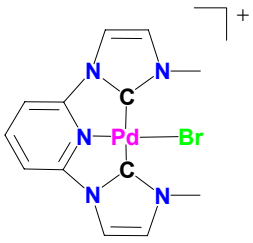

6

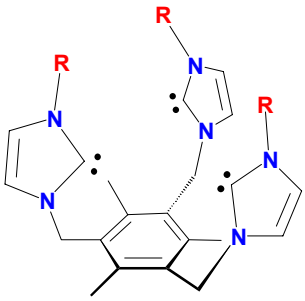

7

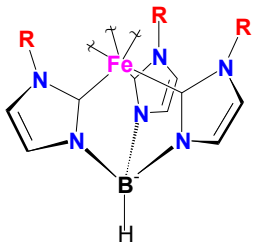

8

Figure 1-6. Polydentate NHC ligands/complexes.

Ligands containing three or more carbene centers are rare. Compound **7** had been the only isolated tris(carbene) ligand prior to our work (Figure 1-6).[42] It was synthesized by Dias and Jin shortly after Arduengo et al. isolated the first free carbene, but no metal complexation could be achieved. Nakai and Meyer thoroughly investigated the coordination chemistry of **7** and its derivatives, but found that the cavity of this ligand system can only host exceptionally large metal ions, such as the thallium(I) cation.[43] Attempts to synthesize transition metal complexes of **7** and alike have been unfruitful to date.

The Fehlhammer group has made the carbene analogues of hydrotris(pyrazolyl)-borate (Tp) ligands.[44] The free carbenes could not be isolated, but metal complexes were prepared by salt metathesis of their lithium complexes.[45] Unfortunately, these anionic ligands tend to form transition metal complexes with two ligand molecules chelating one metal ion (**8**, Figure 1-6).[44,46] The resulting hexakis(carbene) complexes contain coordinatively saturated metal ions with no further reactivity observed. This has greatly limited the application of this class of ligands in metal-assisted small molecule activation chemistry.

1.7. Objectives

The goal of this dissertation work was to develop a tripodal NHC ligand system that is capable of transition metal complexation and apply it in small molecule

activation chemistry (Figure 1-7). NHCs have been widely used as ancillary ligands in homogeneous catalysis, however, their potential in assisting small molecule activation and atom/group transfer reactions has not been exploited fully. On the other hand, the vast success of NHC in catalysis encouraged us to explore in this area.

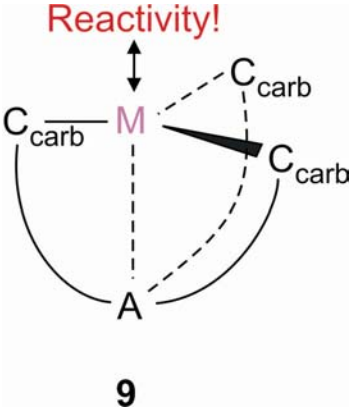

Figure 1-7. A tripodal NHC ligand system for small molecule activation.

The idea of utilizing tripodal NHCs was inspired by the ability of tripodal ligand systems to promote and protect unusual reactivity at distinct metal centers. A well-known example are the Tp ligands (**10**, Figure 1-8).[47] Metal complexes supported by these ligands have been extensively used to promote catalytic transformations, such as C—H activation,[48] C—C,[49] C—O,[50] and C—N bond formation,[51] and serve as structural mimics of metal-containing enzymes.[52] Tripodal ligand systems based on tris(amido)amine frameworks are known to provide powerful platforms for small molecule activation.[53] For instance, using bulky aryl-substituted tris(amido)amine ligands, Schrock et al. isolated and characterized many intermediates

in a hypothetical catalytic dinitrogen reduction reaction (**11**, Figure 1-8).[54] Utilizing an ureayl-functionalized tris(amido)amine ligand, Borovik et al. prepared an unprecedented terminal Fe(III) oxo complex (**12**, Figure 1-8).[55] Tripodal ligands with soft sulfur and phosphorus donors are also popular in coordination chemistry and catalysis.[56] Finally, the recent work by the Peters group nicely illustrates that tripodal ligands can be highly rewarding: with newly developed anionic tris(phosphine) ligands, this group has synthesized the first cobalt(III)[57] and iron(III)[58] terminal imido complexes and the first isolated iron(V) nitride species (**13**, Figure 1-8).[59] The stability of these otherwise transient species originates from the unique geometric and electronic properties enforced by the 3-fold symmetric phosphine tripods.[57,59]

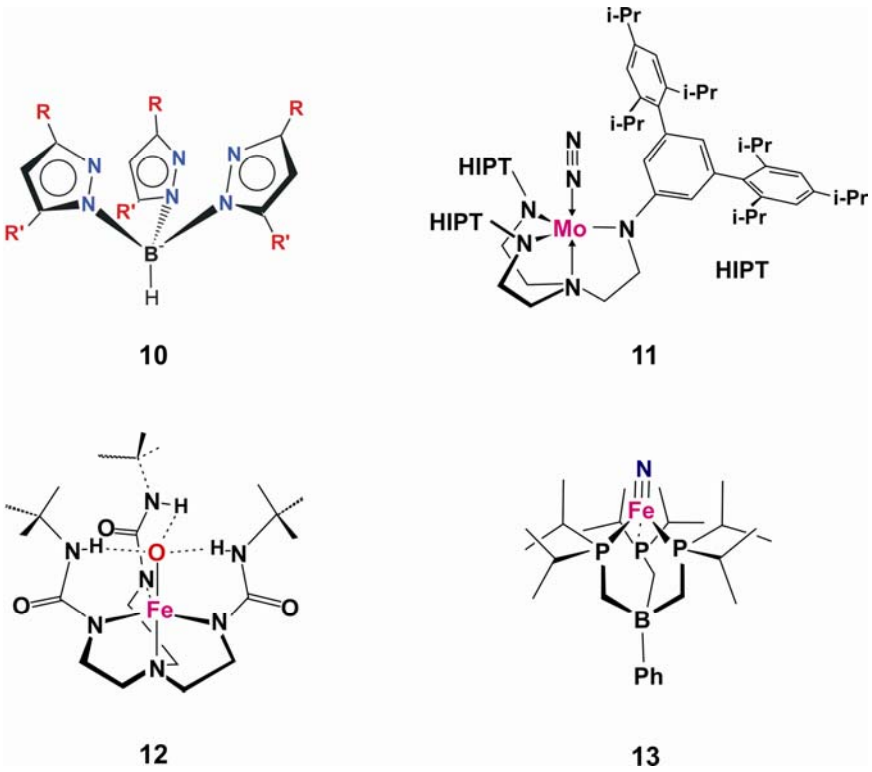

Figure 1-8. Representative tripodal ligands/complexes.

1.8. Acknowledgement

Figure 1-1 and 1-2 were reproduced with permission from *Chemical Reviews*, **2000**, *100*, P41. Copyright 2000, American Chemical Society.

1.9. References

(1) Doering, W. v. E.; Hoffmann, A. K. *J. Am. Chem. Soc.* **1954**, *76*, 6162.

(2) Fischer, E. O.; Maasboel, A. *Angew. Chem.* **1964**, *76*, 645.

(3) Kirmse, W. *Carbene Chemistry*; Academic Press Inc.: New York, 1964.

(4) Bourissou, D.; Guerret, O.; Gabbai, F. P.; Bertrand, G. *Chem. Rev.* **2000**, *100*, 39-91.

(5) Cornils, B.; Herrmann, W. A. *Applied homogeneous catalysis with organometallic compounds : a comprehensive handbook in three volumes*; 2nd ed.; Wiley-VCH: Weinheim, 2002.

(6) Frenking, G.; Frohlich, N. *Chem. Rev.* **2000**, *100*, 717-774.

(7) Bertrand, G., Ed. *Carbene Chemistry, From Fleeting Intermediates to Powerful Reagents*; FontisMedia S.A. and Marcel Dekker, Inc., 2002.

(8) Hoffmann, R. *J. Am. Chem. Soc.* **1968**, *90*, 1475.

(9) Tomioka, H. *Acc. Chem. Res.* **1997**, *30*, 315-321; Tomioka, H. In *Carbene Chemistry, From Fleeting Intermediates to Powerful Reagents*; Bertrand, G., Ed.; FontisMedia S.A. and Marcel Dekker, Inc., 2002, pp 103-152.

(10) Arduengo, A. J. *Acc. Chem. Res.* **1999**, *32*, 913-921.

(11) Herrmann, W. A.; Kocher, C. *Angew. Chem. Int. Ed. Engl* **1997**, *36*, 2163-2187.

(12) Arduengo, A. J.; Harlow, R. L.; Kline, M. *J. Am. Chem. Soc.* **1991**, *113*, 361-363.

(13) Arduengo, A. J.; Dias, H. V. R.; Harlow, R. L.; Kline, M. *J. Am. Chem. Soc.* **1992**, *114*, 5530-5534; Arduengo, A. J.; Goerlich, J. R.; Krafczyk, R.; Marshall, W. J. *Angew. Chem.-Int. Edit.* **1998**, *37*, 1963-1965; Herrmann, W. A.; Elison, M.; Fischer, J.; Kocher, C.; Artus, G. R. J. *Chem.-Eur. J.* **1996**, *2*, 772-780.

(14) Drago, R. S. *Physical Methods for Chemists*; 2nd ed.; Surfside Scientific Publishers: Gainesville, 1992.

(15) Dixon, D. A.; Arduengo, A. J. *J. Phys. Chem.* **1991**, *95*, 4180-4182.

(16) Heinemann, C.; Thiel, W. *Chem. Phys. Lett.* **1994**, *217*, 11-16.

(17) Arduengo, A. J.; Dias, H. V. R.; Dixon, D. A.; Harlow, R. L.; Klooster, W. T.; Koetzle, T. F. *J. Am. Chem. Soc.* **1994**, *116*, 6812-6822.

(18) Boehme, C.; Frenking, G. *J. Am. Chem. Soc.* **1996**, *118*, 2039-2046.

(19) Heinemann, C.; Muller, T.; Apeloig, Y.; Schwarz, H. *J. Am. Chem. Soc.* **1996**, *118*, 2023-2038.

(20) Wanzlick, H. W.; Schonherr, H. J. *Angew. Chem.* **1968**, *80*, 154; Ofele, K. *J. Organomet. Chem.* **1968**, *12*, P42-P43.

(21) Pearson, R. J. *J. Am. Chem. Soc.* **1963**, *85*, 3533-3539.

(22) Herrmann, W. A.; Elison, M.; Fischer, J.; Kocher, C.; Artus, G. R. J. *Angew. Chem. Int. Ed. Engl* **1995**, *34*, 2371-2374.

(23) Huang, J.; Grasa, G.; Nolan, S. P. *Org. Lett.* **1999**, *1*, 1307-1309; Stauffer, S. R.; Lee, S. W.; Stambuli, J. P.; Hauck, S. I.; Hartwig, J. F. *Org. Lett.* **2000**, *2*, 1423-1426.

(24) Herrmann, W. A.; Goossen, L. J.; Kocher, C.; Artus, G. R. J. *Angew. Chem. Int. Ed. Engl* **1996**, *35*, 2805-2807.

(25) Gardiner, M. G.; Herrmann, W. A.; Reisinger, C. P.; Schwarz, J.; Spiegler, M. *J. Organomet. Chem.* **1999**, *572*, 239-247.

(26) Muehlhofer, M.; Strassner, T.; Herrmann, W. A. *Angew. Chem.-Int. Edit.* **2002**, *41*, 1745-1747.

(27) Lee, H. M.; Jiang, T.; Stevens, E. D.; Nolan, S. P. *Organometallics* **2001**, *20*, 1255-1258.

(28) Chen, A. C.; Ren, L.; Decken, A.; Crudden, C. M. *Organometallics* **2000**, *19*, 3459-3461.

(29) Kucukbay, H.; Cetinkaya, B.; Guesmi, S.; Dixneuf, P. H. *Organometallics* **1996**, *15*, 2434-2439.

(30) Desmarets, C.; Kuhl, S.; Schneider, R.; Fort, Y. *Organometallics* **2002**, *21*, 1554-1559.

(31) Louie, J.; Grubbs, R. H. *Chem. Commun.* **2000**, 1479-1480.

(32) Gstottmayr, C. W. K.; Bohm, V. P. W.; Herdtweck, E.; Grosche, M.; Herrmann, W. A. *Angew. Chem. Int. Ed. Engl* **2002**, *41*, 1363-1365.

(33) Yang, C. L.; Lee, H. M.; Nolan, S. P. *Org. Lett.* **2001**, *3*, 1511-1514; McGuinness, D. S.; Cavell, K. J. *Organometallics* **2000**, *19*, 741-748.

(34) Yang, C. L.; Nolan, S. P. *Organometallics* **2002**, *21*, 1020-1022.

(35) Grasa, G. A.; Nolan, S. P. *Org. Lett.* **2001**, *3*, 119-122.

(36) Bohm, V. P. W.; Weskamp, T.; Gstottmayr, C. W. K.; Herrmann, W. A. *Angew. Chem.-Int. Edit.* **2000**, *39*, 1602-1604.

(37) Weskamp, T.; Kohl, F. J.; Hieringer, W.; Gleich, D.; Herrmann, W. A. *Angew. Chem.-Int. Edit.* **1999**, *38*, 2416-2419; Scholl, M.; Trnka, T. M.; Morgan, J. P.;

Grubbs, R. H. *Tetrahedron Lett.* **1999**, *40*, 2247-2250; Scholl, M.; Ding, S.; Lee, C. W.; Grubbs, R. H. *Org. Lett.* **1999**, *1*, 953-956; Huang, J. K.; Schanz, H. J.; Stevens, E. D.; Nolan, S. P. *Organometallics* **1999**, *18*, 5375-5380; Huang, J. K.; Stevens, E. D.; Nolan, S. P.; Petersen, J. L. *J. Am. Chem. Soc.* **1999**, *121*, 2674-2678; Weskamp, T.; Kohl, F. J.; Herrmann, W. A. *J. Organomet. Chem.* **1999**, *582*, 362-365.

(38) Huang, J. K.; Schanz, H. J.; Stevens, E. D.; Nolan, S. P. *Organometallics* **1999**, *18*, 2370-2375.

(39) Herrmann, W. A. *Angew. Chem.-Int. Edit.* **2002**, *41*, 1291-1309.

(40) Peris, E.; Loch, J. A.; Mata, J.; Crabtree, R. H. *Chem. Commun.* **2001**, 201-202.

(41) Herrmann, W. A.; Reisinger, C. P.; Spiegler, M. *J. Organomet. Chem.* **1998**, *557*, 93-96; Tulloch, A. A. D.; Danopoulos, A. A.; Winston, S.; Kleinhenz, S.; Eastham, G. *J. Chem. Soc.-Dalton Trans.* **2000**, 4499-4506; Arnold, P. L.; Scarisbrick, A. C.; Blake, A. J.; Wilson, C. *Chem. Commun.* **2001**, 2340-2341; Danopoulos, A. A.; Winston, S.; Motherwell, W. B. *Chem. Commun.* **2002**, 1376-1377; Loch, J. A.; Albrecht, M.; Peris, E.; Mata, J.; Faller, J. W.; Crabtree, R. H. *Organometallics* **2002**, *21*, 700-706.

(42) Dias, H. V. R.; Jin, W. C. *Tetrahedron Lett.* **1994**, *35*, 1365-1366.

(43) Nakai, H.; Tang, Y. J.; Gantzel, P.; Meyer, K. *Chem. Commun.* **2003**, 24-25.

(44) Kernbach, U.; Ramm, M.; Luger, P.; Fehlhammer, W. P. *Angew. Chem. Int. Ed. Engl* **1996**, *35*, 310-312.

(45) Frankell, R.; Birg, C.; Kernbach, U.; Habereder, T.; Noth, H.; Fehlhammer, W. P. *Angew. Chem.-Int. Edit.* **2001**, *40*, 1907-1910.

(46) Frankel, R.; Kernbach, U.; Bakola-Christianopoulou, M.; Plaia, U.; Suter, M.; Ponikwar, W.; Noth, H.; Moinet, C.; Fehlhammer, W. P. *J. Organomet. Chem.* **2001**, *617*, 530-545.

(47) Trofimenko, S. *Scorpionates, The Coordination Chemistry of Polypyrazolylborate Ligands*; Imperial College Press: London, 1999; Trofimenko, S. *Prog. Inorg. Chem.* **1986**, *34*, 115-210; Trofimenko, S. *Chem. Rev.* **1993**, *93*, 943-980.

(48) Slugovc, C.; Padilla-Martinez, I.; Sirol, S.; Carmona, E. *Coord. Chem. Rev.* **2001**, *213*, 129-157.

(49) Diaz-Requejo, M. M.; Belderrain, T. R.; Trofimenko, S.; Perez, P. J. *J. Am. Chem. Soc.* **2001**, *123*, 3167-3168.

(50) Diaz-Requejo, M. M.; Belderrain, T. R.; Perez, P. J. *Chem. Commun.* **2000**, 1853-1854.

(51) Morilla, M. E.; Diaz-Requejo, M. M.; Belderrain, T. R.; Nicasio, M. C.; Trofimenko, S.; Perez, P. J. *Chem. Commun.* **2002**, 2998-2999.

(52) Parkin, G. *Chem. Commun.* **2000**, 1971-1985.

(53) Cummins, C. C.; Lee, J.; Schrock, R. R.; Davis, W. D. *Angew. Chem. Int. Ed. Engl* **1992**, *31*, 1501-1503; Gudat, D.; Verkade, J. G. *Organometallics* **1989**, *8*, 2772-2779; Schrock, R. R. *Acc. Chem. Res.* **1997**, *30*, 9-16.

(54) Yandulov, D. V.; Schrock, R. R. *Science* **2003**, *301*, 76-78; Yandulov, D. V.; Schrock, R. R.; Rheingold, A. L.; Ceccarelli, C.; Davis, W. M. *Inorg. Chem.* **2003**, *42*, 796-813.

(55) MacBeth, C. E.; Golombek, A. P.; Young, V. G.; Yang, C.; Kuczera, K.; Hendrich, M. P.; Borovik, A. S. *Science* **2000**, *289*, 938-941.

(56) Stavropoulos, P.; Muetterties, M. C.; Carrie, M.; Holm, R. H. *J. Am. Chem. Soc.* **1991**, *113*, 8485-8492; Mayer, H. A.; Kaska, W. C. *Chem. Rev.* **1994**, *94*, 1239-1272; Mandimutsira, B. S.; Yamarik, J. L.; Brunold, T. C.; Gu, W. W.; Cramer, S. P.; Riordan, C. G. *J. Am. Chem. Soc.* **2001**, *123*, 9194-9195.

(57) Jenkins, D. M.; Betley, T. A.; Peters, J. C. *J. Am. Chem. Soc.* **2002**, *124*, 11238-11239.

(58) Brown, S. D.; Betley, T. A.; Peters, J. C. *J. Am. Chem. Soc.* **2003**, *125*, 322-323.

(59) Betley, T. A.; Peters, J. C. *J. Am. Chem. Soc.* **2004**, *126*, 6252-6254.

Chapter 2. A Carbon-Anchored Tripodal N-Heterocyclic Carbene Ligand System and Its Coordination to Group 11 Metal Ions

2.1. Introduction

Neo-pentane based tripodal N-heterocyclic carbenes of type **1** (Figure 2-1) drew our attention for the following reasons: the three pendent arms containing NHC chelators are anchored by a single carbon atom and therefore should provide a binding cavity small enough to host a transition metal ion; the imidazolium precursors for the free carbenes are accessible following the methods reported by Dias and Jin for the preparation of mesitylene-anchored tris(carbene) ligand **8** (in Figure 1-6),[1] and the steric properties of these ligands may be controlled through the substituents on the N3 positions of the imidazoles. The synthesis of substituted imidazoles is well documented, and in addition, there is rich chemistry associated with the phosphine analogues of these ligands.[2] With these considerations, we set out to investigate a carbon-anchored tris(carbene) ligand system, namely 1,1,1-tris(3-alkylimidazol-2-ylidene)methyl]ethane (**TIME**), and its metal complexation.

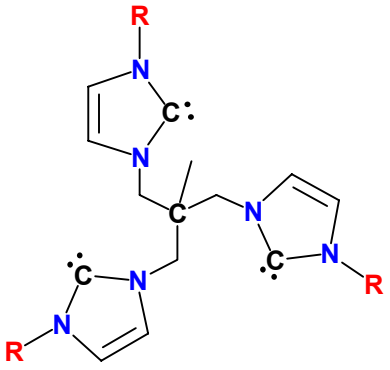

1

Figure 2-1. Carbon-anchored tripodal carbene ligand system **TIME^{R}**

2.2. Results and Discussion

2.2.1. Synthetic protocol for the imidazolium precursors $[H_3TIME^R]X_3$ (R = alkyl, X = Br, PF_6)

Few N-substituted imidazoles such as the N-methyl and N-benzyl imidazoles are commercially available. Other N-substituted imidazoles were synthesized by one-pot condensation reactions of alkyl or aryl amine, formaldehyde, glycol, and ammonium carbonate.[3] The 1,1,1-tris(bromomethyl)ethane was synthesized by bromination of 1,1,1-tris(hydroxymethyl)ethane (2 steps). Quaternization of N-alkylimidazole with 1,1,1-tris(bromomethyl)ethane yields imidazolium salt [1,1,1-tris(3-alkylimidazolium-1-yl)methyl]ethane tribromide $[H_3TIME^R](Br_3)$ (**2a**). Treatment of **2a** with ammonium hexafluorophosphate in methanol affords the precipitation of pure $[H_3TIME^R](PF_6)_3$ (**2b**).

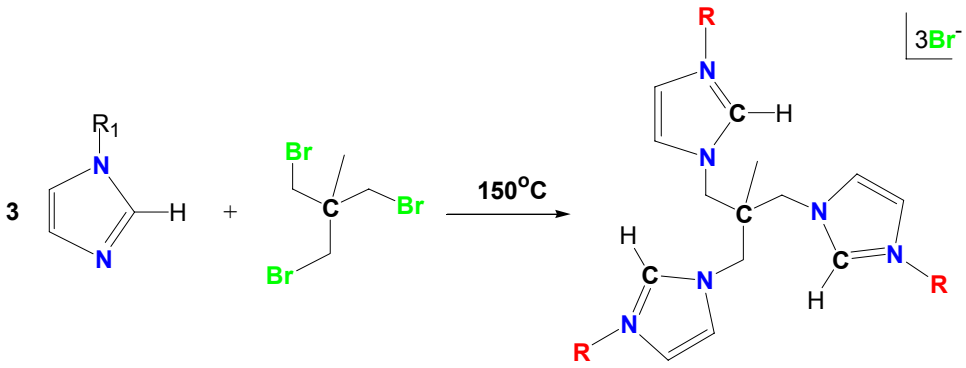

Scheme 2-1. Synthesis of the Tris(Imidazolium) Salts H_3TIME^R (**2a**)

2.2.2. The TIME^{Me} ligand and its coordination to silver(I)

TIME^{Me} is the simplest of the derivatives of TIME ligands. The imidazolium salts [H_3TIME^{Me}]X_3 (**2a**, X = Br; **2b**, X = PF_6) were synthesized in ~ 88 % yield following the method described in Scheme 2-1. Chemical shifts of the resonances in the ^{1}H and ^{13} C NMR spectra of **2a** and **2b** are similar and consistent with those of other reported imidazolium salts.[4] The most prominent features of the ^{1}H and ^{13}C spectra of **2a - b** are the resonances for the imidazolium protons at around 9 ppm and the imidazolium carbons at around 138 ppm. The solid-state molecular structure of **2a** was established by X-ray crystallography (Figure 2-2).

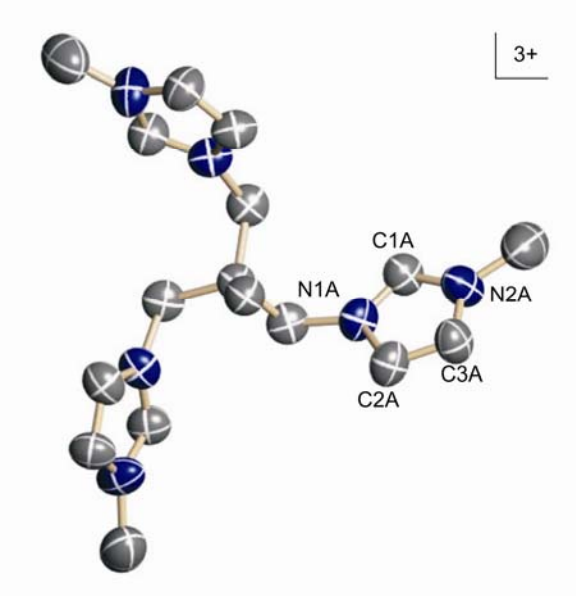

Figure 2-2. Solid-state molecular structure of [H_3TIME^{Me}]Br_3 (**2a**). Hydrogen atoms and counter anions are omitted for clarity; thermal ellipsoids are shown at 50 % probability. Selected bond distances (Å) and angles (deg.): C(1A)-N(1A) 1.313(18), C(1A)-N(2A) 1.339(18), C(2A)-C(3A) 1.34(2), N(1A)-C(1A)-N(2A) 108.5(13).

Treatment of **2a** and **2b** *in situ* with strong bases such as *n*-butyllithium, potassium *tert*-butoxide or benzylpotassium yields free carbene **3**, [1,1,1-tris-(3-methylimidazol-2-ylidene)methyl]ethane ([$TIME^{Me}$]). Attempts to isolate **3**, however, led to reddish, polymeric species that exhibited complicated NMR spectra. Instead, formation of **3** was confirmed by trapping the free carbene with copper triflate and isolating the resulting copper complex (vide infra). Generally, however, reactions between the *in situ* generated free carbene and metal salts often led to the formation of mixtures of complex nature. A more efficient route to metal complexes of $TIME^{Me}$ was thus needed.

Reportedly, reacting imidazolium salts with basic metal fragments has been useful for the preparation of metal NHC complexes when free carbenes are not available. In fact, Ofele et al. and Wanzlick et al. made the first metal NHC complexes via this route.[5] Recently, Wang and Lin reported that reaction of imidazolium salt with silver oxide yielded silver NHC complexes that were capable of transferring carbene ligands to other transition metal ions.[6] This method appeared to be well suited for the $TIME^{Me}$ system and we decided to prepare a silver complex of $TIME^{Me}$.

Reactions of both imidazolium salts, **2a** and **2b,** with Ag_2O in DMSO at 75 ^oC yielded silver carbene complexes [1,1,1-tris(3-methylimidazol-2-ylidene)methyl]-ethane silver bromide, $[(TIME^{Me})_2Ag_3]_2(Ag_8Br_{14})$ (**4a**) and [1,1,1-tris(3-methylimidazol-2-ylidene)methyl]ethane silver hexafluorophosphate, $[(TIME^{Me})_2Ag_3](PF_6)_3$ (**4b**) (Scheme 2-2). Recrystallization from DMSO solution

resulted in colorless, highly light-sensitive crystals of **4a** · 5 DMSO, while diffusion of ether into an acetonitrile solution of **4b** afforded hexagonal, light-stable crystals of **4b**. The formation of the metal carbene complexes was confirmed by ^{1}H and ^{13}C NMR spectroscopy. In the ^{1}H spectra, the signal associated with the imidazolium protons disappeared, and in the ^{13}C spectra, the carbenoid carbons gave rise to signals at around 180 ppm.

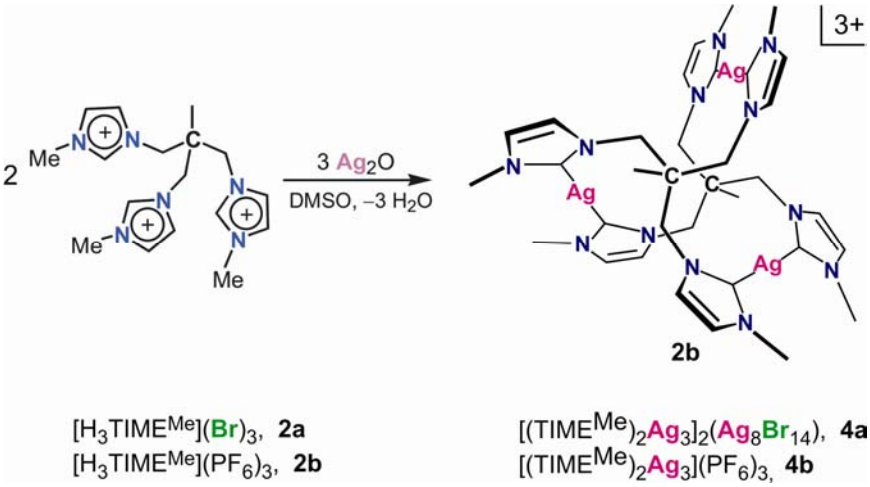

Scheme 2-2. Synthesis of Silver Complexes of the $TIME^{Me}$ Ligand

Single-crystal X-ray diffraction studies were carried out for complexes **4a** and **4b**. In the solid state structure of **4a**, two structurally equivalent $[(TIME^{Me})_2Ag_3]^{3+}$ fragments, linked by an unprecedented $[Ag_8Br_{12}]^{6-}$ cluster through two bridging bromide atoms, were found (Figure 2-3). For the silver cluster, the Ag—Br distances range between 2.5802(15)—2.7712(16) Å, and the Ag—Ag distances range between 2.9300—3.1369(14) Å.

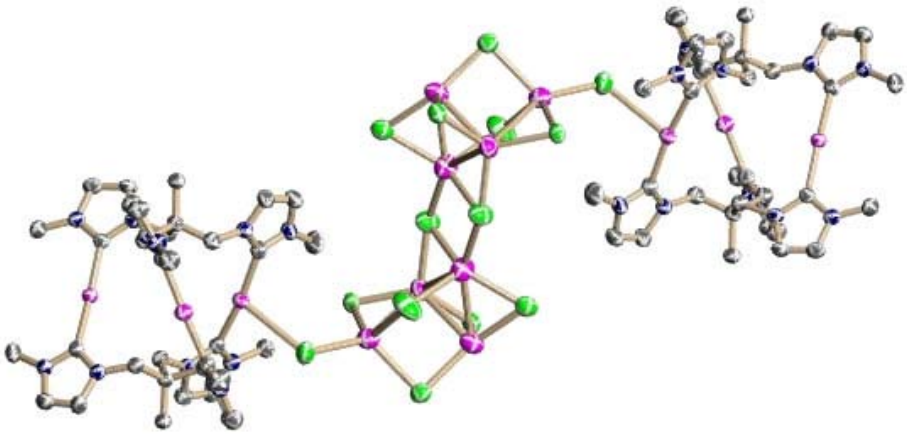

Figure 2-3. Solid-state molecular structure of $[(TIME^{Me})_2Ag_3]_2(Ag_8Br_{12}) \cdot 5DMSO$ (**4a** · 5DMSO). Hydrogen atoms, solvent molecules, and counter ions are omitted for clarity; thermal ellipsoids at 50 % probability.

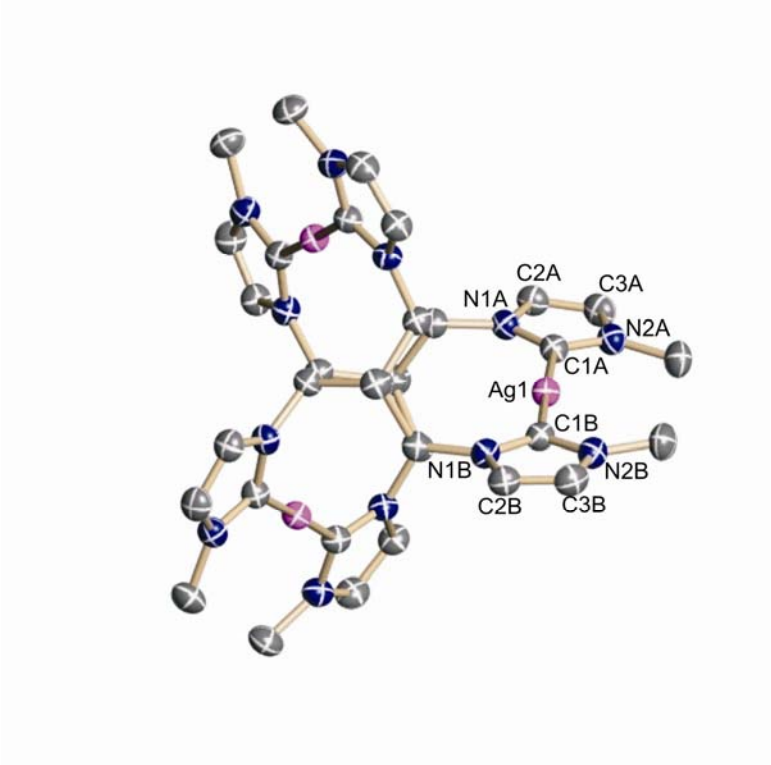

Figure 2-4. Solid-state molecular structure of $[Ag_3(TIME^{Me})_2](PF_6)_3$ (**4b**). Hydrogen atoms and counter ions are omitted for clarity; thermal ellipsoids are shown at 50 % probability. Selected bond distances (Å) and angles (°): Ag(1)-C(1A) 2.082(2), C(1A)-N(1A) 1.359(3), C(1A)-N(2A) 1.347(3), C(2A)-C(3A) 1.341(4), C(1A)-Ag(1)-C(1B) 178.56(13), N(1A)-C(1A)-N(2A) 104.3(2).

The structure of **4b** exhibits D_3 symmetry with the three-fold axis passing through the anchoring C-atoms of the two ligands. In the solid-state structure, three silver atoms bridge two $TIME^{Me}$ ligands through each of the three pendant arms (Figure 2-4). Each silver atom is two-coordinate and the silver—carbene bond distance of 2.082(2) Å is comparable to those found in known Ag–NHC complexes.[7] The carbene—silver units are nearly linear, with a C—Ag—C' angle of 178.56(13) °.

2.2.3. Synthesis and characterization of copper(I) and gold(I) complexes of $TIME^{Me}$

Reaction of **4b** with copper(I) bromide and (dimethylsulfide)gold(I) chloride under a dry N_2 atmosphere yielded the iso-structural and isomorphous corresponding copper(I) and gold(I) complexes $[(TIME^{Me})_2Cu_3](PF_6)_3$ (**5**) and $[(TIME^{Me})_2Au_3](PF_6)_3$ (**6)** (Scheme 2-3). Following these reactions by NMR spectroscopy indicated that the carbene ligand transfer reaction proceeded quantitatively. However, when the reactions were conducted in air, only the imidazolium salts were formed, suggesting that the reaction proceeds via a free carbene intermediate. Similar observations of a free carbene intermediate were previously reported for the formation of a tungsten diaminocarbene complex via a transmetallation reaction.[6]

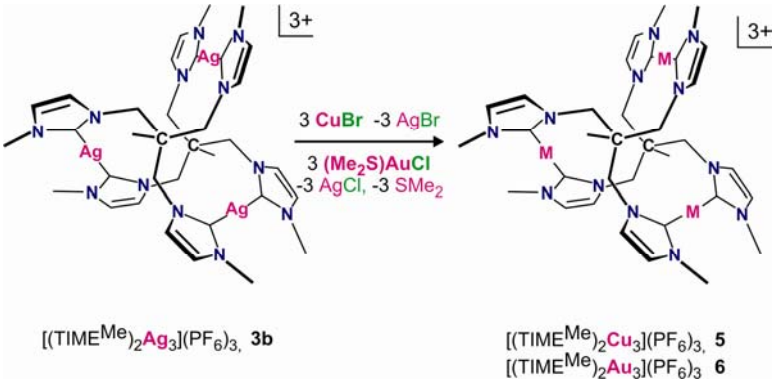

Scheme 2-3. Synthesis of Copper(I) and Gold(I) Complexes of $TIME^{Me}$ via Transmetallation.

Alternatively, *in situ* trapping of free carbene **3** with copper(I) triflate in THF afforded the corresponding $[(TIME^{Me})_2Cu_3]^{3+}$ complex as the triflate salt, which could be further converted into **5** by means of anion exchange

Slow ether diffusion into acetonitrile solutions of complexes **5** and **6** afforded colorless crystals that were characterized by NMR, IR, UV/vis spectroscopy, and X-ray diffraction analysis. The data were compared with those of **2a - b** and **4b**.

In general, the ^{1}H spectra of **4b - 6** are very similar (Table 2-1). The resonances for the 4H/5H protons of the imidazole ring backbone give rise to signal at 7.6/7.5 ppm for **4b**, 7.5/7.4 ppm for **5**, and 7.6/7.5 ppm for **6**. Compared to the analogous nuclei of the imidazolium salts (7.9/7.8 ppm for **2a**, 7.8/7.7 ppm for **2b**), all ring-backbone resonances are shifted slightly upfield. In the ^{13}C spectra, the chemical shifts for the carbenoid carbons were found at 182.5 (**4b**), 180.0 (**5**), and 183.8 (**6**)

ppm, respectively. These results are similar to those of other reported group 11 metal NHC complexes.[7-9]

Table 2-1. NMR Data of the M-TIME^{Me} Carbene Complexes and the Corresponding Imidazolium Salt (in ppm), Recorded in DMSO at 25°C.

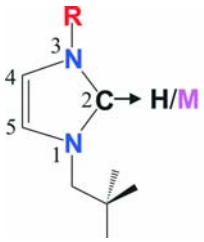

	2b	**4b**	**5**	**6**
H(2)	9.12	-	-	-
H(4)/H(5)	7.8/7.7	7.6/7.5	7.5/7.4	7.6/7.5
C(2)	137.8	182.5	180.0	183.8
C(4)/C(5)	123.5	123.6/123.2	123.0	123.6

In the infra-red vibrational spectra, the characteristic N—C—N stretching frequencies,[10] ν(N—C—N), are 1570 cm^{-1} for **4b**, 1571 cm^{-1} for **5**, and 1572 cm^{-1} for **6**. The vibrational bands around 3200-3100 cm^{-1} can be assigned to the ν(C—H) stretching vibrations of the heterocycle, and bands between 3000-2900 cm^{-1} are known to correspond to the ν(C—H) stretching vibration of the aliphatic groups. The electronic absorption spectra of **4b** - **6** recorded in acetonitrile are characterized by intense absorption bands (λ/nm, ε/M^{-1}cm^{-1}) in the ultra-violet region at 210 (81,000), 224 (77,000), 240 (58,000), and 364 nm (2,000) for **4b**, 210 (46,000), and 256 (24,000), and 270 nm (22,000) for **5**, and 210 (84,000), 216 (76,000), 234 (74,000), 246 (82,000), 260 (73,000) and 290 nm (23,000) for **6** (Figure 2-5). The spectrum of **2b** exhibits only one absorption band at 214 nm (13,000). Although the assignment of

these absorption bands remains largely equivocal, we suggest that they originate from ligand-centered as well as ligand-to-metal and metal-to-ligand charge transfer transitions.

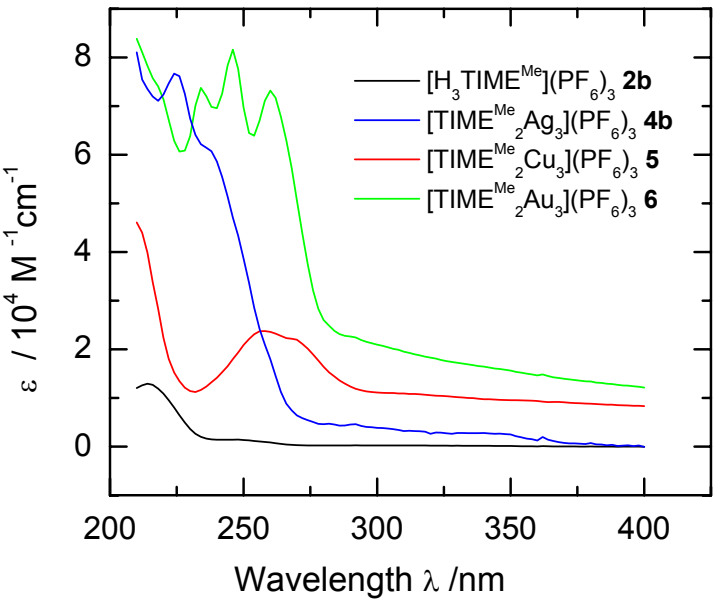

Figure 2-5. Electronic absorption spectra for compounds **2b**, **4b**, **5**, and **6** recorded in acetonitrile at 25°C.

Single crystal X-ray diffraction studies confirmed the isostructural geometries for complexes **4b - 6** (Figure 2-6, 2-7, and Table 2-2). In each of the three solid-state structures, an $\mathbf{M_3L_2}$ composition was found, with three metal ions bridging two $TIME^{Me}$ ligands through each of the three pendant arms. Each metal ion is coordinated to two of the carbenoid carbon atoms, with each carbene center stemming

from a different ligand. All structures exhibit D_3 symmetry, with a 3-fold axis passing through the anchoring C atoms of the two ligands.

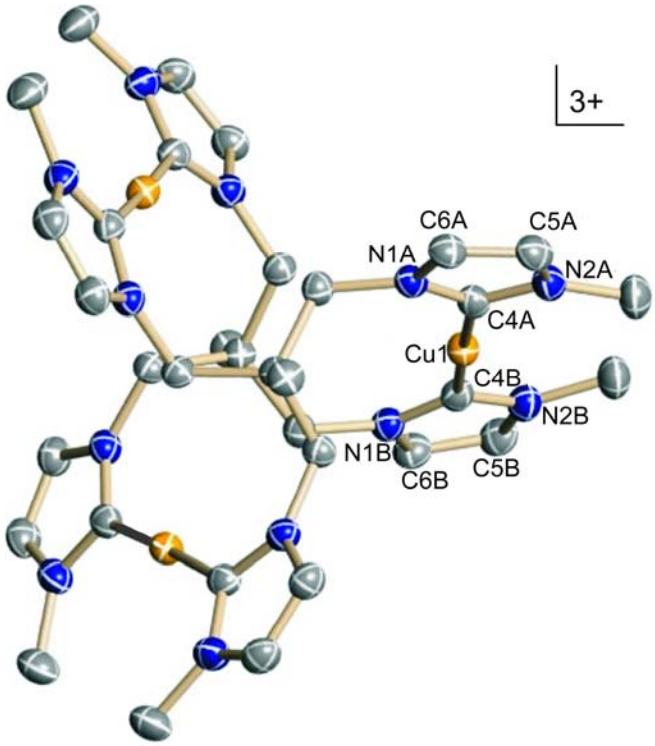

Figure 2-6. Solid-state molecular structure of $[Cu_3(TIME^{Me})_2](PF_6)_3$ (**5**). Counter anions and hydrogen atoms are omitted for clarity; thermal ellipsoids are shown at 50 % probability. Selected bond distances (Å) and angles (deg.): Cu(1)-C(4A) 1.9124(16), C(4A)-N(1A) 1.363(2), C(4A)-N(2A) 1.350(2), C(5A)-C(6A) 1.349(2), C(4A)-Cu (1)-C(4B) 177.70(9), N(1A)-C(4A)-N(2A) 103.78(13).

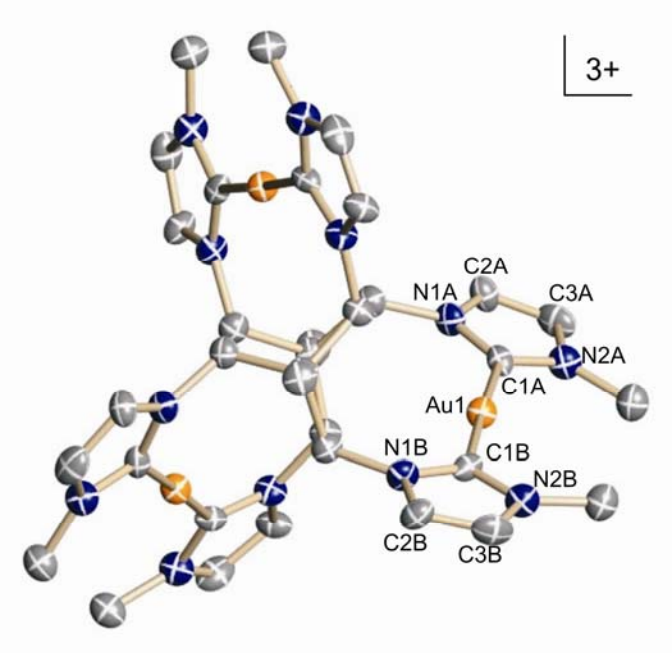

Figure 2-7. Solid-state molecular structure of $[Au_3(TIME^{Me})_2](PF_6)_3$ (**6**). Counter anions and hydrogen atoms are omitted for clarity; thermal ellipsoids are shown at 30 % probability. Selected bond distances (Å) and angles (deg.): Au(1)-C(4A) 2.035(12), C(4A)-N(1A) 1.352(13), C(4A)-N(2A) 1.332(13), C(5A)-C(6A) 1.343(17), C(4A)-Au (1)-C(4B) 177.7(6), N(1A)-C(4A)-N(2A) 110.2(9).

Compound **5** represents a rare example of a crystallographically characterized homoleptic copper(I) NHC complex. In the solid-state structure (Figure 2-6), the average Cu—C distance is 1.9124(16) Å, which is within the range of reported values for typical copper(I) NHC complexes (1.880-1.963 Å).[8,11] Similarly, in the crystal structure of **6** (Figure 2-7), the average Au—C bond distance of 2.035(15) Å is consistent with the values reported for other related two-coordinated gold carbene complexes.[12] The carbene copper entities are nearly linear, with a C—Cu—C' bond angel of 177.70(9)^o, comparable to its analogues: 178.56(13)^o in **4b** and 177.7(6)^o in **6**.

Inter- or intramolecular metal—metal interactions cannot be observed for this series of trinuclear complexes with the shortest metal—metal distances being 5.54, 5.51, and 5.54 Å for **4b**, **5**, and **6**, respectively.

Table 2-2. Selected Bond Lengths (Å) and Angles (deg.) for Group 11 Metal Complexes of $TIME^{Me}$ Ligand $[(TIME^{Me})_2M_3](PF_6)_3$ (M = Ag (**4b**), Cu (**5**), and Au(**6**)).

	4b	**5**	**6**
M—C(4A)	2.082(2)	1.9124(16)	2.035(12)
C(4A)—N(1A)	1.359(3)	1.363(2)	1.352(13)
C(4A)—N(2A)	1.347(3)	1.350(2)	1.332(13)
C(5A)—C(6A)	1.341(4)	1.349(2)	1.343(17)
M—M	5.54	5.51	5.54
C(4A)—M—C(4B)	178.56(13)	177.70(9)	177.7(6)
N(1A)—C(4A)—N(2A)	104.3(2)	103.78(13)	105.3(8)

The imidazole units in the structures of **4b - 6** exhibit typical features of coordinated NHC ligands (Table 2-2). Specifically, the average $C_{carbene}$—N bond distances, $d(N—C_{carbene})_{ave}$, increased from 1.326 Å in imidazolium salt **2a** to 1.353 Å in complex **4b**, to 1.357 Å in **5**, and to 1.346 Å in **6**. The N—$C_{carbene}$—N ring angles are significantly decreased from 108.5° in **2a** to 104.3° in **4b**, 103.8° in **5**, and 105.3° in **6**. Such changes are well documented in the literature[13] and have been attributed to decreased π delocalization in the five-membered ring[4] and increased *p* character of the carbenoid carbon[14] resulting from deprotonation and subsequent coordination.

Additionally, small decreases of the $C_{carbene}$—N bond distances and increases of N—$C_{carbene}$—N bond angles, going from Cu(I), Ag(I) to Au(I) NHC complexes, were observed. This is in agreement with the trends that previously have been found for NHC complexes of the 3*d*, 4*d*, and 5*d* transition metal series.[4] The two imidazole rings coordinated to the same metal ion are nearly co-planar with a dihedral angle of 6.4° (Ag), 7.7° (Cu), and 6.7° (Au).

The electronic structure of **4b - 6** was studied by density functional theory (DFT) calculations. In contrast to the common assumption that NHCs are pure σ-donors, our calculations revealed non-negligible π-interactions between the metal ions and carbene centers in **4b - 6**. The details of this study and that of related complexes are presented in chapter 6.

Attempts to transfer $TIME^{Me}$ to other metal ions by reacting **4b** with metal halides such as $Pd(CH_3CN)_2Cl_2$, $NiCl_2$, $FeCl_3$ etc. were unsuccessful.

2.2.4 The $TIME^{t\text{-}Bu}$ ligand and its coordination to copper(I)

Formation of trinuclear **4b - 6** reflects the tendency of group 11 metal ions to form linear, two-coordinate complexes. The metal centers in these complexes are not situated in a well-protected cavity as desired. To prevent the formation of polynuclear species, we decided to increase the steric bulk at the TIME ligand, e.g., use the *tert*-butyl derivative $TIME^{t\text{-}Bu}$.

The imidazolium salts, $[H_3TIME^{t\text{-}Bu}]X_3$ (**7a**, X = Br; **7b**, X = PF_6) were synthesized according to Scheme 2-1 in ~ 63 % yield. The solid-state molecular structure of **7a** was determined by X-ray crystallography (Figure 2-8).

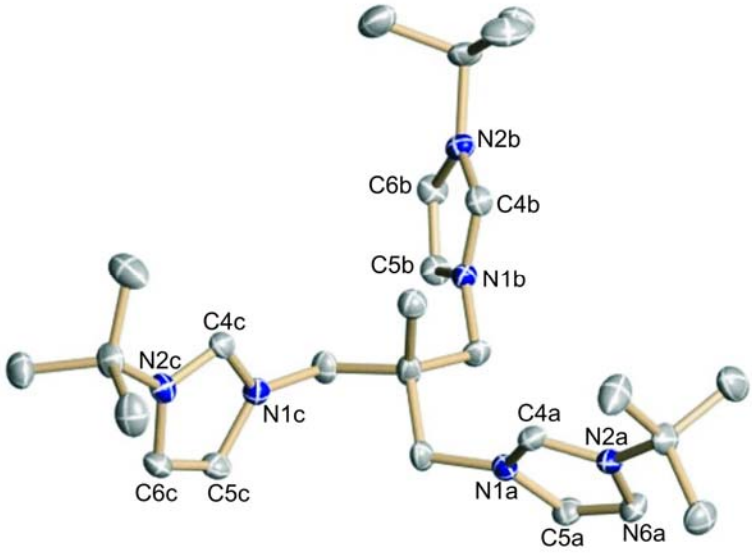

Figure 2-8. Solid-state molecular structure of imidazolium salt $(TIME^{t\text{-}Bu})Br_3$ (**7a**). Hydrogen atoms and anions are omitted for clarity; thermal ellipsoids are shown at 50% probability. Selected bond lengths (Å) and angles (deg.): C4a-N1a 1.332(4), C4a-N2a 1.327(3), C5a-C6a 1.347(4), N1a-C4a-N2a, 108.5(3).

Deprotonation of **7b** with three equivalents of potassium *tert*-butoxide in THF at room temperature yielded free carbene $TIME^{t\text{-}Bu}$ (**8**). NMR spectroscopy confirmed the formation of **8**. In the ^1H spectrum, the signal associated with the imidazolium protons disappeared, and in the ^{13}C spectrum, the carbene carbons gave rise to a signal at 215 ppm. Single crystals of **8** suitable for X-ray diffraction analysis were grown from a saturated solution of ether at –35°C. The solid-state molecular structure of **8** is depicted in Figure 2-9.

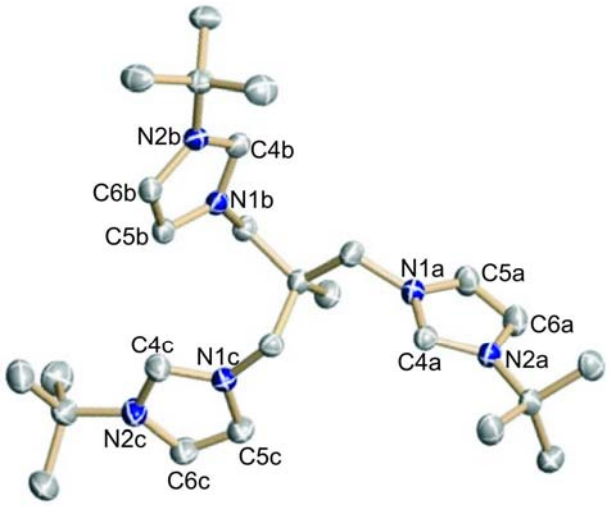

Figure 2-9. Solid-state molecular structure of carbene ligand TIME$^{t\text{-Bu}}$ (**8**). Hydrogen atoms are omitted for clarity; thermal ellipsoids are shown at 50% probability. Selected bond lengths (Å) and angles (deg.): C4a-N1a 1.3680(16), C4a-N2a 1.3633(15), C5a-C6a 1.3394(18), N1a-C4a-N2a, 102.14(10).

The structure of **8** contains three distinct imidazole rings with no appreciable intra or inter-molecular interactions. Each imidazole ring displays structural features similar to those of other reported simple 1,3-disubstituted imidazole-2-ylidenes.[15] The average $C_{carbene}$–N distance is 1.365 Å, and the average N–$C_{carbene}$–N angle is 102.1°.

Reaction of one equivalent of **8** with $[(CH_3CN)_4Cu](PF_6)$ in acetonitrile affords the copper complex $[(TIME^{t\text{-Bu}})_2Cu_2](PF_6)_2$ (**9**) as an off-white powder in ~70% yield (Scheme 2-4).

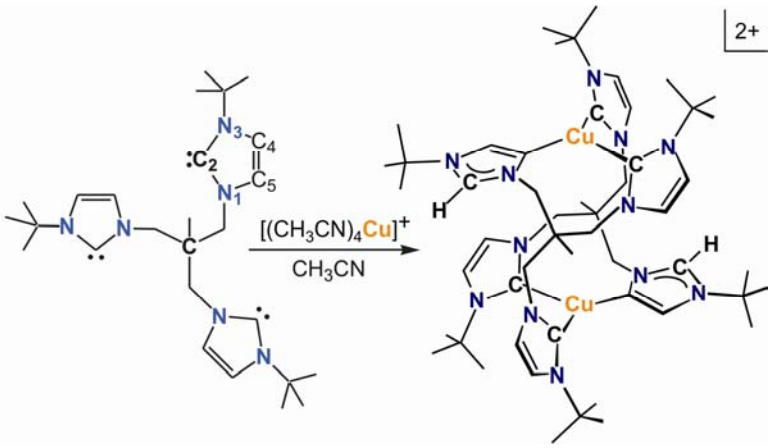

Scheme 2-4. Synthesis of the Complex $[(TIME^{t\text{-}Bu})_2Cu_2](PF_6)_2$ (**9**).

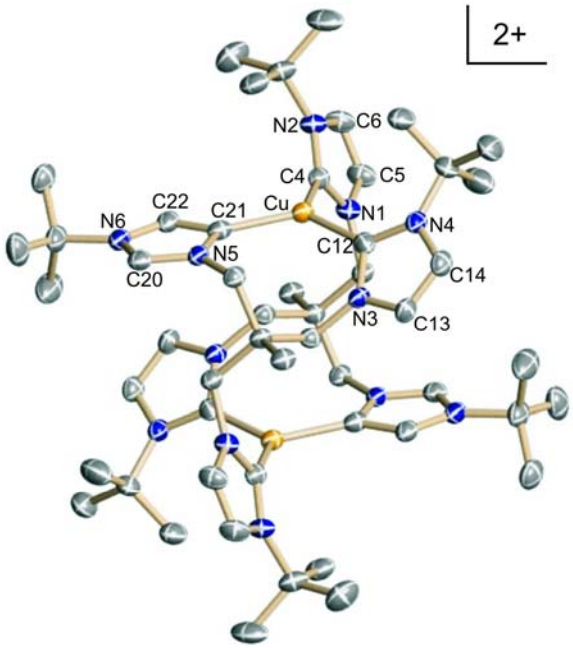

Figure 2-10. Solid-state molecular structure of complex $[(TIME^{t\text{-}Bu})_2Cu_2](PF_6)_2 \cdot$ 4DMSO (**9** · 4DMSO**)**. Hydrogen atoms, anions, and solvent molecules are omitted for clarity; thermal ellipsoids are shown at 50% probability. Selected bond lengths (Å) and angles (deg.): Cu-C4 1.9881(14), Cu-C12 1.9933(13), Cu-C21 1.9938(14), N1-C4-N2 102.84(11), N3-C12-N4 102.60(11), N5-C20-N6 108.52(20), N5-C21-C22 101.51(11), C4-Cu-C12 124.27(5), C12-Cu-C21 116.59(5), C21-Cu-C4 118.34(6).

In the molecular structure of **9** (Figure 2-10), two copper ions are related by a crystallographically defined inversion center. Each copper ion is three-coordinate in a trigonal planar ligand environment of three carbon centers.

Two carbon ligators stem from one ligand forming an unusual eight-membered ring with the cuprous ion, while a third carbon ligator is provided by a pendent arm of a second ligand, which, with its two remaining pendent arms, coordinates to a symmetry-related copper center. The average Cu–C bond distance is 1.996 Å, consistent with those of other reported Cu(I) carbene complexes.[8,11] With 119.73°, the average C–Cu–C angle is close to 120° for an idealized trigonal planar ligand environment.

Remarkably, the structure of **9** reveals the existence of an "alkenyl" binding mode within the Cu–C entity. Two of the three carbon ligands coordinated to the copper ion are "normal" diamino carbene centers corresponding to the carbon centers conventionally labeled as C2 carbon of the imidazole ring (Scheme 2-4). The third carbon ligand, however, formally is the C5 backbone atom of the imidazole ring structure. The formation of such a compound clearly involves C-H activation at the C5 position and subsequent protonation of the C2 carbene carbon. The ligand can thus be considered an alkenyl functionality; a formulation which is further supported by NMR spectroscopy (vide infra). While the crystallographically determined N-C-N angles of two of the imidazole rings are 102.94 and 103.01°, resembling angles typically found for imidazole-2-ylidene entities, the C5-metallated imidazole ring exhibits a much larger N–C–N angle of 108.63°. Although this type of metal binding

to N-heterocyclic carbene ligands was previously reported for complexes synthesized directly from imidazolium salts,[16] this is the first example of this binding mode generated by metal coordination to the free carbene starting material.

The ^{1}H and ^{13}C NMR spectra of **9** are consistent with the atom connectivities determined by X-ray crystallography. In the ^{1}H spectrum, the low field signal of unity intensity (8.41 ppm) was assigned to the imidazole C2 proton, while five signals of unity intensity at higher field (7.33 – 6.63 ppm) were assigned to the backbone protons bound to C4 and C5. Three intense signals at 1.71, 1.42 and 1.30 ppm were readily assigned to three non-equivalent *tert*-butyl groups in **9**. In the ^{13}C spectrum, the "normal" carbene carbons give rise to two well-resolved signals at 188.9 and 188.7 ppm, while the alkenyl carbon appears at 168.7 ppm. These NMR spectroscopic characteristics are known to be diagnostic for these two different modes of carbon metal binding.[8,16]

The formation of a bis(carbene)alkenyl species like **9** instead of a tris(carbene) species most likely has a steric origin, and the copper(I) ion plays an important role here because other metal ions failed to undergo similar reaction with TIME$^{t\text{-Bu}}$. For example, reaction of **8** with a nickel(0) source, i.e., $Ni(PPh_3)_2(CO)_2$, produced a bis(cabene) bis-carbonyl nickel(0) complex [(TIME$^{t\text{-Bu}}$)$Ni(CO)_2$] (**10**). According to ^{1}H and ^{13}C NMR and IR spectroscopy, the tris(carbene) ligand TIME$^{t\text{-Bu}}$ coordinates to nickel only through two of its carbene canters, leaving the third carbene carbon non-coordinating. No alkenyl coordination mode for the carbenes was found.

2.3. Conclusion

In summary, a new tripodal NHC ligand system TIME has been developed and its complexation with group 11 metal ions has been investigated. Spectroscopic and structural studies of the new compounds are described. The methyl derivative $TIME^{Me}$ forms homoleptic trinuclear complexes with group 11 metals. All complexes are isostructural. The structures possess D_3 symmetry, with three metal ions bridging two $TIME^{Me}$ ligands. Each metal ion is linearly coordinated to two carbene centers, with each carbenoid carbon stemming from a different ligand. The *tert*-butyl derivative $TIME^{t\text{-}Bu}$ forms an unusual dinuclear 2:2 complex with copper(I), in which the cuprous ion is in a trigonal-planar ligand environment of three different carbon ligators. NMR spectroscopy and X-ray crystallography revealed both "normal" and "abnormal (alkenyl)" NHC binding modes in this bis(carbene)alkenyl copper(I) complex.

The fact that the tripodal carbene system TIME does not form simple tridentate κ^3 complexes reflects a fundamental problem associated with this class of ligands. Three condensed eight-membered rings of a hypothetical 1:1 complex exhibit significantly lower stability than the more common five-, six-, or seven-membered rings of tris(pyrazolyl) or tris(phosphine) ligands and therefore likely is disfavored. Similarly, the tris(pyrazoyl) analogous of the TIME ligand, 1,1,1-[tris(pyrazol-1-yl)methyl]ethane, reportedly act as bidentate chelators.[17]

Despite this, the work on TIME has laid an important foundation in our study of tripodal NHC ligands: 1) A simple and versatile route to tris(imidazolium) salts was

established and is well suited for the synthesis of poly(imidazolium) salts of other topologies; 2) A free tris(carbene) was isolated suggesting that free polycarbenes in principle can be prepared and handled similar to monodentate NHCs; 3) The coordination of TIME to group 11 metal ions demonstrates the ability of tris-carbenes to chelate transition metals.

2.4. Experimental Section

Methods and Procedures

Manipulation of air-sensitive compounds was performed under a controlled dry nitrogen atmosphere using standard Schlenk-line techniques and inert-gas glove boxes (MBraun Labmaster by M. Braun, Inc.). Solvents were purified using a two-column solid-state purification system (Glasscontour System, Joerg Meyer, Irvine, CA), transferred to the glove box without exposure to air and stored over activated molecular sieves and/or sodium metal. NMR solvents were obtained from Cambridge Isotope Laboratories, degassed and stored over activated molecular sieves prior to use. All NMR spectra were recorded at room temperature (20^{o}C) in d_6-benzene, d_3-acetonitrile and d_6-DMSO solutions on Varian spectrometers operating at 400/300 MHz (^{1}H NMR) and 100 MHz (^{13}C NMR) and referenced to residual solvent peaks unless otherwise noted (δ in ppm). Infrared spectra (400—4000 cm^{-1}) of solid samples were obtained on a Thermo Nicolet Avatar 360 FT-IR spectrophotometer as KBr pellets. Electronic absorption spectra were recorded from 190 nm to 820 nm (HP 8452A Diode Array, UV/vis spectrophotometer). Elemental analyses were performed

by Kolbe Microanalytical Laboratory (Muelheim a. d. Ruhr/Germany) or RuMega Resonance Labs (San Diego, CA/USA).

Synthesis:

Starting materials. N-methylimidazole (Acros), ammonium hexafluorophosphate (Acros), tetrabutylammonium hexafluorophosphate (Acros), potassium *tert*-butoxide (Acros), silver oxide (Fisher), copper(I) bromide (Aldrich), copper(I) trifluoromethanesulfonate (Aldrich), (dimethylsulfide)gold(I) chloride (Aldrich), *n*-butyllithium (2.5 M in hexane) (Aldrich) were obtained from commercial sources and used as received. N-*tert*-butylimidazole, benzylpotassium, and tetrakis(acetonitrile)copper(I) hexafluorophosphate were prepared according to the methods described in the literature.[3,18] 1,1,1-tris(bromomethyl)ethane was prepared using a different approach than the reported method (John M. Derfer, Kenneth W. Greenlee, and Cecil E. Boord, *J. Am. Chem. Soc.* **1949**, **71**, 175-182.)

1,1,1-tris(p-toluenesulfonatemethyl)ethane: 1,1,1-tris(hydroxymethyl)ethane (168.4 g, 1.4 mol) and pyridine (500 ml) were added to a 3 L 3-neck flask. The flask was equipped with a mechanical stir, a thermometer, and a 500 mL additional funnel. The solution was cooled to 0 ^{o}C over an ice-water bath. p-Toluenesulfonyl chloride (820g, 4.2 mol) in 500 ml pyridine was added to the mixture slowly via an additional funnel (the temperature of the solution was kept below 45 ^{o}C during the addition). The addition was completed in 1 hr, and the mixture was removed from the ice-water bath and stirred for another hour. The resulting solution was added slowly to a

mixture of 1 L HCl and 500 methanol. The white solid precipitate was collected by filtration and washed with water and methanol. (800 g; yield: 98 %).

1,1,1-tris(bromomethyl)ethane: 1,1,1-tris(p-toluenesulfonatemethyl)ethane (519 g, 0.9 mol) and sodium bromide (483 g, 4.7 mol) were added to a 3 L flask containing 800 mL ethylene glycol and the mixture was refluxed for 16 hrs. The resulting suspension was cooled to room temperature, and 500 ml water was added. The organic phase was extracted with benzene and evaporated to give a white powder. (139 g; yield: 50 %).

$[H_3TIME^{Me}](Br)_3$ (2a): A 50 mL flask was charged with 1, 1, 1- tris(bromo-methyl)ethane (8.5 g, 0.026 mol) and *N*-methylimidazole (10.8 g, 0.131 mol) and the mixture was heated to 150 °C for 1 day during which a white solid formed. The solid was filtered off, washed with diethyl ether, and re-crystallized from methanol. (12.6 g; yield: 88 %). ^{1}H NMR (400 MHz, d_6-DMSO, 20 °C): δ = 9.28 (s, 3H), 7.89 (s, 3H), 7.81 (s, 3H), 4.37 (s, 6H), 3.89 (s, 9H,), 0.99 ppm (s, 3H). ^{13}C NMR (100 MHz, d_6-DMSO, 20 ^{o}C): δ = 137.5, 123.6, 123.4, 52.9, 38.3, 36.0, 18.9 ppm. Elemental analysis (%) calcd for $C_{17}H_{27}N_6Br_3 \cdot 1.5H_2O$**:** C 35.07, H 5.19, N 14.44; found: C 35.42, H 5.51, N 14.04.

$[H_3TIME^{Me}](PF_6)_3$ (2b): NH_4PF_6 (0.88 g, 5.4 mmol) was added to a solution of **2a** (1 g, 1.8 mmol) in 30 mL methanol. The white hexaflurophosphate salt precipitated immediately, was collected by filtration, washed with small portions of cold methanol, and dried in vacuum. (1.3 g; yield: 96%). ^{1}H NMR (400 MHz, d_6-DMSO, 20 °C): δ = 9.12 (s, 3H), 7.82 (s, 3H), 7.68 (s, 3H), 4.26 (s, 6H), 3.89 (s, 9H,),

0.93 ppm (s, 3H). ^{13}C NMR (100 MHz, d_6-DMSO, 20 ^{o}C): δ = 137.8, 123.8, 123.5, 52.7, 38.3, 36.0, 17.1 ppm. Elemental analysis (%) calcd for $C_{17}H_{27}F_{18}N_6P_3$**:** C 27.21, H 3.62, N 11.20; found: C 26.99, H 3.94, N 11.23.

[(TIME^{Me})$_2$Ag$_3$]$_2$(Ag$_8$Br$_{14}$) (4a): To a solution of 1.4 g (2.52 mmol) of **2a** in 100 mL DMSO was added 1.76 g of Ag_2O (7.58 mmol). The mixture was heated at 75 ^{o}C for 12 h. The resulting suspension was then filtered through Celite and an equal amount of ether was added to give an off-white powder. The precipitate was filtered, washed with ether, and then dried under vacuum (0.98 g, yield: 40%). Colorless crystals suitable for X-ray diffraction analysis were grown from a solution of **4a** in DMSO. ^{1}H NMR (400 MHz, d_6-DMSO, 20 °C): δ = 7.47 (s, 3H), 7.43 (s, 3H), 4.31 (s, br, 6H), 3.86 (s, 9H,), 1.19 ppm (s, 3H). ^{13}C NMR (100 MHz, d_6-DMSO, 20 ^{o}C): δ = 182.1, 123.3, 123.1, 58.8, 40.4, 38.3, 18.5 ppm. Elemental analysis (%) calcd for $C_{34}H_{48}N_{12}Ag_7Br_7$**:** C 21.06, H 2.49, N 8.67; found: C 20.75, H 2.83, N 8.33.

[(TIME^{Me})$_2$Ag$_3$](PF$_6$)$_3$ (4b): **2b** (1.08 g, 1.44 mmol) was dissolved in 100 mL DMSO, and to this solution Ag_2O (0.52 g, 2.24 mmol) was added. The mixture was heated to 75 ^{o}C for 12 h. The resulting suspension was filtered through Celite and to the filtrate an equal amount of water was added to give a white powder. The solid was collected by filtration, washed with diethyl ether, and dried in vacuum (0.67 g, Yield: 67 %). ^{1}H NMR (400 MHz, d_6-DMSO, 20 °C): δ = 7.55 (s, 3H), 7.49 (s, 3H), 4.44 (s, br, 3H), 4.20 (s, br, 3H), 3.90 (s, 9H), 1.24 ppm (s, 3H). ^{13}C NMR (100 MHz, d_6-DMSO, 20 ^{o}C): δ = 182.5, 123.6, 123.2, 59.0, 40.4, 38.2, 18.1 ppm. Elemental

analysis (%) calcd for $C_{34}H_{48}N_{12}Ag_3P_3F_{18}$: C 29.52, H 3.50, N 12.15; found: C 29.26, H 3.46, N 11.77.

[(TIME^{Me})$_2$Cu$_3$](PF$_6$)$_3$ (5) : Method A: A solution of copper(I) bromide (130 mg, 0.9 mmol) in acetonitrile was added dropwise to a solution of **4b** (418.2 mg, 0.3 mmol) in 10 mL acetonitrile. A white precipitate of AgBr formed upon addition of the copper(I) salt. The mixture was filtered through Celite, and to the filtrate 50 mL ether was added to give a white crystalline powder. The solid was collected by filtration, washed with diethyl ether, and dried in vacuum (210 mg; yield: 56%). **Method B:** A solution of 3 equivalent bases (*n*-butyllithium, potassium *tert*-butoxide, or benzylpotassium) in THF was added dropwise to a suspension of **2b** (365 mg, 0.66 mmol) 5 mL THF. A clear colorless solution was formed upon addition of the base. Within 30 minutes, the solution turned into orange-red. The resulting solution was filtered and copper triflate (129 mg, 0.25 mmol) was added to the filtrate. A light-brown precipitate formed immediately. The solid was filtered off, dissolved in 10 mL acetonitrile and to the filtered solution tetrabutylammonium hexaflurophosphate (1 g, 2.6 mmol) was added. The mixture was stirred for 5 minutes, and 50 mL diethyl ether was added to cause precipitation of **5** as an off-white powder. The precipitate was collected by filtration, washed with diethyl ether, and dried in vacuum (110 mg; yield: 27%). Colorless crystals suitable for X-ray diffraction analysis were grown by slow diethyl ether diffusion into a saturated solution of **5** in acetonitrile at room temperature. ^{1}H NMR (400 MHz, d_6-DMSO, 20 °C): δ = 7.49 (s, 3H), 7.44 (s, 3H), 4.55 (s, br, 3H), 4.16 (s, br, 3H), 3.93 (s, 9H), 1.25 ppm (s, 3H). ^{13}C NMR (100 MHz, d_6-DMSO, 20

^{o}C): δ = 178.0, 123.0, 58.6, 40.1, 37.7, 18.1 ppm. Elemental analysis (%) calcd for $C_{34}H_{48}N_{12}Cu_3P_3F_{18}$: C 32.66, H 3.89, N 13.44; found: C 31.59, H 4.14, N 12.94.

[(TIME^{Me})$_2$Au$_3$](PF$_6$)$_3$ (6): A solution of Au(SMe$_2$)Cl (122 mg, 0.41 mmol) in acetonitrile was added dropwise to a solution of **4b** (190.1 mg, 0.14 mmol) in 10 mL acetonitrile. A white precipitate of AgBr formed upon addition of the gold(I) salt. The mixture was filtered through Celite, and to the filtrate 20 mL ether was added to give a white crystalline powder. The solid was collected by filtration, washed with diethyl ether, and dried in vacuum (110 mg; yield: 48%). Colorless crystals suitable for X-ray diffraction analysis were grown by slow diethyl ether diffusion into a saturated solution of **6** in acetonitrile at room temperature. H NMR (400 MHz, d_6-DMSO, 20 °C): δ = 7.61 (s, 3H), 7.48 (s, 3H), 4.80 (d, 3H), 4.20 (d, 3H), 3.94 (s, 9H), 1.26 ppm (s, 3H). ^{13}C NMR (100 MHz, d_6-DMSO, 20 ^{o}C): δ = 183.8, 123.6, 57.6, 40.2, 37.5, 22.5 ppm. Elemental analysis (%) calcd for $C_{34}H_{48}N_{12}Au_3P_3F_{18}$: C 24.74, H 2.93, N 10.18; found: C, 23.45, H, 2.62, N 9.42.

[H$_3$TIME$^{t\text{-}Bu}$]Br$_3$ (7a): A 50 mL flask was charged with 23 g (7.4 mmol) 1, 1, 1- tris(bromomethyl)ethane and 28 g (22.3 mmol) *N-tert*-butylimidazole and the mixture was heated to 150 °C for 3 days during which a white solid formed. The precipitate was filtered, washed with ether, and recrystallized from methanol (32 g, yield: 63 %). Crystals suitable for X-ray diffraction analysis were grown by diffusion of diethylether into a solution of **7a** in DMSO at room temperature. ^{1}H NMR (400 MHz, d_6-DMSO, 20 °C): δ = 8.96 (s, 3H), 7.67 (s, 3H), 7.50 (s, 3H), 4.38 (s, 6H), 1.54 (s, 27H,), 1.20 ppm (s, 3H). ^{13}C NMR (100 MHz, d_6-DMSO, 20 ^{o}C): δ = 135.2,

124.4, 121.1, 54.1, 49.2, 39.9, 29.2, 18.1ppm. Elemental analysis (%) calcd for $C_{26}H_{45}N_6Br_3 \cdot 2H_2O$**:** C 43.53, H 6.88, N 11.71; found: C 43.56, H 6.61, N 12.31.

[H_3TIME$^{t\text{-Bu}}$](PF_6)$_3$ (7b): 0.72 g of NH_4PF_6 (4.4 mmol) were added to a solution of 1 g of **7a** in 30 mL methanol. A white precipitate formed immediately, which was collected by filtration, washed with small portions of cold methanol, and dried in vacuum. (1.25 g, yield: 97%). ^{1}H NMR (400 MHz, d_6-DMSO, 20 °C): δ = 9.28 (s, 3H), 8.18 (s, 3H), 7.88 (s, 3H), 4.24 (s, 6H), 1.61 (s, 27H,), 1.00 ppm (s, 3H). ^{13}C NMR (100 MHz, d_6-DMSO, 20 ^{o}C): δ = 135.6, 124.4, 120.5, 60.1, 53.4, 38.5, 29.0, 17.2 ppm. Elemental analysis (%) calcd for $C_{26}H_{45}F_{18}N_6P_3$**:** C 35.63, H 5.17, N 9.59; found: C 35.49, H 5.49, N 9.49.

[TIME$^{t\text{-Bu}}$] (8): A THF solution of potassium *tert*-butoxide (0.41 g, 3.6 mmol) was added dropwise to a suspension of **7b** (1.08 g, 1.2 mmol) in 5 ml THF. Upon addition of the base, a clear colorless solution was obtained. The solution was evaporated to dryness and the resulting residue was dissolved in 15 ml of ether. The resulting solution was filtered and the filtrate was evaporated to dryness in vacuum. The solid was collected, washed with cold pentane, and dried in vacuum (0.34 g, yield: 65 %). Crystals suitable for X-ray diffraction analysis were grown from a saturated solution of **8** in ether at –35^{o}C. ^{1}H NMR (400 MHz, d_6-Benzene, 20 °C): δ = 7.87 (d, 3H), 6.67 (d, 3H), 4.28 (s, 6H), 1.48 (s, 27H,), 0.79(s, 3H). ^{13}C NMR (100 MHz, d_6-Benzene, 20 ^{o}C): δ = 214.7, 122.5, 115.0, 56.2, 55.3, 42.5, 32.1, 20.9 ppm. Elemental analysis (%) calcd for $C_{26}H_{42}N_6$**:** C 71.19, H 9.65, N 19.16; found: C 71.02, H 9.57, N 19.46.

[(TIME$^{t\text{-Bu}}$)$_2$Cu$_2$](PF$_6$)$_2$ (9): An acetonitrile solution of tetrakis(acetonitrile)copper(I) hexafluorophosphate (1.4 g, 3.75 mmol) was added dropwise to a solution of **8** (1.65 g, 3.75 mmol) in acetonitrile (10 ml). The mixture was allowed to stir for one hour, and then 30 ml ether was added to cause precipitation of **9** as an off-white powder. The precipitate was collected by filtration, washed with ether, and dried under vacuum (1.7 g, yield: 70 %). Crystals suitable for X-ray diffraction analysis were grown from a saturated solution of **9** in DMSO at room temperature. ^{1}H NMR (400 MHz, d_6-DMSO, 20 °C): δ = 8.90 (s, 1H), 7.59 (s, 1H), 7.29 (s, 1H), 7.20 (s, 1H), 7.17 (s, 1H), 6.64 (s, 1H), 4.80 (d, 1H), 4.23 (d, 1H), 4.16 (d, 1H), 3.82 (d, 1H), 3.66 (d, 1H), 2.98(d, 1H), 1.67 (s, 9H), 1.38 (s, 9H), 1.26 (s, 9H), 0.94 (s, 3H). ^{13}C NMR (100 MHz, d_3-Acetonitrile, 20 ^{o}C): δ = 188.9, 188.7, 168.7, 126.3, 123.1, 120.8, 118.9, 117.7, 117.5, 57.5, 57.2, 57.0, 56.8, 53.6, 41.5, 32.1, 31.2, 30.0, 21.2 ppm. Elemental analysis (%) calcd for $C_{26}H_{42}N_6CuPF_6$**:** C 48.25, H 6.54, N 12.99; found: C 48.20, H 6.43, N 13.08.

[(TIME$^{t\text{-Bu}}$)Ni](CO)$_2$ (10): An benzene solution of bis(triphenylphosphine)nickel(0) bis-carbonyl (0.61 g, 0.94 mmol) was added dropwise to a solution of **8** (0.38 g, 0.94 mmol) in benzene (5 ml). The mixture was allowed to stir for one hour, and then evaporated to dryness. 20 mL ether was added to dissolve the solid and the mixture was filtered through a frit. The filtrate was collected and cooled to - 35^{0}C overnight to give **10** as a yellow powder. The precipitate was collected by filtration and dried under vacuum (0.5 g, yield: 67 %). ^{1}H NMR (400 MHz, d_6-benzene, 20 °C): δ = 8.07 (d, 1H), 7.15 (s, 1H), 6.80 (d, 1H),

6.71 (d, 1H), 6.63 (d, 1H), 6.28 (d, 1H), 6.14 (d, 1H), 4.83 (d, 1H), 4.74 (d, 1H), 3.84 (d, 1H), 3.62 (d, 1H), 3.04 (d, 1H), 2.95 (d, 1H), 1.88 (s, 9H), 1.87 (s, 9H), 1.44 (s, 9H), 0.32 (s, 3H). ^{13}C NMR (100 MHz, d_6-benzene, 20 ^{o}C): δ = 213.9, 204.0, 203.8, 199.4, 199.0, 121.7, 121.0, 120.3, 117.0, 116.9, 114.8, 58.7, 58.4, 56.0, 53.4, 52.3, 42.5, 31.3, 31.0, 19.5 ppm. IR (KBr): ν(CO): 1945, 1860, 1846 cm^{-1}. Elemental analysis (%) calcd for $C_{28}H_{42}N_6NiO_2$**:** C 60.64, H 7.58, N 15.26; found: C 60.77, H 7.65, N 15.19.

2.5. Acknowledgement

Text, schemes, and figures of this chapter, in part, are reprints of the materials published in the following papers: **Hu**, **X**.; Tang, Y.-J.; Gantzel, P.; Meyer, K*. "Silver Complexes of a Novel Tripodal N-Heterocyclic Carbene Ligand: Evidence for Significant Metal—Carbene π-Interaction", *Organometallics* **2003**, *22*, 612-614. **Hu**, **X**.; Castro-Rodriguez, I.; Meyer, K*. "A Bis-Carbenealkenyl Copper(I) Complex From a Tripodal Carbene Ligand", *Organometallics* **2003**, *22*, 3016-3018. **Hu**, **X**.; Castro-Rodriguez, I.; Olsen, K.; Meyer, K*. "Group 11 Metal Complexes of N-Heterocyclic Carbene Ligands: Nature of the Metal—Carbene Bond", O*rganometallics* **2004**, *23*, 755-764. The dissertation author was the primary researcher and author. The co-authors listed in these publications also participated in the research.

The permission to reproduce these papers was granted by the American Chemical Society.

2.6. Appendix

Crystallographic Details for 2a, 4a - b, 5 - 6, 7a, and 8 - 9

Table 2-3. Crystal Data and Structure Refinement for $[H_3TIME^{Me}]Br_3$ (**2a**).

Identification code	2-2a	
Empirical formula	C17 H27 Br3 N6	
Formula weight	555.18	
Temperature	100(2) K	
Wavelength	0.71073 Å	
Crystal system	Trigonal	
Space group	*P*-3	
Unit cell dimensions	a = 15.995(2) Å	α = 90°.
	b = 15.995(2) Å	β = 90°.
	c = 5.6388(10) Å	γ = 120°.
Volume	1249.3(3) $Å^3$	
Z	2	
Density (calculated)	1.476 Mg/m^3	
Absorption coefficient	4.855 mm^{-1}	
F(000)	552	
Crystal size	0.08 x 0.18 x 0.28 mm^3	
Theta range for data collection	1.47 to 22.43°.	
Index ranges	-16<=h<=17, -16<=k<=17, -6<=l<=6	
Reflections collected	7099	
Independent reflections	1073 [R(int) = 0.0396]	
Completeness to theta = 22.43°	99.9 %	
Absorption correction	Semi-Empirical	
Refinement method	Full-matrix least-squares on F^2	
Data / restraints / parameters	1073 / 0 / 81	
Goodness-of-fit on F^2	1.234	
Final R indices [I>2sigma(I)]	R_1 = 0.0803, wR_2 = 0.2344	
R indices (all data)	R_1 = 0.0849, $wR2$ = 0.2367	
Largest diff. peak and hole	1.277 and -0.433 e.$Å^{-3}$	

Table 2-4. Crystal Data and Structure Refinement for $[(TIME^{Me})_2Ag_3]_2(Ag_8Br_{14}) \cdot 5DMSO$ (**4a** · 5DMSO)

Identification code	2-4a	
Empirical formula	C44 H48 Ag7 Br7 N12 O5 S5	
Formula weight	2299.70	
Temperature	100(2) K	
Wavelength	0.71073 Å	
Crystal system	Triclinic	
Space group	*P*-1	
Unit cell dimensions	*a* = 15.5320(11) Å	α= 67.7190(10)°.
	b = 16.3539(12) Å	β= 89.5200(10)°.
	c = 17.8793(13) Å	γ= 62.3680(10)°.
Volume	3644.6(5) $Å^3$	
Z	2	
Density (calculated)	2.096 Mg/m^3	
Absorption coefficient	5.867 mm^{-1}	
F(000)	2180	
Crystal size	0.40 x 0.18 x 0.14 mm^3	
Theta range for data collection	1.26 to 27.53°.	
Index ranges	-19<=h<=20, -20<=k<=20, -23<=l<=23	
Reflections collected	30340	
Independent reflections	15817 [*R*(int) = 0.0241]	
Completeness to theta = 27.53°	94.2 %	
Max. and min. transmission	0.4939 and 0.2025	
Absorption correction	Semi-Empirical	
Refinement method	Full-matrix least-squares on F^2	
Data / restraints / parameters	15817 / 0 / 628	
Goodness-of-fit on F^2	1.027	
Final R indices [I>2sigma(I)]	R_1 = 0.0779, wR_2 = 0.2109	
R indices (all data)	R_1 = 0.0852, wR_2 = 0.2171	
Largest diff. peak and hole	8.135 and -2.322 e.$Å^{-3}$	

Table 2-5. Crystal Data and Structure Refinement for $[Ag(TIME^{Me})_2](PF_6)_3$ (**4b**).

Identification code	2-4b
Empirical formula	C34 H48 Ag3 F18 N12 P3
Formula weight	1383.36
Temperature	100(2) K
Wavelength	0.71073 Å
Crystal system	Rhombohedral
Space group	*R*-3*c*
Unit cell dimensions	a = 18.5021(10) Å α= 90°. b = 18.5021(10) Å β= 90°. c = 23.672(3) Å γ = 120°.
Volume	7017.8(10) $Å^3$
Z	6
Density (calculated)	1.964 Mg/m^3
Absorption coefficient	1.461 mm^{-1}
F(000)	4104
Crystal size	0.15 x 0.14 x 0.10 mm^3
Theta range for data collection	2.14 to 27.51°.
Index ranges	-23<=h<=23, -24<=k<=23, -30<=l<=30
Reflections collected	19303
Independent reflections	1797 [R(int) = 0.0267]
Completeness to theta = 27.51°	99.8 %
Absorption correction	Semi-Empirical
Max. and min. transmission	0.8676 and 0.8106
Refinement method	Full-matrix least-squares on F^2
Data / restraints / parameters	1797 / 0 / 119
Goodness-of-fit on F^2	1.078
Final R indices [I>2sigma(I)]	R_1 = 0.0277, wR_2 = 0.0700
R indices (all data)	R_1 = 0.0314, wR_2 = 0.0724
Largest diff. peak and hole	0.795 and -0.275 $e.Å^{-3}$

Table 2-6. Crystal Data and Structure Refinement for $[Cu(TIME^{Me})_2](PF_6)_3$ (**5**).

Identification code	2-5	
Empirical formula	C17 H24 Cu1.50 F9 N6 P1.50	
Formula weight	625.19	
Temperature	100(2) K	
Wavelength	0.71073 Å	
Crystal system	Rhombohedral	
Space group	*R*-3*c*	
Unit cell dimensions	a = 18.5950(8) Å	α = 90°.
	b = 18.5950(8) Å	β = 90°.
	c = 23.0613(18) Å	γ = 120°.
Volume	6905.7(7) $Å^3$	
Z	12	
Density (calculated)	1.804 Mg/m^3	
Absorption coefficient	1.595 mm^{-1}	
F(000)	3780	
Crystal size	0.28 x 0.26 x 0.17 mm^3	
Theta range for data collection	2.17 to 27.52°.	
Index ranges	-23<=h<=24, -24<=k<=24, -29<=l<=28	
Reflections collected	18930	
Independent reflections	1771 [R(int) = 0.0183]	
Completeness to theta = 27.52°	99.7 %	
Absorption correction	Semi-Empirical	
Max. and min. transmission	0.7733 and 0.6637	
Refinement method	Full-matrix least-squares on F^2	
Data / restraints / parameters	1771 / 0 / 113	
Goodness-of-fit on F^2	1.119	
Final R indices [I>2sigma(I)]	R_1 = 0.0286, wR_2 = 0.0808	
R indices (all data)	R_1 = 0.0297, wR_2 = 0.0817	
Largest diff. peak and hole	0.591 and -0.197 $e.Å^{-3}$	

Table 2-7. Crystal Data and Structure Refinement for $[Au(TIME^{Me})_2](PF_6)_3$ (**6**).

Identification code	2-6	
Empirical formula	C34 H48 Au3 F18 N12 P3	
Formula weight	1650.65	
Temperature	100(2) K	
Wavelength	0.71073 Å	
Crystal system	Rhombohedral	
Space group	*R*-3*c*	
Unit cell dimensions	a = 18.3767(14) Å	α = 90°.
	b = 18.3767(14) Å	β = 90°.
	c = 23.425(4) Å	γ = 120°.
Volume	6850.9(13) $Å^3$	
Z	6	
Density (calculated)	2.401 Mg/m^3	
Absorption coefficient	9.836 mm^{-1}	
F(000)	4680	
Crystal size	0.22 x 0.10 x 0.04 mm^3	
Theta range for data collection	2.16 to 23.99°.	
Index ranges	-21<=h<=21, -21<=k<=20, -26<=l<=26	
Reflections collected	14183	
Independent reflections	1198 [R(int) = 0.0567]	
Completeness to theta = 23.99°	100.0 %	
Absorption correction	Semi-Empirical	
Refinement method	Full-matrix least-squares on F^2	
Data / restraints / parameters	1198 / 0 / 109	
Goodness-of-fit on F^2	1.038	
Final R indices [I>2sigma(I)]	R_1 = 0.0416, wR_2 = 0.1078	
R indices (all data)	R_1 = 0.0563, wR_2 = 0.1149	
Largest diff. peak and hole	1.967 and -0.621 $e.Å^{-3}$	

Table 2-8. Crystal Data and Structure Refinement for $[H_3TIME^{t\text{-}Bu}]Br_3$ (**7a**).

Identification code	2-7a	
Empirical formula	C26 H43 Br3 N6	
Formula weight	679.39	
Temperature	100(2) K	
Wavelength	0.71073 Å	
Crystal system	Rhombohedral	
Space group	*R*3*c*	
Unit cell dimensions	a = 19.1240(8) Å	α = 90°.
	b = 19.1240(8) Å	β = 90°.
	c = 14.2798(12) Å	γ = 120°.
Volume	4522.8(5) Å^3	
Z	6	
Density (calculated)	1.497 Mg/m^3	
Absorption coefficient	4.039 mm^{-1}	
F(000)	2076	
Crystal size	0.37 x 0.27 x 0.24 mm^3	
Theta range for data collection	2.13 to 27.49°.	
Index ranges	-24<=h<=24, -10<=k<=24, -16<=l<=15	
Reflections collected	4124	
Independent reflections	1990 [R(int) = 0.0175]	
Completeness to theta = 27.49°	93.4 %	
Absorption correction	Empirical	
Max. and min. transmission	0.4440 and 0.3165	
Refinement method	Full-matrix least-squares on F^2	
Data / restraints / parameters	1990 / 1 / 106	
Goodness-of-fit on F^2	0.983	
Final R indices [I>2sigma(I)]	R_1 = 0.0221, wR_2 = 0.0496	
R indices (all data)	R_1 = 0.0233, wR_2 = 0.0499	
Absolute structure parameter	-0.005(10)	
Largest diff. peak and hole	0.553 and -0.182 e.Å^{-3}	

Table 2-9. Crystal Data and Structure Refinement for $[H_3TIME^{t\text{-}Bu}]Br_3$ (**8**).

Identification code	2-8	
Empirical formula	C26 H42 N6	
Formula weight	438.66	
Temperature	100(2) K	
Wavelength	0.71073 Å	
Crystal system	Monoclinic	
Space group	*C*2/*c*	
Unit cell dimensions	a = 26.317(6) Å	α = 90°.
	b = 11.992(3) Å	β = 125.531(3)°.
	c = 21.092(5) Å	γ = 90°.
Volume	5417(2) Å^3	
Z	8	
Density (calculated)	1.076 Mg/m^3	
Absorption coefficient	0.065 mm^{-1}	
F(000)	1920	
Crystal size	0.39 x 0.30 x 0.20 mm^3	
Theta range for data collection	1.90 to 27.51°.	
Index ranges	-34<=h<=33, -15<=k<=15, -26<=l<=27	
Reflections collected	22985	
Independent reflections	6211 [R(int) = 0.0274]	
Completeness to theta = 27.51°	99.6 %	
Absorption correction	Empirical	
Max. and min. transmission	0.9870 and 0.9749	
Refinement method	Full-matrix least-squares on F^2	
Data / restraints / parameters	6211 / 0 / 314	
Goodness-of-fit on F^2	1.009	
Final R indices [I>2sigma(I)]	R_1 = 0.0468, wR_2 = 0.1154	
R indices (all data)	R_1 = 0.0571, wR_2 = 0.1226	
Largest diff. peak and hole	0.393 and -0.172 e.Å^{-3}	

Table 2-10. Crystal Data and Structure Refinement for $[(TIME^{t\text{-}Bu})_2Cu_2](PF_6)_2 \cdot 4DMSO$(**9** · 4DMSO).

Identification code	2-9	
Empirical formula	C60 H108 Cu2 F12 N12 O4 P2 S4	
Formula weight	1606.84	
Temperature	100(2) K	
Wavelength	0.71073 Å	
Crystal system	Monoclinic	
Space group	*P*2(1)/*c*	
Unit cell dimensions	a = 10.6501(10) Å	α= 90°.
	b = 18.1215(17) Å	β= 93.638(2)°.
	c = 20.3429(19) Å	γ = 90°.
Volume	3918.2(6) $Å^3$	
Z	2	
Density (calculated)	1.362 Mg/m^3	
Absorption coefficient	0.768 mm^{-1}	
F(000)	1688	
Crystal size	0.20 x 0.14 x 0.13 mm^3	
Theta range for data collection	1.51 to 27.51°.	
Index ranges	-13<=h<=13, -23<=k<=23, -26<=l<=26	
Reflections collected	33516	
Independent reflections	8955 [*R*(int) = 0.0280]	
Completeness to theta = 27.51°	99.4 %	
Absorption correction	Empirical	
Max. and min. transmission	0.9271 and 0.8023	
Refinement method	Full-matrix least-squares on F^2	
Data / restraints / parameters	8955 / 0 / 311	
Goodness-of-fit on F^2	0.914	
Final R indices [I>2sigma(I)]	R_1 = 0.0342, wR_2 = 0.0847	
R indices (all data)	R_1 = 0.0406, wR_2 = 0.0865	
Largest diff. peak and hole	0.459 and -0.180 e.$Å^{-3}$	

2.7. References

(1) Dias, H. V. R.; Jin, W. C. *Tetrahedron Lett.* **1994**, *35*, 1365-1366.

(2) Mayer, H. A.; Kaska, W. C. *Chem. Rev.* **1994**, *94*, 1239-1272.

(3) Arduengo, A. J.; Gentry, F. P.; Taverkere, P. K.; Simmons, H. E. In *US Patent*; E. I. du pont de Nemours and Company: U. S. A., 2001.

(4) Herrmann, W. A.; Kocher, C. *Angew. Chem. Int. Ed. Engl* **1997**, *36*, 2163-2187.

(5) Ofele, K. *J. Organomet. Chem.* **1968**, *12*, P42-P43; Wanzlick, H. W.; Schonherr, H. J. *Angew. Chem.* **1968**, *80*, 154.

(6) Wang, H. M. J.; Lin, I. J. B. *Organometallics* **1998**, *17*, 972-975.

(7) Arduengo, A. J.; Dias, H. V. R.; Calabrese, J. C.; Davidson, F. *Organometallics* **1993**, *12*, 3405-3409; Guerret, O.; Sole, S.; Gornitzka, H.; Teichert, M.; Trinquier, G.; Bertrand, G. *J. Am. Chem. Soc.* **1997**, *119*, 6668-6669.

(8) Arnold, P. L.; Scarisbrick, A. C.; Blake, A. J.; Wilson, C. *Chem. Commun.* **2001**, 2340-2341.

(9) Garrison, J. C.; Simons, R. S.; Talley, J. M.; Wesdemiotis, C.; Tessier, C. A.; Youngs, W. J. *Organometallics* **2001**, *20*, 1276-1278.

(10) Frankel, R.; Kniczek, J.; Ponikwar, W.; Noth, H.; Polborn, K.; Fehlhammer, W. P. *Inorg. Chim. Acta* **2001**, *312*, 23-39.

(11) Tulloch, A. A. D.; Danopoulos, A. A.; Kleinhenz, S.; Light, M. E.; Hursthouse, M. B.; Eastham, G. *Organometallics* **2001**, *20*, 2027-2031.

(12) Lee, K. M.; Lee, C. K.; Lin, I. J. B. *Angew. Chem. Int. Ed. Engl* **1997**, *36*, 1850-1852; Raubenheimer, H. G.; Olivier, P. J.; Lindeque, L.; Desmet, M.; Hrusak,

J.; Kruger, G. J. *J. Organomet. Chem.* **1997**, *544*, 91-100; Wang, H. M. J.; Chen, C. Y. L.; Lin, I. J. B. *Organometallics* **1999**, *18*, 1216-1223.

(13) Herrmann, W. A. *Angew. Chem.-Int. Edit.* **2002**, *41*, 1291-1309.

(14) Arduengo, A. J. *Acc. Chem. Res.* **1999**, *32*, 913-921.

(15) Arduengo, A. J.; Harlow, R. L.; Kline, M. *J. Am. Chem. Soc.* **1991**, *113*, 361-363; Bourissou, D.; Guerret, O.; Gabbai, F. P.; Bertrand, G. *Chem. Rev.* **2000**, *100*, 39-91.

(16) Grundemann, S.; Kovacevic, A.; Albrecht, M.; Faller, J. W.; Crabtree, R. H. *Chem. Commun.* **2001**, 2274-2275; Grundemann, S.; Kovacevic, A.; Albrecht, M.; Faller, J. W.; Crabtree, R. H. *J. Am. Chem. Soc.* **2002**, *124*, 10473-10481.

(17) Jacobi, A.; Huttner, G.; Winterhalter, U.; Cunskis, S. *Eur. J. Inorg. Chem.* **1998**, 675-692.

(18) Schlosser, M.; Hartmann, J. *Angew. Chem.* **1973**, *85*, 544-545; Kubas, G. J. *Inorganic Synthesis* **1979**, *19*, 90-92.

Chapter 3. A Nitrogen-Anchored Tripodal N-Heterocyclic Carbene Ligand System and Its Coordination to Copper

3.1. Introduction

In an effort to develop potent tris(carbene) ligand systems for transition metal coordination and application in small molecule activation and homogeneous catalysis, we have synthesized the ligand system 1,1,1-[tris(3-alkylimidazol-2-ylidene)methyl]-ethane ($TIME^{R}$, R = Me, *t*-Bu) and explored its coordination chemistry. With group 11 metal ions the methyl derivative $TIME^{Me}$ exclusively forms isostructural complexes of the general type $[(TIME^{Me})_2M_3]^{3+}$ (M = Cu, Ag, Au), comprising two-coordinate metal centers with a linear binding mode. The sterically more demanding *tert*-butyl derivatized ligand system $TIME^{t\text{-}Bu}$ induces the formation of an interesting dinuclear copper(I) bis(carbene)alkenyl complex, $[(TIME^{t\text{-}Bu})_2Cu_2]^{2+}$ (Chapter 2). These findings demonstrate the versatility of TIME ligands, yet, in our hands, mononuclear metal complexes of these carbon-anchored chelators remained elusive.

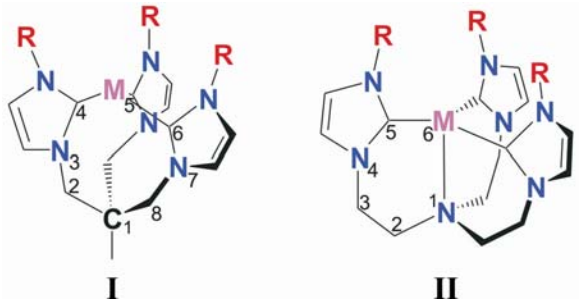

Figure 3-1. Structural models for metal complexes of tripodal C- and N-anchored carbene chelators

Examination of the backbones of the neopentane-based, carbon-anchored tripodal ligands reveals possible reasons for the lack of 1:1 complex formation with these chelators. A hypothetical κ^3 complex of TIME would contain three eight-

membered rings (**I**, Figure 3-1) with much lower stability than the more commonly observed five, six or seven-membered rings formed, for instance, of poly(pyrazolyl)borate[1] or poly(phosphine)[2] ligands. Consequently, the methyl derivative $TIME^{Me}$ yields highly D_3-symmetrical trinuclear complexes and has no tendency for metallacycle formation. Although increased steric bulk at the imidazole N3-position of the *tert*-butyl derivative effectively prevents the formation of trinuclear complexes, formation of three eight-membered rings is still unfavorable and mononuclear complex formation still cannot be observed. Instead, a dinuclear 2:2 complex with only one such unusual eight-membered ring per ligand molecule was isolated. In order to overcome these inherent deficits of TIME, we sought to incorporate a coordinating atom at the anchoring position of the carbene tripod, engendering ligands that favor 1:1 metal complexation by forming three stable six-membered rings (**II**, Figure 3-1). Accordingly, the nitrogen-anchored tris(carbene) ligand system tris[2-(3-alkylimidazol-2-ylidene)ethyl]amine ($TIMEN^R$, R = Me, *t*-Bu, Bz) and the corresponding copper(I) and (II) complexes were synthesized.

3.2. Results and Discussion

3.2.1 Ligand synthesis

The imidazolium precursors, tris-[2-(3-alkylmethylimidazolium-1-yl)-ethyl]amine trichloride $[H_3TIMEN^R]Cl_3$ (R = Me, *t*-Bu, and Bz), were prepared by quaternization of functionalized N-alkylimidazoles with tris-(2-chloroethyl)amine. Treatment of $[H_3TIMEN^R]Cl_3$ in methanol with ammonium hexafluorophosphate

effected complete substitution of chloride and formation of $[H_3TIMEN^R](PF_6)_3$ (**$H_3$1a**, R = Me; **$H_3$1b**, R = *t*-Bu; **$H_3$1c**, R = Bz). Highest yields for all quaternization reactions were achieved by heating the neat reactants at 150 ^oC for 2 days. Deprotonation of **$H_3$1a** with strong base fails to produce free carbene ligand **1a**, however, a copper(I) complex of this ligand is accessible via a transmetallation route[3] employing the corresponding silver complex of this ligand (vide infra). Deprotonation of **$H_3$1b** and **$H_3$1c** with potassium *tert*-butoxide yielded free tris(carbene) ligands **1b** and **1c**, which can be isolated and stored under nitrogen for further transformation. Ligands **1b** and **1c** were characterized by ^1H and ^{13}C NMR spectroscopy. The characteristic ^{13}C signals for the deprotonated carbene carbon atoms were found at δ = 213.6 (**1b**) and 211.8 ppm (**1c**).

3.2.2. Synthesis and characterization of trinuclear $[(TIMEN^{Me})_2Cu_3](PF_6)_3$

Reaction of the methyl derivatized $[H_3TIMEN^{Me}](PF_6)_3$ imidazolium salt **$H_3$1a,** with Ag_2O in DMSO at 75 ^oC yielded a silver complex, $[(TIMEN^{Me})_2Ag_3]$-$(PF_6)_3$ (**2**). Although crystals suitable for X-ray diffraction study were not obtained, complex **2** likely is iso-structural with $[(TIME^{Me})_2M_3]^{3+}$ based on the similarity of characteristic features in their ^1H and ^{13}C NMR spectra. Treatment of **2** with three equivalents of CuBr in acetonitrile led to formation of a copper(I) complex $[(TIMEN^{Me})_2Cu_3](PF_6)_3$ • 2.5 CH_3CN (**3**) (Scheme 3-1). The solid-state structure of **3** • 2.5 CH_3CN reveals a trinuclear complex with two distinctly different coordination geometries of the cuprous ions (Figure 3-2).

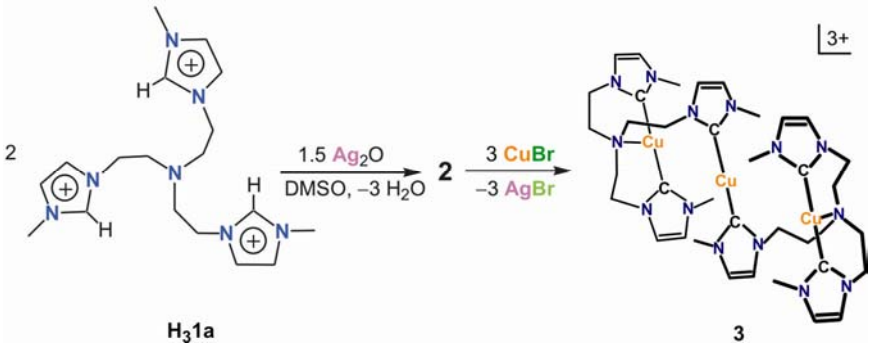

Scheme 3-1. Synthesis of Trinuclear Complex $[(TIMEN^{Me})_2Cu_3](PF_6)_3$ (**3**).

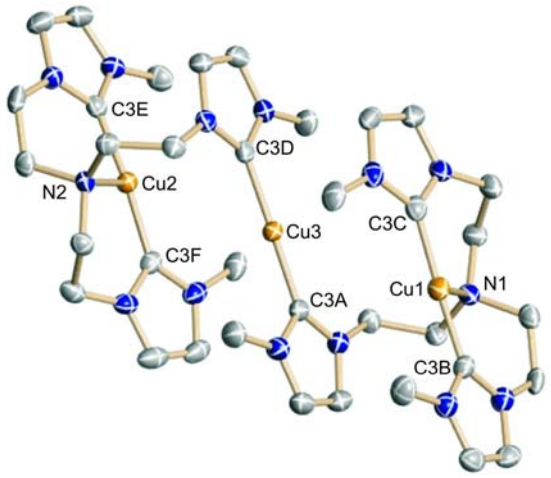

Figure 3-2. Solid-state molecular structure of complex $[(TIMEN^{Me})_2Cu_3](PF_6)_3 \cdot 2.5\ CH_3CN$ (**3** · 2.5 CH_3CN). Hydrogen atoms, anions, and solvent molecules are omitted for clarity; thermal ellipsoids are shown at 50% probability. Selected bond lengths (Å) and angles (deg.): Cu(1)-C(3B) 1.901(4), Cu(1)-C(3C) 1.894(5), Cu(1)-N(1) 2.365(3), Cu(2)-C(3E) 1.892(4), Cu(2)-C(3F) 1.891(4), Cu(2)-N(2) 2.371(3), Cu(3)-C(3A) 1.909(4), Cu(3)-C(3D) 1.910(4), C(3B)-Cu(1)-C(3C) 172.54(19), C(3E)-Cu(2)-C(3F) 166.50(17), C(3A)-Cu(3)-C(3D) 178.74(17).

Each $TIMEN^{Me}$ ligand exhibits coordination to two different Cu(I) centers in nearly centro-symmetric fashion without a crystallographic inversion center. Two of the three pendent carbene ligators and the anchoring nitrogen atom of one ligand

molecule coordinate to one Cu(I) ion to give a T-shaped ligand environment. The third carbene, together with that of the second ligand, coordinates to a central Cu(I) ion in linear fashion. The latter feature is reminiscent to the linear C—M—C fragments in $[(TIME^{Me})_2M_3]^{3+}$.

The Cu—C distances in **3** range between 1.889 – 1.902 Å for the three-coordinate copper ions and 1.908 – 1.911 Å for the two-coordinate copper ions. These values compare well to those found for other reported Cu-NHC complexes.[4] The average Cu—N distance of 2.365 Å for both three-coordinate copper ions is significantly longer than values typically found for tris(2-aminoethyl)amine-based copper(I) complexes of ~2.2 Å.[5] This weak interaction of the nitrogen anchor with the copper ions is also reflected in the crystallographically determined, near linear $C_{carbene}$—Cu–$C_{carbene}$ angles of ~170° for the three-coordinate cuprous and ~180° for the two-coordinate Cu(I) ions. As a result of this weak but significant Cu—N(anchor) interaction, each $TIMEN^{Me}$ ligand forms two of the expected three six-membered rings with one copper ion. Overall, however, formation of the unique structure of **3** was unexpected since no obvious steric hindrance appears to be preventing a 1:1 metal complex formation of the methyl-substituted derivative. We therefore conclude that formation of complex **3** is kinetically controlled. This is likely due to the presence of excess Cu(I) ions in solution resulting from the transmetallation reaction of trinuclear **3** with 3 equivalents of Cu(I) salt to eliminate 3 equiv. of AgBr.

3.2.3. Synthesis and characterization of mononuclear $[(TIMEN^{R})Cu]^{+}$

Reaction of free carbene $TIMEN^{t\text{-}Bu}$ **1b** with one equivalent of $[(CH_3CN)_4Cu](PF_6)$ in acetonitrile afforded the mononuclear 1:1 copper complex **4b** as an off-white powder in high yields (~ 60%) (Scheme 3-2).

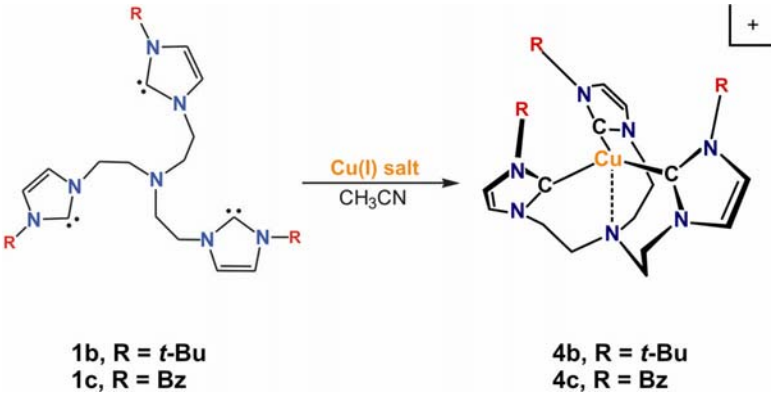

Scheme 3-2. Synthesis of Mononuclear Complexes $[(TIMEN^{R})Cu]^{+}$ (R = *t*-Bu, Bz)

The solid-state structure of mononuclear tris(carbene) copper complex **4b** was determined by single-crystal X-ray diffraction analysis (Figure 3-3). The tripodal carbene ligand **1b** coordinates to the copper ion via the three carbenoid carbons in the predicted tridentate fashion. The long Cu—N distance of 2.567(3) Å and a displacement towards the N-anchor of only 0.02 Å out of the idealized trigonal plane suggest that the interaction of the anchoring nitrogen atom with the copper ion is electronically non-significant. This interaction, however, does stabilize compound **4b** structurally, as it leads to the formation of three six-membered metallacycles (Scheme 3-2). This copper(I) complex represents the first example of a 1:1 transition metal

complex of a polydentate tris(carbene) ligand. The average Cu—$C_{carbene}$ distance of 1.985 Å is slightly longer than that of complex **3**, consistent with the presence of three sterically demanding *tert*-butyl groups at the N3 positions of the imidazole rings. The copper(I) ion is located in an ideal trigonal planar ligand environment with an average C—Cu—C angle of 119.99°.

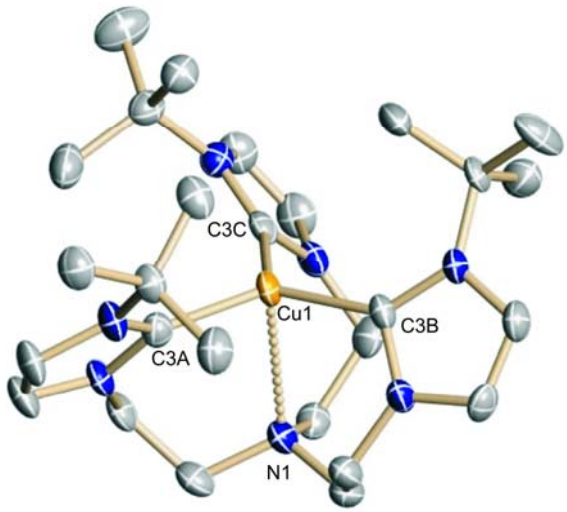

Figure 3-3. Solid-state molecular structure of complex [(TIMEN$^{t\text{-Bu}}$)Cu](PF$_6$) (**4b**). Hydrogen atoms and anions are omitted for clarity; thermal ellipsoids are shown at 50% probability. Selected bond lengths (Å) and angles (deg.): Cu(1)-C(3A) 1.976(3), Cu(1)-C(3B) 1.987(3), Cu(1)-C(3C) 1.993(3), Cu(1)-N(1) 2.567(3), C(3A)-Cu(1)-C(3B) 120.03(12), C(3A)-Cu(1)-C(3C) 117.96(12), C(3B)-Cu(1)-C(3C) 121.98(12).

The NMR spectra of **4b** are consistent with the solid-state structure determined by X-ray crystallography. In the ^{1}H spectrum, the six C4/C5 protons of the imidazole rings give rise to two sets of doublets with equal intensity at δ = 7.19 and 6.92 ppm, and the three *tert*-butyl groups give rise to only one intense signal at δ = 1.52 ppm,

indicative of a C_3 symmetrical molecule in solution. The twelve protons of the ethylene backbones of **4b** give rise to four doublets of doublets with equal intensity and are observed at δ = 3.67, 3.43, 2.90, and 2.34 ppm, respectively. The ^{13}C spectrum exhibits only one signal for the carbenoid carbon at δ = 187 ppm.

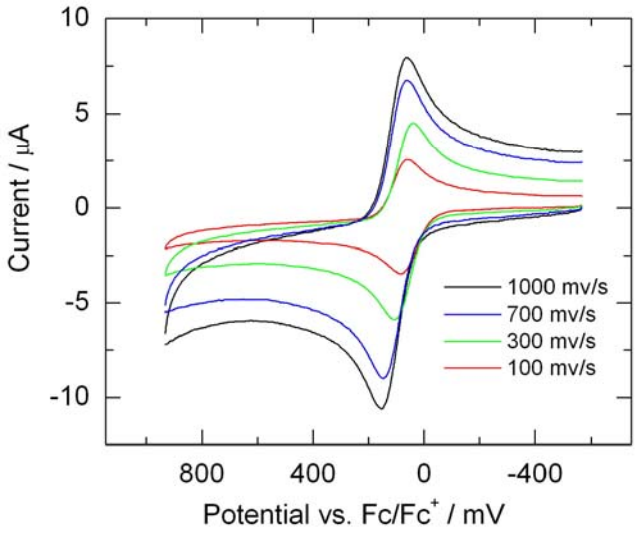

Figure 3-4. Cyclic voltammogram of [(TIMEN$^{t\text{-Bu}}$)Cu](PF$_6$) (**4b**) recorded in acetonitrile solution containing 0.1 M [N(*n*-Bu)$_4$](ClO$_4$) as electrolyte.

The redox behavior of the novel mononuclear compound was examined by electrochemical methods. The cyclic voltammogram of a solution of **4b** in acetonitrile exhibits a reversible one-electron oxidation at a potential of +110 mV vs. Fc/Fc$^+$ (Figure 3-4). The reversibility for the Cu(I)/Cu(II) couple was confirmed by measuring the ratios of I_{ox}/I_{red} as a function of scan rates and the peak separation. For all scan rates, values for I_{ox}/I_{red} were determined to be approx. 1. The peak separation,

$|E_{ox}-E_{red}|$ at 300 mVs^{-1}, was calculated to be 66 mV. This reversible redox behavior indicates that the TIMEN$^{t\text{-Bu}}$ ligand has sufficient structural and electronic flexibility to accommodate the copper ion in both the Cu(I) and Cu(II) oxidation states.

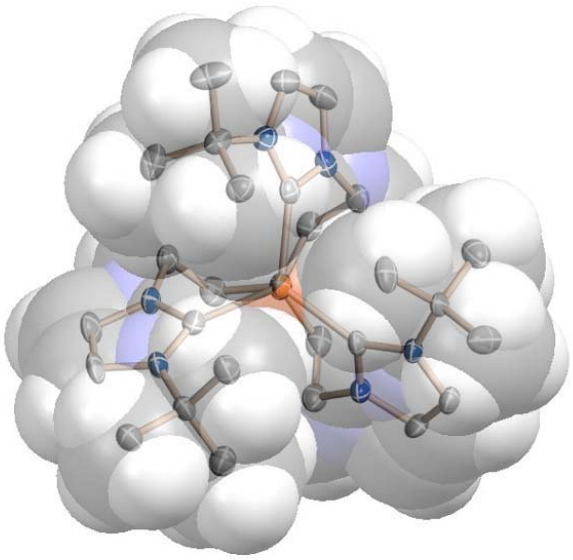

Figure 3-5. Space filling model for [(TIMEN$^{t\text{-Bu}}$)Cu](PF_6) (**4b**).

A space-filling model of complex **4b** (Figure 3-5) suggests that the electron-rich cuprous ion in this complex is well shielded by the three sterically encumbering *tert*-butyl groups. In order to facilitate reactivity at the electron-rich metal center, a Cu(I) complex with the sterically less demanding benzyl-substituted TIMEN^{Bz} ligand, [(TIMEN^{Bz})Cu]Br (**4c**), was synthesized by reacting free carbene **5c** with copper(I) bromide (Scheme 3-2).

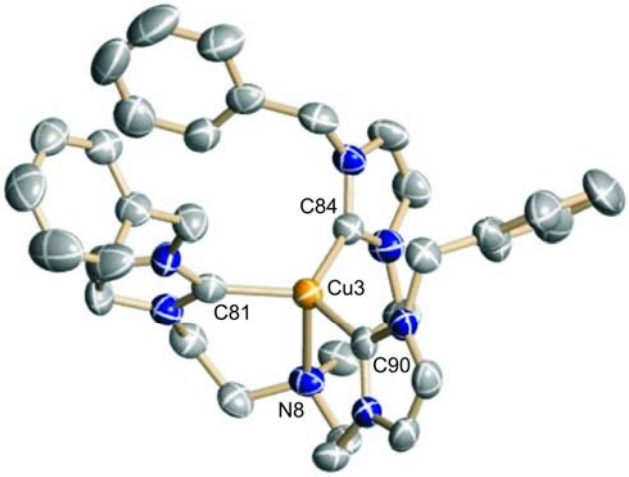

Figure 3-6. Solid-state molecular structure of complex [(TIMEN^{Bz})Cu](Br) (**4c**). Mononuclear **4c** crystallizes with three independent molecules per unit cell, in which bond lengths and angles vary slightly. Hydrogen atoms, anions, and the remaining two independent molecules are omitted for clarity; thermal ellipsoids are shown at 50% probability. Selected bond lengths (Å) and angles (deg.): Cu-$C_{carbene}$ (av.) 1.949, 1.961, and 1.965, Cu-N_{amine} 2.365(4), 2.399(4), and 2.482(4), N-$C_{carbene}$-N (av.) 103.10, 102.78, and 102.61, C-Cu-C (av.) 119.91, 119.68, and 119.56.

The molecular structure of compound **4c** was determined by single-crystal X-ray diffraction study. Complex **4c** crystallizes with three independent molecules in the asymmetric unit. The solid-state structure of one of the three independent molecules is depicted in Figure 3-6. The average Cu-C bond length of 1.958 Å is slightly shorter than that of complex **11b**, consistent with reduced steric bulk of the benzyl substituents. The average Cu(I)-N(amine) interaction of 2.415 Å in **4c**, however, is considerably stronger than that of 2.567(3) Å in **4b.** The space filling model (Figure 3-7) shows the expected open cavity at the Cu(I) ion exposed by the three less protective benzyl groups. The cyclic voltammogram of complex **4c** exhibits a

reversible one-electron oxidation at –100 mV vs. Fc/Fc^{+}; 210 mV lower than that of **4b** (Figure 3-8). The benzyl-substituted ligand **2c** thus seems to be significantly more flexible with regard to structural changes upon oxidation.

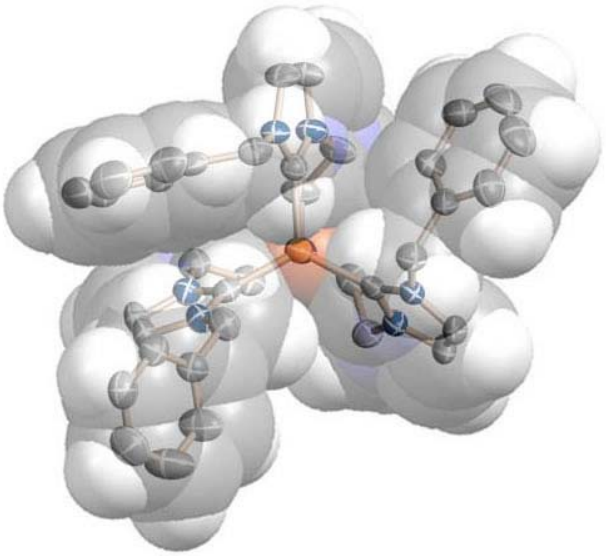

Figure 3-7. Space filling model for [(TIMEN^{Bz})Cu](Br) (**4c**).

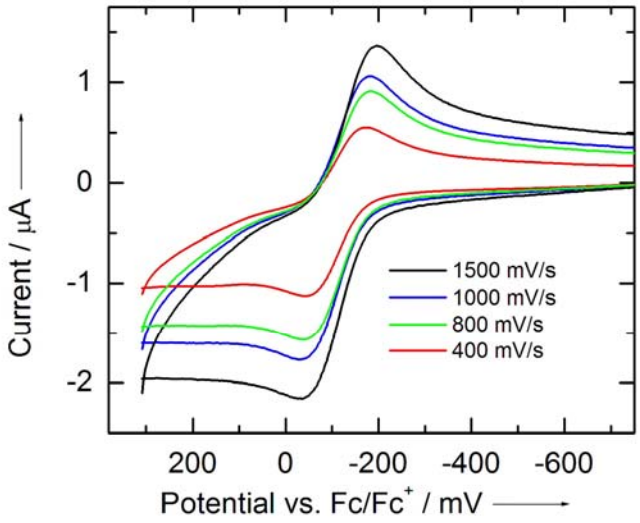

Figure 3-8. Cyclic voltammogram of [(TIMEN^{Bz})Cu](Br) (**4c**) recorded in acetonitrile solution containing 0.1 M [N(*n*-Bu)$_4$](ClO$_4$) as electrolyte.

3.2.4. Synthesis and characterization of [(TIMEN^{Bz})Cu](OTf)$_2$.

The one-electron oxidized corresponding Cu(II) complex, [(TIMEN^{Bz})Cu](OTf)$_2$ (**5**) was synthesized via two different, independent routes. The complex could be obtained by either oxidizing **4c** with silver(I) triflate, or alternatively, by reacting ligand **1c** with copper(II) triflate. Reaction of **1c** with other copper(II) salts, for instance copper(II) bromide, led to formation of unidentified diamagnetic materials.

Paramagnetic compound **5** was characterized by elemental analysis, low-temperature X-band EPR spectroscopy and variable temperature SQUID magnetization measurements. The X-band EPR spectrum of **5,** recorded in frozen acetonitrile/toluene solution at 8 K, exhibits a rhombic signal (Figure 3-9, top). The signal can be simulated to high accuracy with $g_1 = 2.005$, $g_2 = 2.060$ and $g_3 = 2.275$, and a copper hyperfine coupling constant A_3(^{53}Cu, I = 3/2, 100%) of 132 x 10^{-4} cm^{-1} (397 MHz). Copper hyperfine interaction on g_1 and g_2 are not resolved. The EPR spectrum of **5** is consistent with a mononuclear copper(II) complex having one unpaired electron.

The solid-state magnetization measurement of solid samples of **5** confirms the copper(II) oxidation state of the complex. The temperature dependency of the magnetic moment was determined in the temperature range from 5 to 300 K (Figure 3-9, bottom). At room temperature, complex **5** exhibits a magnetic moment of 1.86 μ_B,

which is in good agreement with the calculated value of 1.83 μ_B obtained by applying the average g value of 2.11 determined by EPR spectroscopy. The magnetic moment of 1.86 μ_B at room temperature decreases slightly to ~ 1.71 μ_B at 100 K, then continues to decrease reaching a minimum of 0.91 μ_B at 5 K. This observed temperature behavior indicates weak antiferromagnetic spin-spin coupling in the solid state.

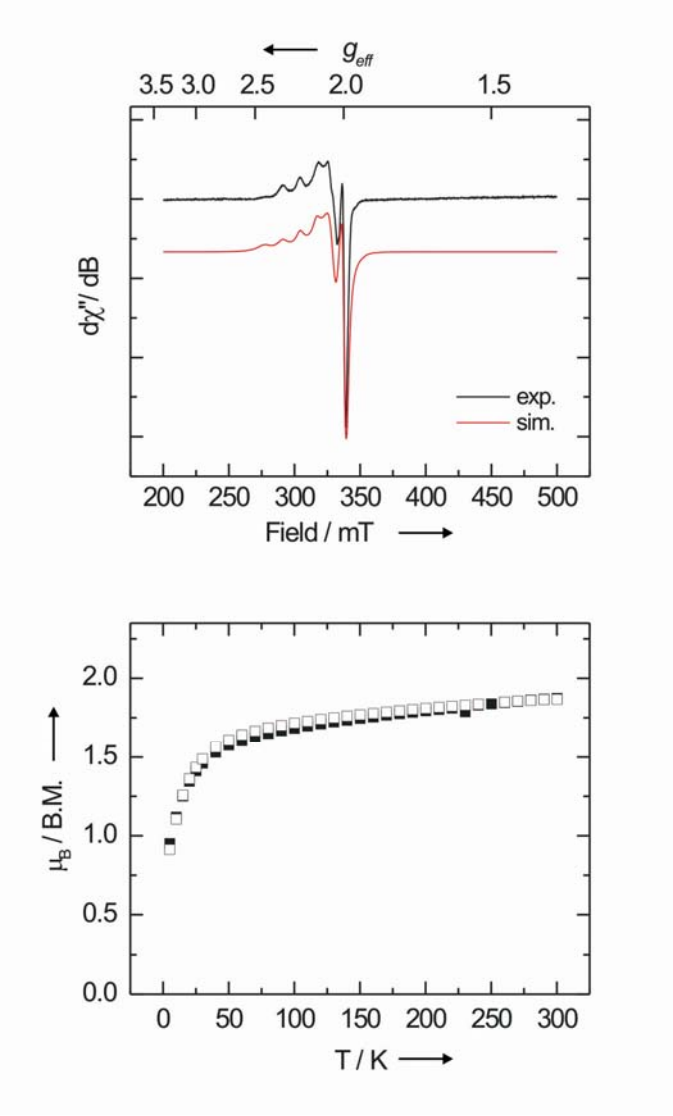

Figure 3-9. X-band EPR spectrum of **5** (top) recorded in frozen acetonitrile/toluene solution at 8 K. Experimental conditions: microwave frequency ν: 9.4666 GHz,

power: 0.63 mW, modulation amplitude: 10 G. Simulated parameters: $g_1 = 2.005$ ($W_1 = 20.00$ G); $g_2 = 2.060$ ($W_2 = 55.00$ G); $g_3 = 2.275$ ($W_3 = 42.00$ G); $A_3 = 132 \times 10^{-4}$ cm^{-1} (397.00 MHz). Plot of the effective magnetic moment, μ_{eff}, versus temperature from temperature-dependent SQUID magnetization measurements for two independently prepared samples of **5** (bottom).

The results from EPR spectroscopy and SQUID magnetization measurements suggest that the unpaired electron in complex **5** resides in the copper $3d(x^2\text{-}y^2)$ orbital. The ground-state electronic structure of **5** was further elucidated with the aid of DFT calculations. Our DFT studies (BP86/TZP, ZORA, ADF 2003.01) on the model complex $[TIMEN^{Me}Cu]^{2+}$ indicate that the copper(II) ion in **5** retains the trigonal-planar ligand environment, with a weak axial Cu-N(amine) interaction ($d_{calcd.}$ Cu-N = 2.54 Å) (Figure 3-10, top). The CuC_3 plane, however, exhibits a Jahn-Teller distortion, rendering one C-Cu-C angle significantly larger (139.7°) than the other two (112.5° and 107.4°). A similar distortion is found in the copper-carbene bond distances. The Cu-C bond opposite to the largest C-Cu-C angle is significantly longer (1.965 Å) than the two Cu-C bonds at 1.935 and 1.936 Å, respectively. This distortion in the Cu-C_3 plane raises the energy of the metal *d*-orbital $d(x^2\text{-}y^2)$ above $d(xy)$ and $d(z^2)$ and thus removes the degeneracy of the $d(x^2\text{-}y^2)$ and $d(xy)$ orbitals. This departure from an idealized trigonal plane, as seen in the Cu(I) complexes of this ligand system, results in a $d(xz)^2d(yz)^2d(xy)^2d(z^2)^2d(x^2\text{-}y^2)^1$ ground-state electronic configuration for the geometry-optimized complex $[TIMEN^{Me}Cu]^{2+}$. The singly occupied molecular orbital (SOMO) is depicted in Figure 3-10, bottom.

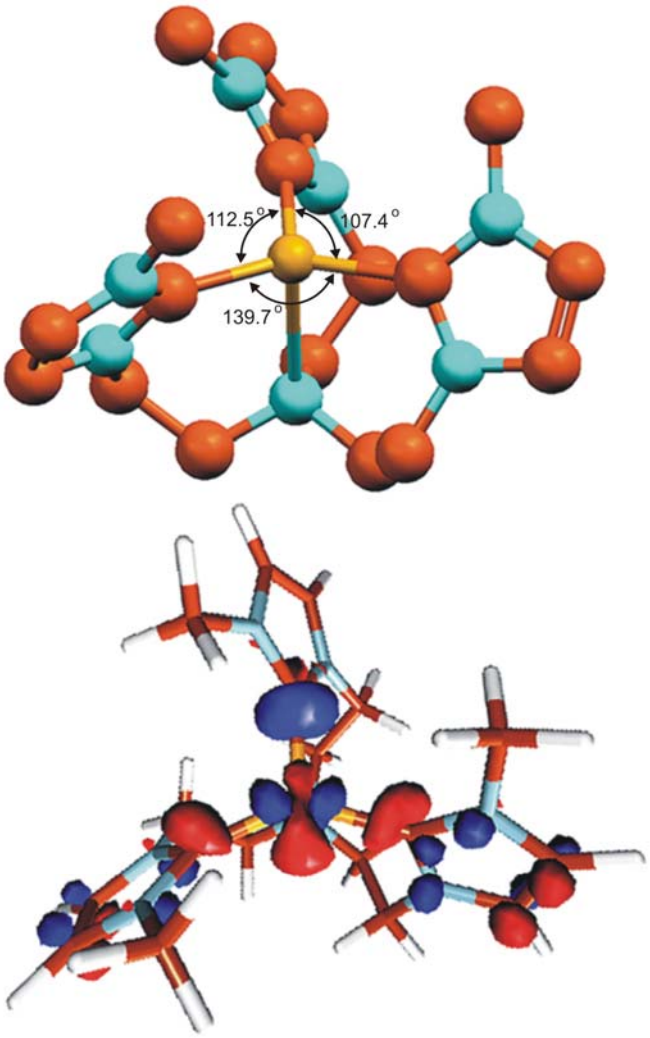

Figure 3-10. Geometry-optimized structure of model compound $[TIMEN^{Me}Cu]^{2+}$ (top) and singly occupied molecular orbital (SOMO) in the system of complex $[TIMEN^{Me}Cu]^{2+}$ (bottom).

3.2.4. Reactivity survey of $[(TIMEN)Cu]^{+}$

Copper(I) complexes **4b-c** were subjected to a variety of reactivity tests. Unfortunately, they are inert towards small molecules such as carbon monoxide,

carbon dioxide, or dihydrogen and they also do not react with trimethylsilyl azide, diazoethylacetate, diphenyldiazomethane, or methyl iodide. Treatment of **4b - c** with dioxygen yielded un-identified products over time. It thus appears that the copper(I) complex **4b – c,** with the trigonal-pyramidal ligand environment of three carbene centers and one additional nitrogen donor provided by TIMEN ligands is too stable and does not allow for further chemical reactivity. This is not too surprising given that the copper(I) ion in these complexes has 18 valence electrons and is encapsulated in a well-protected cavity.

Similarly, the reactivity of copper(II) complex **5** was also investigated but no well-defined reactivity could be observed.

3.3. Conclusion

In summary, strikingly different Cu(I) complexes have been synthesized by employing three derivatives of the same tripodal, tris(carbene) ligand system tris[2-(3-alkylimidazol-2-ylidene)ethyl]amine ($TIMEN^{R}$, R = Me, *t*-Bu, Bz). The methyl substituted ligand, $TIMEN^{Me}$ (**1a**), yields, via a transmetallation route, the trinuclear complex $[(TIMEN^{Me})_2Cu_3]^{3+}$ (**3**) comprising both T-shaped three-coordinate and linear two-coordinate copper(I) centers. In contrast, the sterically more encumbering *tert*-butyl and benzyl derivatized free carbenes $TIMEN^{t\text{-}Bu}$ (**1b**) and $TIMEN^{Bz}$ (**1c**) induce the formation of mononuclear complexes, $[(TIMEN^{R})Cu]^{+}$ (**4b**, R = *t*-Bu; **4c**, R = Bz). To the best of our knowledge, mononuclear complexes **4b** and **4c** represent the first examples of a 1:1 transition metal complex of a polydentate tris(carbene) ligand.

The trigonal planar carbene environment of the Cu(I) and Cu(II) metal centers in all mononuclear complexes presented herein are unprecedented in NHC coordination chemistry. Complex **5** represents the first isolated and spectroscopically characterized copper(II) NHC complex to date.

The successful synthesis of free carbenes derivatized from TIMEN ligand system and their 1:1 copper(I) complexes reprents a breakthrough in our study of tripodal NHC ligands: we were able to prepare several 1:1 metal tris(carbene) complexes and found a simple, versatile, and modular route to monomeric transition metal complexes of tripodal NHCs. The copper complexes were found to be unreactive and therefore have little application in small molecule activation chemistry. We thus decide to explore the coordination of TIMEN ligands with other transition metals.

3.4. Experimental Section

Methods and Procedures

Manipulation of air-sensitive compounds was performed under a controlled dry nitrogen atmosphere using standard Schlenk techniques and inert-gas glove boxes (MBraun Labmaster by M. Braun, Inc.). Solvents were purified using a two-column solid-state purification system (Glasscontour System, Joerg Meyer, Irvine, CA) and transferred to the glove box without exposure to air. NMR solvents were obtained from Cambridge Isotope Laboratories, degassed, and stored over activated molecular sieves prior to use. All NMR spectra were recorded at room temperature (20^{o}C) in d_6-

benzene, d_3-acetonitrile and d_6-DMSO solutions on Varian spectrometers operating at 400/300 MHz (^{1}H NMR) and 100 MHz (^{13}C NMR) and referenced to residual solvent peaks unless otherwise noted (δ in ppm). Cyclic voltammetric measurements were performed on Bioanalytical Systems equipment (BAS, CV-50W) in acetonitrile solutions containing 0.1 M [N(*n*-Bu)$_4$](ClO$_4$) as electrolyte (working electrode: platinum; auxiliary electrode: platinum wire; reference electrode: platinum). Potentials are reported relative to the ferrocene/ferrocenium couple (Fc/Fc$^+$). X-band EPR spectra of dilute complex solutions in a 1:1 mixture of acetonitrile and toluene were recorded on a Bruker Elexsys E500 spectrometer equipped with a helium flow cryostat (Oxford 900). The spectra were simulated using the W95EPR program.[6] Solid-state magnetization measurements of powdered samples were recorded on a SQUID magnetometer (Quantum Design) at 10 kOe between 5 and 300 K. Magnetic susceptibility data were corrected for background and underlying diamagnetic contributions (χ_{dia} = -515 x 10^{-6} cm^{3}mol^{-1}) using tabulated Pascal constants.[7] Data reproducibility was carefully checked in multiple individual measurements of independently synthesized samples. Elemental analyses were performed by Kolbe Microanalytical Laboratory (Muelheim a. d. Ruhr/Germany).

Computational Details. DFT calculations were carried out using the Amsterdam Density Functional program package ADF, release 2003.01.[8] The Vosko, Wilk and Nusair (VWN) local density approximation,[9] Becke's exchange correlation,[10] and Perdew correlation[11] were used. The calculation also included scalar relativistic effects (ZORA)[12] for all atoms. Uncontracted Slater-type Orbitals

(STOs)[13] were used as basis functions. Cu: triple-ζ basis set augmented with a set of *p* functions and frozen core 2*p*. N: triple-ζ basis set augmented with a set of *d* functions and frozen core 1*s*. C: triple ζ-basis set augmented with a set of *d* functions and frozen core 1*s*. O: triple ζ-basis set augmented with a set of *d* functions and frozen core 1*s*. H: triple-ζ basis set augmented with a set of *p* functions. This basis combination is denoted TZP in the ADF program.

For computational economy, calculations were performed on model complex **5m**, in which the three benzyl substitutents on the TIMEN ligand were replaced by methyl groups. No symmetry was specified in the calculations; the counter anion was not included.

Molecular orbitals were visualized using the MOLDEN program package (http://www.cmbi.kun.nl/~schaft/molden/molden.html). ADFrom program was used to convert the TAPE21 file from ADF into a MOLDEN file.

Synthesis:

Starting Materials. N-*tert*-butylimidazole,[14] tris(2-chloroethyl)amine,[15] and tetrakis(acetonitrile)copper(I) hexafluorophosphate[16] were prepared according to literature procedures. N-methylimidazole (Acros), N-benzylimidazole (Aldrich), silver oxide (Fischer), silver triflate (Strem), copper(I) bromide (Acros), copper(II) triflate (Strem), potassium *tert*-butoxide (Acros), ammonium hexafluorophosphate (Aldrich), and tetra(*n*-butyl)ammonium perchlorate (Aldrich) were obtained from commercial sources and used as received.

$[H_3TIMEN^{Me}](PF_6)_3$ ($H_3$1a): A 50 mL flask was charged with tris(2-chloroethyl)amine (4.1 g, 20 mmol) and N-methylimidazole (4.95 g, 60 mmol) and the mixture was heated to 150 °C for 2 days during which a brown solid formed. The solid was filtered off, dissolved in 20 mL methanol and the filtered solution was evaporated to dryness to yield the crude product $[H_3TIMEN^{Me}]Cl_3$ (6.0 g, yield: 67%). The hygroscopic chloride salt was converted to the corresponding, stable hexafluorophosphate salt, $[H_3TIMEN^{Me}](PF_6)_3$, by adding solid NH_4PF_6 (6.5 g, 40.6 mmol) to a solution of $[H_3TIMEN^{Me}]Cl_3$ (6.9 g, 13.3 mmol) in 20 mL methanol. The white hexafluorophosphate salt precipitated immediately, was collected by filtration, washed with small portions of cold methanol, and dried in vacuum. (8.5 g; yield: 82%). ^{1}H NMR (300 MHz, d_6-DMSO, 20 °C): δ = 8.94 (s, 3H), 7.67 (s, 3H), 7.58 (s, 3H), 4.19 (t, ^3J(H,H) = 6.0 Hz, 6H), 3.84 (s, 9H), 2.95 ppm (t, ^3J(H,H) = 6.0 Hz, 6H). ^{13}C NMR (100 MHz, d_6-DMSO, 20 ^{o}C): δ = 136.7, 123.0, 122.3, 52.1, 45.9, 35.8 ppm. Elemental analysis (%) calcd for $C_{18}H_{30}F_{18}N_7P_3$**:** C 27.74, H 3.88, N 12.58; found: C 28.10, H 3.92, N 12.61.

$[H_3TIMEN^{t\text{-}Bu}](PF_6)_3$ ($H_3$1b): A 50 mL flask was charged with tris(2-chloroethyl)amine (2.1 g, 10 mmol) and N-*tert*-butylimidazole (3.9 g, 31 mmol) and the mixture was heated to 150 °C for 3 days during which a brown solid formed. The solid was filtered off, dissolved in 20 mL methanol and the filtered solution was evaporated to dryness to yield the crude product $[H_3TIMEN^{t\text{-}Bu}]Cl_3$ (5.6 g; Yield: 97%). The hygroscopic chloride salt was converted to stable $[H_3TIMEN^{t\text{-}Bu}](PF_6)_3$ by adding NH_4PF_6 (4.8g, 29.4 mmol) to a solution of $[H_3TIMEN^{t\text{-}Bu}]Cl_3$ (5.6 g, 9.7

mmol) in 20 mL methanol. The white hexafluorophosphate salt precipitated immediately, was collected by filtration, washed with small portions of cold methanol, and dried in vacuum (6.7 g; Yield: 76%). ^{1}H NMR (300 MHz, d_6-DMSO, 20 °C): δ = 9.19 (s, 3H), 7.99 (s, 3H), 7.66 (s, 3H), 4.14 (t, ^{3}J (H,H) = 6.0 Hz, 6H), 2.99 (t, ^{3}J(H,H) = 6.0 Hz, 6H), 1.57 ppm (s, 27H). ^{13}C NMR (100 MHz, d_6-DMSO, 20 ^{o}C): δ = 134.3, 122.7, 122.0, 59.6, 52.1, 46.0, 29.0 ppm. Elemental analysis (%) calcd for $C_{27}H_{48}F_{18}N_7P_3$**:** C 35.81, H 5.34, N 10.83; found: C 35.48, H 5.02, N 10.90.

[H$_3$TIMEN^{Bz}](PF$_6$)$_3$ (H$_3$1c): A 50 mL flask was charged with tris(2-chloroethyl)amine (9.85 g, 48.2 mmol) and N-benzylmethylimidazole (22.9 g, 144.8 mmol) and the mixture was heated to 150 °C for 2 days during which a brown solid formed. The solid was isolated, dissolved in 100 mL methanol and the filtered solution was evaporated to dryness to yield the crude product [H_3TIMEN^{Bz}]Cl_3 (32 g; Yield: 98%). The hygroscopic chloride salt was converted to stable [H_3TIMEN^{Bz}](PF_6)$_3$ by adding NH_4PF_6 (22.6 g, 29.4 mmol) to a solution of [H_3TIMEN^{Bz}]Cl_3 (32 g, 47.1 mmol) in 50 mL methanol. The white hexafluorophosphate salt precipitated immediately, was collected by filtration, washed with small portions of cold methanol, and dried in vacuum (39.6 g; Yield: 81%). ^{1}H NMR (300 MHz, d_6-DMSO, 20 °C): δ = 9.20 (s, 3H), 7.76 (s, 3H), 7.63 (s, 3H), 7.37 (m, 15s), 5.41 (s, 6H), 4.13 (t, ^{3}J (H,H) = 6.0 Hz, 6H), 2.93 (t, ^{3}J(H,H) = 6.0 Hz, 6H). ^{13}C NMR (100 MHz, d_6-DMSO, 20 ^{o}C): δ = 136.0, 134.5, 128.8, 128.6, 128.1, 122.8, 122.1, 52.0, 51.8, 46.2 ppm. Elemental analysis (%) calcd for $C_{36}H_{42}F_{18}N_7P_3$**:** C 42.91, H 4.20, N 9.73; found: C 43.30, H 4.19, N 9.87.

[TIMEN$^{t\text{-Bu}}$] (1b): A solution of potassium *tert*-butoxide (0.15 g, 1.35mmol) in THF was added dropwise to a suspension of **$H_3$1b** (0.41 g, 0.45 mmol) in 5 mL THF. A clear colorless solution was formed upon addition of the base. The solution was evaporated to dryness and the white residue was dissolved in 15 mL of diethyl ether. The resulting solution was filtered and the filtrate was evaporated to dryness in vacuum. The white solid was collected, washed with cold pentane, and dried in vacuum (0.15 g; Yield: 71%). ^{1}H NMR (400 MHz, d_6-Benzene, 20 °C): δ = 6.67 (d, ^3J(H,H) = 2.0 Hz, 3H), 6.42 (d, ^3J(H,H) = 2.0 Hz, 3H), 3.84 (t, ^3J(H,H) = 6.0 Hz, 6H), 2.71 (t, ^3J(H,H) = 6.0 Hz, 6H), 1.49 (s, 27H,). ^{13}C NMR (100 MHz, d_6-Benzene, 20 ^{o}C): δ = 213.6, 119.9, 115.3, 57.5, 56.3, 50.5, 32.1 ppm. Elemental analysis (%) calcd for $C_{27}H_{45}N_7$**:** C 69.34, H 9.70, N 20.96; found: C 69.28, H 9.71, N 21.08.

[TIMEN^{Bz}] (1c): A solution of potassium *tert*-butoxide (0.14 g, 1.2 mmol) in THF was added dropwise to a suspension of **$H_3$1c** (0.40 g, 0.4 mmol) in 5 mL THF. A clear colorless solution was formed upon addition of the base. The solution was evaporated to dryness and the white residue was dissolved in 15 mL of diethyl ether. The resulting solution was filtered and the filtrate was evaporated to yield a slightly yellow oily compound (0.16 g; Yield: 70 %). ^{1}H NMR (400 MHz, d_6-Benzene, 20 °C): δ = 7.1 (m, 15H), 6.49 (d, ^3J(H,H) = 2.0 Hz, 3H), 6.22 (d, ^3J(H,H) = 2.0 Hz, 3H), 4.99 (s, 6H), 3.86 (t, ^3J(H,H) = 6.0 Hz, 6H), 2.71 (t, ^3J(H,H) = 6.0 Hz, 6H). ^{13}C NMR (100 MHz, d_6-Benzene, 20 ^{o}C): δ = 211.8, 139.4, 129.1, 128.0, 121.6, 118.4, 57.3, 55.4, 50.0 ppm.

[(TIMEN^{Me})$_2$Ag$_3$](PF$_6$)$_3$ (2): **H$_3$1a** (0.49 g, 0.62 mmol) was dissolved in 50 mL DMSO and to this solution Ag_2O (0.22 g, 0.95 mmol) was added. The mixture was heated to 75 ^oC for 12 h. The resulting suspension was filtered through Celite and to the filtrate an equal amount of water was added to give a white powder. The solid was collected by filtration, washed with ether, and dried under vacuum (0.33 g, Yield: 76 %). ^1H NMR (400 MHz, d_6-DMSO, 20 °C): δ = 7.39 (s, br. 6H), 4.09 (s, br. 6H), 3.73 (s, 9H), 2.96 ppm (s, br. 6H). ^{13}C NMR (100 MHz, d_6-DMSO, 20 ^oC): δ = 179.4, 122.7, 121.9, 54.1, 48.5, 38.1 ppm. Elemental analysis (%) calcd for $C_{36}H_{54}N_{14}Ag_3P_3F_{18}\cdot 3DMSO$: C 30.10, H 4.33, N 11.70; found: C 28.71, H 4.18, N 11.62.

[(TIMEN^{Me})$_2$Cu$_3$](PF$_6$)$_3$ (3): A solution of CuBr (56 mg, 0.40 mmol) in 2 mL acetonitrile was added dropwise to a solution of **2** (190 mg, 0.13 mmol) in 4 mL acetonitrile. The reaction mixture was allowed to stir for one hour and the resulting suspension was filtered. Addition of 10 mL diethyl ether to the filtrate induced precipitation of a white crystalline powder. The precipitate was filtered, washed with diethyl ether, and dried in vacuum (116 mg; Yield: 68%). Colorless crystals suitable for X-ray diffraction analysis were grown by diffusion of diethyl ether into a saturated solution of **3** in acetonitrile at room temperature. ^1H NMR (300 MHz, d_3-acetonitrile, 20 °C): δ = 6.97 (s, 3H), 6.95 (s, 3H), 3.99 (t, ^3J(H,H) = 6.0 Hz, 6H), 3.71 (s, 9H), 2.98 ppm (t, ^3J(H,H) = 6.0 Hz, 6H). ^{13}C NMR (100 MHz, d_3-acetonitrile, 20 ^oC): δ = 178.4, 122.5, 121.9, 57.9, 48.7, 38.6 ppm. Elemental analysis (%) calcd for $C_{36}H_{54}N_{14}Cu_3P_3F_{18}$: C 33.04, H 4.16, N 14.99; found: C 32.79, H 4.12, N 15.08.

[(TIMEN$^{t\text{-Bu}}$)Cu](PF$_6$) (**4b**): A solution of tetrakis(acetonitrile)copper(I) hexafluorophosphate (0.12 g, 0.32 mmol) in acetonitrile was added dropwise to a solution of **1b** (0.15 g, 0.32 mmol) in 3 mL acetonitrile. The reaction mixture was stirred for one hour and 10 mL diethyl ether were added to cause precipitation of **4b** as an off-white powder. The precipitate was collected by filtration, washed with diethyl ether, and dried in vacuum (0.13 g; Yield: 60%). Colorless crystals suitable for X-ray diffraction analysis were grown by diffusion of diethyl ether into a saturated solution of **4b** in THF at room temperature. ^{1}H NMR (400 MHz, d_3-acetonitrile, 20 °C): δ = 7.19 (d, ^3J(H,H) = 2.0 Hz, 3H), 6.92 (d, ^3J(H,H) = 2.0 Hz, 3H), 3.67 (dd, ^3J(H,H) = 14.0 Hz , ^3J(H,H) = 4.0 Hz, 3H), 3.43 (dd, ^3J(H,H) = 14.0 Hz , ^3J(H,H) = 10.0 Hz, 3H), 2.90 (dd, ^3J(H,H) = 14.0 Hz , ^3J(H,H) = 4.0 Hz 3H), 2.34 (dd, ^3J(H,H) = 14.0 Hz , ^3J(H,H) = 10.0 Hz, 3H), 1.52 (s, 27H). ^{13}C NMR (100 MHz, d_3-acetonitrile, 20 ^{o}C): δ = 187.0, 122.3, 117.6, 60.7, 57.8, 51.0, 31.1ppm. Elemental analysis (%) calcd for $C_{27}H_{45}N_7CuPF_6$**:** C 47.96, H 6.71, N 14.50; found: C 48.12, H 6.64, N 14.36.

[(TIMEN^{Bz})Cu](Br) (**4c**): A solution of copper(I) bromide (0.035 g, 0.25 mmol) in acetonitrile was added dropwise to a solution of **1c** (0.14 g, 0.25 mmol) in 3 mL acetonitrile. The mixture was allowed to stir for one hour, and then the solution was evaporated to dryness. The solid residue was dissolved in 10 mL CH_2Cl_2 and the resulting solution was filtered through Celite. Diethyl ether was added to the filtrate to cause precipitation of **4c** as a slightly yellow powder. The precipitate was collected by filtration, washed with diethyl ether, and dried under vacuum (0.1 g; Yield: 56%). Colorless crystals suitable for X-ray diffraction analysis were grown by slow diethyl

ether diffusion into a saturated solution of **4c** in CH_2Cl_2 at room temperature. ^{1}H NMR (400 MHz, d_3-acetonitrile, 20 °C): δ = 7.09 (m, 6H), 6.95 (d, ^3J(H,H) = 2.0 Hz, 3H), 6.83 (m, 9H), 6.76 (d, ^3J(H,H) = 2.0 Hz, 3H), 4.97 (s, br, 6H), 3.75 (s, br. 6H), 2.72 (s, br, 6H) ^{13}C NMR (100 MHz, d_3-acetonitrile, 20 ^{o}C): δ = 189.7, 138.6, 128.9, 127.9, 127.6, 122.0, 118.6, 58.1, 54.3, 48.5 ppm. Elemental analysis (%) calcd for $C_{36}H_{39}N_7CuBr$**:** C 60.60, H 5.51, N 13.75; found: C 60.45, H 5.58, N 13.71.

[(TIMEN^{Bz})Cu](OTf)$_2$ (**5**): Method A: A solution of silver triflate (0.072 g, 0.28 mmol) in acetonitrile was added dropwise to a solution of **4c** (0.1 g, 0.14 mmol) in 5 mL acetonitrile. A black precipitate of Ag^0 formed upon addition of the silver salt. The mixture was filtered through Celite, and the filtrate was evaporated to dryness. The brown solid residue was collected by filtration, washed with diethyl ether, and dried under vacuum (0.052 g; Yield: 40%). Method B: A solution of copper(II) triflate (0.114 g, 0.31 mmol) in benzene was added dropwise to a solution of **1c** (0.18 g, 0.31 mmol) in 10 mL benzene. The reaction mixture was stirred for one hour during which a brown-black precipitate formed. The precipitate was collected by filtration, washed with diethyl ether, and dried in vacuum (0.19 g; Yield: 66%). Elemental analysis (%) calcd for $C_{38}H_{39}N_7CuO_6S_2F_6$**:** C 49.00, H 4.22, N 10.53; found: C 48.78, H 4.20, N 10.62.

3.5. Acknowledgement

Text, schemes, and figures of this chapter, in part, are reprints of the materials published in the following paper: **Hu**, **X**.; Castro-Rodriguez, I.; Meyer, K*. "Copper

Complexes of Nitrogen-Anchored Tripodal N-Heterocyclic Carbene Ligands", *J. Am. Chem. Soc.* **2003**, *125*, 12237-12245. The dissertation author was the primary researcher and author. The co-authors listed in this publication also participated in the research.

3.6. Appendix

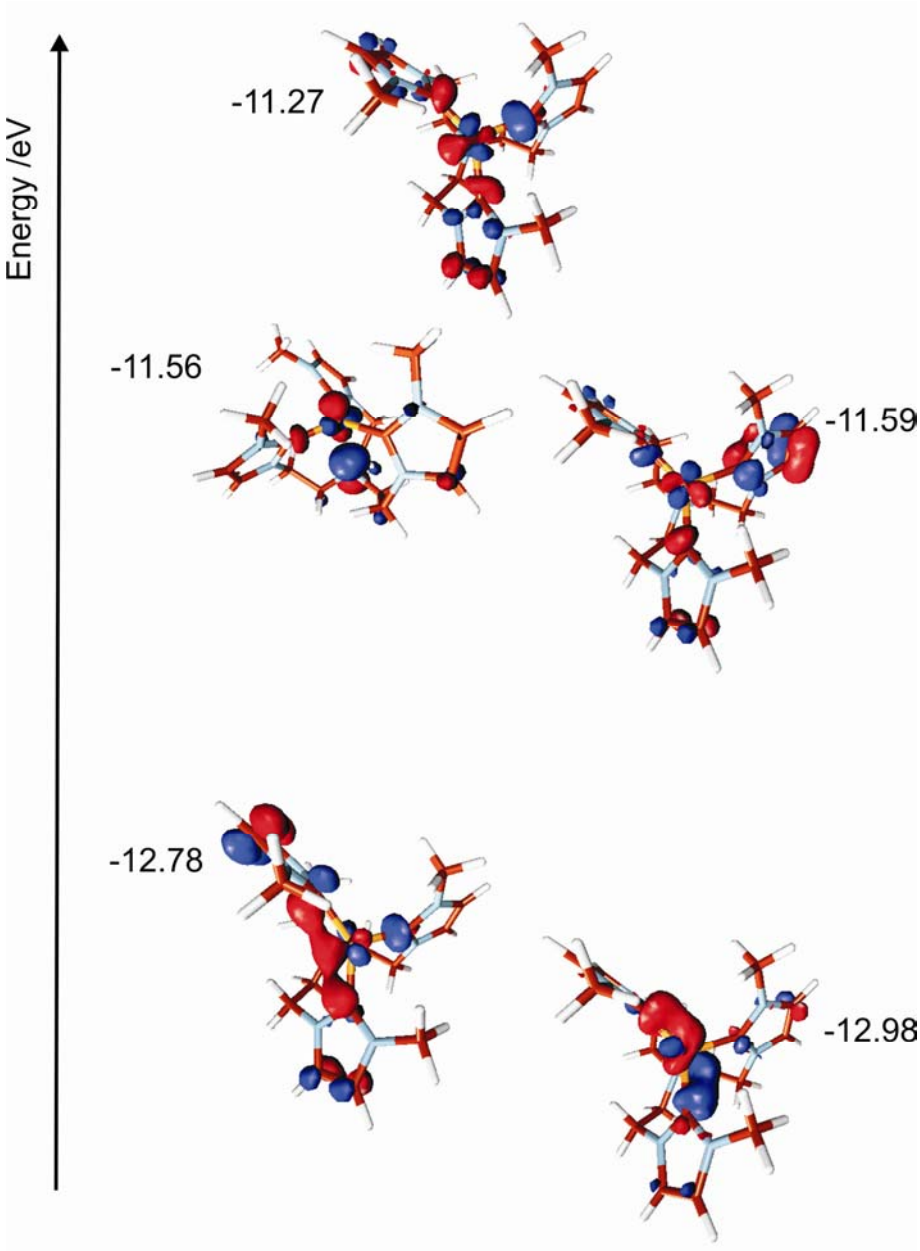

Figure 3-11. Energies and relative positions of metal-based frontier molecular orbitals in the $[(TIMEN^{Me})Cu]^{2+}$ system (alpha spin).

Crystallographic Details for 3, 4b, and 4c.

Table 3-1. Crystal Data and Structure Refinement for $[(TIMEN^{Me})_2Cu_3](PF_6)_3$ (**3**).

Identification code	3-3	
Empirical formula	C41 H61.50 Cu3 F18 N16.50 P3	
Formula weight	1411.10	
Temperature	100(2) K	
Wavelength	0.71073 Å	
Crystal system	Triclinic	
Space group	*P*-1	
Unit cell dimensions	a = 11.6256(18) Å	α = 89.234(3)°.
	b = 12.2828(19) Å	β = 78.523(3)°.
	c = 21.027(3) Å	γ = 71.615(2)°.
Volume	2788.4(8) Å3	
Z	2	
Density (calculated)	1.681 Mg/m3	
Absorption coefficient	1.329 mm-1	
F(000)	1434	
Crystal size	0.17 x 0.13 x 0.05 mm3	
Theta range for data collection	1.75 to 27.51°.	
Index ranges	-15<=h<=14, -15<=k<=15, -27<=l<=27	
Reflections collected	24440	
Independent reflections	12496 [R(int) = 0.0374]	
Completeness to theta = 27.51°	97.5 %	
Absorption correction	Semi-Empirical	
Max. and min. transmission	1.000000 and 0.556710	
Refinement method	Full-matrix least-squares on F^2	
Data / restraints / parameters	12496 / 0 / 736	
Goodness-of-fit on F^2	1.069	
Final R indices [I>2sigma(I)]	R_1 = 0.0597, wR_2 = 0.1407	
R indices (all data)	R_1 = 0.0853, wR_2 = 0.1471	
Largest diff. peak and hole	1.442 and -1.274 e.Å-3	

Table 3-2. Crystal Data and Structure Refinement for [(TIMEN$^{t\text{-Bu}}$)Cu]PF_6 (**4b**).

Identification code	3-4b	
Empirical formula	C27 H45 Cu F6 N7 P	
Formula weight	676.21	
Temperature	293(2) K	
Wavelength	0.71073 Å	
Crystal system	Triclinic	
Space group	*P*-1	
Unit cell dimensions	a = 9.586(4) Å	α = 95.194(6)°.
	b = 11.901(4) Å	β = 102.968(6)°.
	c = 14.205(5) Å	γ = 92.142(6)°.
Volume	1569.9(10) Å3	
Z	2	
Density (calculated)	1.431 Mg/m3	
Absorption coefficient	0.812 mm-1	
F(000)	708	
Crystal size	0.49 x 0.22 x 0.04 mm3	
Theta range for data collection	1.48 to 22.50°.	
Index ranges	-10<=h<=10, -12<=k<=12, -15<=l<=15	
Reflections collected	8778	
Independent reflections	4093 [R(int) = 0.0317]	
Completeness to theta = 22.50°	99.5 %	
Absorption correction	None	
Refinement method	Full-matrix least-squares on F^2	
Data / restraints / parameters	4093 / 0 / 388	
Goodness-of-fit on F^2	0.967	
Final R indices [I>2sigma(I)]	R_1 = 0.0346, wR_2 = 0.0811	
R indices (all data)	R_1 = 0.0438, wR_2 = 0.0838	
Largest diff. peak and hole	0.543 and -0.430 e.Å-3	

Table 3-3. Crystal Data and Structure Refinement for [(TIMEN^{Bz})Cu]Br (**4c**).

Identification code	3-4c	
Empirical formula	C36 H39 Br Cu N7	
Formula weight	713.19	
Temperature	100(2) K	
Wavelength	0.71073 Å	
Crystal system	Triclinic	
Space group	*P*-1	
Unit cell dimensions	a = 14.131(4) Å	α =116.583(5)°.
	b = 20.193(6) Å	β = 98.521(5)°.
	c = 20.713(6) Å	γ = 98.861(5)°.
Volume	5063(2) Å^3	
Z	6	
Density (calculated)	1.404 Mg/m^3	
Absorption coefficient	1.867 mm^{-1}	
F(000)	2208	
Crystal size	0.26 x 0.18 x 0.05 mm^3	
Theta range for data collection	1.13 to 22.50°.	
Index ranges	-15<=h<=15, -21<=k<=21, -22<=l<=22	
Reflections collected	29736	
Independent reflections	13209 [R(int) = 0.0387]	
Completeness to theta = 22.50°	99.8 %	
Absorption correction	Semi-Empirical	
Refinement method	Full-matrix least-squares on F^2	
Data / restraints / parameters	13209 / 0 / 1216	
Goodness-of-fit on F^2	0.932	
Final R indices [I>2sigma(I)]	R_1 = 0.0428, wR_2 = 0.0869	
R indices (all data)	R_1 = 0.0732, wR_2 = 0.1015	
Largest diff. peak and hole	0.469 and -0.554 e.Å^{-3}	

3.7. References

(1) Trofimenko, S. *Prog. Inorg. Chem.* **1986**, *34*, 115-210.

(2) Mayer, H. A.; Kaska, W. C. *Chem. Rev.* **1994**, *94*, 1239-1272.

(3) Wang, H. M. J.; Lin, I. J. B. *Organometallics* **1998**, *17*, 972-975.

(4) Arnold, P. L.; Scarisbrick, A. C.; Blake, A. J.; Wilson, C. *Chem. Commun.* **2001**, 2340-2341; Tulloch, A. A. D.; Danopoulos, A. A.; Kleinhenz, S.; Light, M. E.; Hursthouse, M. B.; Eastham, G. *Organometallics* **2001**, *20*, 2027-2031.

(5) Becker, M.; Heinemann, F. W.; Schindler, S. *Chem.-Eur. J.* **1999**, *5*, 3124-3129; Raab, V.; Kipke, J.; Burghaus, O.; Sundermeyer, J. *Inorg. Chem.* **2001**, *40*, 6964-6971.

(6) Neese, F. *QCPE Bull.* **1995**, *15*, 5.

(7) O'Connor, C. J. *Prog. Inorg. Chem.* **1982**, *29*, 203-283.

(8) ADF2003.01; SCM, Theoretical Chemistry, Vrijie Universiteit: Amsterdam, The Netherlands.

(9) Vosko, S. H.; Wilk, L.; Nusair, M. *Can. J. Phys.* **1980**, *58*, 1200-1211.

(10) Becke, A. D. *Phys. Rev. A* **1988**, *38*, 3098-3100.

(11) Perdew, J. P. *Phys. Rev. B* **1986**, *33*, 8822-8824.

(12) Van Lenthe, E.; Ehlers, A.; Baerends, E. J. *J. Chem. Phys.* **1999**, *110*, 8943-8953.

(13) Snijders, J. G.; Vernooijs, P.; Baerends, E. J. *At. Data Nucl. Tables* **1981**, *26*, 483-509.

(14) Arduengo, A. J.; Gentry, F. P.; Taverkere, P. K.; Simmons, H. E. In *US Patent*; E. I. du pont de Nemours and Company: U. S. A., 2001.

(15) Ward, K. *J. Am. Chem. Soc.* **1935**, *57*, 914-916.

(16) Kubas, G. J. *Inorganic Synthesis* **1979**, *19*, 90-92.

Chapter 4. Synthesis and Characterization of Electron-Rich Nickel Tris(Carbene) Complexes

4.1. Introduction

Reactive nickel complexes employing terminal amido, imido,[1] phosphinidene,[2] and carbene[3] ligands have proven to be excellent group-transfer reagents[4] and hydrocarbation catalysts.[5] Likewise, low valent nickel complexes attract much attention due to their proposed intermediacy in various organometallic transformations. Recent reports show nickel(0) N-heterocyclic carbene (NHC)[6] complexes, formed in-situ, are efficient catalysts for C—C bond formation,[7] C—N coupling,[8] dehalogenation,[9] and transfer hydrogenation reactions.[10] Structurally characterized, well-defined nickel(0) NHC complexes, however, are rare; known examples include a two-coordinate nickel(0) bis-carbene complex, $Ni(IMes)_2$ (IMes = 1,3-dimesitylimidazol-2-ylidene),[11] and few NHC adducts of nickel(0) carbonyls.[12]

We have recently developed the novel tripodal NHC ligand system tris[2-(3-alkylimidazol-2-ylidene)ethyl]amine ($TIMEN^R$) and explored its coordination chemistry with copper (Chapter 3). Inspired by the reported rich chemistry stemming from low-valent nickel complexes, we sought to prepare a reactive nickel(0) complex of the TIMEN ligand system.

Herein we describe the synthesis and full characterization of the tris(carbene) nickel(0) complex, $Ni(TIMEN^{t\text{-}Bu})$ (**1**), as well as the analogous one-electron oxidized nickel(I) complex **2**. To the best of our knowledge, these are the first examples of nickel tris(carbene) complexes.

4.2. Results and Discussion

4.2.1. Synthesis and characterization of the nickel(0) complex [Ni(TIMEN$^{t\text{-Bu}}$)]

Reaction of the free carbene ligand TIMEN$^{t\text{-Bu}}$ with one equiv. of $Ni(COD)_2$ (COD = 1,5-cyclooctadiene) in THF at room temperature yielded the carbene complex Ni(TIMEN$^{t\text{-Bu}}$) (**1**) in 58% isolated yield (Scheme 1).

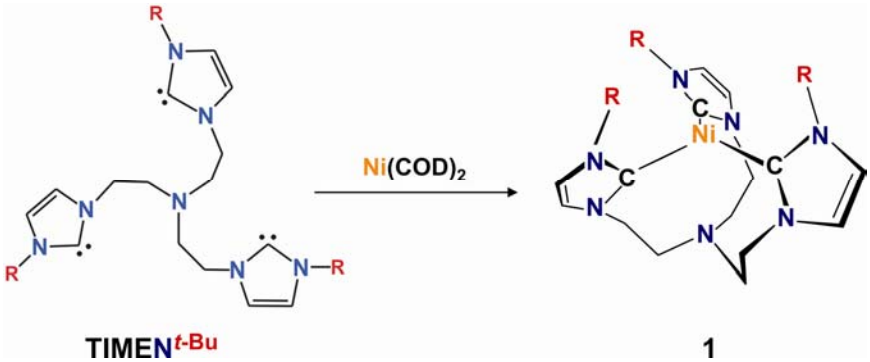

Scheme 4-1. Synthesis of the Nickel(0) Complex of TIMEN$^{t\text{-Bu}}$.

The ^{1}H- and ^{13}C NMR spectra of **1** in solution are consistent with a C_3-symmetrical ligand environment at the diamagnetic nickel(0) center. The ^{1}H NMR spectrum of 1 shows three singlet signals at 1.87, 6.30 and 6.71 ppm, which can be assigned to the tert-butyl substituents and the imadazol-2-ylidene backbone protons, respectively. Four diastereotopic protons on the ethylene backbone give rise to four multiplet signals between 2.42 and 3.92 ppm with unity intensity. The most notable feature in the ^{13}C-NMR spectrum of **1** is a singlet signal at 194.9 ppm, stemming from three equivalent carbenoid carbon atoms. The observed chemical shift is characteristic for Ni(0) bound NHCs.[11,12]

Deep-red, block-shaped single crystals suitable for X-ray diffraction studies were grown from a saturated solution of **1** in diethyl ether at –35°C. Compound **1** crystallized in the cubic space group $P2_13$ with the crystallographically defined 3-fold axis passing through the nickel center and the anchoring nitrogen atom of TIMEN$^{t\text{-Bu}}$, rendering the three pendent arms of the ligand structurally equivalent (Figure 4-1). Due to an increased steric crowding at the nickel center in **1**, the Ni—C bond distance of 1.892(1) Å is slightly longer than that of Ni(IMes)$_2$ with 1.829(6) Å.[11] This Ni—C bond distance is noticeably shorter than those of sterically less hindered nickel NHC carbonyl complexes (1.957-1.986 Å),[12] suggesting a higher degree of metal to ligand π-backbonding in **1**. The C—Ni—C angle of 118.73(2)° reflects the almost perfectly trigonal planar ligand environment at the central nickel atom. A very long Ni—N bond distance of 3.204 Å excludes a possible nickel-amine interaction. It is noteworthy that the solid-state structure of **1** also reveals agostic interactions between the electron-rich nickel center and one hydrogen atom of each of the three *tert*-butyl groups (Figure 4-1), resulting in Ni—HC bond distances of 2.611 Å (d(Ni—$C_{t\text{-}Bu}$ = 3.379 Å). The observed Ni—HC interaction may also account for the observed displacement of the nickel centre from an idealized trigonal plane formed by the three chelating carbenes. The Ni(0) out-of-plane shift in **1** was determined to be d(Ni—C_{plane}) = +0.215 Å. For comparison, the iso-electronic cuprous ion in [Cu(TIMEN$^{t\text{-Bu}}$)]$^+$ shows no evidence for Cu—HC interactions. Accordingly, the Cu(I) ion is suited in a perfect trigonal planar ligand environment of three carbenes (d(Cu—C_{plane}) = –0.02 Å) (see also Chapter 3, complex **4b**).

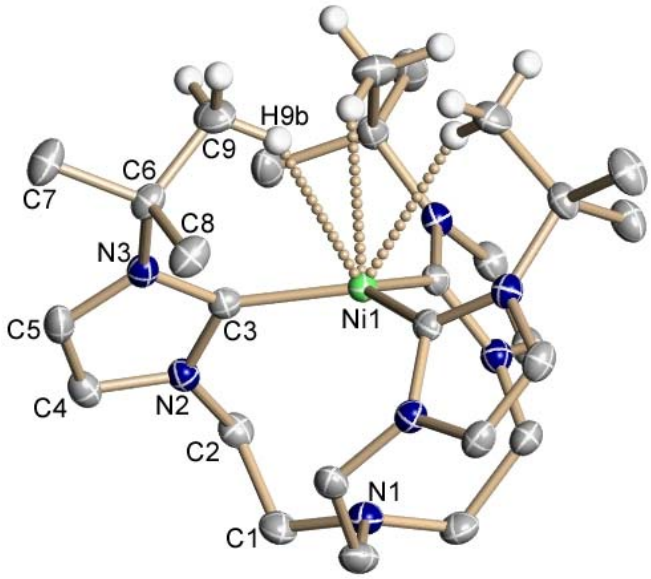

Figure 4-1. Solid-state molecular structure of Ni(TIMEN$^{t\text{-Bu}}$) (1). Most hydrogen atoms are omitted for clarity; thermal ellipsoids are shown at 50% probability. Dotted lines indicate Ni-HC agostic interactions. Selected bond lengths (Å) and angles (deg.): Ni(1)-C(3) 1.8917(12), Ni(1)-H(9b) 2.611, Ni-C(9) 3.379, C(3)-Ni(1)-C(3) 118.728(15).

The redox behavior of complex **1** was examined by electrochemical methods. The cyclic voltammogram (CV) of a solution of **1** in THF exhibits two quasi-reversible one-electron redox processes (Figure 2). The half-wave potential of $E_{1/2} = -2.5$ V *vs.* Fc/Fc^+ corresponds to the Ni(0)/Ni(I) redox couple, while a second redox wave at $E_{1/2} = -1.09$ V is associated with the Ni(I)/Ni(II) couple.

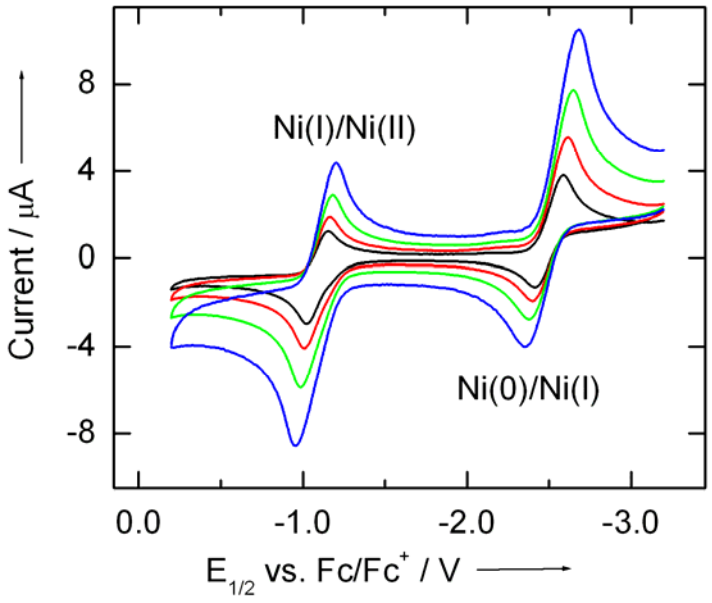

Figure 4-2. Cyclic voltammogram of Ni(TIMEN$^{t\text{-Bu}}$) (**1**) recorded in THF solution containing 0.1 M [N(*n*-Bu)$_4$](ClO$_4$) electrolyte at scan rates of 200 (black), 400 (red) , 800 (green), and 1500 (blue) mV/s.

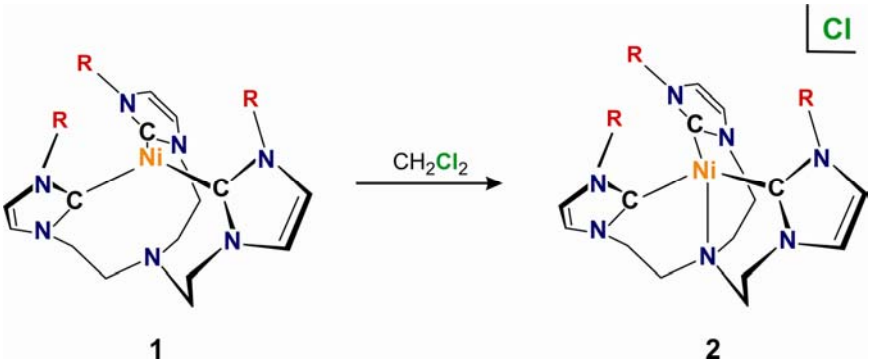

Scheme 4-2. Synthesis of the Nickel(I) Complex of TIMEN$^{t\text{-bu}}$

4.2.1. Synthesis and characterization of the nickel(I) complex $[Ni(TIMEN^{t\text{-}Bu})]^+$

According to its negative redox-potential, **1** may be expected to readily react with one-electron oxidizers to form the cationic Ni(I) complex $[Ni(TIMEN^{t\text{-}Bu})]^+$. For instance, treatment of **1** with stoichiometric amounts of benzyl chloride or neat dichloromethane afforded the cationic complex $[Ni(TIMEN^{t\text{-}Bu})]Cl$ (**2**) in 68% isolated yield (Scheme 4-2). The formation of paramagnetic **2** can be followed by ^{1}H-NMR spectroscopy. The ^{1}H-NMR spectrum of **2** recorded in d_3-acetonitrile exhibits seven paramagnetically shifted and broadened signals. The most intense singlet signal at 6.6 ppm (27H) was readily assigned to the *tert*-butyl groups; six more signals between +35 and –15 ppm integrate properly. Although the assignment remains largely equivocal, the positions of all signals are diagnostic for determination of purity and stability of **2** in solution. The CV of **2** in acetonitrile shows a reversible redox-wave for the Ni(I)/(II) couple at a potential of –1.07 V *vs.* Fc/Fc^+ (Figure 4-3).

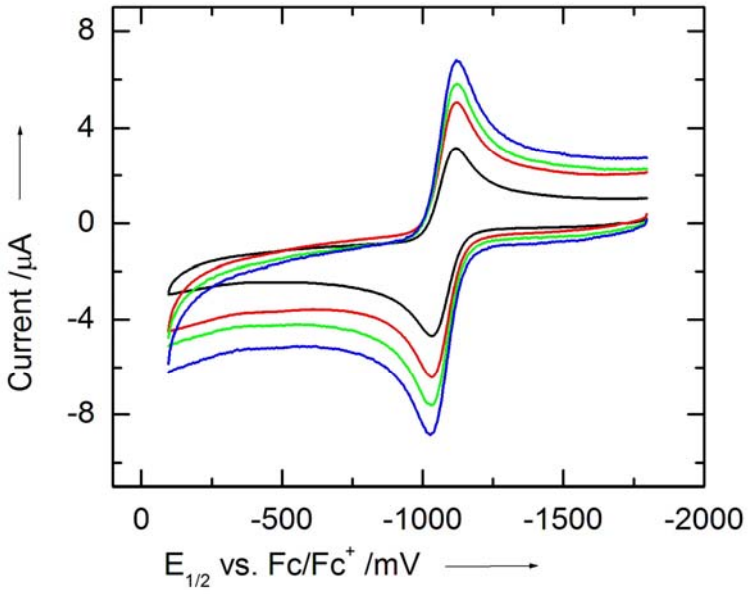

Figure 4-3. Cyclic voltammogram of [Ni(TIMEN$^{t\text{-Bu}}$)]Cl (**2**) recorded in acetonitrile solution containing 0.1 M [N(*n*-Bu)$_4$](ClO$_4$) as electrolyte at scan rates of 200 (black), 400 (red) , 800 (green), and 1500 (blue) mV/s.

The solid-state molecular structure of complex **2** (Figure 4-4) was examined by single-crystal X-ray diffraction study. The coordination polyhedron of the nickel(I) ion can be best described as trigonal pyramidal with three carbenoid carbons forming the trigonal plane and the anchoring nitrogen atom occupying the axial position. The average C—Ni—C bond angle of 119(3)^o is close to the 120^o of an idealized trigonal plane. In contrast to **1**, cationic **2** exhibits a short Ni—N distance of 2.229 Å and an out-of-plane shift of –0.154 Å, indicative of a strong nickel(I)—amine interaction.

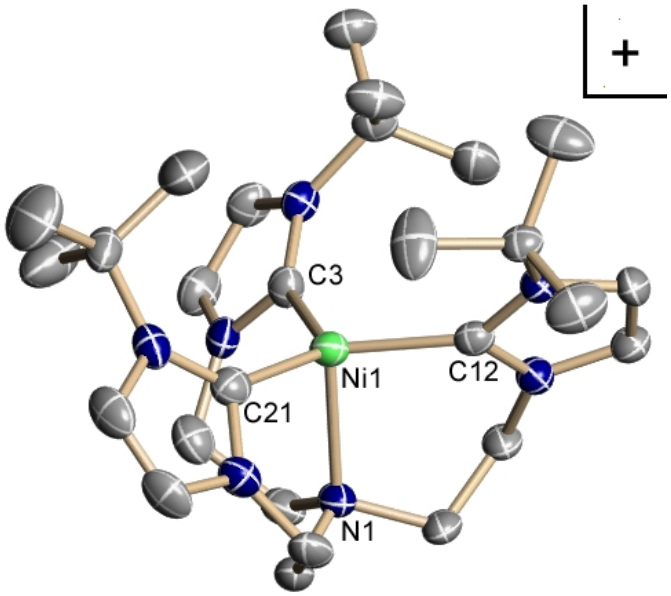

Figure 4-4 Solid-state molecular structure of [Ni(TIMEN$^{t\text{-Bu}}$)]Cl (**2**). Only one of the two independent molecules in each unit cell is shown; hydrogen atoms and counter ions are omitted for clarity; thermal ellipsoids are shown at 50% probability. Selected bond lengths (Å) and angles (deg.): Ni(1)-C(3) 1.988(4), Ni(1)-C(12) 2.004(4), Ni(1)-

C(21) 1.996(4); Ni(1)-N(1) 2.223(3); C(3)-Ni(1)-C(12) 114.68(17), C(12)-Ni(1)-C(21) 123.26(17), C(3)-Ni(1)-C(21) 120.27(18).

Interestingly, despite the smaller radius of the Ni(I) ion, the average Ni—C bond distance of 1.996(4) Å is significantly longer than that of **1**. The latter observation supports recent reports suggesting that the NHC ligand may very well be capable of efficient π-back bonding, thereby stabilizing very electron-rich metal centers (see Chapter 6 for a detailed study). In less electron-rich metal complexes, on the other hand, the NHC ligand serves as excellent σ-donor ligand. This remarkable electronic flexibility of NHC ligands may very well be the reason for their excellent chelating properties with a large variety of transition, lanthanide, and actinide metals in low- and high-oxidation states.

4.3. Conclusion

In summary, the nitrogen anchored tripodal NHC ligand TIMEN$^{t\text{-Bu}}$ exhibits structural and electronic flexibility to coordinate to both Ni(0) and Ni(I) ions, forming the first nickel tris(carbene) complexes. Unfortunately, the low-valent nickel center in these complexes is completely masked for additional ligand binding and inner-sphere redox events. We recently synthesized sterically less-encumbering derivatives of the TIMEN ligand, e.g., TIMEN^{xyl} and TIMEN^{mes} (the synthesis and coordination of these ligands will be discussed in Chapter 5). Interstingly, the nickel(0)/(I) complexes of these aryl-derivatized TIMEN ligands could not be prepared following the methods

described in Scheme 1 and 2, suggesting a substantial difference in the electronic properties of these two classes of ligands.

4.4. Experimental Section

Methods and Procedures

Manipulation of air-sensitive compounds was performed under a controlled dry nitrogen atmosphere using standard Schlenk techniques and inert-gas glove boxes (MBraun Labmaster by M. Braun, Inc.). Solvents were purified using a two-column solid-state purification system (Glasscontour System, Joerg Meyer, Irvine, CA) and transferred to the glove box without exposure to air. NMR solvents were obtained from Cambridge Isotope Laboratories, degassed, and stored over activated molecular sieves prior to use. All NMR spectra were recorded at room temperature (20^{o}C) in d_6-benzene, d_3-acetonitrile and d_6-DMSO solutions on Varian spectrometers operating at 400/300 MHz (^{1}H NMR) and 100 MHz (^{13}C NMR) and referenced to residual solvent peaks unless otherwise noted (δ in ppm). Cyclic voltammetric measurements were performed on Bioanalytical Systems equipment (BAS, CV-50W) in acetonitrile or THF solutions containing 0.1 M [N(*n*-Bu)$_4$](ClO$_4$) as electrolyte (working electrode: platinum; auxiliary electrode: platinum wire; reference electrode: Ag/AgNO$_3$ in acetonitrile). Potentials are reported relative to the ferrocene/ferrocenium couple (Fc/Fc^{+}). Solid-state magnetization measurements of powdered samples were recorded on a SQUID magnetometer (Quantum Design) at 10 kOe between 5 and 300 K. Magnetic susceptibility data were corrected for background and underlying

diamagnetic contributions using tabulated Pascal constants ($\chi_{dia} = 3.61 \cdot 10^{-4}$ cm^3 mol^{-1}).[13] Data reproducibility was carefully checked in multiple individual measurements of independently synthesized samples. Elemental analyses were performed by Kolbe Microanalytical Laboratory (Muelheim a. d. Ruhr/Germany).

Synthesis:

Starting Materials. Tris[2-(3-*tert*-butylimidazol-2-ylidene)ethyl]amine (TIMEN$^{t\text{-Bu}}$) was prepared as describe in Chapter 3. Bis(1,5-cyclooctadiene)nickel(0) was obtained from commercial sources (Strem Chemicals, Inc.) and used as received.

Ni(TIMEN$^{t\text{-Bu}}$) (1): A solution of Ni(COD)$_2$ (0.18 g, 0.67 mmol) in THF was added dropwise to a solution of TIMEN$^{t\text{-Bu}}$ (0.31 g, 0.67 mmol) in 2 mL THF. Upon addition, the solution turned into deep red immediately. The reaction mixture was stirred for one hour and then evaporated under vacuum. The red precipitate was collected by filtration, washed with 5 ml cold diethyl ether, and dried in vacuum (0.20 g; Yield: 58%). Red crystals suitable for X-ray diffraction analysis were grown from a saturated diethyl ether solution of **1** at –35^{o}C. ^{1}H NMR (300 MHz, d_6-benzene, 20 °C): δ = 6.71 (s, 3H), 6.30 (s), 3.92 (t, ^3J(H,H) = 12 Hz , 3H), 3.04 (d, ^3J(H,H) = 12 Hz, 3H), 2.82 (d, ^3J(H,H) = 12 Hz, 3H), 2.42 (t, ^3J(H,H) = 12, 3H), 1.87 (s, 27H). ^{13}C NMR (100 MHz, d_6-benzene, 20 ^{o}C): δ = 194.9, 116.4, 114.3, 64.0, 56.5, 52.9, 30.8ppm. Elemental analysis (%) calcd for $C_{27}H_{45}N_7Ni$**:** C 61.60, H 8.61, N 18.63; found: C 61.53, H 8.56, N 18.71.

[Ni(TIMEN$^{t\text{-Bu}}$)]Cl (2): 1 mL of dichloromethane was added to **1** (58 mg, 0.11 mmol). The resulting yellow solution was stirred for 5 minutes, and then 5 mL of

diethyl ether was added to precipitate **2** as a yellow solid. The solid was collected by filtration, washed with diethyl ether, and dried in vacuum (42 mg; Yield: 68%). Yellow crystals suitable for X-ray diffraction analysis were grown by diffusion of diethyl ether into an acetonitrile solution of **2** at room temperature. ^{1}H NMR (300 MHz, d_3-acetonitrile, 20 °C): δ = 31.1 (s, 3H, $\Delta\nu_{1/2}$ = 20 Hz), 20.4 (s, 3H, $\Delta\nu_{1/2}$ = 13 Hz), 12.7 (s, 3H, $\Delta\nu_{1/2}$ = 11 Hz), 11.1 (s, 9H, $\Delta\nu_{1/2}$ = 22 Hz), 10.8 ppm (s, 3H, $\Delta\nu_{1/2}$ = 15 Hz), 6.5 ppm (s, 27H, $\Delta\nu_{1/2}$ = 30 Hz), -6.1 ppm (s, 3H, $\Delta\nu_{1/2}$ = 11 Hz). Elemental analysis (%) calcd for $C_{27}H_{45}N_7NiCl$**:** C 57.72, H 8.07, N 17.45; found: C 57.41, H 8.06, N 17.52.

4.5. Acknowledgement

Text, schemes, and figures of this chapter, in full, are reprints of the materials published in the following paper: **Hu**, **X**.; Castro-Rodriguez, I.; Meyer, K*. "Synthesis and characterization of Electron-Rich Nickel Tris-Carbene Complexes", *Chem. Comm.* **2004**, 2164-2165. The dissertation author was the primary researcher and author. The co-authors listed in this publication also participated in the research.

4.6. Appendix

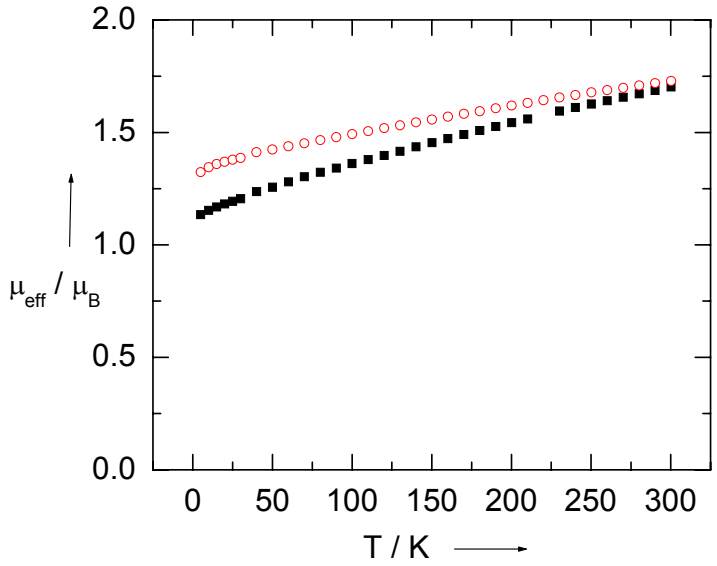

Figure 4-5. Plot of the effective magnetic moment, μ_{eff}, versus temperature from SQUID magnetization measurements for two independently prepared samples of **2** (mass = 16.7 mg, mass = 22.4 mg, $\chi_{dia} = 3.61 \cdot 10^{-4}$ cm^3 mol^{-1}). The observed temperature behavior of the magnetic moment indicates weak antiferromagnetic spin-spin coupling in the solid state, which is sample dependent and, thus, may be accounted for by the different particle size, complex packing in the solids, solvent molecule inclusion, etc. of two independently synthesized microcrystalline samples.

Crystallographic Details for 1 and 2.

Table 4-1. Crystal Data and Structure Refinement for [Ni(TIMEN$^{t\text{-Bu}}$)] (**1**).

Identification code	4-1	
Empirical formula	C27 H45 N7 Ni	
Formula weight	526.41	
Temperature	100(2) K	
Wavelength	0.71073 Å	
Crystal system	Cubic	
Space group	$P2_13$	
Unit cell dimensions	a = 14.0195(3) Å	α= 90°.
	b = 14.0195(3) Å	β= 90°.
	c = 14.0195(3) Å	γ = 90°.
Volume	2755.48(10) Å^3	
Z	4	
Density (calculated)	1.269 Mg/m^3	
Absorption coefficient	0.732 mm^{-1}	
F(000)	1136	
Crystal size	0.26 x 0.22 x 0.20 mm^3	
Theta range for data collection	2.05 to 27.46°.	
Index ranges	-9<=h<=17, -18<=k<=18, -17<=l<=18	
Reflections collected	17469	
Independent reflections	2123 [R(int) = 0.0227]	
Completeness to theta = 27.46°	100.0 %	
Absorption correction	Semi-Empirical	
Max. and min. transmission	1.000 and 0.917	
Refinement method	Full-matrix least-squares on F^2	
Data / restraints / parameters	2123 / 0 / 166	
Goodness-of-fit on F^2	1.113	
Final R indices [I>2sigma(I)]	R_1 = 0.0225, wR_2 = 0.0555	
R indices (all data)	R_1 = 0.0229, wR_2 = 0.0557	
Absolute structure parameter	0.005(10)	
Largest diff. peak and hole	0.360 and -0.123 e.Å^{-3}	

Table 4-2. Crystal Data and Structure Refinement for [Ni(TIMEN$^{t\text{-Bu}}$)]Cl (**2**).

Identification code	4-2	
Empirical formula	C27 H45 Cl N7 Ni	
Formula weight	561.86	
Temperature	100(2) K	
Wavelength	0.71073 Å	
Crystal system	Triclinic	
Space group	*P*-1	
Unit cell dimensions	a = 14.5847(8) Å	α= 103.2710(10)°.
	b = 14.7332(9) Å	β= 99.4650(10)°.
	c = 14.7698(9) Å	γ= 105.2760(10)°.
Volume	2893.1(3) Å^3	
Z	4	
Density (calculated)	1.290 Mg/m^3	
Absorption coefficient	0.791 mm^{-1}	
F(000)	1204	
Crystal size	0.5 x 0.08 x 0.08 mm^3	
Theta range for data collection	1.46 to 22.50°.	
Index ranges	-15<=h<=15, -15<=k<=15, -15<=l<=15	
Reflections collected	16993	
Independent reflections	7554 [R(int) = 0.0519]	
Completeness to theta = 22.50°	99.9 %	
Absorption correction	Semi-Empirical	
Refinement method	Full-matrix least-squares on F^2	
Data / restraints / parameters	7554 / 0 / 667	
Goodness-of-fit on F^2	0.960	
Final R indices [I>2sigma(I)]	R_1 = 0.0495, wR_2 = 0.1078	
R indices (all data)	R_1 = 0.0711, wR_2 = 0.1145	
Largest diff. peak and hole	0.741 and -0.352 e.Å^{-3}	

4.7. References

(1) Mindiola, D. J.; Hillhouse, G. L. *J. Am. Chem. Soc.* **2001**, *123*, 4623-4624.

(2) Melenkivitz, R.; Mindiola, D. J.; Hillhouse, G. L. *J. Am. Chem. Soc.* **2002**, *124*, 3846-3847.

(3) Mindiola, D. J.; Hillhouse, G. L. *J. Am. Chem. Soc.* **2002**, *124*, 9976-9977; Hou, H. Y.; Gantzel, P. K.; Kubiak, C. P. *Organometallics* **2003**, *22*, 2817-2819.

(4) Mindiola, D. J.; Hillhouse, G. L. *Chem. Commun.* **2002**, 1840-1841; Waterman, R.; Hillhouse, G. L. *Organometallics* **2003**, *22*, 5182-5184; Waterman, R.; Hillhouse, G. L. *J. Am. Chem. Soc.* **2003**, *125*, 13350-13351.

(5) Hou, H. Y.; Gantzel, P. K.; Kubiak, C. P. *J. Am. Chem. Soc.* **2003**, *125*, 9564-9565.

(6) Arduengo, A. J. *Acc. Chem. Res.* **1999**, *32*, 913-921; Herrmann, W. A.; Kocher, C. *Angew. Chem. Int. Ed. Engl* **1997**, *36*, 2163-2187; Bourissou, D.; Guerret, O.; Gabbai, F. P.; Bertrand, G. *Chem. Rev.* **2000**, *100*, 39-91; Herrmann, W. A. *Angew. Chem.-Int. Edit.* **2002**, *41*, 1291-1309.

(7) Bohm, V. P. W.; Weskamp, T.; Gstottmayr, C. W. K.; Herrmann, W. A. *Angew. Chem.-Int. Edit.* **2000**, *39*, 1602-1604; Sato, Y.; Sawaki, R.; Mori, M. *Organometallics* **2001**, *20*, 5510-5512.

(8) Desmarets, C.; Schneider, R.; Fort, Y. *J. Org. Chem.* **2002**, *67*, 3029-3036.

(9) Desmarets, C.; Kuhl, S.; Schneider, R.; Fort, Y. *Organometallics* **2002**, *21*, 1554-1559.

(10) Kuhl, S.; Schneider, R.; Fort, Y. *Organometallics* **2003**, *22*, 4184-4186.

(11) Arduengo, A. J.; Gamper, S. F.; Calabrese, J. C.; Davidson, F. *J. Am. Chem. Soc.* **1994**, *116*, 4391-4394.

(12) Ofele, K.; Herrmann, W. A.; Mihalios, D.; Elison, M.; Herdtweck, E.; Scherer, W.; Mink, J. *J. Organomet. Chem.* **1993**, *459*, 177-184; Herrmann, W. A.; Goossen, L. J.; Artus, G. R. J.; Kocher, C. *Organometallics* **1997**, *16*, 2472-2477; Dorta, R.; Stevens, E. D.; Hoff, C. D.; Nolan, S. P. *J. Am. Chem. Soc.* **2003**, *125*, 10490-10491.

(13) O'Connor, C. J. *Prog. Inorg. Chem.* **1982**, *29*, 203-283.

Chapter 5. Cobalt Tris(Carbene) Complexes: Small Molecule Binding, Dioxygen Activation, and Imido Transfer

5.1. Introduction

Ligands that enforce a tripodal topology on coordinated metal ions are known to provide powerful platforms for small molecule activation and functionalization. Recently, Schrock and co-workers have developed such a ligand system based on the tris-amidoamine $[N_3N]^{3-}$ framework,[1] utilizing it for catalytic dinitrogen reduction.[2] The tetradentate tris-amidoamine tripod creates a protected cavity when coordinated to molybdenum, thereby allowing for isolation and characterization of a variety of intermediates of the reductive dinitrogen cleavage reaction.[2,3] Tripodal ligands have also shown to stabilize molecular species with unusual reactive terminal functionalities. For example, using an ureayl-derivatized tris-amidoamine chelator, Borovik and co-workers were able to prepare an unprecedented monomeric iron(III) oxo complex.[4] Peters *et al.* have demonstrated that by employing zwitterionic tris-(phosphine)borate ligands, remarkably reactive late transition metal complexes with terminal imido[5,6] and even nitrido ligands can be synthesized.[7]

Due to the limited accessibility of well-defined polydentate N-heterocyclic carbene (NHC) ligands,[8,9] reports on chelating NHC ligands designed for metal-assisted small molecule activation chemistry are rare. Since the isolation of stable imidazol-2-ylidene carbenes in 1991 by Arduengo et al.,[10] N-heterocyclic carbenes have emerged as a predominant ligand class in organometallic coordination chemistry.[11] This is mainly due to their successful application in homogenous catalysis,[12] especially in C—C bond formation[9,13] and olefin metathesis reactions.[14] We have recently developed a novel nitrogen-anchored tripodal NHC ligand system

TIMEN^{R} (tris[2-(3-alkylimidazol-2-ylidene)ethyl]amine with R = *tert*-butyl, benzyl) and synthesized the corresponding copper(I)/(II) and nickel(0)/(I) complexes (Chapter 3 and 4). The tris(carbene) ligand TIMEN binds to transition metals in a 1:1 fashion and supports controlled reactivity at metal center.

The aryl-derivatized TIMEN^{xyl} and TIMEN^{mes} ligands described herein render the low-valent cobalt(I) tris(carbene) complex [(TIMEN^{xyl})Co]Cl (**1a**) and [(TIMEN^{mes})Co]Cl (**1b**) electronically and structurally flexible for additional ligand binding and various redox events such as small molecule binding, dioxygen activation, and N-atom/group transfer.

Dioxygen activation at transition metal centers is a fundamentally important process due to its postulated role in biological catalyses.[15] Catalytic aerobic oxidation assisted by transition metal complexes remains an attractive, yet, challenging synthetic task.[16,17] There is longstanding interest in the dioxygen chemistry of cobalt complexes owing to their potential use as artificial oxygen carriers[18] and industrial oxidation catalysts.[19] The majority of isolated 1:1 cobalt dioxygen adducts feature the oxygen molecule in an end-on (η^1) binding mode and a cobalt center supported by a chelating polyamine ligand.[20] Cobalt complexes with side-on (η^2) bound dioxygen ligands are uncommon.[21,22]

Transition metal imido species have attracted much attention due to their postulated roles in catalysis and their potential in N-atom transfer chemistry.[23,24] Late transition metal imido complexes, however, are rare, which is likely due to mismatched reactivity of the hard imido ligand and the soft electron-rich metal center.

For about 10 years, Bergman's iridium derivatives of the general formula [(*Cp**)Ir≡NR] (where R = aryl, alkyl, silyl) represented the only structurally characterized late-metal complexes bearing a terminal imido functionality.[25] More recently, the work of Hillhouse and Mindiola on [(*dtbpe*)Ni(N(2,6-$(CHMe_2)_2C_6H_3$))] (*dtbpe* = 1,2-bis(di-*tert*-butylphosphino)ethane) revived this field of research and demonstrated that late first-row metal imido complexes are accessible by employing electron-rich bulky ancillary ligands.[26] Soon after, Peters *et al.* prepared the first mononuclear Co(III) and Fe(III) imido species via oxidative nitrene transfer to a Co(I) and Fe(I) species.[5,6] Following similar strategies, Theopold *et al.* and Warren *et al.* synthesized transient and stable Co(III) imido complexes supported by tris(pyrazolyl)borate and β-diketiminate ligands.[27,28]

We here report a rare example of a side-on (η^2) peroxo complex of a NHC ligand.[29,30] DFT calculations and reactivity studies established the nucleophilic character of the coordinated dioxygen ligand in $[(TIMEN^{xyl})Co(O_2)]^+$. Accordingly, the peroxo complex reacts with strong electrophiles to transfer an oxygen atom. The reactions of **1a** with CO and CH_2Cl_2, yielding the corresponding mononuclear Co(I) carbonyl and Co(II) chloro complexes are also reported.

We additionally report the reaction of **1a** and its mesitylene-analogue, $[(TIMEN^{mes})Co]Cl$ (**1b**), with aryl azides yielding monomeric Co(III) imido complexes. The cobalt—imido fragment in these complexes is electrophilic and, as a result, the imido group readily inserts into the cobalt—carbene bond. To the best of our knowledge, this intramolecular imido insertion reaction had not been observed

before and thus reveals a new type of reactivity of this interesting and valuable class of compounds.

5.2. Results and Discussion

5.2.1. Synthesis of complex [(TIMEN^{xyl})Co]Cl (1a)

Following our previously reported method (Chapter 3), the aryl-substituted tris(carbene) ligand tris[2-(3-xylenylimidazol-2-ylidene)ethyl]amine (TIMEN^{xyl}, xyl = 2,6-dimethylphenyl) were prepared by deprotonation of the corresponding imidazolium salts with potassium *tert*-butoxide. Reaction of TIMEN^{xyl} with a suitable cobalt(I) source, i.e. $Co(PPh_3)_3Cl$, yielded the [(TIMEN^{xyl})Co]Cl (**1a**) target complex, which precipitates from benzene as an analytically pure yellow powder in ~80% yield (Scheme 5-1). Complex **1a** possesses salt-like solubility and is only soluble in polar organic solvents such as acetonitrile and DMSO. It is sparsely soluble in THF, but insoluble in hydrocarbons and diethyl ether.

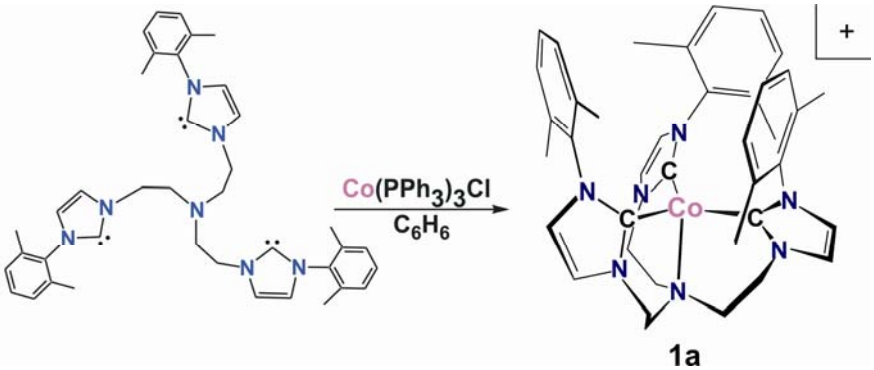

Scheme 5-1. Synthesis of Complex [(TIMEN^{xyl})Co]Cl (**1a**).

The ^{1}H NMR spectrum of **1a** in d_6-DMSO exhibits paramagnetically shifted and broadened peaks and is consistent with the proposed structural formula given in Scheme 5-1. In this complex, the 3-fold symmetry of TIMEN^{xyl} is preserved, giving rise to ten distinctive resonances in the range of 75 to -25 ppm. Although the assignment of these signals remains largely equivocal, their positions are diagnostic for determination of the purity and stability of **1a** in solution.

Under an inert-gas atmosphere, compound **1a** is stable in the solid-state but gradually oxidizes to yield the cobalt(II) species [[(TIMEN^{xyl})CoCl]Cl (**3**) when stored in acetonitrile or THF solution; replacement of the chloride anion with other counter ions does not increase the complexes' stability in solution. This instability in solution greatly hampered our attempt to obtain a crystal structure of **1a** in its pure form. In fact, slow ether diffusion into an acetonitrile solution of **1a** yielded red, plate-shaped crystals, which, according to their NMR spectrum, were a mixture of about 35% of **1a** and 65% of **3**. An X-ray diffraction analysis confirmed the co-crystallization of **1a** and **3**. The overall structure was modeled and refined with the two co-crystallizing components of **1a** (42%) and **3** (58%) (Figure 6-1). In **1a**, the TIMEN^{xyl} ligand is tetradentate coordinated through the three carbenoid carbon atoms and the anchoring nitrogen atom to the cobalt ion; in **3**, the TIMEN^{xyl} binds only through the three carbene centers and the axial coordination site of the cobalt ion is occupied by a chloride anion. The co-crystallization of **3** prevents a detailed discussion of the metric parameters of **1a**, but the structural data still allow for confirmation of atom connectivities and the cationic structure of **1a**. In addition, the structure of **3** deduced

from this experiment agrees well with that of an independently synthesized, pure crystal of **3** (vide infra).

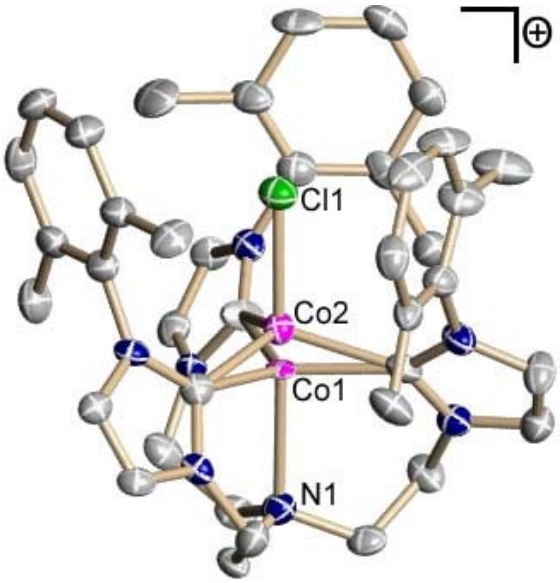

Figure 5-1. Overlay representation of the solid state molecular structures of co-crystallized **1a** and **3**, hydrogen atoms and solvent molecules are omitted for clarity; thermal ellipsoids are shown at 50% probability.

5.2.2. Synthesis and structure of complex [(TIMEN^{xyl})Co(CO)]Cl (2)

In complex **1a** the xylene substituents of the functionalized TIMEN^{xyl} ligand form a well-protected cavity with sufficient access to the cobalt ion for additional ligand binding. To test the reactivity and to further stabilize the electron-rich cobalt(I) ion, complex **1a** was reacted with an excess of CO gas (1 atm, Scheme 5-2). The reaction proceeded smoothly within minutes and the resulting green complex [(TIMEN^{xyl})Co(CO)]Cl (**2**) was isolated in 85% yield. The infra-red vibrational spectrum of **2** shows an intense absorption band at 1927 cm^{-1}, indicative of a terminal

carbonyl ligand.[31] The ^{1}H NMR spectrum of **2** exhibits paramagnetically shifted and broadened resonances between 80 and -15 ppm, suggesting a d^8 high spin (S = 1) electronic configuration of the Co(I) ion.

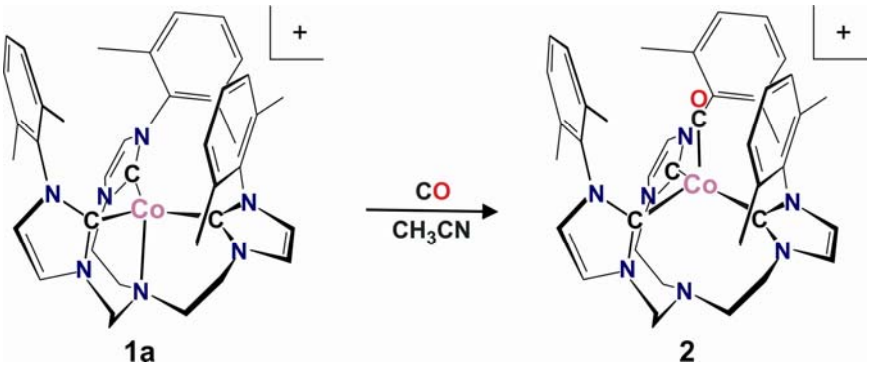

Scheme 5-2. Synthesis of Complex [(TIMEN^{xyl})Co(CO)]Cl (**2**).

The solid-state molecular structure of **2** was determined by X-ray diffraction analysis (Figure 5-2). The average Co—$C_{carbene}$ distance of 2.039(2) Å is slightly longer than those of other cobalt(I) NHC carbonyl complexes (1.888(3)—1.949(11) Å),[32] reflecting a greater degree of steric hindrance, most likely caused by the xylene ortho-methyl groups of the arene substituents. The CO ligand resides on the pseudo-C_3 axis of the [(TIMEN)Co] fragment and is centered within the C_3 propeller-like arrangement of the xylene substituents. The Co—C_{co} and carbonyl C—O bond distances were determined to be 1.8463(19) Å and 1.101(3) Å, respectively. The cobalt center is located +0.392 Å above the idealized trigonal plane defined by the three carbenoid carbon ligands. This, together with an average $C_{carbene}$—Co—$C_{carbene}$

bond angle of 116.42(6)^{o}, suggests that the coordination polyhedron of the cobalt ion in **2** is best described as distorted trigonal pyramidal.

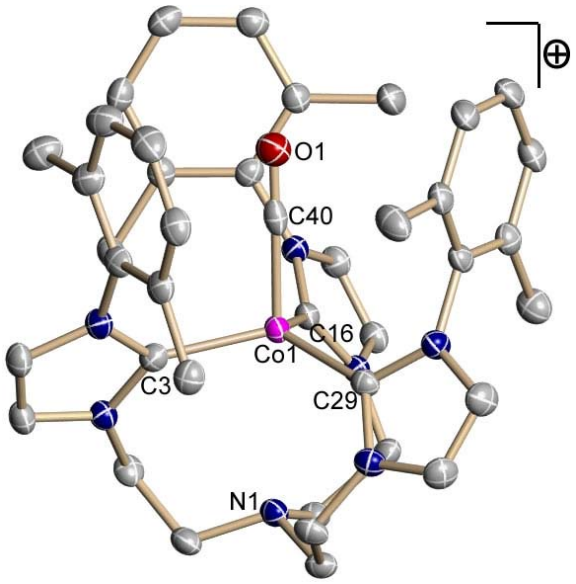

Figure 5-2. Solid-state molecular structure of [(TIMEN^{xyl})Co(CO)]Cl · 2 CH_3CN (**2** · 2 CH_3CN). Hydrogen atoms, anion, and solvent molecules are omitted for clarity; thermal ellipsoids are shown at 50% probability. Selected bond lengths (Å) and angles (deg.): Co(1)-C(3) 2.0347(17), Co(1)-C(16) 2.0545(17), Co(1)-C(29) 2.0267(16), Co(1)-C(40) 1.8463(19), Co(1)-N(1) 3.034, C(40)-O(1) 1.103(2), C(3)-Co(1)-C(16) 117.92(6), C(3)-Co(1)-C(29) 113.02(6), C(16)-Co(1)-C(29) 118.33(6).

5.2.3. Synthesis and structure of complexes [(TIMEN^{xyl})Co(Cl)]Cl (3) and [(TIMEN^{xyl})Co(CH_3CN)](BPh_4)$_2$ (4)

Based on our observation that, when stored in acetonitrile solution over extended periods of time, **1a** slowly oxidizes to form the corresponding cobalt(II) species [(TIMEN^{xyl})Co(Cl)]Cl (**3**), we sought to develop an independent synthesis for

3. Access to **3** was achieved by treatment of **1a** with benzylchloride or chlorinated solvents, such as dichloromethane or chloroform (Scheme 5-3), yielding blue micro-crystals in high yield (> 85%). The paramagnetic ^{1}H NMR spectrum of **3** in CD_2Cl_2 solution shows paramagnetic resonances between 70 and -4 ppm.

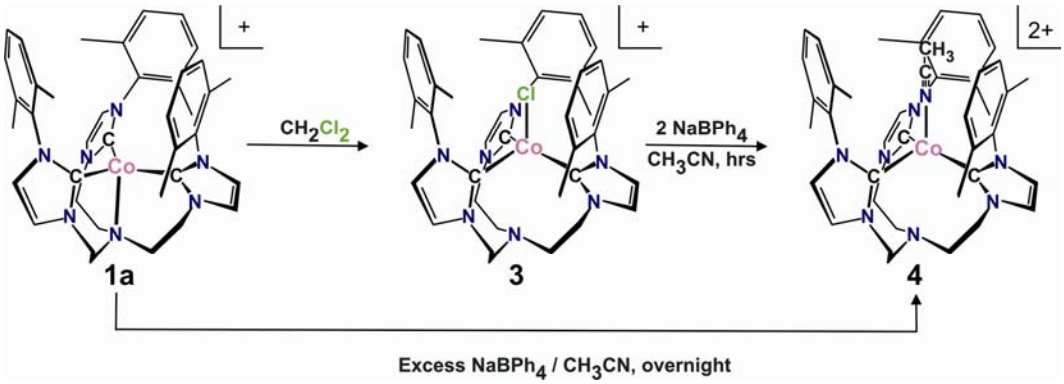

Scheme 5-3. Synthesis of Complexes [(TIMEN^{xyl})Co(Cl)]Cl (**3**) and (TIMEN^{xyl})Co(CH$_3$CN)](BPh$_4$)$_2$ (**4**)

Blue crystals suitable for an X-ray diffraction study were obtained by slow ether diffusion into a DMSO solution of **3**. The complex features a four-coordinate cobalt(II) center with a distorted trigonal-pyramidal geometry (Figure 5-3). The TIMEN^{xyl} ligand coordinates in a tridentate fashion and the axial chloride atom resides inside the pocket provided by the three xylene substituents. The average Co—C distance of 2.077(5) Å and C—Co—C angle of 115.5(2)^{o} are similar to those found in the Co(I) carbonyl complex **2**. In **3**, the displacement of the divalent Co ion from the carbene C_3-plane, however, was found to be +0.448 Å and, thus, is considerably larger than that found in the structure of **2**.

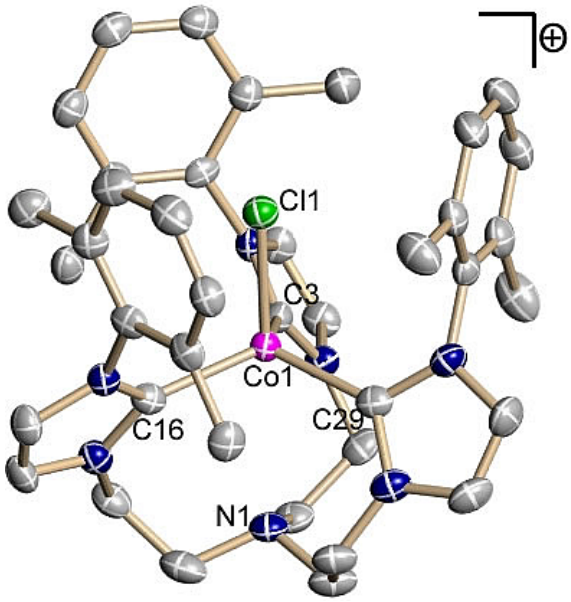

Figure 5-3. Solid-state molecular structure of [(TIMEN^{xyl})Co(Cl)]Cl · DMSO (**3** · DMSO). Hydrogen atoms, anion, and solvent molecules are omitted for clarity; thermal ellipsoids are shown at 50% probability. Selected bond lengths (Å) and angles (deg.): Co(1)-C(3) 2.078(5), Co(1)-C(16) 2.080(5), Co(1)-C(29) 2.074(5), Co(1)-Cl(1) 2.2557(15), Co(1)-N(1) 3.061, C(3)-Co(1)-C(16) 117.57(19), C(3)-Co(1)-C(29) 114.50(19), C(16)-Co(1)-C(29) 114.4(2).

Chloro complex **3** in acetonitrile reacted with $NaBPh_4$ to yield the dicationic acetonitrile complex [(TIMEN^{xyl})Co(CH_3CN)](BPh_4)$_2$ (**4**) (Scheme 5-3) and NaCl precipitation. After filtration of the blue solution and storage at low temperatures, dark-blue plate-shaped crystals of **4** were isolated in 80% yield. Alternatively, an acetonitrile solution of **1** containing $NaBPh_4$ also yields **4** within a few days. The ^{1}H NMR spectrum of **4** exhibits paramagnetically shifted and broadened signals spanning a wider range (100 and -8 ppm) compared to complex **3**.

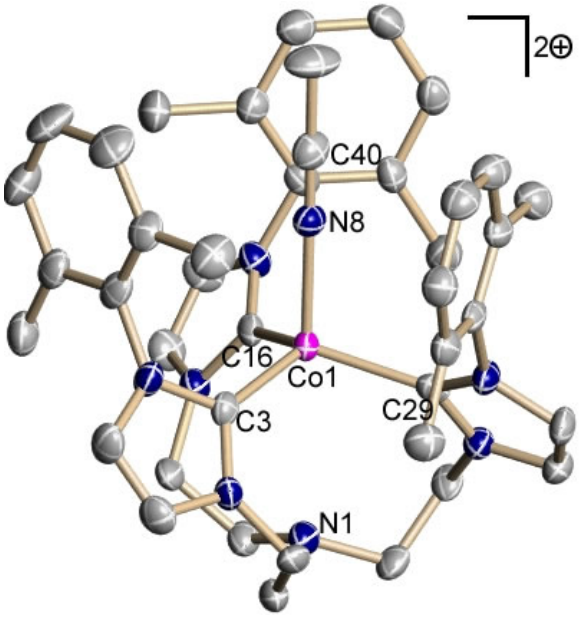

Figure 5-4. Solid-state molecular structure of $[(TIMEN^{xyl})Co(CH_3CN)](BPh_4)_2 \cdot CH_3CN$ (**4** · CH_3CN). Hydrogen atoms, anions, and solvent molecules are omitted for clarity; thermal ellipsoids are shown at 50% probability. Selected bond lengths (Å) and angles (deg.): Co(1)-C(3) 2.028(3), Co(1)-C(16) 2.033(3), Co(1)-C(29) 2.047(3), Co(1)-N(8) 2.035(3), Co(1)-N(1) 3.146, C(3)-Co(1)-C(16) 111.71(13), C(3)-Co(1)-C(29) 111.53(13), C(16)-Co(1)-C(29) 121.24(13), Co(1)-N(1)-C(40) 179.1(3).

The molecular structure of **4** displays features similar to those of **2** and **3**, namely, a four-coordinate cobalt ion and a tris(chelating) $TIMEN^{xyl}$ ligand with distorted trigonal-pyramidal coordination geometry (Figure 5-4). The average Co—C distance is 2.036(3) Å and the C—Co—C angle is 114.83(13)°. The axial acetonitrile molecule is essentially linearly coordinated, with a Co—N—C angle of 179.1(3)°. The displacement of the Co(II) ion from the trigonal plane of the carbene carbon ligands was determined to be +0.469 Å and, thus, is very similar to that found in **3**.

5.2.4. Electronic absorption spectra and magnetic properties of complexes 1a, 2-4

Paramagnetic complexes **1a**, **3 - 4** were characterized by SQUID magnetization measurements and electronic absorption spectroscopy (Figure 5-5 and 5-6).

At room temperature, the cobalt(I) complexes **1a** and **2** exhibit magnetic moments of 3.65 and 3.49 μ_B, respectively. These values are comparable to that of 3.8 μ_B reported for a related cobalt(I) complex $[(Tp)Co(C_2H_4)]$[33] and exceed the calculated spin-only value of 2.83 μ_B for a high-spin d^8 (S = 1) system. Such a deviation is generally considered to be caused by a substantial orbital angular momentum contribution from the cobalt ion. In the temperature range between 300 and 15 K, the magnetic moment of **1a** is nearly constant at 3.65 μ_B, but, likely due to zero-field splitting, decreases rapidly below 15 K until reaching a minimum of 2.60 μ_B at 5 K. In comparison, the magnetic moment of **2** shows little variation over the entire temperature range from 300 and 5 K.

Cobalt(II) complexes **3** and **4** exhibit magnetic properties characteristic for an ion with $3d^7$ high-spin (S = 3/2) electron configuration:[34] Complex **3** exhibits a temperature-independent magnetic moment of 4.23 μ_B in the temperature range between 300 and 5 K. The magnetic moment of complex **4**, on the other hand, has a room temperature value of 4.83 μ_B, which decreases gradually with decreasing temperature until it plateaus between 60 and 15 K. The magnetic moment decreases again at 10 K, reaching a minimum value of 3.80 μ_B at 5 K. The room temperature moments of both complexes, **3** and **4**, fall in the range between 4.3 and 4.8 μ_B. This

range is typically observed for high-spin cobalt(II) complexes with pseudo-tetrahedral or lower symmetry,[34-37] and is suggestive of a quartet magnetic ground state for complexes **3** and **4**.

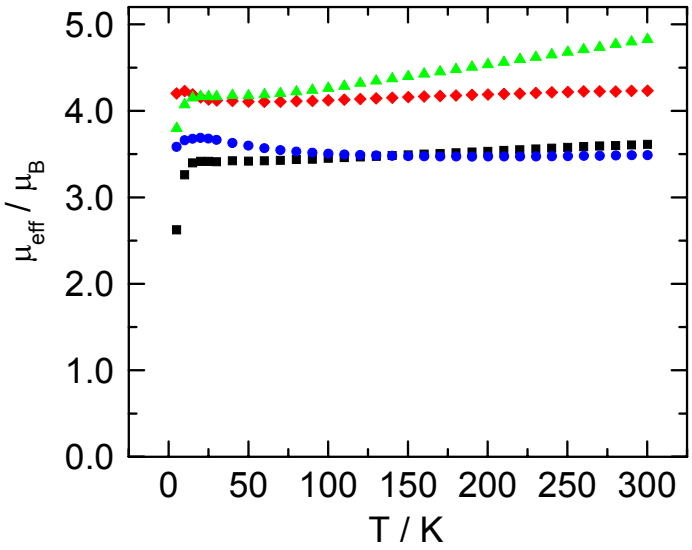

Figure 5-5. Plots of the effective magnetic moments, μ_{eff}, versus temperature from temperature-dependent SQUID magnetization measurements for complexes **1a** (■), **2** (●), **3** (♦), and **4** (▲).

Figure 5-6 and Table 5-1 summarize the UV/vis spectral data for complexes **1a**, **3**—**4**. All absorption spectra are dominated by intense charge-transfer bands in the UV and near visible regions. The visible spectra of cobalt(II) complexes **3** and **4** show d—d transitions around 600 nm (ε = 782 and 581 $M^{-1}cm^{-1}$), characteristic for high-spin Co(II) complexes in a distorted tetrahedral ligand field.[35] The positions and intensities of these bands correlate well with their distorted trigonal-pyramidal geometry (pseudo-C_{3v}).

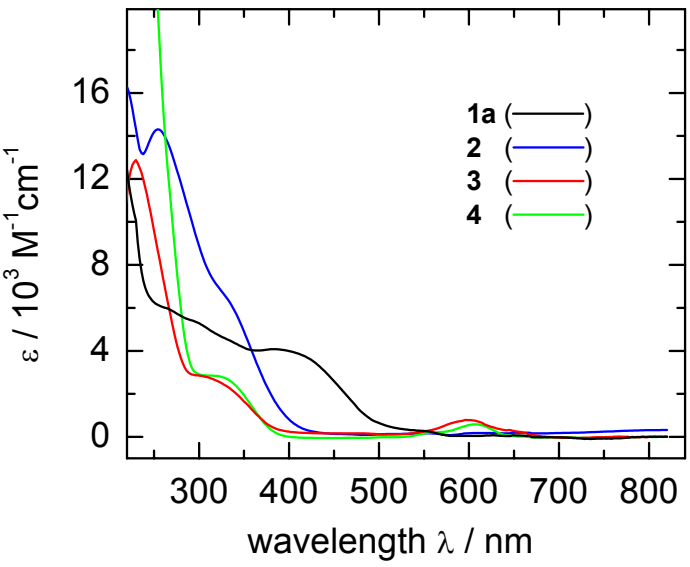

Figure 5-6. UV/vis absorption spectra of complexes **1a**, **2 - 4** recorded in acetonitrile solutions.

Table 5-1. UV/vis Data of Complexes **1a - 4**

Complex	Absorption Maximum λ_{max} / nm (Molar Extinction Coefficient ε / cm^{-1} M^{-1})
1a	220 (12426), 252 (6200), 384 (4080).
2	220 (16274), 254 (14300), 332 (6830).
3	220 (11262), 230 (12880), 308 (2890), 596 (782)
4	220 (78706), 324 (2801), 558 (201), 606 (581)

5.2.5. Synthesis and structure of the cobalt dioxygen complex [(TIMEN^{xyl})Co-(O_2)]BPh_4 (5)

The unusual molecular and electronic structure of the coordinatively unsaturated complex **1** prompted us to investigate its reactivity towards dioxygen. We found that a solution of **1** reacts cleanly with dioxygen at room temperature to form a 1:1 cobalt dioxygen adduct [(TIMEN^{xyl})Co(O_2)]$^+$ (Scheme 5-4). When the reaction was carried out in THF and in the presence of one equivalent of $NaBPh_4$, the resulting complex [(TIMEN^{xyl})Co(O_2)]BPh_4 (**5**) precipitated from the reaction mixture and was isolated as an analytically pure pale pink powder.

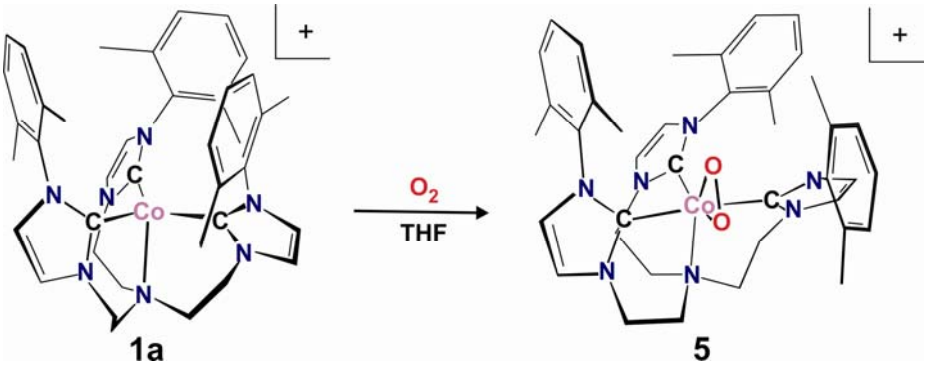

Scheme 5-4. Synthesis of Peroxo Complex [(TIMEN^{xyl})Co(O_2)]BPh_4 **(5)**

Based on the O—O stretching frequency, dioxygen complexes are generally classified as either peroxo (930-740 cm^{-1}) or superoxo (1200-1070 cm^{-1}) species.[38] In the infra-red vibrational spectrum of **5**, the O—O stretching frequency $\nu_{O\text{-}O}$ is found at 890 cm^{-1}, and it shifts to 840 cm^{-1} in the corresponding ^{18}O-labeled compound [(TIMEN^{xyl})Co($^{18}O_2$)]BPh_4. The isotopic shift of 50 cm^{-1} agrees well with the 51 cm^{-1}

calculated using a simple diatomic harmonic oscillator model. Accordingly, the infra-red spectra of **5** suggest the formation of a side-on peroxo complex.

The ^{1}H and ^{13}C NMR spectra of **5** are consistent with a diamagnetic cobalt(III) peroxo species. In the ^{13}C NMR spectrum, signals from the carbenoid carbons are not observed, probably due to coupling with the cobalt ion (I = 7/2, 100 %). Both ^{1}H and ^{13}C spectra, however, indicate a 3-fold symmetry in the coordinated $TIMEN^{xyl}$ ligand, suggesting a fluxional behavior of **5** in solution. The UV/vis absorption spectrum of **5** exhibits two weak d—d transitions centered at 484 (ε = 100 $cm^{-1}\,M^{-1}$) and 646 nm (ε = 35 $cm^{-1}\,M^{-1}$). The low extinction coefficients are consistent with the pseudo-octahedral geometry of the complex (vide infra).

The molecular structure of **5** was established by X-ray crystallography (Figure 5-7). The hexacoordinate cobalt ion is situated in the plane defined by the two oxygen atoms of the dioxygen ligand, the nitrogen atom on the nexus of the TIMEN framework, and one carbene carbon from the $TIMEN^{xyl}$ ligand, thereby bisecting the tetradentate chelator. The pseudo-octahedral coordination sphere is completed by the remaining two carbene carbon pendant arms of $TIMEN^{xyl}$ in the axial positions. The dioxygen ligand coordinates side-on with an O—O distance of 1.429(3) Å. This O—O bond distance falls well within the range of typical peroxide complexes (1.4-1.5 Å)[39] and is comparable with other cobalt(III) peroxo complexes (1.414(12)-1.441(11) Å).[21] This distance differs substantially, however, from the cobalt dioxygen complex [Tp'Co(O_2)] with the structurally related hydridotris(pyrazolyl)borate supporting ligand (1.355(3) Å at T = -123°C and 1.262(8) Å at room temperature).[22,39] It is

noteworthy that the structurally determined O—O bond distance correlates well with the observed O—O stretching frequency.[39] The Co—O bonds are slightly asymmetric with bond distances of 1.855(2) and 1.906(2) Å. With an average value of 1.962(4) Å, the Co—C distances are shorter than those of complexes **2 - 4**, reflecting the smaller radius of the cobalt(III) ion. In **5**, two C—Co—C angles were found to be close to 90° and a third C—Co—C angle close to 180° (C3-Co1-C29 = 98.65(14), C16-Co1-C29 = 91.63(15), and C3-Co1-C16 = 169.67(14)). This, together with an average N—Co—C angle of 90.2(1)°, demonstrates the remarkable flexibility of the TIMEN ligand system, stabilizing complexes with trigonal planar, trigonal pyramidal, and octahedral coordination geometries.

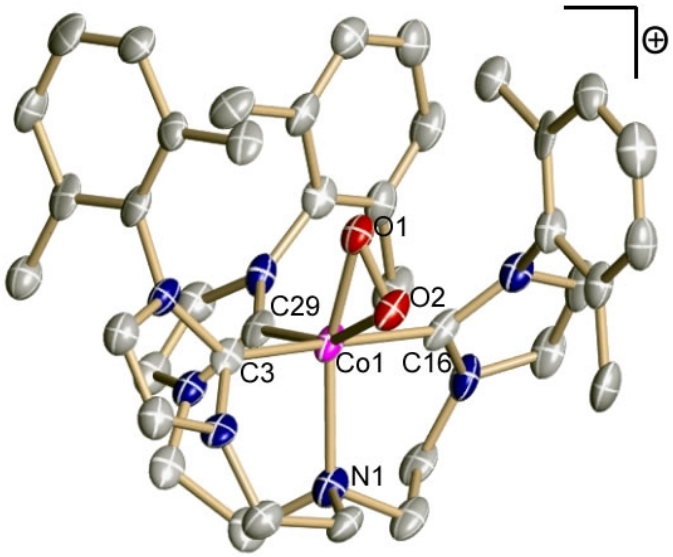

Figure 5-7. Solid-state molecular structure of complex $[(TIMEN^{xyl})Co(O_2)]BPh_4 \cdot Et_2O$ (**5** · Et_2O). Hydrogen atoms, anion, and solvent molecules are omitted for clarity; thermal ellipsoids are shown at 50% probability. Selected bond lengths (Å) and angles (deg.): Co(1)-C(3) 2.003(4), Co(1)-C(16) 1.934(4), Co(1)-C(29) 1.950(4), Co(1)-N(8) 2.137(3), Co(1)-O(1) 1.855(2), Co(1)-O(2) 1.906(2), O(1)-O(2) 1.429(3), C(3)-Co(1)-C(16) 169.67(14), C(3)-Co(1)-C(29) 98.65(14), C(16)-Co(1)-C(29)

91.56(14), O(1)-Co(1)-O(2) 44.64(10), N(1)-Co(1)-C(3) 89.64(13), N(1)-Co(1)-C(16) 91.56(14), N(1)-Co(1)-C(29) 89.27(13).

Complex **5** represents a rare example of a metal NHC complex with a coordinating dioxygen ligand.[30] The ability of $TIMEN^{xyl}$ to stabilize a monomeric cobalt peroxo entity likely arises from several factors: the tetradentate chelator is strongly electron-donating and, thus, is able to accommodate the high-valent Co(III) ion; the ligand backbone is very flexible and enables $TIMEN^{xyl}$ to form octahedral complexes; the three xylene substituents flank the activated dioxygen ligand, thereby effectively blocking the commonly observed bimolecular decomposition pathway to form μ-peroxo dimers.

5.2.6. DFT study on complex $[(TIMEN^{xyl})Co(O_2)]^+$

DFT calculations were carried out on the cationic part of the high-valent peroxo complex **5**. The calculation resulted in a geometry that is in good agreement with the experimentally determined one. The calculated O—O distance of 1.432 Å is very close to that of 1.429(3) Å found in the solid-state molecular structure of **5**, and the Co—O distances 1.852 and 1.905 Å are almost identical to the experimental values of 1.855(2) and 1.906(2) Å. The calculated Co—C and Co—N distances with 1.974 and 2.172 Å are also comparable to their experimental counterparts (1.962(4) and 2.137(3) Å).

Inspection of the frontier orbitals of complex **5** confirms that the complex's diamagnetism originates from a d^6 low-spin (S = 0) cobalt(III) center with a dative

peroxo ligand (Figure 5-8). The HOMO is predominantly composed of dioxygen π^* orbitals with some minor contribution from the metal *d* orbital. Five nearby orbitals, namely, LUMO+1, LUMO, HOMO-1, HOMO-2, and HOMO-3, are mainly metal *d*-orbital based. The shapes and relative positions of these orbitals indicate that the cobalt ion has a $d(xy)^2d(xz)^2d(yz)^2d(z^2)^0d(x^2\text{-}y^2)^0$ electronic configuration. The presence of a high-lying, filled dioxygen π^* orbital suggests the coordinated dioxygen ligand to be nucleophilic.

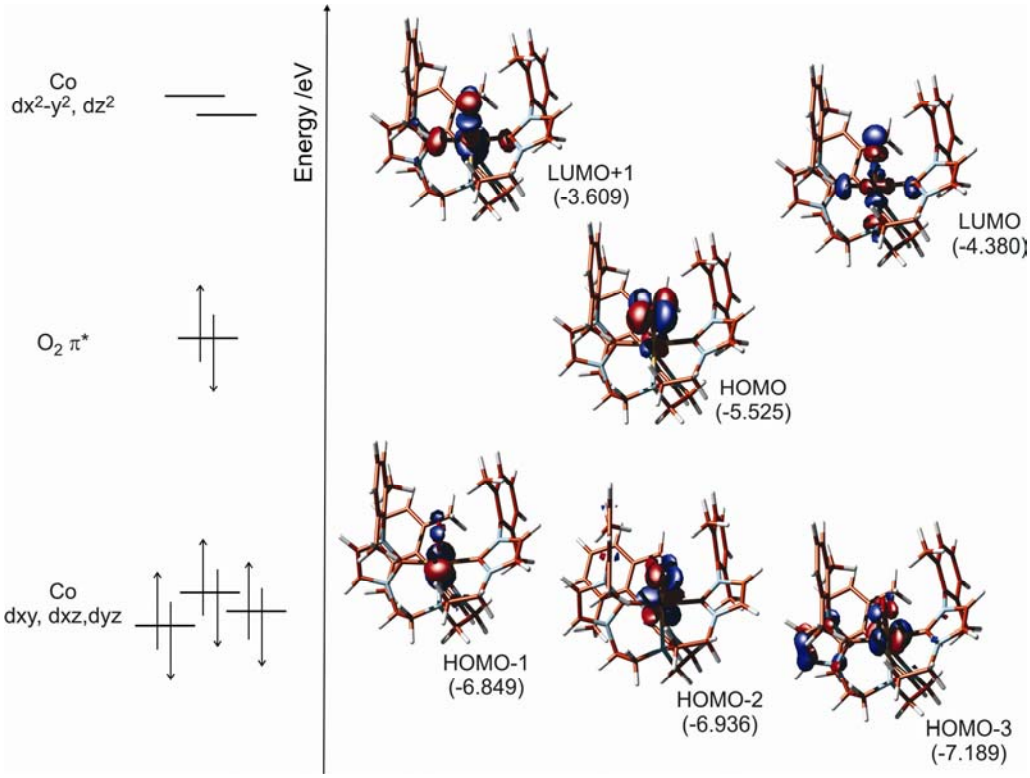

Figure 5-8. Energies and relative positions of the frontier molecular orbitals of $[(TIMEN^{xyl})Co(O_2)]^+$. Calculations are performed at the BP86/ZORA/TZP level using the ADF 2003.01 program suites.

5.2.7. Reactivity of [(TIMEN^{xyl})Co(O_2)]BPh_4 (5)

Transition metal peroxo complexes are classified as either nucleophiles or electrophiles according to their reactivity with organic substrates.[16,40] While reaction with triphenylphosphine to give triphenylphosphine oxide is used to assess metal peroxides' electrophilicity,[41] the nucleophilicity of peroxo species is assessed by reaction with the extremely electron-deficient olefin tetracyanoethylene (TCNE).[42] Early transition metal peroxides, such as [(porphyrin)Ti(O_2)],[41] reportedly react as electrophiles; late transition metal peroxides, like [(PPh_3)$_2$Pt(O_2)][42] and [(porphyrin)Fe(O_2)]$^-$,[41,43] generally are nucleophilic. In accord with the prediction of the DFT study, peroxo complex **5** is nucleophilic and only reacts with electron-deficient organic substrates.

An acetonitrile solution of complex **5** reacts with benzoyl chlorides, for instance, yielding complex **4** and phenyl benzoate quantitatively. The NMR and absorption spectra of **4** isolated from this reaction are identical to those of an independently synthesized sample prepared as described above. The only tractable organic product identified in this reaction was phenyl benzoate, identified by NMR, IR, and GC-MS spectroscopy. A possible reaction mechanism is shown in Scheme 5-5. In the first step, the coordinated dioxygen attacks benzoyl chloride to form a cobalt(III) peroxyphenyl acetate [(TIMEN)CoOOC(O)Ph]$^{2+}$,[44] which undergoes homolytic Co—O bond cleavage[16] to give a cobalt(II) species and a ·OOC(O)Ph radical. The organic radical then decomposes into CO_2 and a ·OPh radical, which in turn reacts with another molecule of benzoyl chloride to form the final PhOC(O)Ph product.[45] In

support of this mechanism, we found that $Ph^{18}OC(O)Ph$ was produced when an $^{18}O_2$ labeled sample of **5** was employed in the reaction. Unfortunately, we are unable to detect any CO_2 evolution from the reaction mixture. This is likely due to the small, stoichiometric quantities of CO_2 released in this reaction.

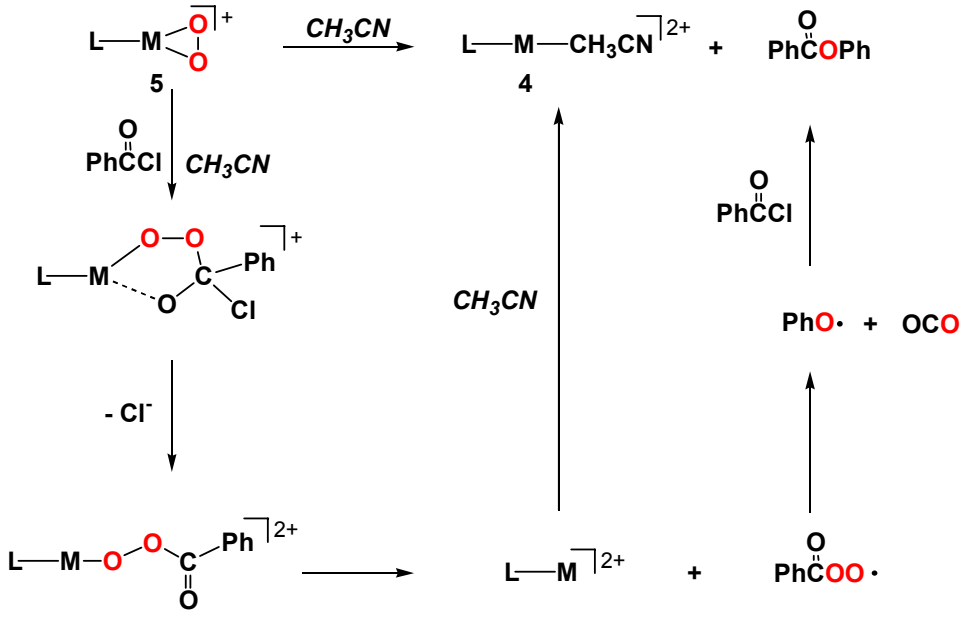

Scheme 5-5. Proposed Mechanism for the Reaction of **5** with Bnzoyl Chloride

Complex **5** also reacts with electron-deficient alkenes. Reaction of **5** with benzylidenemalonitrile yields **4** and benzyl aldehyde, and reaction of **5** with TCNE yields **4** and unidentified organic compounds. The mechanisms of these reactions are currently under investigation, but based on the reaction products, we suspect homolytic Co—O bond cleavage as part of the mechanism. Palladium and platinum peroxo complexes undergo similar reactions via a 2+2 cycloaddition pathway to give cyclic peroxy-adducts.[42,46]

We also treated **5** with α,β-unsaturated alkenes such as 2-cyclohexene-1-one, 1,4-naphthoquinone, and 2-methyl-1,4-naphthoquinone but no reaction was observed during an extended period of time. Likewise, complex **5** is also inert toward styrene, cyclohexene, and triphenylphosphine, confirming its lack of electrophilicity.

Valentine and co-worker have classified peroxo species into class I and class II nucleophiles according to their relative nucleophilicity.[41] Class I nucleophiles react not only with highly electron-deficient substrates such as TCNE and acyl halide, but also with enones and quinones. Class II nucleophiles, on the other hand, merely react with TCNE and acyl halides. Accordingly, the reactivity of complex **5** identifies it as class II nucleophile. Other class II nucleophiles include group VIII metal peroxides, such as $[(PPh_3)_2Pd(O_2)]$, $[(PPh_3)_2Pt(O_2)]$, and $[(PPh_3)_2Ir(CO)(O_2)]I$.[42,46,47]

5.2.8. Comparison of the tris(carbene) TIMEN and analogous tris(phosphine) ligand systems

The unique electronic properties of NHCs render the N-anchored tris(carbene) TIMEN ligand system considerably diverse from known analogous polydentate phosphine chelators,[48] such as the neutral NP_3 ($P = PPh_2$) ligand by Sacconi[49,50] and the anionic $PhBP_3^-$ system ($P = PPh_2$, P^iPr_2) developed by Peters *et al*.[5,6,36,51] These differences are reflected in the coordination polyhedra and electronic properties of the isolated Co-TIMEN complexes **1a**, **2**–**4**. While, with cobalt(I) for instance, the TIMEN ligand system forms the high-spin carbonyl species $[(TIMEN)Co(CO)]^+$, phosphine based ligand systems NP_3 and $PhBP_3^-$ ($P = PPh_2$) form diamagnetic

complexes $[(NP_3)Co(CO)]^+$ and $[(PhBP_3)Co(CO)_2]$, respectively. The cobalt(II) halide $[(TIMEN^{xyl})CoCl]^+$ is four-coordinate, distorted trigonal-pyramidal and high-spin; the equivalent phosphine species $[(NP_3)CoCl]^+$, however, is five-coordinate, trigonal-bipyramidal and high-spin;[49] $[(PhBP_3)CoI]$ is four-coordinate, pseudo-tetrahedral and low-spin.[36]

The steric properties of the TIMEN ligand system are also unique and are generally beneficial for the stabilization of reactive intermediates. While the sterics of coordinated polyphosphine ligands are regulated by substituents on the coordinating phosphorus atom, the sterics of TIMEN are controlled by substituents at the imidazole N3 position. Upon formation of (distorted) tetrahedral metal phosphine complexes, the substituents all point away from the metal center. As a result, the axial binding site in these complexes is exposed and dimeric compounds form readily via binuclear decomposition pathways. Even the sterically encumbering and versatile $PhB(^iPr_2P)_3^-$ ligand system does not prevent such dimerization as evidenced by a unique but highly reactive terminal iron(IV) nitrido complex $[(PhB(^iPr_2P)_3)Fe{\equiv}N]$ that forms a dinitrogen-bridged dinuclear ferrous species.[7] Due to constrains of the sp^2 hybridized ring nitrogen, aryl substituents in complexes of the $TIMEN^R$ ligand are oriented perpendicular to the trigonal tris(carbene) metal plane, thereby forming a deep, well-protected binding cavity. As a result, in complexes of the type $[(TIMEN)\text{-}M(L_{ax})]^{n+}$, binuclear decomposition pathways are effectively suppressed.

This steric difference is similarly evident for TIMEN and β-diketiminate ligand systems.[28,52] It was reported that the cobalt(I) complex of the xylene-

functionalized β-diketiminate ligand, namely [(Me_2NN)Co(η^6-toluene)] (Me_2NN = 2,4-bis(2,6-dimethylphenyllimido)pentane), reacted with dioxygen to form a dinuclear [(Me_2NN)Co(μ-O)$_2$Co(NNMe_2)] complex. Monomeric dioxygen adducts could not be isolated from this reaction.[28] The differences in dioxygen reactivity of [(Me_2NN)Co(η^6-toluene)] and [(TIMEN^{xyl})Co]$^+$ may thus also be steric in origin.

5.2.9. Synthesis of cobalt(II) azido complex [(TIMEN^{xyl})Co(N_3)]$^+$ (6)

Transition metal imido species might be synthesized by reaction of low-valent transition metal precursors with organic azides. In an initial attempt to prepare a Co(III) imido species, we treated **1a** with trimethylsilyl azide. The reaction proceeds smoothly, but only the one-electron oxidized [(TIMEN^{xyl})Co(N_3)]Cl (**6**) was isolated (92% yield). Complex **6** was fully characterized, including paramagnetic ^{1}H NMR, IR, UV-Vis spectroscopy, SQUID measurements and CHN analysis. An X-ray diffraction analysis on single-crystal of **6**(BPh_4) (Figure 5-9) shows that the distorted trigonal-pyramidal ligand environment of the Co(II) ion in **6** is composed of three carbenoid carbon atoms and an axial azido ligand.

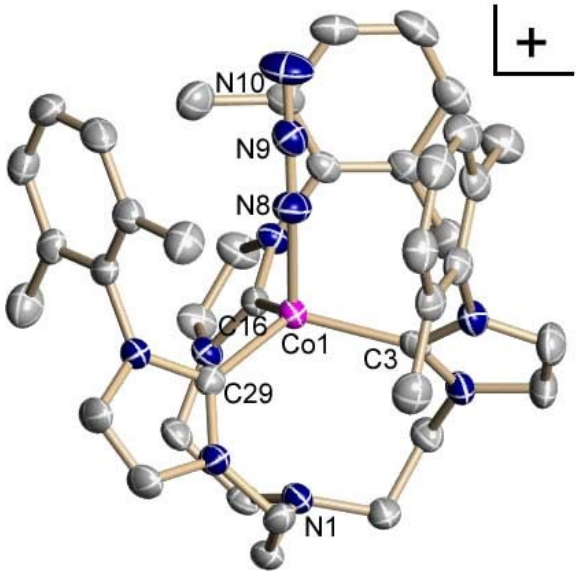

Figure 5-9. Solid-state molecular structure of **6**(BPh_4) • CH_3CN. Hydrogen atoms, counter ions, and solvent molecules are omitted for clarity; thermal ellipsoids are shown at 50% probability. Selected bond lengths (Å) and bond angles (deg.): Co(1)-C(3) 2.052(2), Co(1)-C(16) 2.049(2), Co(1)-C(29) 2.047(2), Co(1)-N(8) 1.938(2), N(8)-Co(1)-C(29) 110.48(8), N(8)-Co(1)-C(16) 101.85(8), C(29)-Co(1)-C(16) 110.52(8), Co(1)-N(8)-N(9), 166.31(18).

5.2.10. Synthsis and characterization of cobalt(III) imido complexes $[(TIMEN^{R})Co(NAr^{R'})]^{+}$ (7a - 8b)

To circumvent the tendency of silyl azides to form azide radicals, we decided to use aryl azides. Reactions of **1a** and **1b** with aryl azides at -35°C produced the desired Co(III) imido complexes $[(TIMEN^{R})Co(NAr^{R'})]Cl$ (**7a** - **8b**, Scheme 5-6) that could be isolated at low temperature in near quantitative yields. Complexes **7a** – 8**b** are diamagnetic (d^6 low-spin, S = 0), and the ^1H spectra suggest a C_3-symmetry of these molecules in solution. All complexes are deep-green, and their UV/vis spectra consist of characteristic absorption bands at 298, 430, and 604 nm (Figure 5-10).

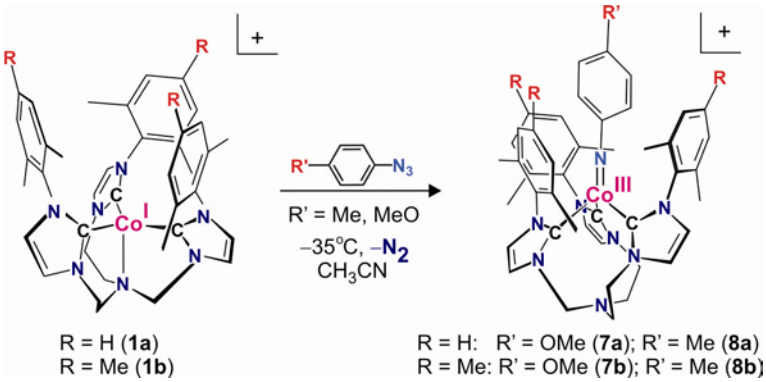

Scheme 5-6. Synthesis of Cobalt Imido Species [(TIMEN^{R})Co(NAr$^{R'}$)]Cl.

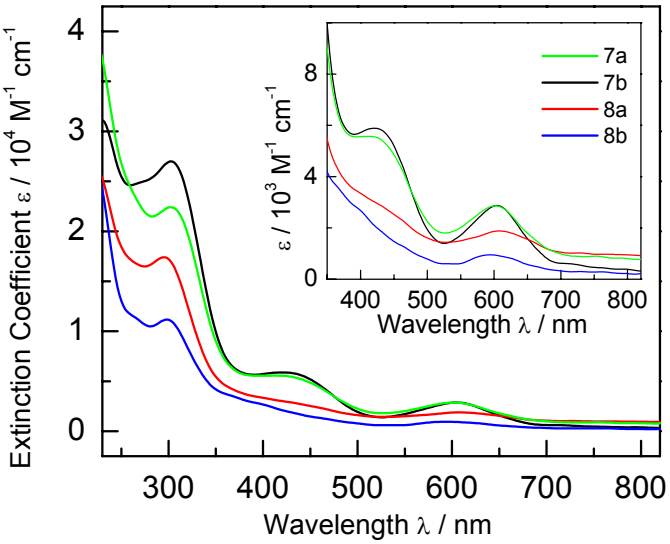

Figure 5-10. UV/vis Spectra of complexes **7a - 8b** recorded in acetonitrile solution.

X-ray quality crystals of **7b**(BPh_4) were grown by applying a weak vacuum on a cold acetonitrile solution of **7b** in the presence of excess of $NaBPh_4$. The complex displays a pseudo-tetrahedral geometry (Figure 5-11). The TIMEN^{mes} ligand is co-

ordinated in a tridentate fashion, rendering the complex in a pseudo-tetrahedral geometry. The average Co—C bond distance of 1.947(3) Å is similar to 1.962(4) found in octahedral Co(III) peroxo complex $[(TIMEN^{xyl})Co(O_2)](BPh_4)$. The Co—N distance of 1.675(2) Å compares well with that of 1.624(4) and 1.658(2) Å in the only other two reported terminal Co(III) imido species.[5,28] This short distance, together with an almost linear Co—N—C angle of 168.6(2)°, is indicative of strong multiple bond character within the Co—NAr entity. The N—C distance of 1.386(4) Å is significantly smaller than that of a normal N—C single bond (sum of the N and C covalent radii is 1.52 Å),[53] suggesting a substantial degree of electron delocalization within the aryl imido ligand. Also noticeable from the crystal structure is the short distance between the imido nitrogen (N8) and one of the coordinated carbene carbon (C3) ligands: the N8—C3 distance of 2.982 Å is considerably smaller than the sum of their van der Waals radii (3.25 Å).[53]

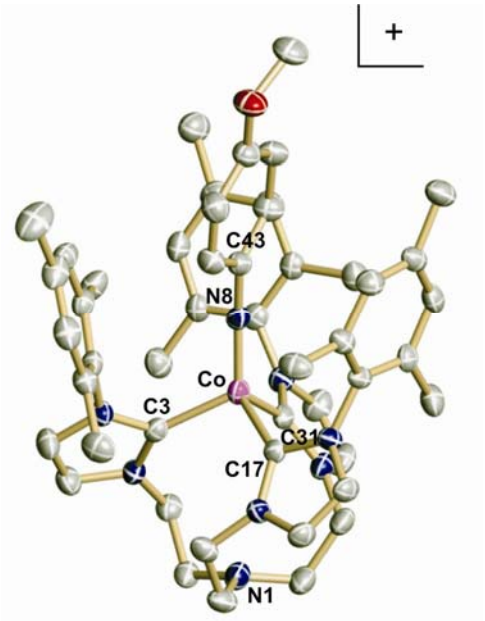

Figure 5-11. Solid-state molecular structures of **7b**(BPh_4). Hydrogen atoms and counter anions are omitted for clarity; thermal ellipsoids are shown at 50% probability. Selected bond lengths (Å) and angles (deg.): Co-C3 1.940(3), Co-C17 1.938(3), Co-C31 1.962(3), Co-N8 1.675(2), N8-C43 1.386(4), Co-N8-C43 168.6(2).

To gain insight into the electronic structure of complexes **7a**–**8b**, DFT calculations (ADF 2003.1, ZORA/TZP, BP86) were carried out on the model compound **7bm**, in which the TIMEN mesitylene substituents were replaced by methyl groups. The calculation results in a core geometry that is in good agreement with the experimentally determined structure of **7b**(BPh_4). In the orbital splitting diagram (Figure 5-12), the Co(III) ion adopts a $d(xy)^2d(x^2\text{-}y^2)^2d(z^2)^2d(xz)^0d(yz)^0$ ground state electron configuration. As expected, MOs of d(xz) and d(yz) parentage are greatly destabilized by strong π-bonding interaction with the imido π-lone pairs and thus lie at highest energies (Figure 5-13a). The orbital of $d(z^2)$ parentage interacts with the σ-lone pair of the imido nitrogen and is positioned well below the π* orbitals. Orbitals of d(xy) and $d(x^2\text{-}y^2)$ origin have minimal interaction with ligand orbitals and thus are most stabilized among the set of d-orbitals. The six d-electrons therefore occupy MOs up to the $d(z^2)$ orbital, which is σ-antibonding with respect to the Co—NR bond; the π* orbitals d(xz) and d(yz) remain unoccupied (LUMOs). Although the metal—imido group is often formulated as a formal triple bond, consisting of two degenerate π- and one σ-type orbital interactions[24], the bonding within the cobalt imido unity reported here is best described as a formal double bond. Interestingly, the DFT study also suggests that there is a considerable amount of electron density donated from one of the σ-orbitals of the carbenoid carbon into the π-orbital of the

imido nitrogen (Figure 5-13b). This finding corroborates well with the short distance between the C3 and N8 atom observed in the crystal structure and the tendency of the imido group to insert into the Co—C bond in solution (vide infra).

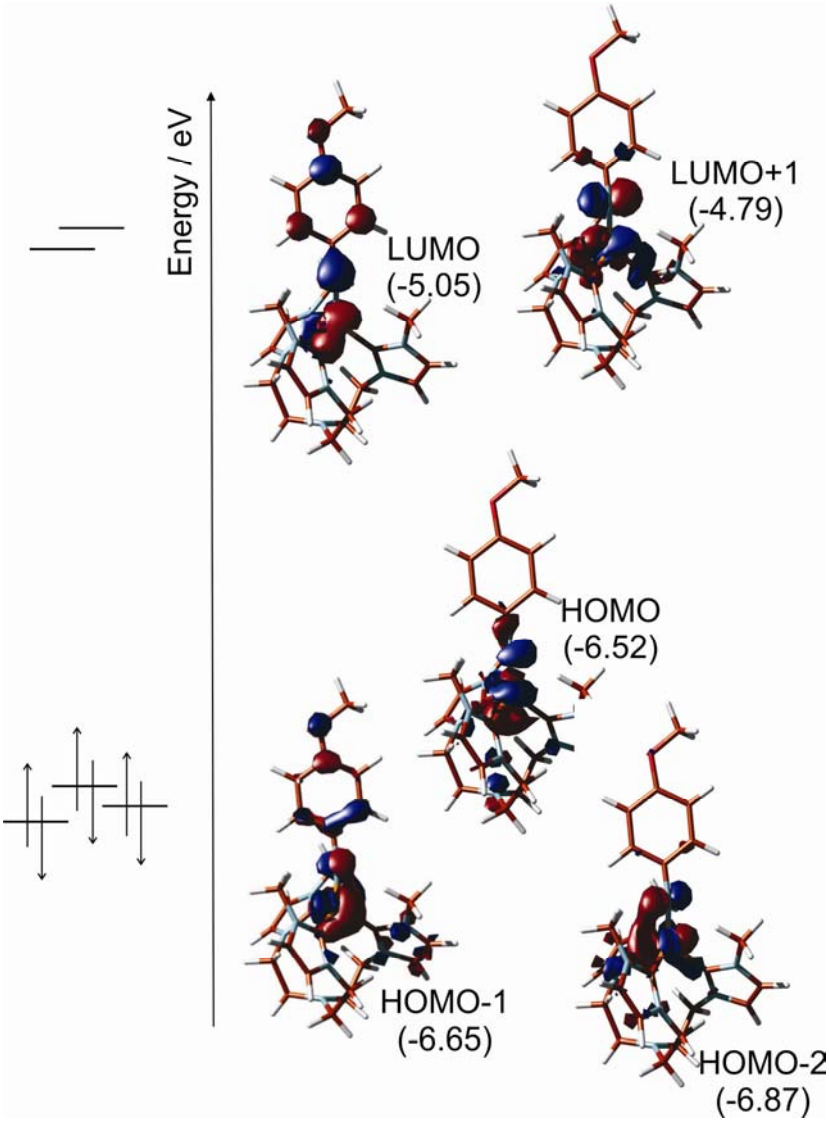

Figure 5-12. Orbital energy diagram for model complex **7bm**.

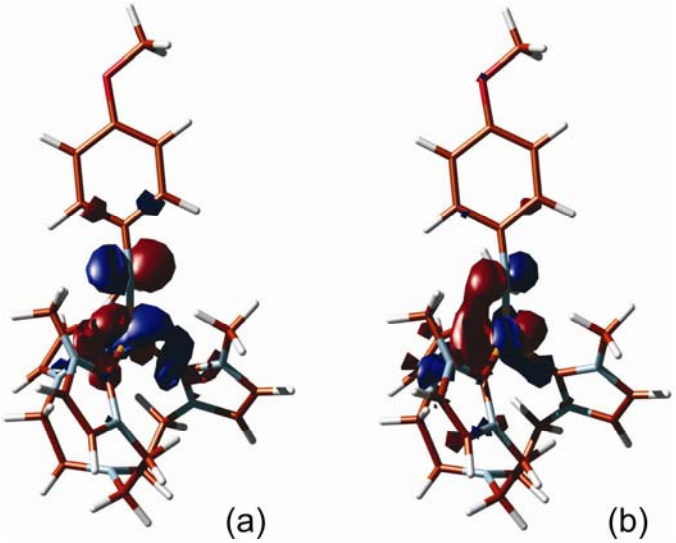

Figure 5-13. Representative frontier orbitals for model complex **7bm**. (a) One of the two π-antibonding orbitals, LUMO+1, with d(xz)/d(yz) parentage (b). HOMO-2 orbital showing interaction between carbene carbon and imido nitrogen.

5.2.11. Intra-Molecular imido insertion in $[(TIMEN^{R})Co(NAr^{R'})]^{+}$ complexes

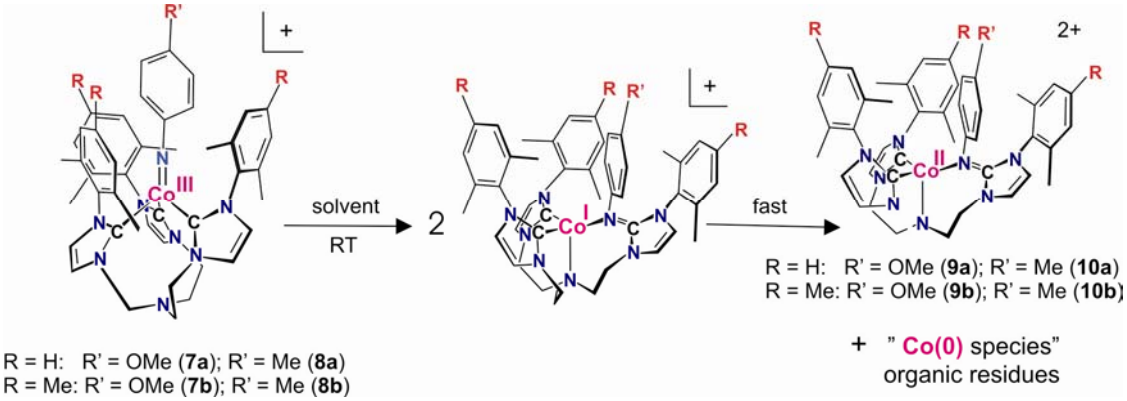

Scheme 5-7. Imido Insertion into the Cobalt—Carbene Bond in Complexes $[(TIMEN^{R})Co(NAr^{R'})]^{+}$

Complexes **7a** – **8b** are stable in solid-state and in solution at -35^{0}C. In solution at room temperature, however, the imido group readily inserts into one of the cobalt—carbene bonds as established by ^{1}H NMR spectroscopy and X-ray crystallography. We propose that the immediate reaction product is a cobalt(I) imine species, which further disproportionates to form cobalt(II) imine complexes $[(TIMEN^{aryl})*Co]^{2+}$ (**9a** – **10b**), metallic cobalt(0) species, and unidentified organic side-products (Scheme 5-7). The molecular structure of **9b**$(BPh_4)_2 \cdot 1.5Et_2O$ and **10a**$(BPh_4)_2 \cdot Et_2O$ exhibit iso-structural geometries (**9b**, Figure 5-14; **10a**, Figure 5-15). The modified TIMEN' ligand coordinates to the Co ion through two of its remaining carbenoid carbons, the anchoring nitrogen and the newly formed imine N atom.

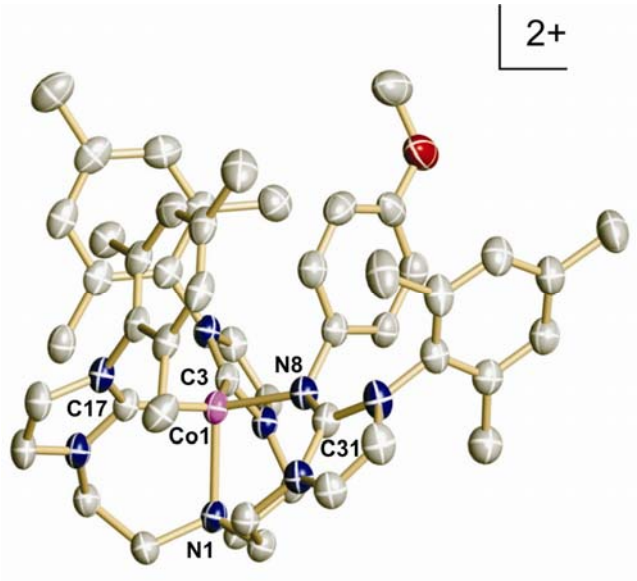

Figure 5-14. Solid-state molecular structures of **9b**(BPh4)2·1.5Et2O. Hydrogen atoms and counter anions are omitted for clarity; thermal ellipsoids are shown at 50% probability. Selected bond lengths (Å) and angles (deg.): Co1-C3 2.043(2), Co1-C17 2.019(2), Co1-N1 2.169(2), Co1-N8 1.9973(19), N8-C31 1.330(3).

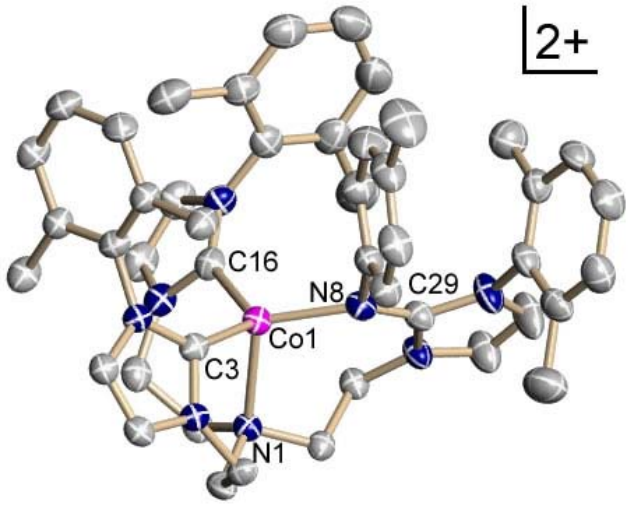

Figure 5-15. Solid-state molecular structure of **10a**$(BPh_4)_2$•Et_2O. Hydrogen atoms, counter ions, and solvent molecules are omitted for clarity; thermal ellipsoids at 50% probability. Selected bond lengths (Å) and bond angles (deg.): Co(1)-C(3) 2.033(3), Co(1)-C(16) 2.033(3), Co(1)-N(1) 2.199(2), Co(1)-N(8) 1.990(2), N(8)-C(29) 1.326(4), N(8)-Co(1)-C(3) 116.52(10), N(8)-Co(1)-C(16) 119.05(11), N(8)-Co(1)-N(1) 106.65(9), C(3)-Co(1)-N(1) 94.04(10), C(16)-Co(1)-N(1) 96.70(10).

The disproportionation rate is likely faster than that of the imido insertion, thereby preventing the isolation of the cobalt(I) imine complexes. However, monitoring this reaction by UV/vis spectroscopy confirmed that the reaction follows first-order kinetics and that the rate-limiting step is indeed the imido insertion (Figure 5-16 and 5-17). The rate of these reactions is independent of the solvent and was determined to be $1.6*10^{-4}$ for (**7a**), $8.7*10^{-5}$ (**7b**), $3.4*10^{-4}$ (**8a**), and $3.0*10^{-4}$ s^{-1} (**8b**) at 20°C, respectively. In general, the insertion is faster for less electron rich species, suggesting that the reaction proceeds via an electrophilic attack of the imido group on the Co—C bond.

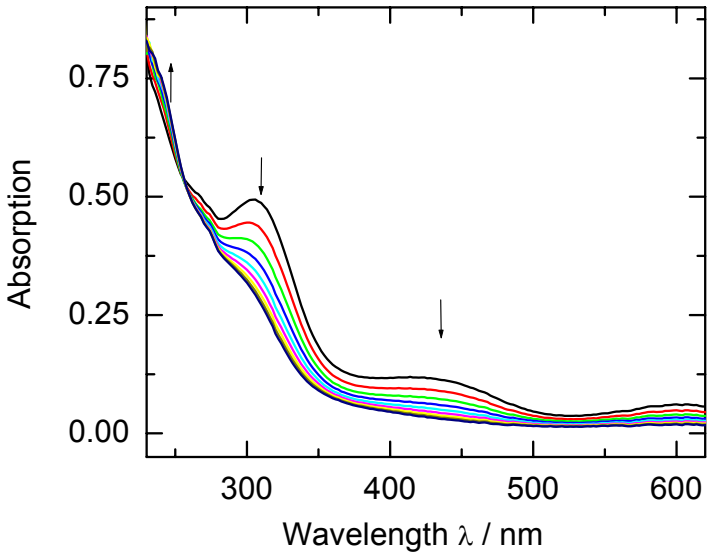

Figure 5-16. Time-dependent spectra of **7a** in acetonitrile solution showing an isosbestic point at 256 nm wavelength; spectra were recorded every 30 minutes.

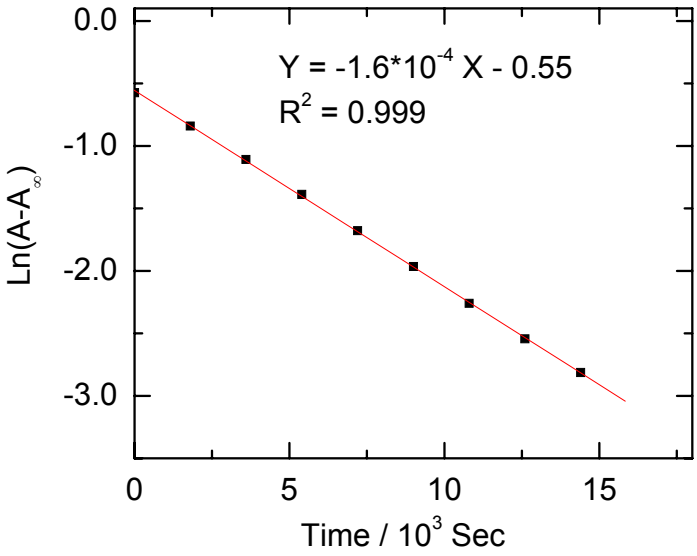

Figure 5-17. First-order imido insertion with respect to the concentration of **7a**. A: absorption at 298 nm; rate constant was determined to be $1.6 * 10^{-4}\ s^{-1}$.

5.2.13. Aziridination of styrene catalyzed by $[(TIMEN^{xyl})Co]^{+/2+}$ complexes

Table 5-2. Catalytic Aziridination of Styrene Employing Iminoiodinane as the Nitrogen Source. [a] Reactions are conducted at room temperature in a dry-nitrogen atmosphere in 1 mL solvent. Yields are based on NMR and referred to the limiting reagent. Scale: 0.5 mmol limiting agent. [b] $[(TIMEN^{xyl})CoCl]Cl$. [c] Control. [d] Referred to styrene.

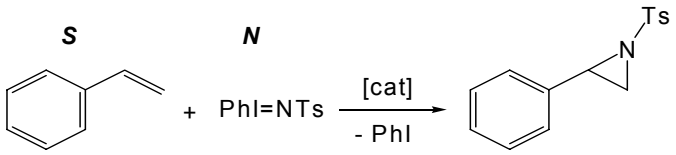

entry	***S*** : ***N***	[cat][b] (mol %)	solvent	Time (h)	yield (%)[a]
1	1:1	5	CH_3CN	7	80
2	5:1	5	CH_3CN	2	82
3	1:1	1	CH_3CN	48	77
4[c]	1:1	0	CH_3CN	24	<15
5	1:1	5	CH_2Cl_2	1.5	84
6	5:1	5	CH_2Cl_2	0.6	87
7	1:2	5	CH_2Cl_2	2.5	74 (>95[d])
8	1:1	1	CH_2Cl_2	8	81

The cobalt(II) complex $[(TIMEN^{xyl})CoCl]Cl$ (**3**) catalyzes the aziridination of olefins with (N-tosylimino)phenyliodinane (PhINTs). Employing standard experimental conditions, i.e., 5 mol % catalyst loading, 5:1 substrate (S):PhINTs (N) ratio, the aziridination of styrene completed in 1.5 hours in 87 % yield. When the reaction was carried out with a 1:1 S:N ratio, no significant decrease in yield (84 %)

was observed, demonstrating a high efficiency of the nitrene transfer in this system. In this regard, the cobalt(II) system out-performs most of the known copper(I) catalyst,[54] and is comparable to a copper(I) scorpionate system developed by Perez.[55] Table 5-2 also suggests that dichloromethane is a better solvent than the commonly used acetonitrile in these reactions. We found that the cobalt(I) complex [(TIMEN^{xyl})Co]Cl (**1a**) also catalyzed the aziridination with similar yields, albeit with slower reaction rates. The first step of these reactions presumably is the oxidation of **1a** to **3** in solution.

In light of the tendency of cobalt(III) imido species **7a** – **8b** to undergo intra-molecular imido transfer reactions, a cobalt(IV) nitrene intermediate in the catalytic aziridination reactions reported here is highly unlikely. Rather, a radical-type mechanism likely is the preferred mechanism, given the accessibility of the Co(II)/(III) couple with this ligand system.

5.3. Conclusion

The low-valent and coordinatively unsaturated cobalt(I) tris(carbene) complex [(TIMEN^{xyl})Co]Cl (**1a**) has been synthesized and characterized. This versatile starting material reacts with CO, CH_2Cl_2, and O_2 to yield the cobalt carbonyl [(TIMEN^{xyl})-Co(CO)]Cl (**2**), the chloro [(TIMEN^{xyl})Co(Cl)]Cl (**3**), and peroxo [(TIMEN^{xyl})Co-(O_2)](BPh$_4$) (**5**) complexes. Spectroscopic and structural characterization of all complexes **1a**, **2**-**5** (including the acetonitrile complex [(TIMEN^{xyl})Co(NCCH$_3$)]-(BPh$_4$)$_2$ (**4**)) has allowed important insights into structure/reactivity relations. The X-ray analyses revealed the remarkable flexibility of the tripodal ligand system TIMEN,

stabilizing distorted trigonal-pyramidal, four-coordinate cobalt(I) and cobalt(II) complexes as well as a six-coordinate cobalt(III) complex with pseudo-octahedral geometry. This structural flexibility, allowing formation of a large variety of 1:1 metal complexes, is provided by the anchoring nitrogen atom of the carbene tripod. We have demonstrated that this nitrogen atom additionally holds potential to serve as a two electron σ-donor ligand to aid stabilization of higher valent complexes such as the cobalt(III) peroxo complex reported here. The stability of the monomeric cobalt(III) peroxo complex $[(TIMEN^{xyl})Co(O_2)](BPh_4)$ is increased by steric protection of the bulky xylene substituents on the TIMEN imidazole rings. The sterically well-protected coordinated dioxygen ligand reacts with electron-deficient organic substrates. This experimentally determined dioxygen reactivity correlates well with the theoretically predicted reactivity established by DFT calculations. One-electron reduction of complex **5** is expected to further increase the nucleophilicity of the dioxygen ligand.

The ability of the polydentate carbene ligand $TIMEN^R$ (R = aryl) to stabilize both low- and high-valent metal ions and its unique steric properties suggest that the $[(TIMEN^R)M]$ scaffold is well-suited for hosting other highly reactive terminal functionalities, e.g., monodentate imido, nitrido, and oxo ligands. This has been demonstrated by the synthesis of the terminal cobalt(III) imido species $[(TIMEN^R)Co(NAr^{R'})]Cl$ (**7a - 8b**).

As evidenced by their unusual intra-molecular imido insertion reactions, the highly electrophilic imido complexes **7a** – **8b** are distinctively different from other

isolated terminal cobalt(III) imido species, which are either unreactive[28] or slightly neucleophilic.[5] Noteworthy, reactions of **7a** – **8b** with an excess of nucleophiles, such as styrene and tetramethylimidazol-2-ylidene, do not result in inter-molecular imido transfer proving the intra-molecular reaction to be favored (fast). Our results support the perspective of using well-defined late metal imido complexes as N-group transfer agents for nucleophilic organic substrates, such as alkenes, in the absence of intra-molecular reactive sites.

5.4. Experimental Section

Methods and Procedures

Manipulations of air-sensitive compounds were performed under a dry nitrogen atmosphere using standard Schlenk techniques and inert-gas glove boxes (MBraun Labmaster by M. Braun, Inc.). Solvents were purified using a two-column solid-state purification system (Glasscontour Systems, Joerg Meyer, Irvine, CA) and transferred to the glove box without exposure to air. NMR solvents were obtained from Cambridge Isotope Laboratories, degassed, and stored over nitrogen and activated molecular sieves prior to use. All NMR spectra were recorded on Varian spectrometers operating at 400/300 MHz (^{1}H NMR) and 100 MHz (^{13}C NMR) at room temperature (20^{o}C) in d_6-benzene, d_3-acetonitrile, d_2-dichoromethane, and d_6-DMSO solutions respectively. The signals were referenced to residual solvent peaks unless noted otherwise (δ in ppm). Solid-state magnetization measurements of powdered samples were recorded on a SQUID magnetometer (Quantum Design) at 10 kOe

between 5 and 300 K. Magnetic susceptibility data were corrected for background and underlying diamagnetic contributions using tabulated Pascal constants.[56] Data reproducibility was carefully checked in multiple individual measurements of independently synthesized samples. Infrared spectra (400—4000 cm^{-1}) of solid samples were obtained on a Thermo Nicolet Avatar 360 FT-IR spectrophotometer as KBr pellets. Electronic absorption spectra were recorded from 190 nm to 820 nm (HP 8452A Diode Array, UV/vis spectrophotometer). High resolution mass spectral data were obtained on a ThermoFinnigan MAT900XP spectrometer (UCSD Mass Spec Facility). 3-Nitrobenzyl alcohol was used as the matrix, and polypropylene glycol was used as the internal reference. Elemental analyses were performed by Kolbe Microanalytical Laboratory (Mülheim a. d. Ruhr/Germany).

Computational Details. DFT calculations were carried out using the Amsterdam Density Functional program package ADF, release 2003.01.[57] The Vosko, Wilk and Nusair (VWN) local density approximation,[58] Becke's exchange correlation,[59] and Perdew correlation[60] were used. The calculation also included scalar relativistic effects (ZORA)[61] for all atoms. Uncontracted Slater-type Orbitals (STOs)[62] were used as basis functions. Co: triple-ζ basis set augmented with a set of p functions and frozen core 2p. N: triple-ζ basis set augmented with a set of d functions and frozen core 1s. C: triple ζ-basis set augmented with a set of d functions and frozen core 1s. O: triple ζ-basis set augmented with a set of d functions and frozen core 1s. H: triple-ζ basis set augmented with a set of p functions. This basis combination is denoted TZP in the ADF program.

For complex **5**, calculations start from X-ray defined geometry of the cationic portion of **5**; for complex **7b**, calculations were performed on model complex **7bm**, in which the three mesitylene substitutents on the TIMEN ligand were replaced by methyl groups. No symmetry was specified in the calculations; the counter anions were not included.

Molecular orbitals were visualized using the MOLDEN program package (http://www.cmbi.kun.nl/~schaft/molden/molden.html). ADFrom program was used to convert the TAPE21 file from ADF into a MOLDEN file.

Synthesis:

Starting Materials. Tris(2-chloroethyl)-amine,[63] 1-(2,6-xylyl)imidazole, 1-(2,4,6-trimethyl)imidazole,[64] tolyl azide and 4-methoxy azide[65] , and [N-(p-toluenesulfonyl)imino]phenyliodinane (PhINTs)[66]were prepared following literature procedures. Chlorotristriphenylphosphine cobalt(I) (Aldrich), azidotrimethylsilane (Aldrich), tetracyanoethylene (Aldrich), benzylidenemalonitrile (Aldrich), styrene (Aldrich), benzoyl chloride (Fischer), sodium tetraphenylborate (Acros), and potassium *tert*-butoxide (Acros) were obtained from commercial sources and used as received. Carbon monoxide and dioxygen gases were purchased from Matheson Tri-gas, 95% ^{18}O-labeled O_2 was ordered from Cambridge Isotope Laboratories, Inc.

C**aution:** *Although we have not encountered any problems, it should be noted that organic azides are shock sensitive and potentially explosive and should be handled with care.*

$[H_3TIMEN^{xyl}](PF_6)_3$: A 50 mL flask was charged with tris(2-chloroethyl)amine (1.58 g, 7.7 mmol) and 1-(2,6-xylyl)imidazole (4.00 g, 60 mmol) and the mixture was heated to 150 °C for 2 days. During this time, a brown solid precipitated from the solution. The solid was filtered off, dissolved in 20 mL methanol and the solution filtered. This solution was evaporated to dryness to yield the crude product $[H_3TIMEN^{xyl}]Cl_3$. The hygroscopic chloride salt was converted to the corresponding, stable hexafluorophosphate salt, $[H_3TIMEN^{xyl}](PF_6)_3$, by addition of a solution of $NaPF_6$ (3.88 g, 23.1 mmol) in 20 mL methanol. The white hexafluorophosphate salt precipitated immediately, was collected by filtration, washed with small volumes of cold methanol, re-dissolved in acetone, and filtered. The solvent was evaporated to dryness and the resulting solid was dried in a vacuum. (6.5 g; yield: 80%). ^{1}H NMR (300 MHz, d_6-DMSO, 20 °C): δ = 9.46 (s, 3H), 8.09 (d, ^3J(H,H) = 1.1 Hz, 3H), 8.02 (d, ^3J(H,H) = 1.1 Hz, 3H), 7.49 (t, ^3J(H,H) = 7.8 Hz, 3H), 7.39 (d, ^3J(H,H) = 7.8 Hz, 6H), 4.48 (t, ^3J(H,H) = 6.0 Hz, 6H), 3.26 (s, 9H), 2.12 ppm (s, 18H). ^{13}C NMR (100 MHz, d_6-DMSO, 20 ^{o}C): δ = 137.3, 136.6, 133.5, 130.6, 128.7, 123.6, 123.4, 52.2, 46.9, 17.0 ppm.

$[H_3TIMEN^{mes}](PF_6)_3$: A 50 mL flask was charged with tris(2-chloroethyl)amine (1.62 g, 7.9 mmol) and 1-(2,4,6-trimethyl)imidazole (4.44 g, 23.8 mmol) and the mixture was heated to 150 °C for 2 days. During this time, a brown solid precipitated from the solution. The solid was filtered off, dissolved in 20 mL methanol and the solution filtered. This solution was evaporated to dryness to yield the crude product $[H_3TIMEN^{mes}]Cl_3$. The hygroscopic chloride salt was converted to the

corresponding, stable hexafluorophosphate salt, $[H_3TIMEN^{mes}](PF_6)_3$, by addition of a solution of $NaPF_6$ (4.12 g, 24.5 mmol) in 20 mL methanol. The off-white hexafluorophosphate salt precipitated immediately, was collected by filtration, washed with small volumes of cold methanol, re-dissolved in acetone, and filtered. The solvent was evaporated to dryness and the resulting solid was dried in a vacuum. (6.74 g; yield: 78%). ^{1}H NMR (300 MHz, d_6-DMSO, 20 °C): δ = 9.40 (s, 3H), 8.05 (d, ^3J(H,H) = 1.1 Hz, 3H), 7.98 (d, ^3J(H,H) = 1.1 Hz, 3H), 7.17 (s, 6H), 4.38 (t, ^3J(H,H) = 6.0 Hz, 6H), 3.15 (t, ^3J(H,H) = 6.0 Hz, 6H), 2.33 (s, 9H), 2.01 ppm (s, 18H). ^{13}C NMR (100 MHz, d_6-DMSO, 20 ^{o}C): δ = 140.4, 137.3, 133.5, 134.2, 131.0, 129.2, 123.8, 123.3, 52.2, 46.8, 20.6, 16.9 ppm.

[TIMEN^{xyl}]: A solution of potassium *tert*-butoxide (0.428 g, 3.81 mmol) in THF was added dropwise to a suspension of $[H_3TIMEN^{xyl}](PF_6)_3$ (1.00 g, 0.95 mmol) in 5 mL THF and stirred for 1 h. The solution was evaporated to dryness and the solid residue dissolved in 15 mL of diethyl ether. The resulting solution was filtered and the filtrate was evaporated to dryness in vacuum. The solid was collected, washed with cold pentane, and dried in a vacuum (0.43 g; Yield: 75%). ^{1}H NMR (300 MHz, d_6-DMSO, 20 °C): δ = 7.32 (d, ^3J(H,H) = 1.1 Hz, 3H), 7.21 (m, 3H), 7.14 (m, 6H), 7.06 (d, ^3J(H,H) = 1.1 Hz, 3H), 4.08 (t, ^3J(H,H) = 6.0 Hz, 6H), 3.01 (t, J(H,H) = 6.0 Hz, 6H), 1.94 (s, 18H,). ^{13}C NMR (100 MHz, d_6-Benzene, 20 ^{o}C): δ = 211.8, 141.4, 135.8, 121.3, 120.5, 120.3, 119.9, 119.6, 67.5, 56.6, 49.7, 32.2, 18.4 ppm.

[TIMEN^{mes}]: A solution of potassium *tert*-butoxide (0.411 g, 3.66 mmol) in THF was added dropwise to a suspension of $[H_3TIMEN^{mes}](PF_6)_3$ (1.00 g, 0.92mmol)

in 5 mL THF and stirred for 1 h. The solution was evaporated to dryness and the solid residue dissolved in 15 mL of diethyl ether. The resulting solution was filtered and the filtrate was evaporated to dryness in vacuum. The solid was collected, washed with cold pentane, and dried in a vacuum (0.51 g; Yield: 72%). ^{1}H NMR (300 MHz, d_6-benzene, 20 °C): δ = 7.54 (s, 6H), 7.16 (s, 6H), 6.73 (s, 3H), 4.44 (t, ^{3}J(H,H) = 6.0 Hz, 6H), 3.28 (t, J(H,H) = 6.0 Hz, 6H), 2.51 (s, 9H), 2.50 (s, 18H). ^{13}C NMR (100 MHz, d_6-benzene, 20 ^{o}C): δ = 211.3, 138.9, 135.3, 129.2, 120.5, 120.0, 67.5, 56.7, 49.7, 32.3, 18.3 ppm.

[(TIMEN^{Xyl})Co]Cl (**1a**): A solution of $(PPh_3)_3CoCl$ (1.1 g, 1.24 mmol) in 5 mL benzene was added dropwise to a solution of TIMEN^{Xyl} (0.76 g, 1.24 mmol) in 5 mL benzene. The reaction mixture was allowed to stir for one hour during which a yellow-brown precipitate formed. The precipitate was filtered, washed with benzene, diethyl ether, and dried in a vacuum (0.69 g; Yield: 79%). ^{1}H NMR (300 MHz, d_6-DMSO, 20 °C): δ = 72.1 (s, 3H, $\Delta\nu_{1/2}$ = 62 Hz), 27.3 (s, 3H, $\Delta\nu_{1/2}$ = 51 Hz), 15.5 (s, 3H, $\Delta\nu_{1/2}$ = 46 Hz), 7.8 (s, 9H, $\Delta\nu_{1/2}$ = 81 Hz), 7.0 (s, 6H, $\Delta\nu_{1/2}$ = 37 Hz), 5.5 (s, 3H, $\Delta\nu_{1/2}$ = 30 Hz), 4.4 (s, 3H, $\Delta\nu_{1/2}$ = 32 Hz), -2.8 (s, 3H, $\Delta\nu_{1/2}$ = 18 Hz), -5.0 (s, 9H, $\Delta\nu_{1/2}$ = 93 Hz), -24.0 ppm (s, 3H, $\Delta\nu_{1/2}$ = 20 Hz). Elemental analysis (%) calcd for $C_{39}H_{45}N_7CoCl$: C 66.33, H 6.42, N 13.88; found: C 66.09, H 6.22, N 13.57.

[(TIMEN^{mes})Co]Cl (**1b**): A solution of $(PPh_3)_3CoCl$ (1.1 g, 1.24 mmol) in 5 mL benzene was added dropwise to a solution of TIMEN^{mes} (0.81 g, 1.24 mmol) in 5 mL benzene. The reaction mixture was allowed to stir for one hour during which a yellow-brown precipitate formed. The precipitate was collected, washed with

benzene, diethyl ether, and dried in a vacuum (0.65 g; Yield: 74%). ^{1}H NMR (300 MHz, d_3-acetonitrile, 20 °C): δ = 69.0 (s, 3H, $\Delta\nu_{1/2}$ = 11 Hz), 26.3 (s, 3H, $\Delta\nu_{1/2}$ = 54 Hz), 16.7 (s, 3H, $\Delta\nu_{1/2}$ = 43 Hz), 7.2 (s, 9H, $\Delta\nu_{1/2}$ = 71 Hz), 6.9 (s, 6H, $\Delta\nu_{1/2}$ = 14 Hz), 6.3 (s, 9H, $\Delta\nu_{1/2}$ = 21 Hz), 4.6 (s, 3H, $\Delta\nu_{1/2}$ = 13 Hz), -1.8 (s, 3H, $\Delta\nu_{1/2}$ = 32 Hz), -3.6 (s, 9H, $\Delta\nu_{1/2}$ = 57 Hz), -22.1 ppm (s, 3H, $\Delta\nu_{1/2}$ = 9 Hz). Elemental analysis (%) calcd for $C_{42}H_{51}N_7CoCl$: C 67.47, H 6.82, N 13.12; found: C 67.54, H 6.74, N 13.05.

[(TIMEN^{Xyl})Co(CO)]Cl (**2**): A yellow solution of [(TIMEN^{Xyl})Co]Cl (30 mg, 0.04 mmol) in acetonitrile was sparged with carbon monoxide gas, resulting in an immediate color change to green. The reaction mixture was stirred for 30 minutes, filtered through Celite, and evaporated to give **2** as a green solid. The precipitate was collected by filtration, washed with diethyl ether, and dried in a vacuum (25 mg; Yield: 85%). Green crystals suitable for X-ray diffraction analysis were grown by diffusion of diethyl ether into a saturated acetonitrile solution of **2** at room temperature. ^{1}H NMR (300 MHz, d_3-Acetonitrile, 20 °C): δ = 76.0 (s, 3H, $\Delta\nu_{1/2}$ = 15 Hz), 36.1 (s, 3H, $\Delta\nu_{1/2}$ = 53 Hz), 25.7 (s, 3H, $\Delta\nu_{1/2}$ = 11 Hz), 11.7 (s, 3H, $\Delta\nu_{1/2}$ = 17 Hz), 10.1 (s, 3H, $\Delta\nu_{1/2}$ = 15 Hz), 5.8 (s, 3H, $\Delta\nu_{1/2}$ = 29 Hz), 3.9 (s, 3H, $\Delta\nu_{1/2}$ = 37 Hz), 1.4 (s, 9H, $\Delta\nu_{1/2}$ = 49 Hz), -3.4 (s, 3H, $\Delta\nu_{1/2}$ = 39 Hz), -10.7 ppm (s, 9H, $\Delta\nu_{1/2}$ = 106 Hz). IR (KBr): ν(CO) = 1927 cm^{-1}. Elemental analysis (%) calcd for $C_{40}H_{45}N_7OCoCl$**:** C 65.43, H 6.17, N 13.35; found: C 65.37, H 5.96, N 13.28.

[(TIMEN^{Xyl})CoCl]Cl (**3**): [(TIMEN^{Xyl})Co]Cl (50 mg, 0.71 mmol) was dissolved in 2 mL dichloromethane to form a blue solution. Diethyl ether was then diffused into the solution at room temperature to give blue crystals of **3** overnight.

The crystals were collected by filtration, washed with diethyl ether, and dried in a vacuum (46 mg; Yield: 87%). Crystals suitable for X-ray diffraction analysis were grown by diffusion of diethyl ether into a solution of **3** in DMSO at room temperature. ^{1}H NMR (300 MHz, d_2-dichloromethane, 20 °C): δ = 67.4 (s, 3H, $\Delta\nu_{1/2}$ = 66 Hz), 33.3 (s, 3H, $\Delta\nu_{1/2}$ = 94 Hz), 31.2 (s, 3H, $\Delta\nu_{1/2}$ = 96 Hz), 9.5 (s, 6H, $\Delta\nu_{1/2}$ = 24 Hz), 6.8 (s, 3H, $\Delta\nu_{1/2}$ = 72 Hz), 6.4 (s, 3H, $\Delta\nu_{1/2}$ = 53 Hz), 5.7 (s, 3H, $\Delta\nu_{1/2}$ = 71 Hz), 1.9 (s, 9H, $\Delta\nu_{1/2}$ = 114 Hz), 0.6 (s, 9H, $\Delta\nu_{1/2}$ = 103 Hz), -3.3 ppm (s, 3H, $\Delta\nu_{1/2}$ = 24 Hz). Elemental analysis (%) calcd for $C_{39}H_{45}N_7CoCl_2$**:** C 63.16, H 6.11, N 13.22; found: C 63.17, H 5.88, N 13.16.

[(TIMEN^{Xyl})Co(CH$_3$CN)](BPh$_4$)$_2$ (4): Method A. 2 equivalents of $NaBPh_4$ were added to a blue solution of [(TIMEN^{Xyl})CoCl]Cl (120 mg, 0.16 mmol) in acetonitrile and the mixture was filtered through Celite. Blue crystals started to form from this filtrate within 30 min. The crystals were collected by filtration, washed with diethyl ether, and dried in a vacuum (168 mg; yield: 80%). Method B. Excess of $NaBPh_4$ was added to a yellow solution of [(TIMEN^{Xyl})Co]Cl (30 mg, 0.04 mmol) in acetonitrile. The solution gradually turns blue and blue needle-like crystals precipitated within 1 day. The crystals were collected by filtration, washed with diethyl ether, and dried in a vacuum (20 mg; Yield: 38%). ^{1}H NMR (300 MHz, d_3-DMSO, 20 °C): δ = 98.3 (s, 3H, $\Delta\nu_{1/2}$ = 15 Hz), 30.7 (s, 3H, $\Delta\nu_{1/2}$ = 42 Hz), 19.6 (s, 3H, $\Delta\nu_{1/2}$ = 20 Hz), 12.5 (s, 9H, $\Delta\nu_{1/2}$ = 15 Hz), 7.8 (s, 3H, $\Delta\nu_{1/2}$ = 33 Hz), 7.16 (m, 16H), 6.92 (m, 16H), 6.80 (dd, 8 H), 4.3(s, 6H, $\Delta\nu_{1/2}$ = 29 Hz), 1.3 (s, 9H, $\Delta\nu_{1/2}$ = 35

Hz), -3.2 (s, 3H, $\Delta\nu_{1/2}$ = 8 Hz), -6.0 ppm (s, 3H, $\Delta\nu_{1/2}$ = 7 Hz). Elemental analysis (%) calcd for $C_{89}H_{88}N_8B_2Co$**:** C 79.17, H 6.57, N 8.30; found: C 80.69, H 6.11, N 7.53.

[(TIMEN^{Xyl})Co(O$_2$)]BPh$_4$ (5): 1 equivalent of $NaBPh_4$ was added to a suspension of [(TIMEN^{Xyl})Co]Cl (100 mg, 1.4 mmol) in 3 mL THF. All solids dissolved immediately and the resulting solution was filtered and transferred to a Schlenk flask. The flask was evacuated and cooled to -78^{o}C. Neat dioxygen gas was transferred to the flask and the reaction mixture was allowed to warm up to room temperature. A pale-pink solid started to precipitate from the solution within 1 h. The solid was collected by filtration, washed with diethyl ether, and dried in a vacuum (90 mg; yield: 57%). ^{1}H NMR (300 MHz, d_6-DMSO, 20 °C): δ = 7.50 (s, 3H), 7.16 (s, br, 8H), 6.92 (m, 14H), 6.78 (d, ^3J(H,H) = 6 Hz, 3H), 6.75 (s, 3H), 6.71 (s, 3H), 4.25 (s, br, 3H), 3.60 (s, br, 3H), 3.50(s, br, 3H), 2.65 (s, br, 3H), 1.64 (s, 9H), 1.25 ppm (s, 9H). ^{13}C NMR (100 MHz, d_6-DMSO, 20 ^{o}C): δ = 164.8, 164.3, 163.8, 163.3, 140.6, 136.2, 135.3, 127.6, 127.4, 126.1, 126.0, 125.9, 125.7, 123.5, 122.2, 47.7, 18.6, 17.8 ppm. IR(KBr): ν(OO) = 890 cm^{-1}. Elemental analysis (%) calcd for $C_{73}H_{65}N_7BO_2Co$**:** C 76.77, H 5.70, N 8.59; found: C 76.34, H 5.43, N 8.28. The ^{18}O-labeled [(TIMEN^{Xyl})Co(^{18}O$_2$)]BPh$_4$ complex was synthesized by applying 95 % $^{18}O_2$ labeled gas.

Reactions of [(TIMEN^{Xyl})Co(O$_2$)]BPh$_4$ with benzoyl chloride: 1 equivalent of benzoyl chloride was added to a stirring solution of **5** (30 mg, 0.026 mmol) in acetonitrile. The reaction was allowed to stir for 1 day, and the resulting blue solution was evaporated to dryness. Diethyl ether was added to extract the organic product,

which, after workup, was identified as phenyl benzoate by IR, NMR, and GC-MS. The solid residue was also collected and identified as complex **4** by NMR spectroscopy (30 mg; yield: 79%). The same reaction products were isolated when excess benzoyl chloride was used. NMR reaction showed that **4** was the only traceable cobalt complex formed.

Reactions of [(TIMEN^{Xyl})Co(O_2)]BPh_4 with benzylidenemalonitrile: 1 equivalent of benzylidenemalonitrile was added to a solution of **5** (15 mg, 0.013 mmol) in acetonitrile resulting in a blue solution within 30 mins. The solution was evaporated to dryness and diethyl ether was added to extract the organic product that was identified by NMR and GC-MS. The solid residue was also collected and identified as complex **4** by NMR (10 mg; yield: 53%). Performing the reaction on a small scale in an NMR tube showed that **4** is the only tractable cobalt complex formed.

Reactions of [(TIMEN^{Xyl})Co(O_2)]BPh_4 with TCNE: 1 equivalent of benzylidenemalonitrile was added to a stirring solution of **5** (15 mg, 0.013 mmol) in acetonitrile. The resulting blue solution was evaporated to dryness and diethyl ether was added to extract any organic products. The solid residue was collected and identified as complex **4** by NMR spectroscopy (12 mg; yield: 64%). An NMR reaction showed that **4** is the only traceable cobalt complex formed.

Reactions of [(TIMEN^{Xyl})Co(O_2)]BPh_4 with alkenes and triphenylphosphine: The reactivity of **5** with 2-cyclohexene-1-one, 1,4-naphthaquinone, 2-methyl-1,4-naphthaquinone, styrene, cyclohexene, and triphenylphosphine was examined. In a typical reaction, an NMR tube was loaded

with equal molar amounts of **5** and alkene (or phosphine) and the reaction was monitored by NMR spectroscopy. In all cases, no changes in the NMR spectra were observed after 2 days.

[(TIMEN^{xyl})Co(N$_3$)]Cl (**6**): Excess of trimethylsilylazide (46 mg, 0,4 mmol) was added to a yellow solution of **1a** (60 mg, 0.08 mmol) in 1 mL acetonitrile. Upon addition, the color of the solution immediately changed to blue. The reaction mixture was stirred for 5 minutes, filtered through Celite, and evaporated to give **6** as a blue solid. The precipitate was collected, washed with diethyl ether, and dried in a vacuum (55 mg; Yield: 92%). Blue crystals of **6**(BPh_4) • CH_3CN suitable for X-ray diffraction analysis were grown by diffusion of diethyl ether into a saturated acetonitrile solution of **6** in the presence of excess of tetrabutylammonium tetraphenylborate at room temperature. ^{1}H NMR (300 MHz, d_3-Acetonitrile, 20 °C): δ = 76.6 (s, 3H, $\Delta\nu_{1/2}$ = 11 Hz), 33.4 (s, 3H, $\Delta\nu_{1/2}$ = 36 Hz), 32.2 (s, 3H, $\Delta\nu_{1/2}$ = 50 Hz), 9.6 (s, 3H, $\Delta\nu_{1/2}$ = 15 Hz), 8.8 (s, 3H, $\Delta\nu_{1/2}$ = 23 Hz), 7.2 (s, 6H, $\Delta\nu_{1/2}$ = 24 Hz), 5.8 (s, 3H, $\Delta\nu_{1/2}$ = 24 Hz), 2.0-1.2 (br, 18H,), -3.9 (s, 3H, $\Delta\nu_{1/2}$ = 18 Hz). IR (KBr): $\nu(N_3)$ = 2045 cm^{-1}. Elemental analysis (%) calcd for $C_{39}H_{45}N_{10}CoCl$**:** C 62.65, H 6.02, N 18.74; found: C 62.47, H 5.84, N 18.55.

[(TIMEN^{xyl})Co(NAr^{OMe})]Cl (**7a**): 1 equiv. of 4-methoxyphenylazide (10.5 mg, 0.07 mmol) was added to a solution of **1a** (50 mg, 0.07 mmol) in 1 mL acetonitrile at -35 ^{0}C. Upon addition, the solution color immediately turned into green with evolution of nitrogen. The reaction mixture was stirred for 5 minutes, filtered through Celite, and evaporated to give **7a** as a green solid (56 mg; Yield: 95%). ^{1}H

NMR (300 MHz, d_3-acetonitrile, 20 °C): δ = 7.41 (s, 3H), 7.33 (s, 3H), 6.95-6.83 (m, 6H), 6.45 (d, ^3J(H,H) = 3 Hz, 3H), 5.88 (d, ^3J(H,H) = 7.5 Hz, 2H), 5.66 (d, ^3J(H,H) = 7.5 Hz, 2H), 3.68 (t, ^3J(H,H) = 14 Hz, 3H), 3.55 (s, 3H), 3.00 (m, 6H), 2.30(t, ^3J(H,H) = 14 Hz, 3H), 2.09 (s, 9H), 1.42 (s, 9H). Elemental analysis (%) calcd for $C_{46}H_{52}N_8CoOCl$**:** C 66.83, H 6.30, N 13.56; found: C 66.67, H 6.15, N 13.42.

[(TIMEN^{mes})Co(NAr^{OMe})]Cl (**7b**): Same as **7a** with the exception of **1a** being substituted by **1b** (60 mg; Yield: 96%). Green crystals of **7b**(BPh_4) suitable for X-ray diffraction analysis were grown by applying a slow vacuum on a cold acetonitrile solution of **7b** in the presence of excess of sodium tetraphenylborate. ^{1}H NMR (400 MHz, d_3-acetonitrile, 20 °C): δ = 7.38 (s, 3H), 7.32 (s, 3H), 6.76 (s, 3H), 6.26 (s, 3H), 6.01 (d, ^3J(H,H) = 7.5 Hz, 2H), 5.83 (d, ^3J(H,H) = 7.5 Hz, 2H), 3.67 (t, ^3J(H,H) = 14 Hz, 3H), 3.55 (s, 3H), 3.05 (m, 6H), 2.29(t, ^3J(H,H) = 14 Hz, 3H), 2.02 (s, 18H), 1.42 (s, 9H). Elemental analysis (%) calcd for $C_{49}H_{58}N_8CoOCl$**:** C 67.74, H 6.68, N 12.90; found: C 66.36, H 6.49, N 12.58.

[(TIMEN^{xyl})Co(NAr^{Me})]Cl (**8a**): Same as **7a** with the exception of 4-methoxyphenyl azide being substituted by tolyl azide (9.3 mg, 0.07 mmol; Yield: 48 mg, 85%). ^{1}H NMR (300 MHz, d_3-acetonitrile, 20 °C): δ = 7.43 (s, 3H), 7.28 (s, 3H), 6.9-6.8 (m, 8H), 6.44 (d, ^3J(H,H) = 7.5 Hz, 2H), 5.86 (s, 3H), 4.25 (m, 3H), 3.05 (m, 6H), 2.30(m, 3H), 2.08 (s, 9H), 1.44 (s, 9H), 1.18 ppm (s, 3H). Elemental analysis (%) calcd for $C_{46}H_{52}N_8CoOCl$**:** C 68.15, H 6.42, N 13.83; found: C 68.23, H 6.34, N 13.71.

[(TIMEN^{mes})Co(NAr^{Me})]Cl (**8b**): Same as **8a** with the exception of **1a** being substituted by **1b** (55 mg; Yield: 92%). ^{1}H NMR (300 MHz, d_3-acetonitrile, 20 °C): δ = 7.43 (d, 3H), 7.35 (d, 3H), 6.76(s, 3H), 6.26(s, 3H), 5.99 (d, 2H), 5.95(d, 2H), 3.65(m, 3H), 3.00 (m, 6H), 2.20 (m, 3H), 2.06(s, 9H), 2.05(s, 9H), 1.43 (s, 9H), 1.24 ppm (s, 3H). Elemental analysis (%) calcd for $C_{49}H_{58}N_8CoOCl$**:** C 69.01, H 6.81, N 13.15; found: C 68.84, H 6.65, N 13.04.

[(TIMEN^{xyl})*Co(NAr^{OMe})']Cl (**9a**): From a solution of **7a** (50 mg, 0.07 mmol) in 1 mL acetonitrile a black solid precipitated overnight. The reaction mixture was filtered through Celite and evaporated to give **9a** as a yellow-green solid. The solid was collected by filtration, washed with diethyl ether, and dried in a vacuum (18 mg; Yield: 36%). ^{1}H NMR (300 MHz, d_3-Acetonitrile, 20 °C): The NMR spectrum of **9a**-**10b** is very complicated due to paramagnetism and lack of symmetry, however, the peaks in the paramagnetic region (> 10 and < 0 ppm) are distinctive and reproducible: δ= 68.2, 38.8, 35.0, 25.6 17.9, -1.3, -3.9, -20.6 ppm. HR-MS (FAB): 791.3572 (M-2Cl; calc. 791.3591).

[(TIMEN^{mes})*Co(NAr^{OMe})']Cl (**9b**): Same as **9a** with the exception of **7a** being substituted by **7b** (24 mg; Yield: 41%). Green crystals of **9b**$(BPh_4)_2$ • $2Et_2O$ suitable for X-ray diffraction analysis were grown by diffusion of diethyl ether into a saturated acetonitrile solution of **9b** in the presence of excess of sodium tetraphenylborate at room temperature. ^{1}H NMR (300 MHz, d_3-Acetonitrile, 20 °C): δ= 69.2, 40.1, 38.4, 26.2, 16.4, -3.8, -21.8 ppm. HR-MS (FAB): 833.4068 (M-2Cl; calc. 833.4060).

[(TIMEN^{xyl})*Co(NAr^{Me})']Cl (**10a**): Same as **9a** with the exception of **7a** being substituted by **8a** (20 mg; Yield: 35%). Green crystals of **10a**$(BPh_4)_2$ • Et_2O suitable for X-ray diffraction analysis were grown by diffusion of diethyl ether into a saturated acetonitrile solution of **10a** in the presence of excess of sodium tetraphenylborate at room temperature. ^{1}H NMR (300 MHz, d_3-Acetonitrile, 20 °C): δ= 69.0, 35.2, 34.5, 30.3, 28.0 27.1, 24.6, 19.6, 14.4, 13.5, 12.4, 11.5, 9.3, 7.8, -5.3, -3.3, -0.8, -9.6 ppm. HR-MS (FAB): 775.3627 (M-2Cl; calc. 775.3641).

[(TIMEN^{mes})*Co(NAr^{Me})']Cl (**10b**): Same as **10b** with the exception of **7b** being substituted by **8b** (22 mg; Yield: 37%). ^{1}H NMR (300 MHz, d_3-Acetonitrile, 20 °C): δ= 69.3, 39.2, 37.1, 31.9, 30.8, 28.1, 27.0, 26.1, 19.2, 12.1, 11.2, 10.1, -3.1, -4.4 ppm. HR-MS (FAB): 817.4101 (M-2Cl; calc. 817.4111)

Aziridination of styrene with PhINTs by catalyst [(TIMEN^{xyl})Co]$^{+/2+}$: Reactions were performed by stirring mixtures of PhINTs, styrene, and the cobalt catalyst in 1 mL anhydrous acetonitrile or dichloromethane at room temperature under a dry nitrogen atmosphere. The stoichiometric ratios of the reactants are given in Table 5-2. After PhINTs was completely consumed, the reaction mixture was filtered through Celite, evaporated to dryness, and the remaining solid was collected. Reaction yields were determined by NMR.

5.6. Acknowledgement

Text, schemes, and figures of this chapter, in part, are reprints of the materials published in the following papers: **Hu**, **X**.; Meyer, K*. "Terminal Cobalt(III) Imido

Species Supported by Tris(Carbene) Ligands: Imido Insertion into the Cobalt—Carbene Bond", *J. Am. Chem. Soc.*, ASAP article, DOI: 10.1021/ja044271b. **Hu**, **X**.; Castro-Rodriguez, I.; Meyer, K*. "Dioxygen Activation by a Low-Valent Cobalt Complex with a Flexible Tripodal N-Heterocyclic Carbene Ligand", *J. Am. Chem. Soc.* **2004**, *126*, 13464-13473. The dissertation author was the primary researcher and author. The co-authors listed in these publications also participated in the research.

5.6. Appendix

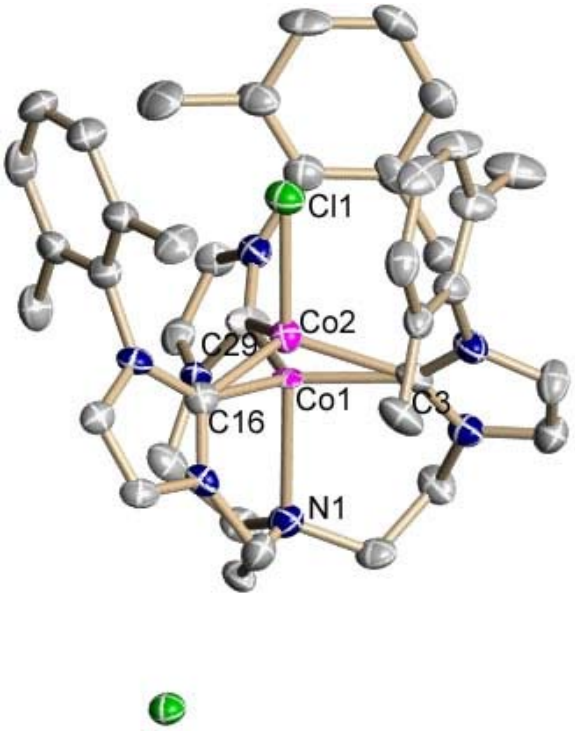

Figure 5-18. Solid-sate molecular structure of **1amix** • $2CH_3CN$. Hydrogen atoms and solvent molecules are omitted for clarity; thermal ellipsoids are shown at 50% probability. Selected bond lengths (Å): Co(1)-C(3) 2.038(9), Co(1)-C(16) 1.922(10), Co(1)-C(29) 2.040(10), Co(1)-N(1) 2.360(10), Co(2)-C(3) 2.059(9), Co(2)-C(16) 2.088(10), Co(2)-C(29) 2.071(9), Co(2)-Cl(1) 2.272(5).

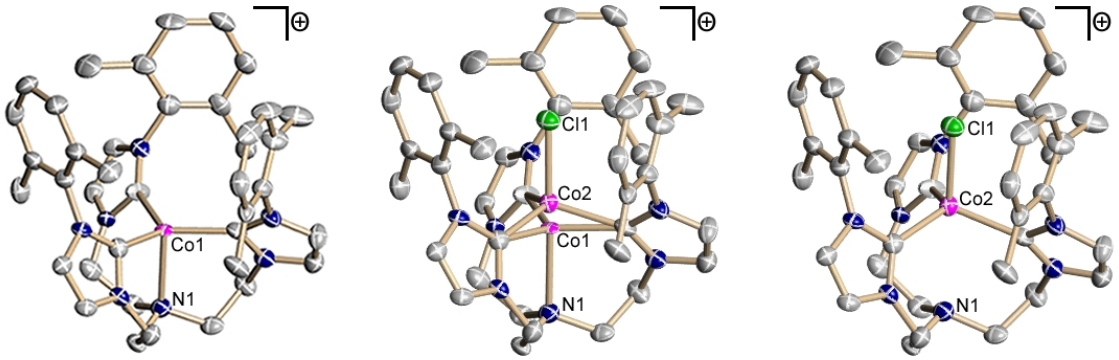

Figure 5-19. Co-crystallization of **1a** (left) and **3** (right) in **1amix** • $2CH_3CN$ (middle). Hydrogen atoms, counter ions, and solvent molecules are omitted for clarity; thermal ellipsoids are shown at 50% probability.

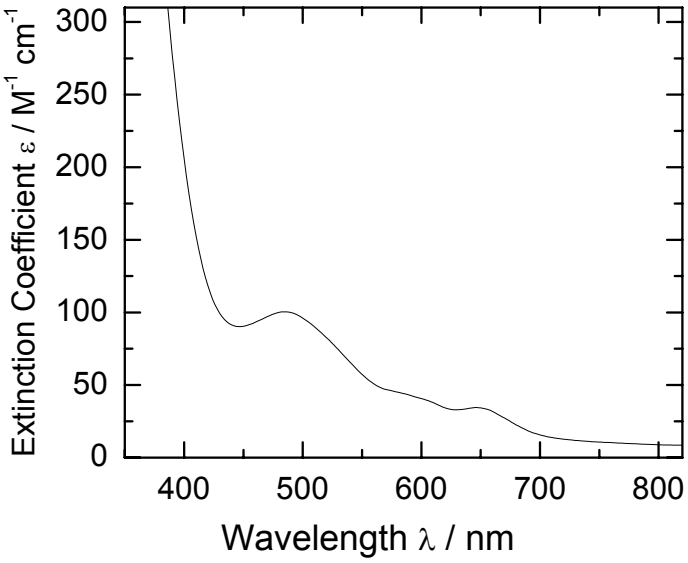

Figure 5-20. UV/vis Spectrum of complex **5** recorded in DMSO solution.

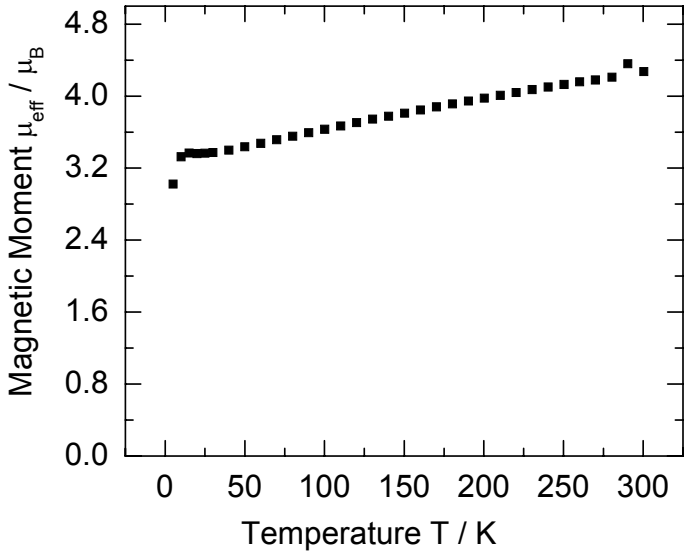

Figure 5-21. Temperature-dependent SQUID magnetization measurements for complex **6**; plot of the effective magnetic moments, μ_{eff}, versus temperature.

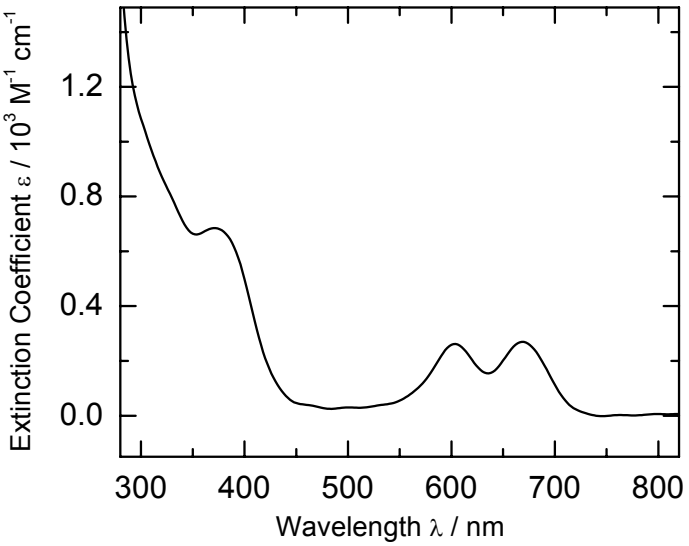

Figure 5-22. UV/vis Spectrum of complex **6** recorded in acetonitrile solution.

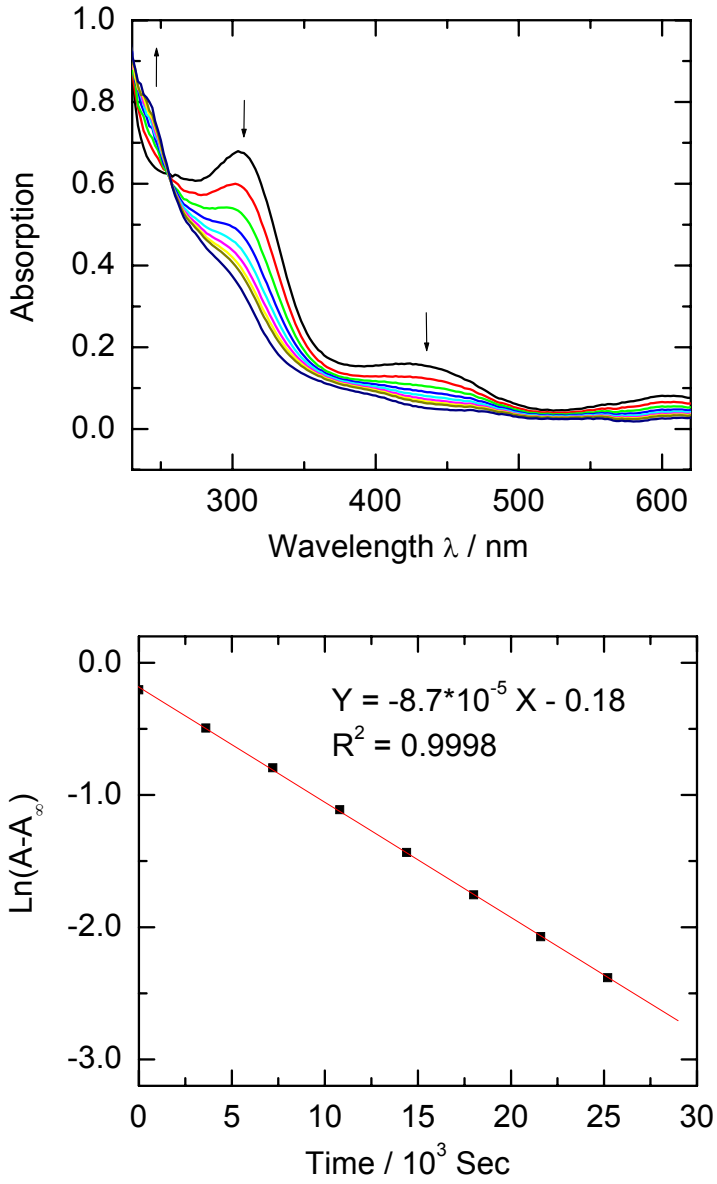

Figure 5-23. Intra-molecular imido insertion of complex **7b** monitored by UV/vis spectroscopy. Top: Time-dependent spectra of **7b** in acetonitrile solution showing an isosbestic point at 256 nm wavelength; spectra were recorded every 60 minutes. Bottom: First-order reaction with respect to the concentration of **7b**. A: absorption at 298 nm; rate constant was determined to be $8.7 * 10^{-5}\ s^{-1}$.

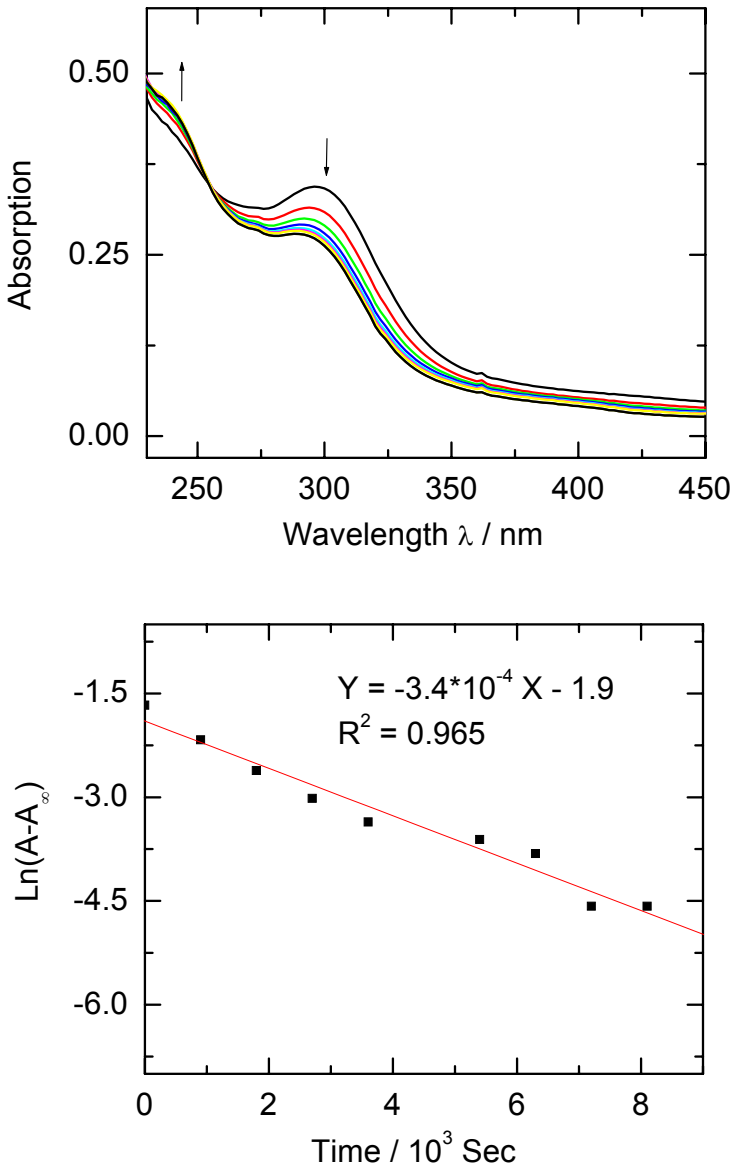

Figure 5-24. Intra-molecular imido insertion of complex **8a** monitored by UV/vis spectroscopy. Top: Time-dependent spectra of **8a** in acetonitrile solution showing an isosbestic point at 256 nm wavelength; spectra were recorded every 15 minutes. Bottom: First-order reaction with respect to the concentration of **8a**. A: absorption at 298 nm; rate constant was determined to be $3.4 * 10^{-4}$ s^{-1}.

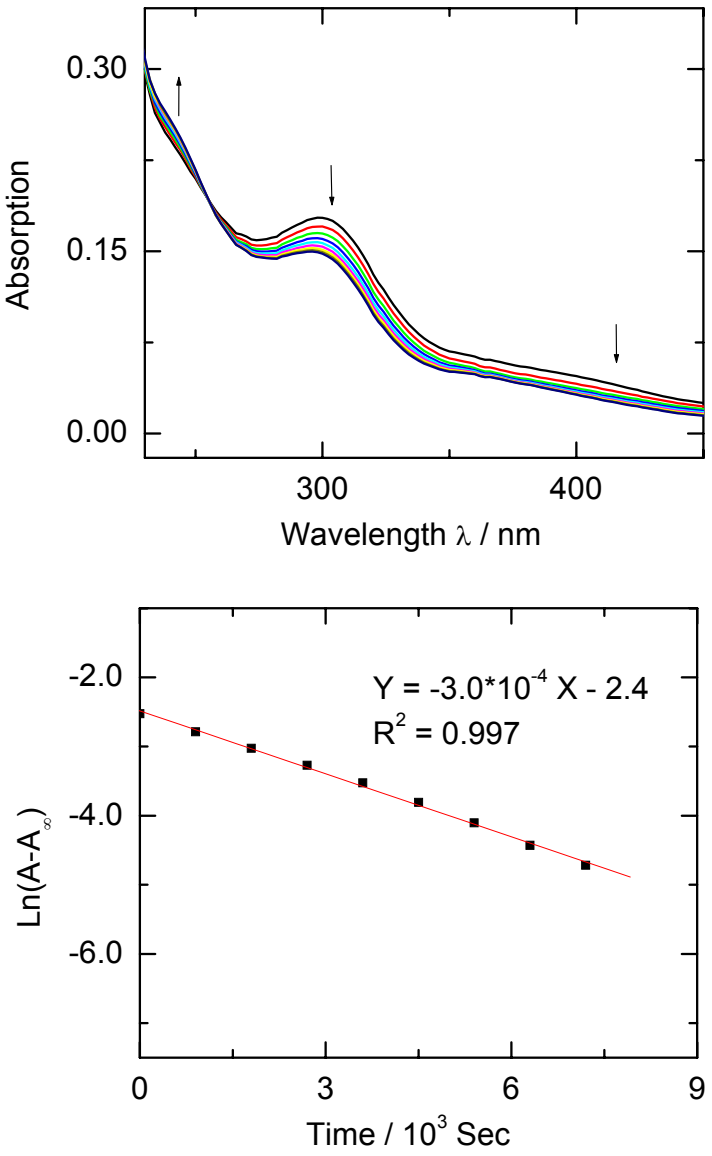

Figure 5-25. Intra-molecular imido insertion of complex **8b** monitored by UV/vis spectroscopy. Top: Time-dependent spectra of **8b** in acetonitrile solution showing an isosbestic point at 256 nm wavelength; spectra were recorded every 15 minutes. Bottom: First-order reaction with respect to the concentration of **8b**. A: absorption at 298 nm; rate constant was determined to be $3.0 * 10^{-4}\ s^{-1}$.

Crystallographic Details for Complexes 1a-mix, 2-6, 7b, 9b, and 10a.

Table 5-3. Crystal Data and Structure Refinement for **1a-mix**.

Identification code	5-1amix	
Empirical formula	C43 H51 Cl1.58 Co N9	
Formula weight	808.87	
Temperature	100(2) K	
Wavelength	0.71073 Å	
Crystal system	Triclinic	
Space group	*P*-1	
Unit cell dimensions	a = 10.6509(19) Å	α= 93.521(3)°.
	b = 10.6886(19) Å	β= 93.052(3)°.
	c = 20.955(4) Å	γ = 119.836(2)°.
Volume	2055.8(6) Å^3	
Z	2	
Density (calculated)	1.307 Mg/m^3	
Absorption coefficient	0.563 mm^{-1}	
F(000)	852	
Crystal size	0.4 x 0.2 x 0.1 mm^3	
Theta range for data collection	1.96 to 22.50°.	
Index ranges	-11<=h<=11, -11<=k<=11, -22<=l<=22	
Reflections collected	11483	
Independent reflections	5263 [R(int) = 0.0223]	
Completeness to theta = 22.50°	97.6 %	
Absorption correction	Semi-empirical from equivalents	
Max. and min. transmission	1.000 and 0.849	
Refinement method	Full-matrix least-squares on F^2	
Data / restraints / parameters	5263 / 0 / 513	
Goodness-of-fit on F^2	1.252	
Final R indices [I>2sigma(I)]	R_1 = 0.1112, wR_2 = 0.2599	
R indices (all data)	R_1 = 0.1122, wR_2 = 0.2602	
Largest diff. peak and hole	1.060 and -0.483 e.Å^{-3}	

Table 5-4. Crystal Data and Structure Refinement for **[(TIMEN^{xyl})Co(CO)]Cl (2)**.

Identification code	5-2
Empirical formula	C44 H51 Cl Co N9 O
Formula weight	816.32
Temperature	100(2) K
Wavelength	0.71073 Å
Crystal system	Triclinic
Space group	*P*-1
Unit cell dimensions	a = 10.5775(9) Å α= 94.2400(10)°. b = 10.6288(9) Å β= 93.0000(10)°. c = 21.2014(18) Å γ= 119.2060(10)°.
Volume	2064.1(3) Å^3
Z	2
Density (calculated)	1.313 Mg/m^3
Absorption coefficient	0.527 mm^{-1}
F(000)	860
Crystal size	0.41 x 0.33 x 0.08 mm^3
Theta range for data collection	0.97 to 27.51°.
Index ranges	-13<=h<=13, -13<=k<=13, -27<=l<=26
Reflections collected	17360
Independent reflections	8901 [R(int) = 0.0190]
Completeness to theta = 27.51°	93.7 %
Absorption correction	Semi-empirical from equivalents
Max. and min. transmission	1.000 and 0.7957
Refinement method	Full-matrix least-squares on F^2
Data / restraints / parameters	8901 / 0 / 513
Goodness-of-fit on F^2	1.033
Final R indices [I>2sigma(I)]	R_1 = 0.0367, wR_2 = 0.0903
R indices (all data)	R_1 = 0.0429, wR_2 = 0.0939
Largest diff. peak and hole	0.740 and -0.344 e.Å^{-3}

Table 5-5. Crystal Data and Structure Refinement for **[(TIMEN^{xyl})CoCl]Cl (3)**.

Identification code	5-3	
Empirical formula	C41 H45 Cl2 Co N7 O S	
Formula weight	813.73	
Temperature	100(2) K	
Wavelength	0.71073 Å	
Crystal system	Triclinic	
Space group	*P*-1	
Unit cell dimensions	a = 10.667(2) Å	α= 87.212(3)°.
	b = 10.702(2) Å	β= 83.314(3)°.
	c = 20.707(4) Å	γ= 60.477(3)°.
Volume	2042.7(7) Å^3	
Z	2	
Density (calculated)	1.323 Mg/m^3	
Absorption coefficient	0.643 mm^{-1}	
F(000)	850	
Crystal size	0.30 x 0.13 x 0.02 mm^3	
Theta range for data collection	1.98 to 22.50°.	
Index ranges	-11<=h<=11, -11<=k<=11, -22<=l<=22	
Reflections collected	11898	
Independent reflections	5352 [R(int) = 0.0259]	
Completeness to theta = 22.50°	99.8 %	
Absorption correction	Semi-empirical from equivalents	
Max. and min. transmission	1.000 and 0.842	
Refinement method	Full-matrix least-squares on F^2	
Data / restraints / parameters	5352 / 0 / 501	
Goodness-of-fit on F^2	1.071	
Final R indices [I>2sigma(I)]	R_1 = 0.0618, wR_2 = 0.1654	
R indices (all data)	R_1 = 0.0732, wR_2 = 0.1724	
Largest diff. peak and hole	1.682 and -0.429 e.Å^{-3}	

Table 5-6. Crystal Data and Structure Refinement for **[(TIMEN^{xyl})Co(CH$_3$CN)]-(BPh$_4$)$_2$ (4)**.

Identification code	5-4	
Empirical formula	C91 H91 B2 Co N9	
Formula weight	1391.28	
Temperature	100(2) K	
Wavelength	0.71073 Å	
Crystal system	Monoclinic	
Space group	*P*2(1)/*c*	
Unit cell dimensions	*a* = 23.7912(19) Å	α= 90°.
	b = 11.5916(9) Å	β= 94.8400(10)°.
	c = 27.394(2) Å	γ= 90°.
Volume	7527.6(10) Å^3	
Z	4	
Density (calculated)	1.228 Mg/m^3	
Absorption coefficient	0.282 mm^{-1}	
F(000)	2948	
Crystal size	0.4 x 0.1 x 0.05 mm^3	
Theta range for data collection	1.49 to 22.50°.	
Index ranges	-25<=h<=25, -12<=k<=12, -29<=l<=29	
Reflections collected	42407	
Independent reflections	9860 [*R*(int) = 0.0697]	
Completeness to theta = 22.50°	100.0 %	
Absorption correction	Semi-empirical from equivalents	
Max. and min. transmission	1.000 and 0.671	
Refinement method	Full-matrix least-squares on F^2	
Data / restraints / parameters	9860 / 0 / 936	
Goodness-of-fit on F^2	1.049	
Final R indices [I>2sigma(I)]	R_1 = 0.0491, wR_2 = 0.1065	
R indices (all data)	R_1 = 0.0736, wR_2 = 0.1155	
Largest diff. peak and hole	0.476 and -0.249 e.Å^{-3}	

Table 5-7. Crystal Data and Structure Refinement for **[(TIMEN^{xyl})Co(O$_2$)]BPh$_4$ (5)**.

Identification code	5-5	
Empirical formula	C63 H65 B Co N7 O2	
Formula weight	1021.96	
Temperature	100(2) K	
Wavelength	0.71073 Å	
Crystal system	Triclinic	
Space group	*P*-1	
Unit cell dimensions	a = 13.600(2) Å	α = 95.254(3)°.
	b = 14.788(3) Å	β = 109.027(3)°.
	c = 16.356(3) Å	γ = 106.392(3)°.
Volume	2921.7(9) Å^3	
Z	2	
Density (calculated)	1.162 Mg/m^3	
Absorption coefficient	0.341 mm^{-1}	
F(000)	1080	
Crystal size	0.12 x 0.08 x 0.02 mm^3	
Theta range for data collection	1.34 to 25.00°.	
Index ranges	-16<=h<=16, -17<=k<=17, -19<=l<=19	
Reflections collected	20992	
Independent reflections	10206 [R(int) = 0.0605]	
Completeness to theta = 25.00°	99.1 %	
Absorption correction	Semi-empirical from equivalents	
Max. and min. transmission	1.000 and 0.725	
Refinement method	Full-matrix least-squares on F^2	
Data / restraints / parameters	10206 / 0 / 673	
Goodness-of-fit on F^2	0.953	
Final R indices [I>2sigma(I)]	R_1 = 0.0650, wR_2 = 0.1356	
R indices (all data)	R_1 = 0.1071, wR_2 = 0.1483	
Largest diff. peak and hole	0.670 and -0.355 e.Å^{-3}	

Table 5-8. Crystal Data and Structure Refinement for **[(TIMEN^{xyl})Co(N$_3$)]BPh$_4$ (6**(BPh$_4$)**)**.

Identification code	5-6	
Empirical formula	C65 H68 B Co N11	
Formula weight	1073.04	
Temperature	123(2) K	
Wavelength	0.71073 Å	
Crystal system	Monoclinic	
Space group	*P*2(1)/*n*	
Unit cell dimensions	a = 17.5814(10) Å	α= 90°.
	b = 17.6895(10) Å	β= 100.8740(10)°.
	c = 18.7229(11) Å	γ= 90°.
Volume	5718.4(6) Å^3	
Z	4	
Density (calculated)	1.246 Mg/m^3	
Absorption coefficient	0.351 mm^{-1}	
F(000)	2268	
Crystal size	0.45 x 0.10 x 0.05 mm^3	
Theta range for data collection	1.46 to 25.00°.	
Index ranges	-18<=h<=20, -18<=k<=21, -22<=l<=18	
Reflections collected	29983	
Independent reflections	10071 [R(int) = 0.0377]	
Completeness to theta = 25.00°	100.0 %	
Absorption correction	Semi-empirical from equivalents	
Max. and min. transmission	1.000 and 0.818	
Refinement method	Full-matrix least-squares on F^2	
Data / restraints / parameters	10071 / 0 / 710	
Goodness-of-fit on F^2	1.032	
Final R indices [I>2sigma(I)]	R_1 = 0.0440, wR_2 = 0.0937	
R indices (all data)	R_1 = 0.0597, wR_2 = 0.1002	
Largest diff. peak and hole	0.429 and -0.306 e.Å^{-3}	

Table 5-9. Crystal Data and Structure Refinement for **[(TIMEN^{mes})Co(NAr^{OMe})]-BPh$_4$ (7b**(BPh$_4$)**)**.

Identification code	5-7b	
Empirical formula	C73 H78 B Co N8 O	
Formula weight	1153.17	
Temperature	293(2) K	
Wavelength	0.71073 Å	
Crystal system	Monoclinic	
Space group	*P*2(1)/*n*	
Unit cell dimensions	a = 18.715(3) Å	α= 90°.
	b = 14.361(2) Å	β= 95.175(3)°.
	c = 22.967(4) Å	γ = 90°.
Volume	6147.4(16) Å^3	
Z	4	
Density (calculated)	1.246 Mg/m^3	
Absorption coefficient	0.331 mm^{-1}	
F(000)	2448	
Crystal size	0.40 x 0.08 x 0.03 mm^3	
Theta range for data collection	1.35 to 25.00°.	
Index ranges	-22<=h<=22, -17<=k<=17, -27<=l<=27	
Reflections collected	43772	
Independent reflections	10825 [R(int) = 0.0717]	
Completeness to theta = 25.00°	100.0 %	
Absorption correction	Semi-empirical from equivalents	
Max. and min. transmission	1.000 and 0.787	
Refinement method	Full-matrix least-squares on F^2	
Data / restraints / parameters	10825 / 0 / 767	
Goodness-of-fit on F^2	1.034	
Final R indices [I>2sigma(I)]	R_1 = 0.0532, wR_2 = 0.1070	
R indices (all data)	R_1 = 0.0894, wR_2 = 0.1195	
Largest diff. peak and hole	1.006 and -0.560 e.Å^{-3}	

Table 5-10. Crystal Data and Structure Refinement for **[(TIMEN^{mes})*Co(NAr'^{OMe})]-(BPh$_4$)$_2$ (9b**(BPh$_4$)$_2$**)**.

Identification code	5-9b	
Empirical formula	C103 H113 B2 Co N8 O2.50	
Formula weight	1583.56	
Temperature	100(2) K	
Wavelength	0.71073 Å	
Crystal system	Triclinic	
Space group	*P*-1	
Unit cell dimensions	*a* = 13.2685(13) Å	α= 85.323(2)°.
	b = 17.2830(17) Å	β= 79.331(2)°.
	c = 20.673(2) Å	γ = 69.009(2)°.
Volume	4349.1(7) Å^3	
Z	2	
Density (calculated)	1.209 Mg/m^3	
Absorption coefficient	0.254 mm^{-1}	
F(000)	1688	
Crystal size	0.40 x 0.10 x 0.02 mm^3	
Theta range for data collection	1.00 to 25.00°.	
Index ranges	-15<=h<=15, -20<=k<=20, -24<=l<=24	
Reflections collected	31739	
Independent reflections	15215 [*R*(int) = 0.0336]	
Completeness to theta = 25.00°	99.3 %	
Absorption correction	Semi-empirical from equivalents	
Max. and min. transmission	1.000 and 0.832	
Refinement method	Full-matrix least-squares on F^2	
Data / restraints / parameters	15215 / 0 / 992	
Goodness-of-fit on F^2	0.983	
Final R indices [I>2sigma(I)]	R_1 = 0.0498, wR_2 = 0.1245	
R indices (all data)	R_1 = 0.0707, wR_2 = 0.1329	
Largest diff. peak and hole	0.697 and -0.480 e.Å^{-3}	

Table 5-11. Crystal Data and Structure Refinement for **[(TIMEN^{xyl})*Co(NAr^{Me})]-(BPh$_4$)$_2$ (10a**(BPh$_4$)$_2$**)**.

Identification code	5-10a	
Empirical formula	C98 H102 B2 Co N8 O	
Formula weight	1488.43	
Temperature	100(2) K	
Wavelength	0.71073 Å	
Crystal system	Monoclinic	
Space group	*P*2(1)/*c*	
Unit cell dimensions	*a* = 20.741(2) Å	α= 90°.
	b = 20.118(2) Å	β= 92.424(2)°.
	c = 19.862(2) Å	γ = 90°.
Volume	8280.5(17) Å^3	
Z	4	
Density (calculated)	1.194 Mg/m^3	
Absorption coefficient	0.261 mm^{-1}	
F(000)	3164	
Crystal size	0.3 x 0.1 x 0.05 mm^3	
Theta range for data collection	1.41 to 25.00°.	
Index ranges	-24<=h<=24, -23<=k<=23, -23<=l<=23	
Reflections collected	59015	
Independent reflections	14573 [*R*(int) = 0.0666]	
Completeness to theta = 25.00°	99.9 %	
Absorption correction	Semi-empirical from equivalents	
Max. and min. transmission	1.000 and 0.818	
Refinement method	Full-matrix least-squares on F^2	
Data / restraints / parameters	14573 / 0 / 1000	
Goodness-of-fit on F^2	1.024	
Final R indices [I>2sigma(I)]	R_1 = 0.0529, wR_2 = 0.1196	
R indices (all data)	R_1 = 0.0886, wR_2 = 0.1352	
Largest diff. peak and hole	0.529 and -0.355 e.Å^{-3}	

5.7. References

(1) Cummins, C. C.; Lee, J.; Schrock, R. R.; Davis, W. D. *Angew. Chem. Int. Ed. Engl* **1992**, *31*, 1501-1503.

(2) Yandulov, D. V.; Schrock, R. R. *Science* **2003**, *301*, 76-78.

(3) Yandulov, D. V.; Schrock, R. R. *J. Am. Chem. Soc.* **2002**, *124*, 6252-6253; Yandulov, D. V.; Schrock, R. R.; Rheingold, A. L.; Ceccarelli, C.; Davis, W. M. *Inorg. Chem.* **2003**, *42*, 796-813.

(4) MacBeth, C. E.; Golombek, A. P.; Young, V. G.; Yang, C.; Kuczera, K.; Hendrich, M. P.; Borovik, A. S. *Science* **2000**, *289*, 938-941.

(5) Jenkins, D. M.; Betley, T. A.; Peters, J. C. *J. Am. Chem. Soc.* **2002**, *124*, 11238-11239.

(6) Brown, S. D.; Betley, T. A.; Peters, J. C. *J. Am. Chem. Soc.* **2003**, *125*, 322-323.

(7) Betley, T. A.; Peters, J. C. *J. Am. Chem. Soc.* **2004**, *126*, 6252-6254.

(8) Kernbach, U.; Ramm, M.; Luger, P.; Fehlhammer, W. P. *Angew. Chem. Int. Ed. Engl* **1996**, *35*, 310-312; Arnold, P. L.; Scarisbrick, A. C.; Blake, A. J.; Wilson, C. *Chem. Commun.* **2001**, 2340-2341; Danopoulos, A. A.; Winston, S.; Motherwell, W. B. *Chem. Commun.* **2002**, 1376-1377; Douthwaite, R. E.; Houghton, J.; Kariuki, B. M. *Chem. Commun.* **2004**, 698-699.

(9) Peris, E.; Loch, J. A.; Mata, J.; Crabtree, R. H. *Chem. Commun.* **2001**, 201-202.

(10) Arduengo, A. J.; Harlow, R. L.; Kline, M. *J. Am. Chem. Soc.* **1991**, *113*, 361-363.

(11) Herrmann, W. A.; Kocher, C. *Angew. Chem. Int. Ed. Engl* **1997**, *36*, 2163-2187; Bourissou, D.; Guerret, O.; Gabbai, F. P.; Bertrand, G. *Chem. Rev.* **2000**, *100*, 39-91.

(12) Herrmann, W. A. *Angew. Chem.-Int. Edit.* **2002**, *41*, 1291-1309.

(13) Herrmann, W. A.; Elison, M.; Fischer, J.; Kocher, C.; Artus, G. R. J. *Angew. Chem. Int. Ed. Engl* **1995**, *34*, 2371-2374; Gstottmayr, C. W. K.; Bohm, V. P. W.; Herdtweck, E.; Grosche, M.; Herrmann, W. A. *Angew. Chem. Int. Ed. Engl* **2002**, *41*, 1363-1365.

(14) Scholl, M.; Ding, S.; Lee, C. W.; Grubbs, R. H. *Org. Lett.* **1999**, *1*, 953-956; Huang, J. K.; Stevens, E. D.; Nolan, S. P.; Petersen, J. L. *J. Am. Chem. Soc.* **1999**, *121*, 2674-2678.

(15) Solomon, E. I.; Brunold, T. C.; Davis, M. I.; Kemsley, J. N.; Lee, S. K.; Lehnert, N.; Neese, F.; Skulan, A. J.; Yang, Y. S.; Zhou, J. *Chem. Rev.* **2000**, *100*, 235-349; Solomon, E. I.; Chen, P.; Metz, M.; Lee, S. K.; Palmer, A. E. *Angew. Chem.-Int. Edit.* **2001**, *40*, 4570-4590; Que, L.; Ho, R. Y. N. *Chem. Rev.* **1996**, *96*, 2607-2624; Que, L.; Tolman, W. B. *Angew. Chem.-Int. Edit.* **2002**, *41*, 1114-1137; Lewis, E. A.; Tolman, W. B. *Chem. Rev.* **2004**, *104*, 1047-1076; Kim, E.; Chufan, E. E.; Kamaraj, K.; Karlin, K. D. *Chem. Rev.* **2004**, *104*, 1077-1133.

(16) Sheldon, R. A.; Kochi, J. K. *Metal-Catalyzed Oxidation of Organic Compounds*; Academic Press, Inc.: New York, U.S.A., 1981.

(17) Martell, A. E.; Sawyer, D. T., Eds. *Oxygen Complexes and Oxygen Activation by Transition Metals*; Plenum Press: New York, U.S.A., 1988; Simandi, L. I., Ed. *Advances in catalytic Activation of Dioxygen by Metal Complexes*; Kluwer Academic Publishers: Dordrecht, The Netherlands, 2003.

(18) Busch, D. H.; Alcock, N. W. *Chem. Rev.* **1994**, *94*, 585-623.

(19) Hanzlik, R. P.; Williamson, D. *J. Am. Chem. Soc.* **1976**, *98*, 6570-6573; Reetz, M. T.; Tollner, K. *Tetrahedron Lett.* **1995**, *36*, 9461-9464; Jain, S. L.; Sain, B. *Angew. Chem.-Int. Edit.* **2003**, *42*, 1265-1267; Reinaud, O. M.; Yap, G. P. A.; Rheingold, A. L.; Theopold, K. H. *Angew. Chem. Int. Ed. Engl* **1995**, *34*, 2051-2052.

(20) Brown, L. D.; Raymond, K. N. *Inorg. Chem.* **1975**, *14*, 2595-2601; Gall, R. S.; Rogers, J. F.; Schaefer, W. P.; Christoph, G. G. *J. Am. Chem. Soc.* **1976**, *98*, 5135-5144; Schaefer, W. P.; Huie, B. T.; Kurilla, M. G.; Ealick, S. E. *Inorg. Chem.* **1980**, *19*, 340-344; Jameson, G. B.; Robinson, W. T.; Rodley, G. A. *J. Chem. Soc.-Dalton Trans.* **1978**, 191-196; Cini, R.; Orioli, P. *J. Chem. Soc., Chem. Commun.* **1981**, 196-198; Hohenester, E.; Kratky, C.; Krautler, B. *J. Am. Chem. Soc.* **1991**, *113*, 4523-4530; Busch, D. H.; Jackson, P. J.; Kojima, M.; Chmielewski, P.; Matsumoto, N.; Stevens, J. C.; Wu, W.; Nosco, D.; Herron, N.; Ye, N. D.; Warburton, P. R.; Masarwa, M.; Stephenson, N. A.; Christoph, G.; Alcock, N. W. *Inorg. Chem.* **1994**, *33*, 910-923.

(21) Terry, N. W.; Amma, E. L.; Vaska, L. *J. Am. Chem. Soc.* **1972**, *94*, 653-655; Halpern, J.; Goodall, B. L.; Khare, G. P.; Lim, H. S.; Pluth, J. J. *J. Am. Chem. Soc.* **1975**, *97*, 2301-2303; Crump, D. B.; Stepaniak, R. F.; Payne, N. C. *Can. J. Chem* **1977**, *55*, 438-446; Ohishi, T.; Kashiwabara, K.; Fujita, J.; Ohba, S.; Ishii, T.; Saito, Y. *Bull. Chem. Soc. Jpn.* **1986**, *59*, 385-393.

(22) Egan, J. W.; Haggerty, B. S.; Rheingold, A. L.; Sendlinger, S. C.; Theopold, K. H. *J. Am. Chem. Soc.* **1990**, *112*, 2445-2446.

(23) Groves, J. T.; Takahashi, T. *J. Am. Chem. Soc.* **1983**, *105*, 2073-2074; Wigley, D. E. In *Prog. Inorg. Chem.*, 1994; Vol. 42, pp 239-482; DuBois, J.; Tomooka, C. S.; Hong, J.; Carreira, E. M. *Acc. Chem. Res.* **1997**, *30*, 364-372; Eikey, R. A.; Abu-Omar, M. M. *Coord. Chem. Rev.* **2003**, *243*, 83-124.

(24) Nugent, W. A.; Mayer, J. M. *Metal-Ligand Multiple Bonds*; John Wiley and Sons: New York, 1988.

(25) Glueck, D. S.; Hollander, F. J.; Bergman, R. G. *J. Am. Chem. Soc.* **1989**, *111*, 2719-2721; Glueck, D. S.; Wu, J. X.; Hollander, F. J.; Bergman, R. G. *J. Am. Chem. Soc.* **1991**, *113*, 2041-2054.

(26) Mindiola, D. J.; Hillhouse, G. L. *J. Am. Chem. Soc.* **2001**, *123*, 4623-4624; Mindiola, D. J.; Hillhouse, G. L. *Chem. Commun.* **2002**, 1840-1841.

(27) Thyagarajan, S.; Shay, D. T.; Incarvito, C. D.; Rheingold, A. L.; Theopold, K. H. *J. Am. Chem. Soc.* **2003**, *125*, 4440-4441.

(28) Dai, X. L.; Kapoor, P.; Warren, T. H. *J. Am. Chem. Soc.* **2004**, *126*, 4798-4799.

(29) Dioxygen reactivity of a nickel(II) NHC complex has been reported, see: Dible, B. R.; Sigman, M. S. *J. Am. Chem. Soc.* **2003**, *125*, 872-873.

(30) Stahl et al. recently synthesized a palladium(II) peroxo complex with two monodentate NHCs as supporting ligands, see: Konnick, M. M.; Guzel, L. A.; Stahl, S. S. *J. Am. Chem. Soc.* **2004**, *126*, 10212-10213.

(31) Nakamoto, K. *Infrared and Raman Spectra of Inorganic and Coordination Compounds*; 5th ed.; John Wiley & Sons, Inc.: New York, 1997; Vol. 2.

(32) Simms, R. W.; Drewitt, M. J.; Baird, M. C. *Organometallics* **2002**, *21*, 2958-2963; Gibson, S. E.; Johnstone, C.; Loch, J. A.; Steed, J. W.; Stevenazzi, A. *Organometallics* **2003**, *22*, 5374-5377; van Rensburg, H.; Tooze, R. P.; Foster, D. F.; Slawin, A. M. Z. *Inorg. Chem.* **2004**, *43*, 2468-2470.

(33) Jewson, J. D.; Liable-Sands, L. M.; Yap, G. P. A.; Rheingold, A. L.; Theopold, K. H. *Organometallics* **1999**, *18*, 300-305.

(34) Boudreaux, E. A.; Mulay, L. N. *Theory and Applications of Molecular Paramagnetism*; John Wiley & Sons, Inc.: New York, 1976.

(35) Cotton, F. A.; Wilkinson, G.; Murillo, C. A.; Bochmann, M. *Advanced Inorganic Chemistry*; 6th ed.; John Wiley & Sons, Inc.: New York, 1999.

(36) Jenkins, D. M.; Di Bilio, A. J.; Allen, M. J.; Betley, T. A.; Peters, J. C. *J. Am. Chem. Soc.* **2002**, *124*, 15336-15350.

(37) Drago, R. S. *Physical Methods for Chemists*; 2nd ed.; Surfside Scientific Publishers: Gainesville, 1992.

(38) Jones, R. D.; Summerville, D. A.; Basolo, F. *Chem. Rev.* **1979**, *79*, 139-179.

(39) Cramer, C. J.; Tolman, W. B.; Theopold, K. H.; Rheingold, A. L. *Proc. Natl. Acad. Sci. USA* **2003**, *100*, 3635-3640.

(40) Ballistreri, F. P.; Tomaselli, G. A.; Toscano, R. M.; Conte, V.; Difuria, F. *J. Am. Chem. Soc.* **1991**, *113*, 6209-6212; Adam, W.; Haas, W.; Lohray, B. B. *J. Am. Chem. Soc.* **1991**, *113*, 6202-6208; Kitajima, N.; Morooka, Y. *Chem. Rev.* **1994**, *94*, 737-757.

(41) Sisemore, M. F.; Selke, M.; Burstyn, J. N.; Valentine, J. S. *Inorg. Chem.* **1997**, *36*, 979-984.

(42) Sheldon, R. A.; Vandoorn, J. A. *J. Organomet. Chem.* **1975**, *94*, 115-129.

(43) Sisemore, M. F.; Burstyn, J. N.; Valentine, J. S. *Angew. Chem. Int. Ed. Engl* **1996**, *35*, 206-208.

(44) An iron peroxyacetate complex was identified in the reacton of peroxo complex [(porphrin)Fe(O_2)]$^-$ with acylating agents, see: Khenkin, A. M.; Shteinman, A. A. *J. Chem. Soc., Chem. Commun.* **1984**, 1219-1220.

(45) The fate of the chlorine radical generated in this reaction is not clear. Formation of Co(II)-Cl species was not observed.

(46) Mimoun, H. *J. Mol. Catal.* **1980**, *7*, 1-29.

(47) Regen, S. L.; Whitesides, G. M. *J. Organomet. Chem.* **1973**, *59*, 293-297.

(48) Mayer, H. A.; Kaska, W. C. *Chem. Rev.* **1994**, *94*, 1239-1272.

(49) Sacconi, L.; Bertini, I. *J. Am. Chem. Soc.* **1968**, *90*, 5443-5446.

(50) Sacconi, L.; Ghilardi, C. A.; Mealli, C.; Zanobini, F. *Inorg. Chem.* **1975**, *14*, 1380-1386; Ghilardi, C. A.; Midollini, S.; Sacconi, L. *Inorg. Chem.* **1975**,

14, 1790-1795; Ghilardi, C. A.; Sabatini, A.; Sacconi, L. *Inorg. Chem.* **1976**, *15*, 2763-2767.

(51) Betley, T. A.; Peters, J. C. *Inorg. Chem.* **2003**, *42*, 5074-5084; Betley, T. A.; Peters, J. C. *Journal of the American Chemical Society* **2004**, *126*, 6252-6254.

(52) Basuli, F.; Bailey, B. C.; Tomaszewski, J.; Huffman, J. C.; Mindiola, D. J. *J. Am. Chem. Soc.* **2003**, *125*, 6052-6053; Holland, P. L.; Tolman, W. B. *J. Am. Chem. Soc.* **1999**, *121*, 7270-7271; Spencer, D. J. E.; Aboelella, N. W.; Reynolds, A. M.; Holland, P. L.; Tolman, W. B. *J. Am. Chem. Soc.* **2002**, *124*, 2108-2109; Smith, J. M.; Lachicotte, R. J.; Pittard, K. A.; Cundari, T. R.; Lukat-Rodgers, G.; Rodgers, K. R.; Holland, P. L. *J. Am. Chem. Soc.* **2001**, *123*, 9222-9223; Dai, X. L.; Warren, T. H. *Chem. Commun.* **2001**, 1998-1999.

(53) Winter, M. *WebElements*, http://www.webelements.com.

(54) Halfen, J. A.; Uhan, J. M.; Fox, D. C.; Mehn, M. P.; Que, L. *Inorg. Chem.* **2000**, *39*, 4913-4920.

(55) Mairena, M. A.; Diaz-Requejo, M. M.; Belderrain, T. R.; Nicasio, M. C.; Trofimenko, S.; Perez, P. J. *Organometallics* **2004**, *23*, 253-256.

(56) O'Connor, C. J. *Prog. Inorg. Chem.* **1982**, *29*, 203-283.

(57) ADF2003.01; SCM, Theoretical Chemistry, Vrijie Universiteit: Amsterdam, The Netherlands.

(58) Vosko, S. H.; Wilk, L.; Nusair, M. *Can. J. Phys.* **1980**, *58*, 1200-1211.

(59) Becke, A. D. *Phys. Rev. A* **1988**, *38*, 3098-3100.

(60) Perdew, J. P. *Phys. Rev. B* **1986**, *33*, 8822-8824.

(61) Van Lenthe, E.; Ehlers, A.; Baerends, E. J. *J. Chem. Phys.* **1999**, *110*, 8943-8953.

(62) Snijders, J. G.; Vernooijs, P.; Baerends, E. J. *At. Data Nucl. Tables* **1981**, *26*, 483-509.

(63) Ward, K. *J. Am. Chem. Soc.* **1935**, *57*, 914-916.

(64) Arduengo, A. J.; Gentry, F. P.; Taverkere, P. K.; Simmons, H. E. In *US Patent*; E. I. du pont de Nemours and Company: U. S. A., 2001.

(65) Smith, P. A. S.; Brown, B. B. *J. Am. Chem. Soc.* **1951**, *73*, 2438-2441.

(66) Yamada, Y.; Yamamoto, T.; Okawara, M. *Chem. Lett.* **1975**, 361-362.

Chapter 6. The Nature of the Metal—Carbene Bond in Metal N-Heterocyclic Carbene Complexes

6.1. Introduction

Since the discovery of their remarkable activity in homogeneous catalysis,[1,2] enormous research interest has emerged for the chemistry of metal complexes supported by N-heterocyclic carbenes (NHCs).[3] Numerous metal NHC complexes have been synthesized and their structures have been determined by single-crystal X-ray diffraction studies.[1,4] In most cases, single M—C bonds were observed, which in many reports has led to the assumption that NHCs are pure σ donor ligands. The successful synthesis of main group metal NHC complexes, such as the beryllium tris(carbene) complex $[(IM^{Me})_3BeCl]Cl$[5], which one considered as empirical evidence for this bonding model.[6] It is noteworthy that NHC complexes of main group metals, such as lithium,[7] beryllium,[5] and thallium(I),[8] are often air, moisture, and even temperature sensitive, while NHC complexes of transition metals (TMs) generally exhibit much higher stabilities. The above mentioned main-group-metal NHC complexes are not capable of back-donating electrons into the carbene p-π orbitals, which might be one reason for their relatively weak M—C bonds. In recent years, NHCs are almost exclusively referred to as pure σ-donors. However, as early as 1975, Taube and Clarke reported the existence of π-backbonding in ruthenium(II) NHC (carbon-bound xanthine) complexes.[9] Several recent theoretical studies also suggest various degree of π-bonding in transition metal NHC complexes.[10-13] For example, density functional theory (DFT) calculations predicted correctly that metal-to-ligand π-backbonding effects allow for the isolation of an air stable vanadium(V) tri-chloro-oxo NHC complex.[12] In addition, a DFT study suggested the involvement of metal-

carbene *d-pπ* hybrid orbitals in transition states of an alkyl-carbene elimination from Pd(II) NHC complexes.[14] However, careful computational studies on crystallographically characterized metal NHC complexes are still scarce and, as a result, the detailed nature of metal carbene bonds remains to be unveiled.

During the last decade, quantum mechanical methods have gained widespread acceptance in the study of TM compounds.[15,16] This is mostly due to the recent development of modern density functional theories. Analyzing the calculated electronic structures resulting from DFT calculations provides insight into the nature of bonding in TM compounds.[16,17] Bonding models based on quantum mechanical concepts have thus been developed to qualitatively understand and, furthermore, predict the structures and reactivities of inorganic and organometallic compounds, such as metal carbonyl complexes,[18] Fischer-type and Schrock-type metal carbene complexes,[18-20] alkene and alkyne π-complexes[21], as well as an unusual silver phosphorous compound, $[Ag(\eta^2\text{-}P_4)_2]^+$.[22] Surprisingly, only very few quantum mechanical investigations on metal NHC complexes, especially TM NHC complexes, have been reported.[10-13,23] This is in contrast to their vast popularity in organometallic chemistry.

In the course of developing tris(carbene) ligand systems for transition metal coordination and application in small molecule activation, we recently synthesized a novel tripodal polycarbene ligand system [1,1,1-tris-(3-methylimidazol-2-ylidene)methyl]ethane ($TIME^{Me}$) and its corresponding silver complex (Chapter 2). The silver-carbene complex has proven to be a useful carbene transfer reagent for the

otherwise unstable free polycarbene $TIME^{Me}$ (see Chapter 2). Cu(I) and Au(I) complexes of the polycarbene ligand $TIME^{Me}$ have been synthesized via Ag(I) carbene transfer routes (Chapter 2).[24] Our previously reported DFT study on the D_3-symmetrical $[(TIME^{Me})_2Ag_3]^{3+}$ complex suggests the existence of π interaction in the silver-carbene moieties.[25] The successful synthesis of the analogous copper and gold $TIME^{Me}$ complexes prompted our interest in a comprehensive DFT investigation of these group 11 complexes and analogues, closely related species. The main goal of the DFT study reported herein is to provide further insight into the nature of bonding in NHC complexes and aims at defining the concept of π-interaction in metal-NHC complexes in a more general manner.

6.2. Results and Discussion

All calculations were carried out using the ADF program suite at the BP86 level with relativistic effects accounted for by ZORA.[26] Geometry optimizations and single point calculations were carried out for trinuclear $[(TIMEMe)_2M_3]^{3+}$ (M = Ag (**1**), Cu(**2**), and Au(**3**)) and the closely related palladium complex $Pd(CN_2Bu^t_2C_2H_2)_2$ (**4**).[27] Calculations carried out on the free carbene 1,3-dimethylimidazol-2-ylidene (**5**, **Im**)[28] served as a starting point for the construction of molecular orbital diagrams (*vide infra*). The metal-ligand bonding interactions were analyzed by using the energy-decomposition scheme introduced by Ziegler and Rauk.[29] The energy-decomposition analyses were carried out on the D_3 symmetrical complexes **1**-**3**, D_{2d}-symmetrical complex **4**, and simplified model complexes for **1 - 3**, namely the D_{2h}-symmetrical

complexes $M(Im^{Me})_2$, (M = Ag (**6**), Cu(**7**), and Au (**8**)) (Figure 6-1). To compare the π-acceptor strength of NHCs with that of the strong π-acid carbon monoxide, geometry optimization and energy decomposition analyses were carried out on hypothetical bis-carbonyl species $M(CO)_2$, (M = Ag^+ (**9**), Cu^+ (**10**), Au^+ (**11**), and Pd(0) (**12**). In these species, the two carbonyl ligands coordinate to the metal in a linear fashion ($D_{\infty h}$ symmetry).

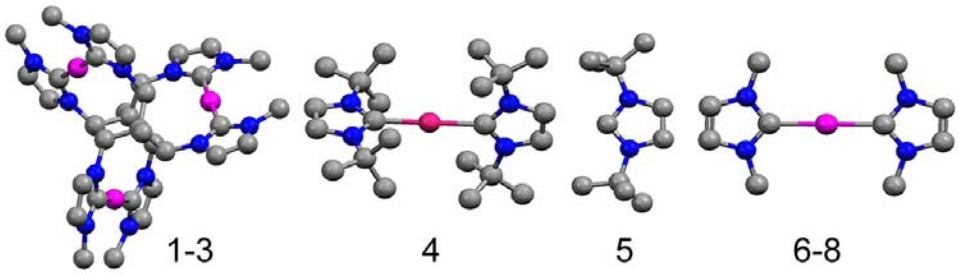

Figure 6-1. Structural representations of complexes **1 - 8**.

6.2.1. Optimized geometries

The calculations result in structural parameters that reproduce the experimentally determined bond lengths and angles of complexes **1 - 4** (Table 6-1). Even the small decrease in the $C_{carbene}$—N bond distances and increase in N—$C_{carbene}$—N bond angles in going from Cu to Ag and Au are observed. The structure of the free carbene 1,3-dimethylimidazol-2-ylidene (**Im**, **5**) is unknown, however, the calculated structure is in good agreement with those of the crystallographically characterized analogues mesityl and adamantyl derivatives.[3,28] For example, the calculations resulted in an average N—$C_{carbene}$ bond length of 1.373 Å, that is very

similar to 1.370 Å in 1,3-di-1-adamantyl-imidazol-2-ylidene,[3] and 1.368 Å in 1,3-bis(2,4,6-trimethylphenyl)-imidazol-2-ylidene.[28] Also, the calculated N—$C_{carbene}$—N bond angle of 101.6° agrees well with the X-ray crystallographically determined 102.2° and 101.4° of the mesityl and adamantyl derivatives.

Table 6-1. Selected Structural Parameters for the Geometry-Optimized Species **1-5** (Bond Distances in Å and Bond Angles in Deg. Parameters for the Crystallographically Characterized Complexes **1 - 4** are Listed for Comparison.)

Structural parameters	**1**		**2**		**3**		**4**		**5**
	Calc.	Expt.	Calc.	Expt.	Calc.	Expt.	Calc.	Expt.	Calc.
M—C_{carb}	2.087	2.082	1.901	1.912	2.054	2.028	2.057	2.041	-
Ave. N—C_{carb}	1.366	1.353	1.371	1.357	1.365	1.347	1.388	1.361	1.373
C=C	1.359	1.341	1.360	1.349	1.360	1.344	1.357	1.357	1.362
Ave. N—C	1.390	1.384	1.387	1.380	1.389	1.395	1.389	1.374	1.394
N—C_{carb}—N	103.9	104.3	103.5	103.8	104.4	105.2	102.8	105.3	101.6
C_{carb}—M—C'_{carb}	177.6	178.6	176.9	177.7	177.5	177.6	180.0	180.0	-

Table 6-2. Selected Structural Data for the Geometry-Optimized Species **9 - 12** (Bond Distances in Å and Bond Angles in Deg.)

Structural parameters	**9**	**10**	**11**	**12**
M—C_{CO}	2.089	1.865	1.989	1.942
C≡ O	1.129	1.131	1.130	1.148

Calculated geometries for the hypothetical complexes **9** – **12** are listed in Table 6-2. Structurally characterized examples for **9** – **12** are unknown, but a related complex, $[Ag(CO)_2][B(OTeF_5)_4]$, in which the $[Ag(CO)_2]^+$ ion is stabilized by weakly coordinating $B(OTeF_5)_4^-$ anion, has been reported.[30] In this complex the $Ag(CO)_2$ is almost linear and the average Ag—C and C—O distances of 2.14(5) Å and 1.08(5) Å are slightly different from those of **9**, reflecting a significant degree of structural influence imposed by the coordinating counter anion.

6.2.2. Bonding in the metal-NHC complexes

I. Molecular orbital analysis

All metal-ligand interactions in complexes **1-3** were analyzed using a "fragment approach". This approach applied to complex **2** with three copper ions and two $TIME^{ME}$ ligands arranged in D_3 symmetry, for instance, results in a molecular orbital interaction diagram comprising the $\mathbf{M_3}$ and $\mathbf{L_2}$ fragment of the $\mathbf{M_3L_2}$ complex. Analysis of the corresponding molecular orbitals (MOs) allows for deriving σ-bonding and π-backbonding models that describe the metal-ligand electronic interactions involved. The complicated MOs of the $\mathbf{L_2}$ fragment are easier to understand when correlated to those of the much simpler free carbene **5**, followed by superimposing D_3 symmetry.

The orbital energy diagram of **5** is shown in Figure 6-2, left. The highest occupied molecular orbital 19A (HOMO) of **5** mainly contains the lone pair of the carbene center. This orbital has σ symmetry, and the energetic accessibility of this

orbital allows NHC ligands to act as superb σ donors. Near the HOMO, there are five more π-type orbitals that originate from the "aromaticity" of the imidazole ring.[4] Only two of these π-type orbitals, 18A and 21A, meet the requirements to interact with the MOs of the metal fragment of the complex. While occupied orbitals such as 18A do not result in net bonding with occupied metal *d*-π orbitals, they can mix with their unoccupied counterparts like orbital 21A and interact with fully occupied metal *d*-π orbitals, resulting in overall stabilizing contributions (vide infra).

Considering all possible bonding interactions, a simplified orbital diagram of $(TIME^{Me})_2$ containing all relevant σ and π orbitals was constructed. The L_2 ligand fragment $(TIME^{Me})_2$ contains six imidazole rings arranged in D_3 symmetry. Therefore, the MOs of $(TIME^{Me})_2$ can be treated as linear combinations of six 19A-like σ-type orbitals and twelve 18A- and 21A-like π-type orbitals (Figure 6-2, right).

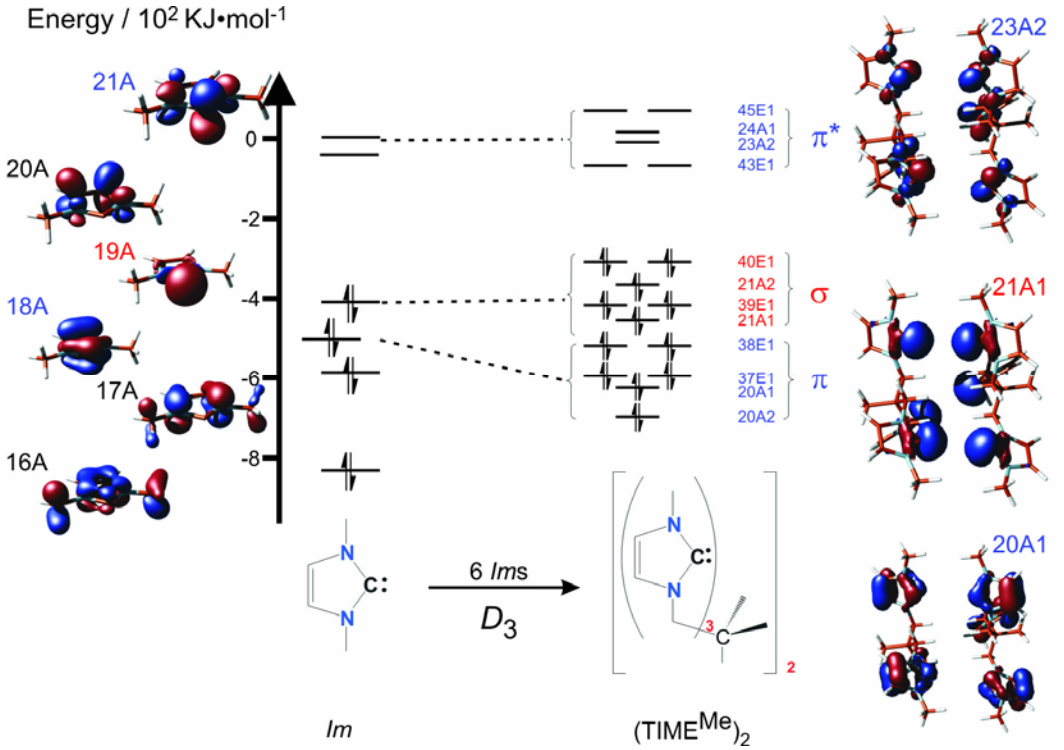

Figure 6-2. Orbital diagram of carbene **Im** (left) and ligand fragment $(TIME^{Me})_2$ (right).

Accordingly, a qualitative molecular orbital correlation diagram of complex **2** is accessible by combining the two fragments, $(TIME^{Me})_2$ and Cu_3 (Figure 6-3).[31] From this diagram it is apparent that both σ and π-type bonding exist between the metal and the ligand fragments. Two types of σ-bonding are involved (Figure 6-3); the dominant σ contribution results from interaction of the ligand fragment is σ orbitals with the $3d(z^2)+4s$ hybrid orbitals of the metal fragment. A representative bonding orbital, 20A1, has 33% metal $d + s$ character and 64% ligand character (Figure 6-4 left, bottom). The interaction between the σ ligand orbitals and the $4p(z)$

orbitals of the metal ions additionally produces a small but noticeable contribution. A representative bonding orbital with 14% metal *p* and 86% ligand character, 21A2, is shown in Figure 6-4, left top. While all ligand σ orbitals and the metal *d* orbitals are fully occupied, the metal *s* and *p* orbitals are empty. This results in an overall σ-donation from the ligand to the metal fragment. Since the σ orbitals of the ligand fragment originate from the lone pairs of the carbene centers, the σ bonding model described here is in accord with the well-known, strong Lewis-basicity of NHCs.

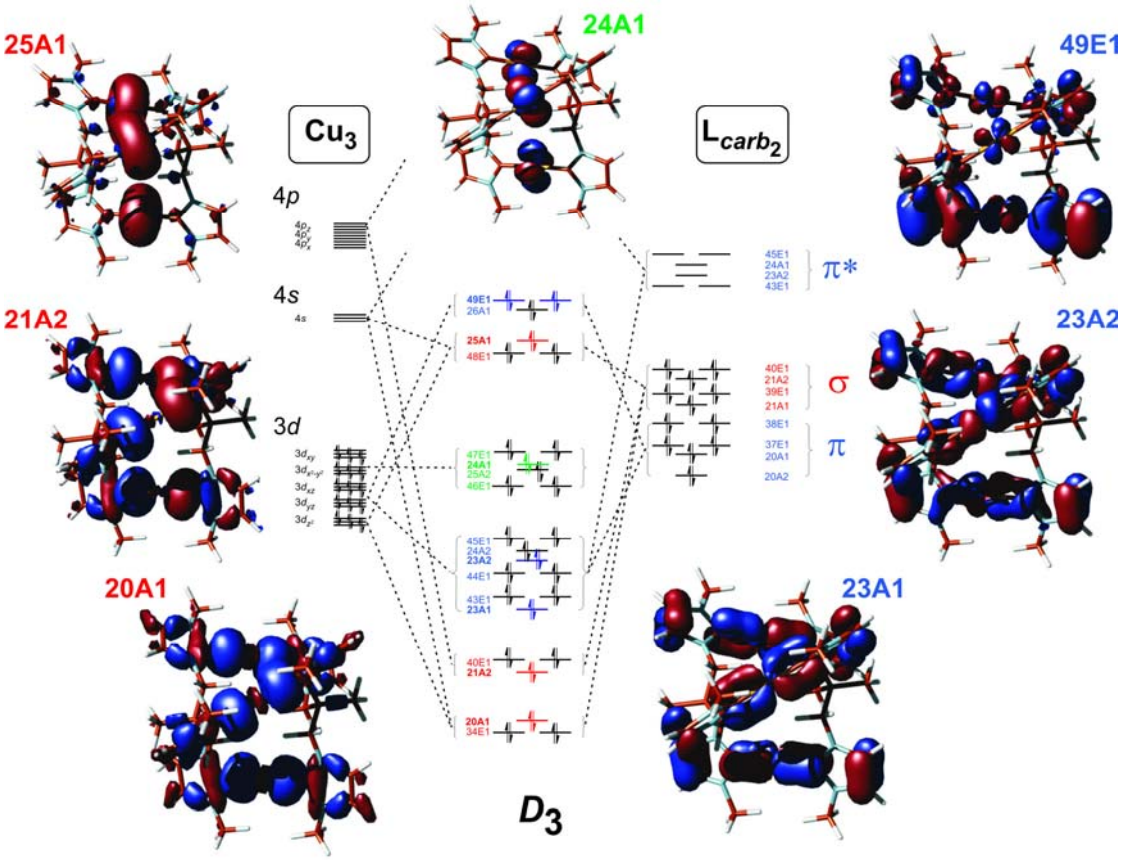

Figure 6-3. Qualitative orbital correlation diagram of complex **2**, $[(TIME^{Me})_2Cu_3]^{3+}$: σ-type orbitals are labeled red, π-type orbitals are labeled blue, and metal-based, non-bonding orbitals are labeled green. The z-axis is defined along the C—M—C entity.

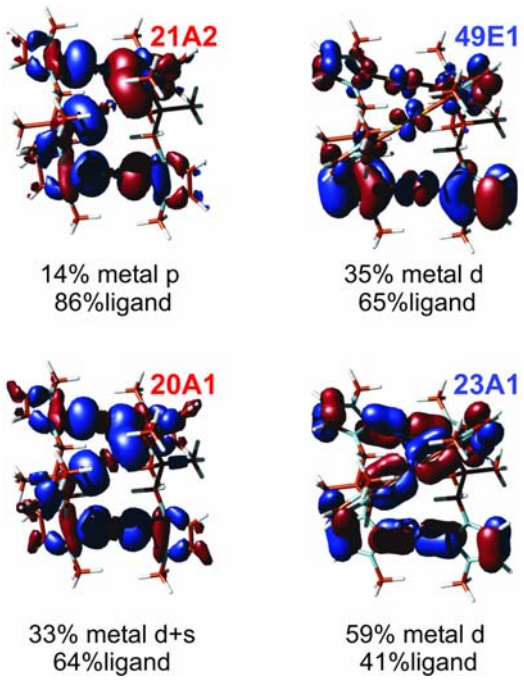

Figure 6-4. Representative molecular orbitals in complex **4**: left, σ-type orbitals; right, π-type orbitals.

The MO diagram shown in Figure 6-3 also reveals a detailed picture of the π bonding interactions in complex **2**. The metal *d*(xz)/*d*(yz) orbitals interact with both, the π and π^* orbitals, of the carbene ligands and form bonding, quasi-antibonding, and antibonding orbitals (Figure 6-4, orbitals with π symmetry are labeled in blue).[31] Typical π-type MOs are shown in Figure 6-4, right. Orbital 23A1 has apparent bonding character, with 59% metal *d* and 41% ligand π/π^* contributions. Orbital 49E1 has quasi-antibonding character with 35% metal *d* and 65% ligand π/π^* contribution. This significant overlap of the fully occupied metal *d*(xz)/(yz) orbitals

and the partially empty ligand π/π^* orbitals,[32] stemming from the carbene p-π orbitals, is indicative of π-backbonding interaction between the metal ions and the NHCs.

This π bonding between the metal ions and NHC ligands is not limited to D_3 symmetrical complexes of group 11 metal ions such as **1**-**3**. In fact, calculations on complex **4** similarly revealed π interactions of various degrees. MO diagrams similar to that of complex **2** were constructed and analyzed. The corresponding representative π-bonding MOs are presented in Figure 6-5.

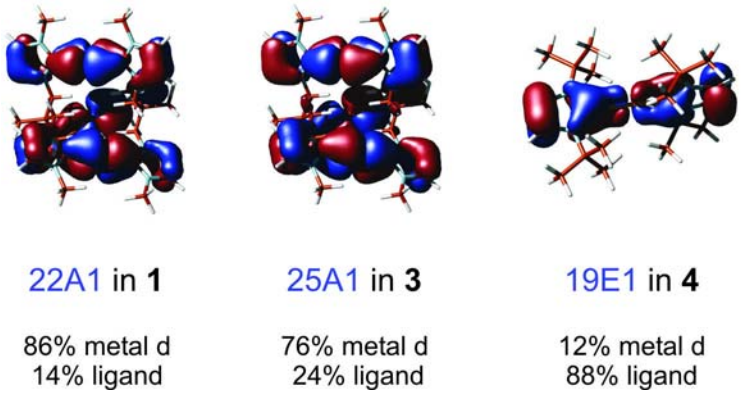

Figure 6-5. Representative π-type molecular orbitals in complexes **1**, **3**, and **4**.

II. Energy decomposition analysis

The nature of the M-$C_{carbene}$ bond in complexes **1 - 4** was additionally explored using the Ziegler and Rauk energy-decomposition schemes[29] incorporated in the ADF program. The central element of such an analysis is the interaction energy (ΔE_{int}) between the bonding fragments. It is calculated as the energy difference between the geometry-optimized complex and the complex fragments with frozen geometry. This

energy difference can be broken down into three separate energy terms: $\Delta E_{int} = \Delta E_{pauli} + \Delta E_{elst} + \Delta E_{orb}$. The pauli energy term (ΔE_{pauli}) refers to the four-electron destabilizing interactions between occupied orbitals; the electrostatic energy term (ΔE_{elst}) term gives the attractive electrostatic contributions; and the orbital energy term (ΔE_{orb}) gives the stabilizing orbital interaction energy arising when the Kohn-Sham orbitals relax to their optimal form. This latter energy term can be broken down into orbital contributions from different irreducible representations of the interacting system. This allows the calculation of stabilizing contributions stemming from orbitals with σ, π, or δ symmetry.

The bond energy (ΔE_{bond}) of the complexes was calculated by adding the preparation energy (ΔE_{prep}) to the interaction energy (ΔE_{int}) as given by the above energy-decomposition analysis ($\Delta E_{bond} = \Delta E_{int} + \Delta E_{prep}$). The preparation energy is the energy that is necessary to promote two of the interacting fragments, e.g. A and B, from their equilibrium geometry to the geometry that they exhibit in the geometry-optimized species, e.g AB. The bond dissociation energy (D_e) for each metal-carbene bond can in turn be deduced from the overall bond energy.

The results are summarized in Table 6-3. Our calculations reveal relatively high M—$C_{carbene}$ bond dissociation energies, which is in agreement with the reported stabilities of TM NHC complexes. The strongest M—C bond was found for complex **2** with a D_e of 81.5 kcal/mol for each Cu—C bond. This value is even higher than that reported for the classical Fischer-carbene complex $(CO)_5$W-CH(OH) (D_e = 75.0 kcal/mol at CCSD(T) level).[19] In cationic complexes **1**-**3**, the metal—carbene bonds

were found to be much stronger than in their iso-electronic neutral counterpart **4** (Table 6-3). The calculated D_e values of complexes **1**-**3** are slightly different from those found for the (*Im*C**:**)M(Cl) (M = Cu, Ag, and Au) model system with D_e values of 67.4, 56.5, and 82.8 kcal/mol for the Cu(I), Ag(I), and Au(I) complexes, respectively.[10]

Table 6-3. Energy Decomposition Analysis of Metal-NHC Complexes in the D_3 (**1 - 3**) and D_{2d} (**4**) Groups at the BP86 Level.

Contribution (kcal/mol)	Description	**1**	**2**	**3**	**4**
ΔE_{Pauli}	Pauli repulsion	697.1	628.0	1066.3	323.6
ΔE_{elst}	electrostatic interaction	-827.7	-848.4	-1127.5	-289.2
ΔE_{orb}	stabilizing orbital interactions	-358.7	-428.8	-525.0	-120.3
ΔE_{int}	bond interaction energy	-467.8	-624.5	-558.2	-83.0
ΔE_{prep_m}	prep. energy for the metal fragment	127.9	120.8	89.3	0
ΔEprep_l	prep. energy for the ligand fragment	8.9	14.9	11.7	8.08
ΔE_{bond}	bond energy	-330.9	-488.7	-457.2	-75.0
De (M-C)	BDE for each metal-carbene bond	55.2	81.5	76.2	37.5

Generally, partitioning the stabilizing orbital interaction energy (ΔE_{orb}) into contributions from different symmetry allows separation of σ and π interactions.[11,16,17,22,33] The D_3 symmetrical group 11 metal NHC complexes with three metal ions in each molecule will not allow for such a separation. However, a mononuclear palladium bis-carbene complex **4** possesses D_{2d} symmetry with three

main contributions to the orbital interaction energy stemming from different irreducible representations in the D_{2d} group (Figure 6-6). The major contribution arises from donation of carbene lone pair electrons into the palladium $4d(z^2) + 5s$ hybrid (a1, -74.31 kcal/mol). The donation of carbene lone pair electrons into the palladium $5p(z)$ orbital results in much less stabilization energy (b2, -5.94 kcal/mol). Overall, the sum of all σ-type contribution totals -79.35 kcal/mol. Notably, the interaction between the palladium *d* orbitals and the carbene p-π orbitals is also significant (e1, -36.28 kcal/mol) and cannot be neglected. The ratio of σ-donation/π-backdonation (d/b value) in **4** is 2.2, and the π bonding contributes 30% to the overall stabilizing orbital interaction energy (E_{orb} = -120.34 kcal/mol).

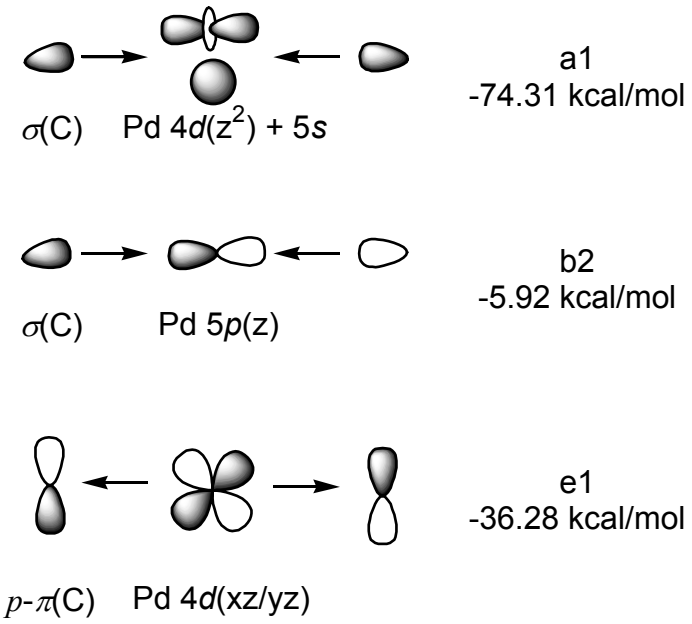

Figure 6. Main contributions of the irreducible representations to the stabilizing orbital-interaction energy (ΔE_{orb}) in $Pd(CN_2Bu^t_2C_2H_2)_2$, **4** (D_{2d}).

As mentioned earlier, quantitative separation of σ and π interaction energy in trinuclear complexes **1-3** is not possible due to their D_3 symmetry. However, approximate results can be obtained by analysis of the simplified D_{2h}-symmetrical model compounds $M(CN_2Me_2C_2H_2)_2$, (M = Ag (**6**), Cu(**7**), and Au(**8**)). The geometry of these mononuclear model compounds closely resembles the individual linear carbene-metal-carbene entities found for complexes **1-3** (see Figure 6-1). Calculations show that in these model complexes the main σ-donations (a_{1g}) have energy contributions of -57.4 (**6**), -67.8 (**7**), and -73.7 (**8**) kcal/mol, while the π-interactions (b_{2g}) have energy contributions of -10.2 (**6**), -15.5 (**7**) and -12.6 (**8**) kcal/mol. Thus, the d/b ratios are 5.6, 4.4, and 5.8, and therefore the π bonding contributes to approximately 15%, 18%, and 15% of the overall stabilizing orbital interaction energy for Ag(I), Cu(I), and Au(I) respectively. The results are slightly different from that of hypothetical NHC ligand metal adducts (*Im*C**:**)M(Cl) (M = Ag, Cu, and Au), with the d/b being 6.6, 9.7, and 4.3 for Cu(I), Ag(I), and Au(I) respectively.[10] The smaller π-backbonding contribution in complexes **6**-**8** relative to that in complex **4** might be attributed to the positive charge on the group 11 metal ions. Also in complexes **6**-**8** only one *d*-π orbital can be involved in the π-bonding, while in **4**, the two *d*-π orbitals can both take part in such interactions.

The above study leads to the conclusion that NHCs are not only excellent σ donors, but also fairly good π-acceptors. This is true even for the cationic closed-shell d^{10} metal centers discussed here. The magnitude of such interactions, however, may vary. We generally do not agree with the use of a term such as “negligible” to

describe the π-backbonding in metal NHC complexes. It is true that of the few calculated metal NHC complexes to date,[10,11,13] σ-bonding accounts for more than 70 % of the overall stabilizing orbital energy. Even so, it is important to recognize the potential π-acceptor properties of NHC ligands. As we and others[13] have shown, for electron rich metal centers, π-backbonding can be significant and contributes up to 20 - 30% of the orbital interaction energy of a metal NHC complex, e.g. in palladium complex **6** or in iridium complex [Cp(NHC)Ir=CH_2].[13] It was found that in the NHC-Ir fragment of the latter complex, π-backbonding contributes to 20% of the covalent bonding energy of the fragment, while in a Schrock-type carbene fragment {M=CH_2}, a benchmark fragment for the σ-bonding/π-backbonding model, π-backbonding contributes 25% to the covalent bonding energy.[13]

6.2.3. Bonding in metal carbonyl complexes

To compare the degree of π-backbonding in metal NHC complexes discussed here and that of metal carbonyls, we also carried out energy decomposition analysis of hypothetical bis-carbonyl complexes **9** – **12**. We only focused on the relative contributions of σ- and π-bonding to the overall stabilizing orbital interaction energies in these complexes (Table 6-4). Calculations show that the CO σ to metal *d* bonding (σ_g symmetry) has energy contributions of -39.47, -52.23, -59.23, and -68.71 kcal/mol, and the metal *d* to CO π* backbonding (π_g symmetry) has energy contributions of -17.89, -31.28, -29.17, and -66.80 kcal/mol for **9** - **12**, respectively. Thus the d/b ratios

are 2.2, 1.7, 2.0, and 1.0, and the *d*-π* backbonding contributes to approximately 24%, 30%, 27%, and 48% of the overall stabilizing orbital interaction energy for Ag(I), Cu(I), Au(I), and Pd(0) bis-carbonyls, respectively (σ- and π-bonding between metal *s* and *p* orbitals and CO frontier orbitals also contribute substantially to the orbital interaction in these complexes). Overall, the calculations suggest that for electron-rich low-valent late metals, carbonyl is a much stronger π-acceptor ligand than NHCs.

Table 6-4. Energy Decomposition of the Metal Bis-Carbonyl Complexes (**9 - 12**) in $D_{\infty h}$ symmetry at the BP86 Level.

Contribution (kcal/mol)	Description	**9**	**10**	**11**	**12**
$\mathbf{\Delta E_{Pauli}}$	Pauli repulsion	155.5	170.8	309.1	309.1
$\mathbf{\Delta E_{elst}}$	electrostatic interaction	-127.8	-154.2	-230.8	-239.8
$\mathbf{\Delta E_{orb}}$	stabilizing orbital interactions	-73.6	-105.7	-107.9	-138.4
$\mathbf{\Delta E_{\sigma(g)}}$	energy from σ(g) symmetry	-39.5	-52.2	-53.4	-68.71
$\mathbf{\Delta E_{\sigma(u)}}$	energy from σ(u) symmetry	-11.0	-15.8	-11.9	-4.14
$\mathbf{\Delta E_{\pi(u)}}$	energy from π(g) symmetry	-17.9	-31.3	-29.2	-66.80
$\mathbf{\Delta E_{\pi(u)}}$	energy from π(u) symmetry	-5.3	-7.5	-7.47	-1.28

6.3. Conclusion

The electronic structure of group 11 metal complexes of $TIME^{Me}$ was elucidated with the aid of molecular orbital analyses based on results from DFT calculations. The analyses revealed the expected and well-known σ-type interactions

in addition to non-negligible π- interactions between the electron rich metal ions and the carbene p-π orbitals. Energy decomposition analyses of the closely related D_{2d}-symmetrical Pd complex, $Pd(CN_2Bu^t_2C_2H_2)_2$ and the D_{2h}-symmetrical model complexes $M(Im^{Me}C:)_2$ (M = Ag, Cu, and Au) allowed for a quantitative comparison of π and σ contributions. It was found that the π-backbonding interactions in these diaminocarbene species contribute to approximate 15 - 30% of the complexes' overall orbital interaction energies.

This finding of non-negligible or even significant π-bonding interactions in metal NHC complexes is in contrast to the common assumption that NHC ligands are pure σ donors. However, the latter assumption generally was based on the "single-bond" character of the M—$C_{carbene}$ crystallographically determined. While it is customary, and often instructive, to correlate a given bond length with the bond order in a certain class of compounds, such a correlation is purely empirical and by itself is not sufficient to corroborate the nature of any given metal-ligand interaction. Instead, for the investigation of π-backbonding from the metal to the π* orbitals of NHC ligands it is more instructive to compare structural parameters of the imidazole rings in a series of isostructural NHC complexes containing electron-rich, less electron-rich, and electron-poor metal centers. If π-backbonding from the metal to NHC ligand exists, one would expect a decrease of the nitrogen-to-carbene π-bonding and, thus, an increase of the C—N bond lengths for the more electron-rich metal centers. Extensive search in the Cambridge Crystallographic Data Center (CCDC) does in fact provide convincing structural evidence for metal-NHC π-backbonding: For example,

comparison of structural parameters for the bis-carbene complexes $(IM^{Mes}C:)_2M$ (with $IM^{Mes}C:$ = 1,3-dimesitylimidazol-2-ylidene, M = Ni(0), Ag(I), and I^+).[34] These complexes are iso-structural and bare the same set of NHC ligands. All structural data were collected at low temperature. It is apparent that from I^+ (electron poor, not capable of π-backbonding) to Ag^+ (less electron-rich, capable of π-backbonding) to Ni(0) (electron-rich, very capable of π-backbonding), the average C—N bond lengths increase from 1.346 Å in $[(IM^{Mes}C:)_2I]^+$ to 1.358 Å in $[(IM^{Mes}C:)_2Ag]^+$ to 1.375 Å in $[(IM^{Mes}C:)_2Ni]$. These structural changes provide indeed very definitive experimental evidence for the existence of metal-NHC π-backbonding. Nevertheless, quantum mechanical calculations are more straightforward and essential in unveiling the "true" nature of the metal-carbene bond. While some may argue that 15% of π-bonding is "negligible", such a simplification would certainly overlook the exact nature of the metal NHC bond, as well as the potential role of metal-carbene π-backbonding in the diverse NHC chemistry.

Additional note: after publication of this work, a paper by Frenking et al. entitled "The Significance of π-Interactions in Group 11 Complexes with N-Heterocyclic Carbenes" described similar study and concluded that "The EDA results suggest that R_2C—ML_n π back-donation in complexes with N-heterocyclic carbenes is not substantially smaller than in Fischer carbene complexes bearing two p donor groups R."[35]

6.4. Experimental Section

Computational details. All DFT calculations were carried out using the Amsterdam Density Functional (ADF) program package, release 2002.01.[26] The Vosko, Wilk and Nusair (VWN) local density approximation,[36] Becke's exchange correlation,[37] and Perdew correlation[38] were used. The calculation also included scalar relativistic effects (ZORA)[39] for all atoms. Uncontracted Slater-type Orbitals (STOs)[40] were used as basis functions. Cu: triple-ζ basis set augmented with a set of *p* functions and frozen core 2*p*. Ag: triple-ζ basis set augmented with a set of *p* functions and frozen core 3*d*. Au: triple-ζ basis set augmented with a set of *p* functions and frozen core 4*d*. N: triple-ζ basis set augmented with a set of *d* functions and frozen core 1*s*. O: triple-ζ basis set augmented with a set of *d* functions and frozen core 1*s*. C: triple ζ-basis set augmented with a set of *d* functions and frozen core 1*s*. H: triple-ζ basis set augmented with a set of *p* functions. This basis combination is denoted TZP in the ADF program. For the analyses of the metal—ligand bonds, Ziegler and Rauk's energy decomposition scheme was employed.[29]

Molecular orbitals were visualized using the MOLDEN program package (http://www.cmbi.kun.nl/~schaft/molden/molden.html).

6.5. Acknowledgement

Text and figures of this chapter, in part, are reprints of the materials published in the following paper: **Hu**, **X**.; Castro-Rodriguez, I.; Olsen, K.; Meyer, K*. "Group 11 Metal Complexes of N-Heterocyclic Carbene Ligands: Nature of the Metal-

Carbene Bond", *Organometallics* **2004**, *23*, 755-764. The dissertation author was the primary researcher and author. The co-authors listed in this publication also participated in the research.

6.6. References

(1) Bourissou, D.; Guerret, O.; Gabbai, F. P.; Bertrand, G. *Chem. Rev.* **2000**, *100*, 39-91; Herrmann, W. A. *Angew. Chem.-Int. Edit.* **2002**, *41*, 1291-1309.

(2) Huang, J. K.; Stevens, E. D.; Nolan, S. P.; Petersen, J. L. *J. Am. Chem. Soc.* **1999**, *121*, 2674-2678; Scholl, M.; Ding, S.; Lee, C. W.; Grubbs, R. H. *Org. Lett.* **1999**, *1*, 953-956.

(3) Arduengo, A. J.; Harlow, R. L.; Kline, M. *J. Am. Chem. Soc.* **1991**, *113*, 361-363.

(4) Herrmann, W. A.; Kocher, C. *Angew. Chem. Int. Ed. Engl* **1997**, *36*, 2163-2187.

(5) Herrmann, W. A.; Runte, O.; Artus, G. *J. Organomet. Chem.* **1995**, *501*, C1-C4.

(6) Frohlich, N.; Pidun, U.; Stahl, M.; Frenking, G. *Organometallics* **1997**, *16*, 442-448.

(7) Frankell, R.; Birg, C.; Kernbach, U.; Habereder, T.; Noth, H.; Fehlhammer, W. P. *Angew. Chem.-Int. Edit.* **2001**, *40*, 1907-1910.

(8) Nakai, H.; Tang, Y. J.; Gantzel, P.; Meyer, K. *Chem. Commun.* **2003**, 24-25.

(9) Clarke, M. J.; Taube, H. *J. Am. Chem. Soc.* **1975**, *97*, 1397-1403.

(10) Boehme, C.; Frenking, G. *Organometallics* **1998**, *17*, 5801-5809.

(11) Deubel, D. V. *Organometallics* **2002**, *21*, 4303-4305.

(12) Abernethy, C. D.; Codd, G. M.; Spicer, M. D.; Taylor, M. K. *J. Am. Chem. Soc.* **2003**, *125*, 1128-1129.

(13) Termaten, A. T.; Schakel, M.; Ehlers, A. W.; Lutz, M.; Spek, A. L.; Lammertsma, K. *Chem.-Eur. J.* **2003**, *9*, 3577-3582.

(14) McGuinness, D. S.; Saendig, N.; Yates, B. F.; Cavell, K. J. *J. Am. Chem. Soc.* **2001**, *123*, 4029-4040.

(15) Davidson, E. R. *Chem. Rev.* **2000**, *100*, 351-352; Torrent, M.; Sola, M.; Frenking, G. *Chem. Rev.* **2000**, *100*, 439-493.

(16) Frenking, G.; Frohlich, N. *Chem. Rev.* **2000**, *100*, 717-774.

(17) Frenking, G.; Wichmann, K.; Frohlich, N.; Loschen, C.; Lein, M.; Frunzke, J.; Rayon, V. M. *Coord. Chem. Rev.* **2003**, *238*, 55-82.

(18) Jacobsen, H.; Ziegler, T. *Inorg. Chem.* **1996**, *35*, 775-783.

(19) Vyboishchikov, S. F.; Frenking, G. *Chem.-Eur. J.* **1998**, *4*, 1428-1438.

(20) Vyboishchikov, S. E.; Frenking, G. *Chem.-Eur. J.* **1998**, *4*, 1439-1448; Jacobsen, H.; Ziegler, T. *Organometallics* **1995**, *14*, 224-230.

(21) Li, J. A.; Schreckenbach, G.; Ziegler, T. *Inorg. Chem.* **1995**, *34*, 3245-&; Kovacs, A.; Frenking, G. *Organometallics* **1999**, *18*, 887-894.

(22) Deubel, D. V. *J. Am. Chem. Soc.* **2002**, *124*, 12312-12318.

(23) Green, J. C.; Scurr, R. G.; Arnold, P. L.; Cloke, F. G. N. *Chem. Commun.* **1997**, 1963-1964.

(24) Wang, H. M. J.; Lin, I. J. B. *Organometallics* **1998**, *17*, 972-975.

(25) Hu, X.; Tang, Y.; Gantzel, P.; Meyer, K. *Organometallics* **2003**, *22*, 612-614.

(26) ADF2002.01; SCM, Theoretical Chemistry, Vrijie Universiteit: Amsterdam, The Netherlands; Velde, G. T.; Bickelhaupt, F. M.; Baerends, E. J.; Guerra, C. F.; Van Gisbergen, S. J. A.; Snijders, J. G.; Ziegler, T. *J. Comput. Chem.* **2001**, *22*, 931-967; Guerra, C. F.; Snijders, J. G.; te Velde, G.; Baerends, E. J. *Theor. Chem. Acc.* **1998**, *99*, 391-403.

(27) Arnold, P. L.; Cloke, F. G. N.; Geldbach, T.; Hitchcock, P. B. *Organometallics* **1999**, *18*, 3228-3233.

(28) Arduengo, A. J.; Dias, H. V. R.; Harlow, R. L.; Kline, M. *J. Am. Chem. Soc.* **1992**, *114*, 5530-5534.

(29) Ziegler, T.; Rauk, A. *Theor. Chim. Acta* **1977**, *46*, 1-10; Ziegler, T.; Rauk, A. *Inorg. Chem.* **1979**, *18*, 1558-1565.

(30) Hurlburt, P. K.; Rack, J. J.; Dec, S. F.; Anderson, O. P.; Strauss, S. H. *Inorg. Chem.* **1993**, *32*, 373-374.

(31) The unoccupied orbitals are omitted for clarity.

(32) The π orbitals of the ligand fragment are preoccupied, but the π* orbitals are empty, and there is a mixing between these π and π* orbitals when the ligands coordinates to the metal ions. Accordingly, the hybrid π/π* orbitals are "partially empty" in the metal NHC complex.

(33) Massera, C.; Frenking, G. *Organometallics* **2003**, *22*, 2758-2765.

(34) Arduengo, A. J.; Gamper, S. F.; Calabrese, J. C.; Davidson, F. *J. Am. Chem. Soc.* **1994**, *116*, 4391-4394; Arduengo, A. J.; Dias, H. V. R.; Calabrese, J. C.; Davidson, F. *Organometallics* **1993**, *12*, 3405-3409; Arduengo, A. J.; Tamm, M.; Calabrese, J. C. *J. Am. Chem. Soc.* **1994**, *116*, 3625-3626.

(35) Nemcsok, D.; Wichmann, K.; Frenking, G. *Organometallics* **2004**, *23*, 3640-3646.

(36) Vosko, S. H.; Wilk, L.; Nusair, M. *Can. J. Phys.* **1980**, *58*, 1200-1211.

(37) Becke, A. D. *Phys. Rev. A* **1988**, *38*, 3098-3100.

(38) Perdew, J. P. *Phys. Rev. B* **1986**, *33*, 8822-8824.

(39) Van Lenthe, E.; Ehlers, A.; Baerends, E. J. *J. Chem. Phys.* **1999**, *110*, 8943-8953.

(40) Snijders, J. G.; Vernooijs, P.; Baerends, E. J. *At. Data Nucl. Tables* **1981**, *26*, 483-509.